REFERENCE ONLY

UNIVERSITY OF LONDON THESIS

Degree	Year	Name of Author
PhD	2005	McDARBY, J. M.

Modelling of Turbulent Rotor-Blade Flow and Ground Effect

John Michael McDarby
University College London
University of London

A thesis submitted for the degree of
Doctor of Philosophy.
Supervisor: Prof. F.T. Smith F.R.S.
October 2004

ProQuest LLC
789 East Eisenhower Parkway
P.O. Box 1346
Ann Arbor, MI 48106-1346

Abstract

Rotor blade flows occur in numerous physical systems from helicopters to fans, and from propellers to food mixers. Many previous studies have concentrated on the laminar flow generated by a set of rotors but in many practical cases the flow is turbulent, a setting in which previous research appears to be mainly experimental or purely numerical. The thesis examines turbulent rotor flow as its prime feature, before moving on to the impact of the ground and side structures on the flow. Whilst there exists a wide variety of rotor blade flows in industry, the present research is motivated by the application to helicopters. Using asymptotic analysis and computational methods the thesis first examines the turbulent boundary layer on a flat plate with a moving surface and, second, a rotating disc. Analytical and numerical predictions are then derived and compared with previous results. Asymmetry about the axis of rotation is introduced next and the problem of a rotating cut-disc is studied as an approximation to a set of rotors. A numerical solution is obtained and is supported by analytical results. Blade inclination and thickness are then incorporated into the three-dimensional case, with asymmetric blade shape being analyzed as if in two dimensions only. The influence of ground effect is examined firstly through the use of an image potential in the two-dimensional asymmetric blade shape problem and secondly in the axisymmetric case of flow between a stationary and a rotating disc. A numerical solution is determined and compared with existing research, whilst an analytical solution is produced for large radii. The flow between a stationary disc and a rotating cut disc is then briefly discussed before, finally, the possible extension of this thesis to the problem of turbulent jets is examined.

Acknowledgements

Firstly I would like to thank my supervisor, Prof. FT Smith, FRS, for all his support, guidance and encouragement, and for giving me the opportunity to undertake this research. I would also like to thank Roger Gent, Judith Miller, Mohammed Soliman and Colin Young of QinetiQ for their advice, support and technical expertise, all of which have proven to be invaluable. My gratitude also goes to EPSRC and QinetiQ for the financial support provided to enable me to complete this research.

Recognition is also deserved for all the members of the UCL mathematics department and my fellow postgraduates who have helped me so much along the way.

Personally I also know that I would not have been able to achieve what I have done without the support of my friends and, in particular, my family throughout, so I would like to take this opportunity to thank my mum, dad, Martina, Julie, Tara and all my friends for everything they have done for me.

Finally I would like to thank all the maths teachers that have taught me and who helped encourage and challenge me. In particular I would like to mention Mr J Dolan, Mr A Larson and Mr D Smith for giving me such a strong grounding in maths that I have been able to study it this far.

Contents

List of Figures

List of Tables

Chapter 1

Introduction

Rotating machinery and the resultant fluid flows they induce form an integral part of our lives. Personally my room is often cooled by a desk-top fan whilst a CD plays in the background and the news regularly features incidents involving the use of helicopters in military manoeuvres. These three examples are just the tip of the iceberg and there are many more related occurrences such as with food mixers, lawn mowers, sycamore seeds and propeller blades. Of these, the chief motivation here is the application to helicopter dynamics. Even in this one particular context the range of practical uses is impressive. Perhaps the most obvious of these, especially in light of recent world events, is the military helicopter but this is by no means the only regular use of the technology. Coastal search-and-rescue, police emergency response teams and air-ambulance services all involve helicopters and are an essential component of national emergency services. Less urgent, although nonetheless important, alternative uses range from passenger transport to tourism and even traffic reporting. This variety of applications emphasizes why our interest in rotary flows is focussed on the application to helicopter dynamics since such usage

pervades much of our lives. This interest is mirrored in industrial research, as evidenced by the support and sponsorship of this research by QinetiQ.

In all the different capacities mentioned above, helicopters are chosen for their very special abilities. These include being able to land and take-off in compact locations (as well as to take-off and land vertically), the ability to hover and the general manoeuvrability of helicopters when compared to other aircraft. Unfortunately all these advantages come at a price: the typical fluid flow generated by a helicopter is incredibly complicated. This leads to the dual problem that helicopters are both very difficult to fly and to model.

The complexity inherent in flying a helicopter requires an array of control features to ensure successful flight (Gent et al[32]). These include continuously varying blade inclination as the rotor spins in order that the lift generated by each blade remains approximately constant regardless of whether it is advancing (travelling in the same direction as the helicopter itself) or receding (travelling in the direction opposite to that of the helicopter motion). The variation in the lift produced by advancing and receding blades arises due to the different relative velocities of each blade and so blade inclination is used to adjust for these changes.

Another complication is that the inclination of a blade to the horizontal is not even constant for a given blade at any time. This is due to 'blade twist' and is an important design feature of modern helicopters. It is used to improve the distribution of lift generation along the radius of the blade as an untwisted blade would generate an increasing amount of lift as the radius increased up to the tip, where there is a rapid reduction in lift. This would create strain on the rotors so a twist is introduced to even out the lift distribution.

A further feature is rotor tilt, where the [illegible] rotor can be tilted

relative to the helicopter body. These aspects of helicopter design also help explain the second problem of helicopter dynamics, namely that the modelling of the resultant fluid flow is also very difficult, and not just for the reasons mentioned above. Now blade-wake interaction, and the influence of the fuselage and (where appropriate) a tail rotor, a second set of rotors, the ground and side structures on the flow can be involved. Moreover, based on typical tip velocities, turbulence is an aspect of helicopter dynamics which cannot necessarily be ignored.

The problem of helicopter aerodynamics has been the subject of a large body of literature including Bramwell[8], Conlisk[19], Riley & Brotherhood[60], Seddon[65] and Stepniewski & Keys[73], and the scope of investigation includes empirical, experimental, numerical and analytical work. Each of these approaches has its own advantages and disadvantages. Empirical methods, such as prescribed wake models (where the unknown wake between two blades is estimated from existing data), can be accurate and efficient but require knowledge of the flow (or at least similar ones) beforehand. Experimental techniques can also be reliable but tend to be very expensive and may not highlight all aspects of the flow. Numerical and analytical models are useful but often involve significant simplifications being assumed to enable a solution to be determined. Often this means that simple models or approximations are used to enable certain aspects of the flow, such as turbulence or ground effect, to be focussed on.

In the case of turbulence one such model is to introduce the concept of turbulent stress (known as Reynolds stress) and prescribe the additional stress terms using a simple model based on the viscosity and involving a new term - the effective viscosity. This approach has been used by a range of authors and

for a variety of different flow problems, including Bayley & Owen[3], Cebeci & Smith[13], Cooper[20], Neish & Smith[50] and Wilson[80]. An important feature of turbulence which is particularly relevant in the current context of helicopter dynamics arises in rotating turbulent flows. In such systems, at small radii typical flow speeds are low (at least relative to the tip velocity) and so the flows are laminar at sufficiently low radii. Moving further away from the centre, the blade speed, and hence that of the fluid also, increases and eventually turbulence occurs. This 'transition' to turbulence occurs over some radial range although for the purposes of a solution certain authors take transition to occur at a particular point. The work of Cooper[20] for a free rotating disc is an example of this approach. In the present thesis only the turbulent flow region of rotating flows will be considered. Turbulence will be deemed to occur for all radii beyond a transition radius, and no consideration will be given to the flow at lower radii.

A related problem is that of turbulent intermittency. This is where the fluid is not always turbulent at a given radius and instead 'pockets' of laminar flow may occur. For the present purposes it is assumed that all the systems considered are 'fully turbulent', meaning that such intermittency does not feature.

Turbulent flows are extremely complex and the aspects mentioned above are by no means the only ones which occur. Other important contributions to turbulent modelling, for example adverse pressure gradients and separation, include the work of Prandtl[56], Bradshaw, Ferriss & Atwell[7], Durbin[28] and Spalart[71] however it is not deemed necessary for these particular aspects to be considered here.

The influence of ground effect has also been considered with respect to

helicopter dynamics. This aspect is important as not only is it a phenomenon which occurs widely, it can also have a dramatic effect on the performance of the helicopter. In particular a helicopter hovering close to the ground requires less power to maintain its state than the same craft out of ground effect. This is discussed by amongst others Bramwell[8] [1] and Seddon[65], while Purvis[58] has considered the impact of the ground on rotating laminar flow regimes.

Vertical blade asymmetry is another crucial facet of helicopter design and one which is essential in producing lift. Whilst this is far from straightforward to model, it is possible to consider a variety of more basic flows, each of which incorporates some aspect of the asymmetric case. Such features include interaction of the upper and lower halves of the flow (i.e. some of the flow over one blade may become part of the flow beneath the next one), variable pressure in the outer inviscid region, and lift generation.

In the present work use is made of the **boundary layer** approximation to simplify the governing equations for the central problems. This enables ground effect to be modelled in two ways. Firstly in 2D the fluid region outside the boundary layer is taken to be inviscid (potential) flow. Here ground effect can be incorporated into the system by an image potential; this leads to qualitative agreement with Bramwell[8] and Seddon[65] that the close presence of the ground increases lift. Attention is then turned to a simple system where the boundary layer directly interacts with the ground (or indeed any flat co-axial impervious body).

The boundary layer on a [illegible] rotor has been examined by Smith & Timoshin[68]. Here the Prandtl shift was employed to reduce the flow to that on a cut-disc which is taken to be a body of infinitesimal thickness made up of alternating surfaces and wakes. As a simplification the blade surfaces were taken

1. This particular solution was updated by Done & Balmforth.

to be radial, so that a similarity solution can be applied. Smith & Timoshin[68] then showed that for laminar flow this was a reasonable approximation to non-radial blades as the far-field behaviour of both cases is similar. Understanding the boundary layer on a [illegible] rotor is important but does not allow for the determination of important aspects of the flow such as the pressure exerted on the blades and the wake shape. As such, Smith & Timoshin[69] then proceeded to consider the flow system outside the boundary layer. In the case of symmetric blades the system is reasonably straightforward and can be determined. In the case of asymmetric blade shape however they then show that the inviscid flow problem, and in particular the pressure outside the boundary layer, cannot be solved without knowledge of the wake shape and boundary layer thickness. Unfortunately, in turn these cannot be specified without information about the pressure. This is **viscous-inviscid interaction** and couples the flows in the two regions of concern. This viscous-inviscid interaction is overcome in the 2D problem through an iterative numerical procedure. Purvis[58] then takes this work further by considering ground effect.

This thesis now extends the approach of, amongst others, Bowles & Smith, Smith & Timoshin, Jones and Purvis, by examining the effects of turbulence on rotor blade dynamics. This involves the investigation of a range of turbulent flows which can be classified in the following way:

1. *Simple flows.* Initially some simple two and three-dimensional flow problems are examined in Chapters 2 and 3 in order to understand the elementary principals of rotor blade flow;

2. *Non-axisymmetry.* Vertically symmetric 3D rotating flows without symmetry about the axis of rotation are then considered in Chapters 4 and 5;

3. *Blade shape.* Various practical aspects of rotor blade flow, in particular blade shape and thickness, are analyzed in Chapters 5, 6 and 7;

4. *Ground effect.* Finally ground effect is examined on an inviscid length scale at the end of Chapter 7 and on a viscous length scale in Chapter 8.

As the flows modelled here are ones which either occur widely in practical applications or have relevance to more complicated rotor blade flows, it is of course important to make comparisons with existing research and the predictions and data of other authors. This is especially true when models for the turbulent stress or boundary layer structure are used. Hence, where possible, qualitative and quantitative direct comparisons are made between the current work and earlier studies. Often such comparisons will be illustrated or tabulated as appropriate, subject to the limitations discussed in subsequent chapters.

In Chapter 2, in an initial attempt to understand a relevant turbulent boundary layer (and as a direct precursor to the analysis of Chapter 3 in fact), the case of a 2D finite stationary flat plate with a moving surface travelling at a constant velocity is considered. This problem is similar to that examined by Afzal[2], Sakiadis[61,62] and Tsou, Sparrow & Goldstein[77]. A particular turbulence model is specified here, namely the Cebeci-Smith eddy viscosity model (see Cebeci & Smith[13]). The appropriate boundary layer structure and scalings are determined and reveal that the boundary layer is thicker than might have been anticipated. In particular it is thicker than that on a flat plate in a moving free stream (or, equivalently, that on a flat plate moving at constant speed through a fluid otherwise at rest). The boundary layer structure and the asymptotic behaviour of the flow lead onto an analytical solution for the skin friction on the surface; this is found to be in good agreement with existing

predictions and measurements. A numerical scheme is then proposed and used to determine the velocity within the turbulent boundary layer and the displacement thickness. As with skin friction, it is found that both of these quantities are in good agreement with earlier work. This healthy correlation with other authors' findings supports both our use of the Cebeci-Smith eddy viscosity and the taking of the boundary layer thickness to be relatively large.

Chapter 3 is concerned with the flow generated by a rotating disc (with constant rotation velocity) in an unbounded fluid. This problem has been studied by a range of authors, in particular Cebeci & Abbott[11] and Cooper[20]. Both these studies derived a numerical solution using a Cebeci-Smith eddy viscosity model. Symmetry about the axis of rotation allows this problem to be treated as a quasi-2D system and the same boundary layer structure as used in Chapter 2 is applied along with the Cebeci-Smith model. The use of a similarity variable then simplifies the flow problem further and leads to an analytical description of the skin friction equivalent to that of the flat plate flow considered in the previous chapter. Again this turns out to be in reasonable agreement with earlier results (both experimental and numerical). A similar numerical investigation to that in Chapter 2 is performed and yields velocity profiles in the turbulent boundary layer which are in close correlation with existing data. Predictions for the displacement thickness of the boundary layer are also possible, although these differ numerically from the work of von Karman[79] and Cooper. This may be due to the assumption of a similarity solution which necessitates a linear growth in the displacement thickness, a growth which is not noted by other authors (they tend to find that the displacement thickness grows less rapidly).

Attention is then switched to the matter of a rotating body which does not

have symmetry about its axis of rotation (non-axisymmetry) and this is examined in Chapter 4. A new boundary layer structure is required for such flows. The one used here is based on the axisymmetric turbulent boundary layer used in Chapter 3 and the work of Neish & Smith[50] for the uniform stream past a flat plate and subsequent wake. A similarity variable is then introduced and the problem is thereby reduced to a quasi-2D flow. An important parameter which arises here and in subsequent chapters is the disc (or surface) solidity. This is defined as the ratio of the total surface area of the body to the total area of the surface and wakes. With this definition a rotating disc has unit solidity. Velocity profiles are derived for a region of the boundary layer where exact details of the rotating body are not required (only specification of the disc solidity is necessary). Those parts of the boundary layer which are dependent on the precise nature of the non-axisymmetric surface are considered in the next chapter when a particular body-type is used.

Chapter 5 then examines the flow generated by a rotating cut-disc, focussing particularly on the main region (a sublayer) of the boundary layer to have azimuthal dependence. The velocity in this area is determined for a variety of cut-disc configurations, although for ease of analysis only ones with evenly spaced identical blades are considered here. The problem is then extended to incorporate blade inclination by assuming that each blade is inclined at a fixed angle to the horizontal. The precise details of the wake are not of concern here and instead results are produced for different values of the wake shift, which is defined as the vertical distance from the leading edge of one blade to the wake centre line of the preceding blade. This enables us to consider an important aspect of rotor blade dynamics, namely the interaction of the flow above and below the blades, without having to undertake the more

difficult problem of determining the wake shape. Finally in this chapter the limit as the disc solidity decreases to zero is dealt with, particularly to see if the flow approaches that of an isolated blade. Here analytical approximations are possible and are contrasted with the earlier numerical findings of this chapter.

Another important aspect of rotor blade flow is then considered in Chapters 6 and 7: blade shape. In Chapter 6 the cut-disc model of the previous chapter is extended to include vertically symmetric blade thickness. The Prandtl shift (or transposition) is then invoked to reduce the boundary layer to that on a cut-disc so that the results of Chapter 5 now apply here in terms of the Prandtl co-ordinates. The flow in the inviscid region outside the boundary layer is then examined so as to determine the pressure exerted on the blades. In practice this requires the solution of Laplace's equation for the pressure, subject to a boundary condition at the bottom of the inviscid region which is based on the blade shape and the boundary layer thickness. Here the latter is taken to be negligible in comparison to the blade shape and so the outer pressure problem can be divorced from the boundary layer calculations. As an illustration, a solution is derived for a highly simplified configuration and particular blade shape.

In Chapter 7 an essential aspect of helicopter dynamics is addressed: vertically asymmetric blade shape. As in the symmetric case examined in Chapter 6, the boundary layer is initially reduced to that on a cut-disc and the flow in the inviscid region is then considered. As a simplification, and encouraged by the low solidity extreme considered in Chapter 5, the flow past a succession of 2D asymmetric blades is investigated. This is an extension of the work of Smith & Timoshin[69] who studied the flow past thin multi-blade configurations. Again the boundary layer thicknesses are taken to be insignificant when com-

pared to the blade shapes. Accordingly the fluid downwash across the wakes and the pressure difference on the blades can be determined without resorting to the boundary layer part of the problem. The results of Smith & Timoshin are then used directly to derive solutions on a local and a global length scale in the limit as the surface solidity decreases to zero. These solutions show that the flow on a local scale is approximately that of an isolated blade whilst, in the case of an infinite number of identical blades, the flow is periodic on a global scale. In particular the global solution can then be used to determine a complex potential for the flow on that length scale. This is combined with an image potential to incorporate ground effect into the model on an inviscid length scale. The model yields qualitative agreement with Bramwell and Seddon as to the effect of the ground on the power required to sustain a helicopter in hover.

Ground effect is then considered in Chapter 8 on a viscous scale by examining the flow between two discs, one rotating and the other stationary. The problem here is one which has been subject to many previous investigations, largely through experiments and numerical techniques. Of these, the most relevant to the current work is that of Cooper & Reshotko[22] who considered the boundary layers on each disc and used the Cebeci-Smith model to solve for the turbulent flow in the gap between the two discs. Unfortunately Cooper & Reshotko's work is restricted to a finite radial range and hence the appropriate form of the Cebeci-Smith model to use for this flow is only defined for a limited range of values of the Reynolds number. In particular, we examine the flow at large radii where the boundary layers are deemed to have merged and where the flow can be taken to be approximately antisymmetric about the gap centre line. This leads to analytical and numerical solutions to the

velocity profiles and an analytical prediction for the skin friction. Significant differences exist between our results and those of Cooper & Reshotko although reasonable agreement does exist between our analytical work and the comparable numerical results of Cooper & Reshotko. The present work also seems to agree well with Afzal[1] for turbulent Couette flow.

Finally, in Chapter 9 the conclusions of our research are presented and summarized, and possible extensions to the current work are proposed and discussed. This includes the brief examination of an alternative occurrence of turbulent flow: 2D turbulent jets and the possible relevance of the earlier work of this thesis to this type of flow.

Chapter 2

Flat Plate with a Moving Surface

2.1 Introduction

Initially we examine the flow generated by a flat plate with a fixed leading edge, the surface of which is moving with constant velocity U through a fluid at rest. Although we consider this flow to be something of a model problem which is not directly related to the flow induced by a rotor, nonetheless the present problem is sufficiently significant to warrant investigation in its own right and in detail it turns out to have a solution structure similar in parts to the rotor case.

Flows past moving surfaces occur widely in engineering applications and the present problem is physically similar to that of the flow past a moving belt, such as a conveyor belt or any mechanism with a belt-drive, such as the fan belt in a motor. In addition to the practical applications of the flow, and the inherent value of understanding any physical problem, the flow also has relevance to the flow due to a rotating disc, which we shall examine later, as a rotating disc can also be considered to be a stationary body which is fixed

in space but has a moving surface. Thus we might anticipate that the present flow shares several features with the rotating disc flow whilst the advantage in considering the current problem is that, being essentially two-dimensional, it is much simpler to solve.

To understand this problem we consider the two-dimensional turbulent boundary layer (2DTBL). The boundary layer on a stationary flat plate with a moving surface differs from the physically similar problem of the boundary layer on a flat plate moving with a constant velocity, and the equivalent case of the boundary layer on a stationary flat plate in a uniform stream. The most obvious difference is the relative thicknesses of the two boundary layers, as is seen in this present problem and again later when we examine the problem of the rotating disc; the 2DTBL here is larger than for a flat plate moving at a constant speed through a stationary fluid. In fact the height of the 2DTBL is found to be to be $O(k_1^2)$, where k_1 is the von Karman constant, and it is assumed that k_1^2 is sufficiently small for the boundary layer equations to hold. Another advantage of the present problem is that it serves as a good test of the validity of this 'k_1^2 assumption' as there exists a variety of relevant studies with which we can compare our predictions.

The flow examined here, as illustrated in Figure 2.1, is similar to the flow on a continuous flat plate with a moving surface as studied by Afzal[2], Sakiadis[61,62] and Tsou, Sparrow & Goldstein[77]. In particular, Afzal also examined the 2DTBL. The main difference between the present problem and the work of those authors named above is that the continuous flat plate is semi-infinite and not finite as is the case for the current flow.

Our approach takes the following form. Firstly we compose the relevant governing equation for the 2DTBL - the Reynolds equation - then proceed

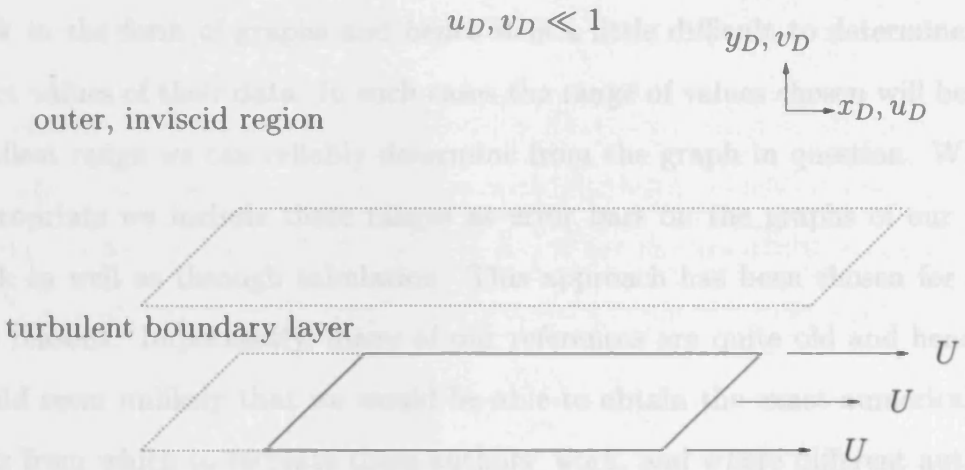

Figure 2.1: *Diagram of a flat plate with a moving surface. x_D measures distance along the plate and y_D measures distance normal to the surface. The upper dotted lines represent the edge of the boundary layer, outside of which the velocity is negligible.*

to model the boundary layer as being composed of two distinct regions, one where viscosity is negligible and one where turbulence effects are comparable to viscous effects. This is the same approach as Afzal except that we are concerned with a finite plate instead of the continuous one which Afzal examined. Further, Afzal makes no predictions for the displacement thickness. This approach is contrasted with that of Sakiadis who assumed a one-seventh power law for the velocity profile to determine predictions for, amongst others, the displacement thickness and skin friction coefficient, and Tsou et al. who combined analytical results with direct experimental data.

Throughout, comparisons are made between the results of the authors named above and our own predictions. In such comparisons we will include our own results, usually graphically, and present other author's work as lying within a range of possible values to illustrate how our predictions compare with existing work. This is because most of these authors also present their

work in the form of graphs and hence it is a little difficult to determine the exact values of their data. In such cases the range of values chosen will be the smallest range we can reliably determine from the graph in question. Where appropriate we include these ranges as error bars on the graphs of our own work as well as through tabulation. This approach has been chosen for several reasons. Importantly, many of our references are quite old and hence it would seem unlikely that we would be able to obtain the exact numerical results from which to recreate these authors' work, and where different authors have produced predictions for the same quantities, such as skin friction or the velocity profile, their results often differ from one another, albeit only within a small range of values. As such, we might also anticipate that our results too may differ, but hopefully not by much, from those of other authors; thus it is important that our results follow the same trends as previous results, and not necessarily match the exact same figures. Finally, the original results of those authors referenced are available within the references quoted.

In the present chapter the appropriate governing equation (the Reynolds equation) for this flat plate flow is derived in §2.2 before discussing a particular method of modelling turbulence, namely the Cebeci-Smith eddy viscosity (§2.3). Then the Reynolds equation is non-dimensionalized (§2.4) and a structure for the boundary layer described in §2.5. Analytical and numerical solutions to different regions of the boundary layer are produced in §2.6 and §2.7 respectively. Finally an analytical prediction for the skin friction is derived in §2.8.

2.2 The Reynolds Equation

We take the two-dimensional turbulent boundary layer on a flat surface, where x_D and y_D are Cartesian co-ordinates with y_D being normal to and x_D measuring distance along the surface. If $\overline{u}$ and $\overline{v}$ are the velocities in the x_D and y_D directions respectively then the appropriate boundary layer equation is

$$\frac{\partial \overline{u}}{\partial t} + \overline{u}\frac{\partial \overline{u}}{\partial x_D} + \overline{v}\frac{\partial \overline{u}}{\partial y_D} = \nu \frac{\partial^2 \overline{u}}{\partial y_D^2}. \tag{2.1}$$

For completeness the time-derivative is included here although the flows which are examined herein are steady and so subsequently when the Reynolds equations are used the time-derivatives are omitted. Note also that since there is negligible flow outside the boundary layer, and negligible variation in pressure across the boundary layer, the pressure is constant within the 2DTBL and can be taken to be zero without loss of generality.

Now the velocities are considered to be composed of a time-averaged mean part and a turbulent fluctuating part and so the following substitutions are introduced,

$$\overline{u} = u_D + u^*, \tag{2.2}$$

$$\overline{v} = v_D + v^*, \tag{2.3}$$

where u_D and v_D are the mean velocities and u^* and v^* are the turbulent fluctuations from the mean velocities in the x_D and y_D directions. Now if the time average over a sufficiently large time interval is taken, the equation of motion (after some rearrangement) is

$$\frac{\partial u_D}{\partial t} + u_D\frac{\partial u_D}{\partial x_D} + v_D\frac{\partial u_D}{\partial y_D} = \nu\frac{\partial^2 u_D}{\partial y_D^2} - \frac{\partial}{\partial y_D}(< u^* v^* >), \tag{2.4}$$

where $< s >$ denotes the time average of the quantity s and ν is the kinematic

viscosity of the fluid. This equation is the two-dimensional Reynolds equation and a full derivation is contained in Smith & Cebeci[66].

2.3 Eddy Viscosity

The term $< u^*v^* >$ is the Reynolds stress and is an unknown which needs to be modelled. Herein we adopt a particular model for the turbulent stress which involves the use of an eddy viscosity, as in Bush & Fendell[9]. The present approach regards the turbulent term as being similar to viscous stress and so proposes the relation

$$< u^*v^* >= -\nu_{tD}\frac{\partial u_D}{\partial y_D}, \tag{2.5}$$

where ν_{tD} is known as the eddy viscosity, which is also unknown and so needs to be modelled in some way. This is done by invoking the Cebeci-Smith model. The origins of the Cebeci-Smith model lie in the work of Prandtl, specifically Prandtl's two mixing-length hypotheses, but this is not of primary concern here since a more detailed description of the motivation for this particular choice for the eddy viscosity can be found in, amongst others, Smith & Cebeci[66], Schlichting[64] and Wilson[80]. Rather, this particular choice of eddy viscosity has been chosen as it has been used successfully in the examination of various different earlier investigations, including Neish & Smith[50] for the flow past a flat plate, Cebeci & Abbott[11] and Cooper[20] for the flow past a rotating disc, and Wilson[80] for the flow through a curved duct. The Cebeci-Smith model is also a particularly simple form for the eddy viscosity which, combined with its apparent effectiveness, makes it a suitable choice for a mathematical examination of the turbulent boundary layer.

The exact form of the Cebeci-Smith model varies between papers but the

essential features remain present. Most notable is the two-tier form that it takes. For the purposes of the current problem we use the following form:

$$\nu_{tD} = \begin{cases} k_2 U \delta_D^* & \text{for } y_D \geq y_{Dk}, \\ k_1^2 y_D^2 [1 - \exp(-\frac{y_D u_{\tau D}}{26\nu})]^2 |\frac{\partial u_D}{\partial y_D}| & \text{for } y_D \leq y_{Dk}. \end{cases} \tag{2.6}$$

Here y_{Dk} is known as the critical value of y_D and is defined[1] by

$$(k_1^2 y_D^2 [1 - \exp(-\frac{y_D u_{\tau D}}{26\nu})]^2 \frac{\partial u_D}{\partial y_D})_{y_D = y_{Dk}} = k_2 U \delta_D^* \tag{2.7}$$

where

$$\delta_D^* = \int_0^\infty \frac{u_D}{U} dy_D, \tag{2.8}$$

$$u_{\tau D} = (\frac{\tau_{WD}}{\rho})^{\frac{1}{2}}, \tag{2.9}$$

$$\tau_{WD} = \mu(\frac{\partial u_D}{\partial y_D})_{y_D = 0}, \tag{2.10}$$

which are the dimensional displacement thickness, friction velocity and shear stress on the plate respectively. Also, k_1 and k_2 are constants and μ, ρ and ν are the viscosity, density and kinematic viscosity of the fluid respectively. For the purposes of this study it is assumed that $y_{Dk} = O(k_1^2)$.

2.4 Problem Formulation

As discussed previously the relevant equation of motion is the two-dimensional Reynolds equation taken with the Cebeci-Smith eddy viscosity model; thus

$$u_D \frac{\partial u_D}{\partial x_D} + v_D \frac{\partial u_D}{\partial y_D} = \nu \frac{\partial^2 u_D}{\partial {y_D}^2} + \frac{\partial}{\partial y_D} \begin{cases} k_2 U \delta_D^* \frac{\partial u_D}{\partial y_D} & \text{for } y_D \geq y_{Dk} \\ k_1^2 y_D^2 [1 - \exp(-\frac{y_D u_{\tau D}}{26\nu})]^2 |\frac{\partial u_D}{\partial y_D}| \frac{\partial u_D}{\partial y_D} & \text{for } y_D \leq y_{Dk} \end{cases} \tag{2.11}$$

with continuity equation

$$\frac{\partial u_D}{\partial x_D} + \frac{\partial v_D}{\partial y_D} = 0, \tag{2.12}$$

1. It is assumed that y_{D_c} exists and is unique.

and the unknown junction position y_{Dk} determined by continuity of eddy viscosity at the junction. The constants k_1 and k_2 are 0.4 and 0.0168 respectively and the boundary conditions for this system are $u_D = U$ at $y_D = 0$ and $u_D \rightarrow 0$ as $y_D \rightarrow \infty$. Since $u_D = U$ on the plate but is zero outside the boundary layer we will assume that u_D decays monotonically and hence $|\frac{\partial u_D}{\partial y_D}| = -\frac{\partial u_D}{\partial y_D}$. Taking $u_D = Uu, v_D = k_1^2 Uv, x_D = lx$ and $y_D = k_1^2 ly$, where l is the plate length we have the following non-dimensional form of the problem,

$$u\frac{\partial u}{\partial x} + v\frac{\partial u}{\partial y} = \frac{1}{R}\frac{\partial^2 u}{\partial y^2} + \frac{\partial}{\partial y}\begin{cases} k_3\delta^*\frac{\partial u}{\partial y} & \text{for } y \geq y_k \\ -y^2[1-\exp(-\frac{yRu_\tau}{26})]^2(\frac{\partial u}{\partial y})^2 & \text{for } y \leq y_k \end{cases} \tag{2.13}$$

and

$$\frac{\partial u}{\partial x} + \frac{\partial v}{\partial y} = 0 \tag{2.14}$$

where

$$R = \frac{k_1^4 Ul}{\nu} = k_1^4 Re, \tag{2.15}$$

$$Re = \frac{Ul}{\nu}, \tag{2.16}$$

$$u_{\tau D} = (\frac{\tau_{WD}}{\rho})^{\frac{1}{2}} = k_1^2 U u_\tau, \tag{2.17}$$

$$\tau_{WD} = \mu(\frac{\partial u_D}{\partial y_D})_{y_D=0}, \tag{2.18}$$

$$\delta^* = \int_0^\infty u dy, \tag{2.19}$$

$$k_3 = \frac{k_2}{k_1^2} = 0.105, \tag{2.20}$$

with the boundary conditions

$$u(0) = 1, \tag{2.21}$$

$$u(\infty) = 0, \tag{2.22}$$

$$\frac{\partial u}{\partial y}|_{y=y_k} = -k_3\delta^*. \tag{2.23}$$

In the condition of continuity of eddy viscosity at y_k, (2.23), we have omitted the exponential term in the lower tier of (2.13) since we shall take the junction position y_k to be O(1), so that with $R \gg 1$ the exponential term is negligible. Note also that the non-dimensionalization above absorbs the factor k_1^2 for convenience and it also confirms that the ratio of the y_D-scale to the x_D-scale is proportional to k_1^2 which is taken to be small. This corresponds to the notion which is described subsequently that the height of the boundary layer is $O(k_1^2)$.

2.5 Boundary Layer Structure

Since we are interested in the boundary layer on a flat plate the flow is taken to be composed of a thin boundary layer attached to the surface of the plate and a larger inviscid region where there is negligible variation from the free stream if one is present. Thus for the purposes of this problem we are only interested in the 2DTBL which is taken to consist of two coupled layers. This model has the same two layer structure as that of Bush & Fendell[9] and Mellor[46] who describe the 2DTBL in terms of an outer defect layer and a thinner, inner wall layer but now the outer layer is nonlinear and not linear as in both Bush & Fendell and Mellor. The important physical properties of these two layers are that in the defect layer the velocity differs from the free stream (which is zero here) only by a small perturbation and that this layer is characterized by a balance between the inertial and turbulent terms, whilst in the wall layer we have a balance between the viscous and turbulent stresses, and the velocity is given by the velocity of the surface (non-zero in this case) plus a small perturbation which we take to be of the same order as that in the defect layer.

For this particular problem such a description of the turbulent boundary

layer is sufficient for our purposes, but a more complicated structure is needed in Chapters 4 and 5 in order to understand the three-dimensional turbulent boundary layer (3DTBL) on a [illegible] rotor [illegible]. The issue of the appropriate boundary layer structure for other flows is addressed later but for now it can be assumed that the 2DTBL has the two-layer structure outlined above - a small inner layer where viscous stresses are important and a large inertial-turbulent balance layer. In reality there exists a thin transitional layer sharing the characteristics of these two main parts of the boundary layer and which exists between them. We regard this layer as an overlap region where the asymptotic expansions for the two main layers, which are derive herein, are matched to each other using logarithmic matching. This approach has been used by many authors previously, notably by Mellor and Bush & Fendell, but also by Afzal and Neish & Smith, which are of particular interest with regard to the present flow on a flat plate.

We now note that the turbulent boundary layer is taken to have height $O(k_1^2)$, where k_1 is the von Karman constant, as illustrated in Figure 2.2. This is necessary to ensure the balance of inertial and turbulent terms in the outer layer which we shall see later. Also, we call the outer defect layer and the inner wall layer, the inertial-turbulent layer and the laminar sublayer respectively, to stress the importance of the inertial terms in the outer layer and also to later allow for wakes as well as boundary layers. The particular inertial-turbulent layer and laminar sublayer for this flow are taken to have heights of $O(1)$ and $O(\epsilon^{-1}R^{-1})$[1] respectively, relative to the non-dimensional height y, and we proceed by examining each of the two layers separately, determining the relevant governing equations and solution structure, then matching the asymptotic forms of the solution to produce a coupled system. This coupled

1. ϵ here is defined as: $\epsilon = (\ln R)^{-1}$

problem is calculated numerically by solving for the inertial-turbulent layer only, then using our results to establish predictions for the skin friction, velocity profiles and displacement thickness.

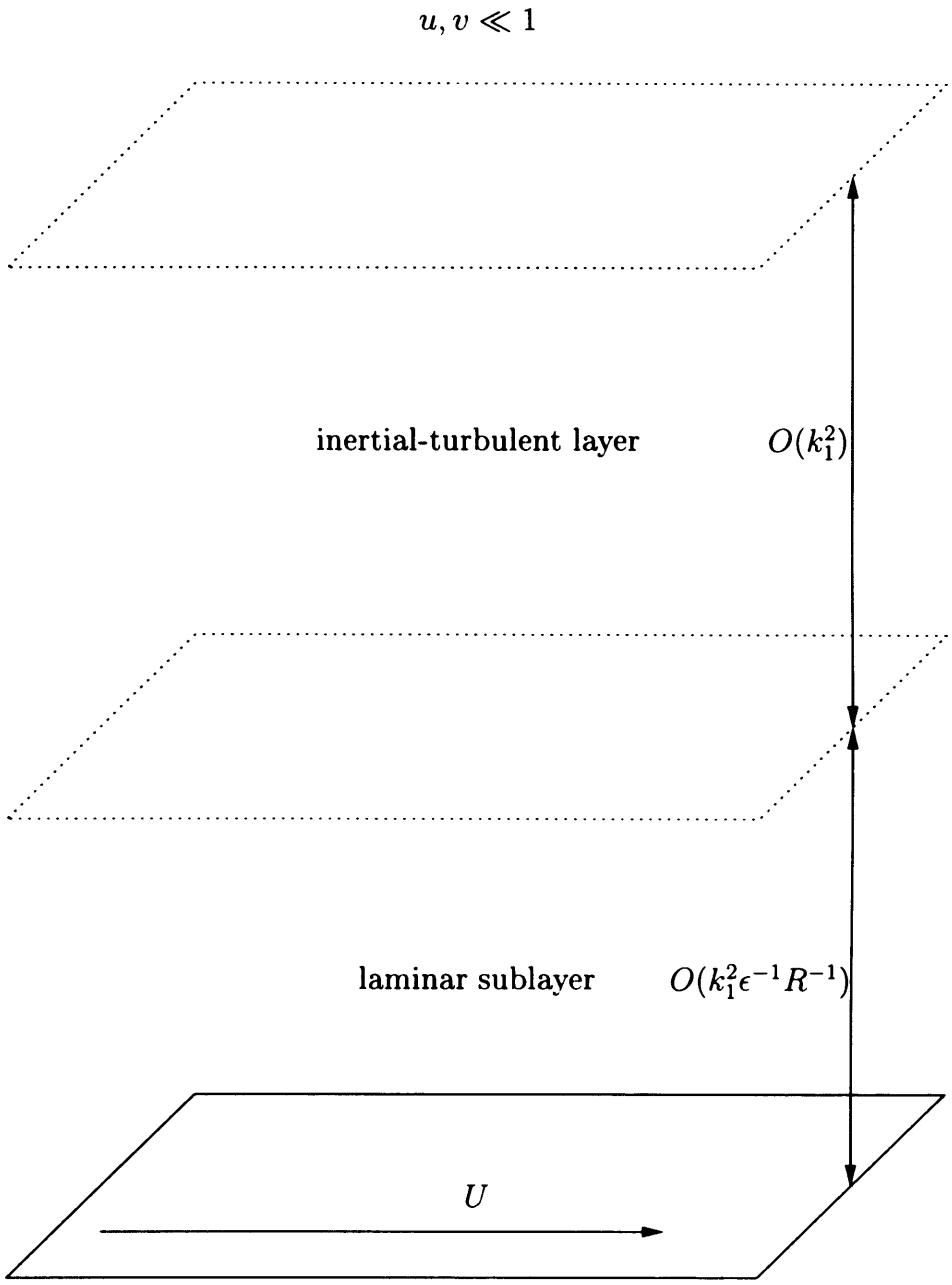

Figure 2.2: *Diagram of the turbulent boundary layer on a flat plate with a moving surface. Note that for clarity we have drawn the two layers as comparable in height, whereas in truth the inertial-turbulent layer comprises almost all of the total boundary layer. The height scales are given relative to the (dimensional) height* y_D.

2.5.1 Inertial-Turbulent Layer

In the inertial-turbulent layer (ITL) we have $x = O(1)$ and since we guess that the velocity here is the same as the free stream (zero here) plus a small perturbation, $u = O(\epsilon)$ where $\epsilon = (\ln R)^{-1}$, as in Neish & Smith[50]. In this problem the ITL must be taken to be considerably thicker than might be expected for the following reason.

Supposing that, as in Neish & Smith, the boundary layer height is also $O(\epsilon)$ and hence $v = O(\epsilon^2)$. Examining the limit as $R = \frac{k_1^4 U l}{\nu} \to \infty$ leads to

$$0 = \frac{\partial}{\partial y_1} \begin{cases} k_3 \delta_1^* \frac{\partial u_1}{\partial y_1} & \text{for } y_1 \geq y_{1k} \\ -{y_1}^2 [1 - \exp(-\frac{y_1 \epsilon R u_\tau}{26})]^2 (\frac{\partial u_1}{\partial y_1})^2 & \text{for } y_1 \leq y_{1k} \end{cases} \tag{2.24}$$

where

$$u = \epsilon u_1 + ..., \tag{2.25}$$

$$v = \epsilon^2 v_1 + ..., \tag{2.26}$$

$$y = \epsilon y_1 + ..., \tag{2.27}$$

and the scaling of the normal velocity is determined by the continuity equation which implies that $v = O(uy)$. However, this choice of scaling leaves no terms to balance the turbulent stresses. Thus we could just have the following solution for u_1,

$$u_1 = \alpha y_1 + \beta \tag{2.28}$$

for $y_1 \geq y_{1k}$ and for some constants α and β, and

$$u_1 = \gamma + \delta \ln y_1 \tag{2.29}$$

for $y_1 \leq y_{1k}$ ignoring the exponential term in (2.24), with constants γ and δ. This solution is incorrect as it does not satisfy the boundary condition

that $u_1 \to 0$ as $y_1 \to \infty$, unless $\alpha = \beta = 0$ and hence $u_1 = 0$; but this solution then means we cannot have continuity of $\frac{\partial u_1}{\partial y_1}$, and hence stress, at the junction position, unless $\gamma = \delta = 0$ also. This then means that there is a zero flow in the ITL, which cannot match with the $O(1)$ velocity required in the laminar sublayer (see below). Thus the following scalings for the ITL are instead proposed

$$u = \epsilon u_1 + ..., \tag{2.30}$$

$$v = \epsilon v_1 + ..., \tag{2.31}$$

$$y = y_1 + ..., \tag{2.32}$$

which lead to the following equations for the ITL,

$$\epsilon^2 u_1 \frac{\partial u_1}{\partial x} + \epsilon^2 v_1 \frac{\partial u_1}{\partial y_1} = \frac{\epsilon}{R} \frac{\partial^2 u_1}{\partial y_1^2} + \epsilon^2 \frac{\partial}{\partial y_1}(\nu_t \frac{\partial u_1}{\partial y_1}) \tag{2.33}$$

and

$$\frac{\partial u_1}{\partial x} + \frac{\partial v_1}{\partial y_1} = 0. \tag{2.34}$$

Since $R \gg 1$, in the ITL the viscous term $\frac{\partial^2 u_1}{\partial y_1^2}$ can be neglected and we are left with the nonlinear system

$$u_1 \frac{\partial u_1}{\partial x} + v_1 \frac{\partial u_1}{\partial y_1} = \frac{\partial}{\partial y_1}(\nu_{t1} \frac{\partial u_1}{\partial y_1}). \tag{2.35}$$

Also now

$$\nu_{t1} = \begin{cases} k_3 \delta_1^* & \text{for } y_1 \geq y_{1k} \\ -y_1^2 [1 - \exp(-\frac{y_1 R u_\tau}{26})]^2 \frac{\partial u_1}{\partial y_1} & \text{for } y_1 \leq y_{1k} \end{cases} \tag{2.36}$$

where

$$\delta_1^* = \int_0^\infty u_1 dy_1. \tag{2.37}$$

This is similar to the system which Afzal has for his outer wake layer with nonlinear inertial terms and negligible viscosity. In fact, Afzal's governing

equation for the outer wake layer reduces to a form equivalent to the equation which is subsequently derived for the ITL if only the upper tier of the Cebeci-Smith model is used. To solve (2.35) and (2.36) we try the similarity solution

$$u_1 = x^m f'(\frac{y_1}{x^n}), \tag{2.38}$$

which, from the continuity equation and defining $f(0) = 0$, leads to the following form for the normal velocity v_1,

$$v_1 = x^{m+n-1}(nzf' - (m+n)f) \tag{2.39}$$

where $z = \frac{y_1}{x^n}$. Subsequently (2.35) and (2.36) become

$$x^{2m-1}(mf'^2 - (m+n)ff'') = x^{2m-n}\frac{\partial}{\partial z}\begin{cases} k_3 f_\infty f'' & \text{for } z \geq z_k, \\ -z^2 f''^2 & \text{for } z \leq z_k, \end{cases} \tag{2.40}$$

where $'$ denotes differentiation with respect to z. The exponential term in the lower form of the eddy viscosity is negligibly small and so has been omitted.

By comparison of both sides, and to balance the momentum and Reynolds terms, as is characteristic of the ITL, $n = 1$ is taken, while from consideration of the necessary matching with the laminar sublayer which follows later, $m = 0$. Thus the governing equation for the ITL is now the nonlinear ordinary differential equation

$$-ff'' = \frac{\partial}{\partial z}\begin{cases} k_3 f_\infty f'' & \text{for } z \geq z_k, \\ -z^2 f''^2 & \text{for } z \leq z_k, \end{cases} \tag{2.41}$$

with

$$f(0) = 0, \tag{2.42}$$

$$f'(0) = 1, \tag{2.43}$$

$$f'(\infty) = 0, \tag{2.44}$$

while the non-dimensional normal velocity is now given by

$$v_1 = zf' - f. \tag{2.45}$$

Now we have the junction position z_k constant as (2.35) is reduced to a first-order equation. This implies that the actual junction position y_k is proportional to x. Finally we note that in his outer wake layer Afzal has

$$h''' + hh'' = 0 \tag{2.46}$$

subject to

$$h(0) = 0, \tag{2.47}$$

$$h'(0) = 1, \tag{2.48}$$

$$h'(\infty) = 0, \tag{2.49}$$

which is equivalent to the upper form of our system.

2.5.2 Laminar Sublayer and Matching

In the laminar sublayer (LS) we again have $x = O(1)$ and in order to match with the perturbation in the ITL we take the perturbation of u from the unit velocity of the moving surface to be $O(\epsilon)$ also. Since in this layer a balance between the laminar and turbulent terms is expected, this dictates that $y = O(\epsilon^{-1}R^{-1})$, as in Neish & Smith, so that

$$u = 1 + \epsilon u_2 + ..., \tag{2.50}$$

$$v = R^{-1}v_2 + ..., \tag{2.51}$$

$$y = \epsilon^{-1}R^{-1}y_2 + ..., \tag{2.52}$$

where y_2, u_2 and v_2 are $O(1)$. Substituting these into (2.13) obtains

$$\epsilon\frac{\partial u_2}{\partial x} + \epsilon^2 u_2\frac{\partial u_2}{\partial x} + \epsilon^2 v_2\frac{\partial u_2}{\partial y_2} \tag{2.53}$$
$$= \epsilon^3 R\frac{\partial^2 u_2}{\partial {y_2}^2} - \epsilon^3 R\frac{\partial}{\partial y_2}(y_2^2[1-\exp(-\frac{y_2 u_\tau}{26\epsilon})]^2(\frac{\partial u_2}{\partial y_2})^2).$$

Thus in the LS the inertial terms can be neglected and there is the linear system

$$\frac{\partial^2 u_2}{\partial {y_2}^2} - \frac{\partial}{\partial y_2}(y_2^2[1-\exp(-\frac{y_2 u_\tau}{26\epsilon})]^2(\frac{\partial u_2}{\partial y_2})^2) = 0. \tag{2.54}$$

Integrating (2.54):

$$\frac{\partial u_2}{\partial y_2} - y_2^2[1-\exp(-\frac{y_2 u_\tau}{26\epsilon})]^2(\frac{\partial u_2}{\partial y_2})^2 = -C_1^2, \tag{2.55}$$

where C_1 is a constant suggesting that $u_2 \sim C_1 \ln y_2$ as $y_2 \to \infty$. We now have the solutions, in structured form, to the present flow in the two main regions of the boundary layer and these now need to be matched where the regions merge. This is done by means of a logarithmic matching procedure.

We need

$$1 + \epsilon u_2(x, y_2 \to \infty) = \epsilon x^m f'(z \to 0). \tag{2.56}$$

Seeking logarithmic behaviour in this matching region, as implied by (2.55), the following asymptotes are assumed

$$u_2(x, y_2 \to \infty) = \overline{u}(x, y_2)\ln y_2, \tag{2.57}$$
$$f'(z \to 0) = \overline{f}(z)\ln z, \tag{2.58}$$

which when matched imply

$$1 + \epsilon\overline{u}(x, y_2)\ln y_2 = \epsilon x^m \overline{f}(z)\ln z, \tag{2.59}$$

as $y_2 \to \infty$ and $z \to 0$. Here we are taking $u_1 = x^m f'(z)$ where m is no longer necessarily zero as stated previously. Thus,

$$1 + \epsilon\overline{u}(x, y_2)(\ln y + \ln R + \ln\epsilon) = \epsilon x^m \overline{f}(z)(\ln y - \ln x). \tag{2.60}$$

Remembering that $\epsilon = (\ln R)^{-1}$ and that as $z \ll 1$ we have $y \ll x$, we can take $|\ln y| \gg |\ln x|$ and neglect the term in $\ln x$ as being relatively small. Thus it is found that $\overline{u} = -1, \overline{f} = -1$ and $m = 0$ as assumed earlier. This shows that $C_1 = -1$. Hence, as $y_1 \to \infty$,

$$u = 1 + \epsilon u_2 \sim 1 - \epsilon \ln y_2 \tag{2.61}$$

while as $z \to 0$,

$$u = \epsilon f'(z) \sim -\epsilon \ln z. \tag{2.62}$$

Therefore in the ITL the solution is

$$\begin{aligned} u &= \epsilon u_1, && (2.63)\\ u_1 &= f'(z), && (2.64)\\ z &= \frac{y}{x}, && (2.65)\\ u_1(z \to 0) &\sim -\ln z, && (2.66) \end{aligned}$$

and for the LS

$$\begin{aligned} u &= 1 + \epsilon u_2(x, y_2), && (2.67)\\ y_2 &= R\epsilon y, && (2.68)\\ u(x, y_2 \to \infty) &\sim 1 - \epsilon \ln y_2. && (2.69) \end{aligned}$$

Although we have only considered the logarithmic behaviour of the asymptotes, more completely we have

$$\begin{aligned} f'(z) &\sim c_1 - \ln z && (2.70)\\ u_2(x, y_2) &\sim c_2 - \ln y_2 && (2.71) \end{aligned}$$

as $z \to 0$ and $y_2 \to \infty$ respectively, where c_1 and c_2 are constants. We might anticipate that the matching of these additional constant terms would lead to

$c_1 = c_2$ but this is not necessarily true. In the same way that logarithmic behaviour of order ϵ balances an $O(1)$ constant, $O(\epsilon^2)$ logarithmic terms in each region can match with a non-zero difference in the first-order constant terms $c_1 - c_2$. Hence we proceed assuming that c_1 and c_2 are not necessarily equal. The present problem is now in a form suitable for solution, which we shall construct in two parts - first a (mainly) analytical solution for the laminar sublayer, then a numerical solution for the inertial-turbulent layer.

2.6 Analytical Solution in the Laminar Sublayer

In the LS

$$\frac{\partial u_2}{\partial y_2} - y_2^2[1 - \exp(-\frac{y_2 u_\tau}{26\epsilon})]^2(\frac{\partial u_2}{\partial y_2})^2 = -1, \tag{2.72}$$

which can be rearranged to

$$\alpha_2^2(y_2) - F(y_2)\alpha_2(y_2) - F(y_2) = 0. \tag{2.73}$$

Here

$$\alpha_2(y_2) = \frac{\partial u_2}{\partial y_2}, \tag{2.74}$$

$$F(y_2) = y_2^{-2}[1 - \exp(-\frac{y_2 u_\tau}{26\epsilon})]^{-2}, \tag{2.75}$$

and $u_\tau = \frac{\epsilon}{k_1}$, the proof of which follows later. The above leads to the following solution for α_2,

$$\alpha_2 = \frac{1}{2}(F - \sqrt{(F^2 + 4F)}) \tag{2.76}$$

where the sign of the square root is chosen to satisfy the condition $\alpha_2(0) = -1$. This condition comes from letting $y_2 \to 0$ in (2.72). Thus we can determine α_2 and hence $\frac{\partial u_2}{\partial y_2}$ analytically but to calculate u_2 we now choose to integrate (2.76) numerically. For this we use a Runge-Kutta-Fehlberg (RKF)

algorithm, similar to the RKF algorithm presented in Appendix *A*. Hence, with $u_2(0) = 0$, we obtain the solution illustrated in Figure 2.3, along with a plot of $\ln y_2$ for comparison. The solution suggests the asymptotic form,

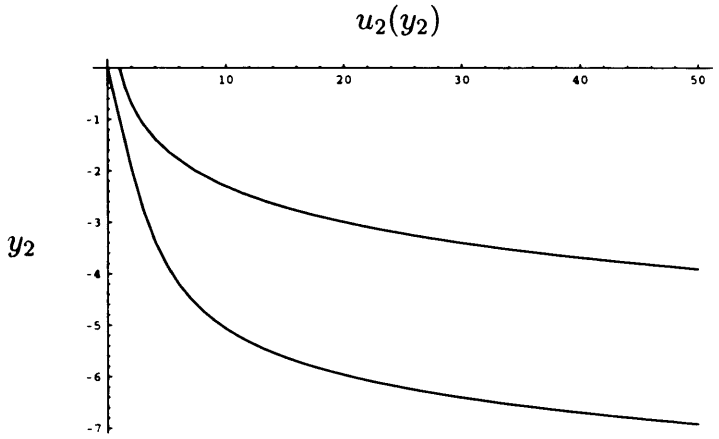

Figure 2.3: *Lower curve: Analytical solution for* $u_2(y_2)$ *in the laminar sublayer. Upper curve: Plot of* $\ln y_2$.

$$u_2 \rightarrow -\ln y_2 - 3.001 \tag{2.77}$$

as $y_2 \rightarrow \infty$, where the constant term in the asymptote comes from examining the numerical solution for u_2 at large values of y_2.

In a similar vein, Afzal proposes the following asymptotic form,

$$\frac{u_D}{U} \rightarrow 1 - \epsilon k_1 B - \epsilon \ln y_+, \tag{2.78}$$

where $y_2 = k_1 y_+$ and B is approximately five. Taking $B = 5$, in our terminology (2.78) equates to

$$u_2 \rightarrow -\ln y_2 - 2.9, \tag{2.79}$$

although it should be pointed out that Afzal actually uses $k_1 = 0.41$, instead of $k_1 = 0.4$ as we have, but to one decimal place this does not affect the value of the constant in the asymptotic form.

2.7 Numerical Solution in the Inertial-Turbulent Layer

Since we are unable to progress any further through analytical means, a numerical solution is now tried. Here consideration is limited to the ITL, as the ITL constitutes most of the boundary layer, and so we can consider the LS to be negligible for this purpose. Hence we seek a numerical solution to the governing equation for the ITL, which from §2.5.1 is

$$-ff'' = \frac{\partial}{\partial z}\begin{cases} k_3 f_\infty f'' & \text{for } z \geq z_k, \\ -z^2 f''^2 & \text{for } z \leq z_k. \end{cases} \tag{2.80}$$

A solution is attempted using a shooting method, specifically a Runge-Kutta-Fehlberg algorithm, where the scheme used shoots downward, in a manner which is explained in more detail later. For convenience the substitutions $z = z_k t$ and $f(z) = f_\infty F(t)$ are introduced into (2.80), which then becomes

$$-z_k FF'' = \frac{\partial}{\partial t}\begin{cases} k_3 F'' & \text{for } t \geq 1, \\ -t^2 F''^2 & \text{for } t \leq 1, \end{cases} \tag{2.81}$$

with the conditions

$$F(0) = 0, \tag{2.82}$$

$$F''(1) = -k_3, \tag{2.83}$$

$$F(\infty) = 1, \tag{2.84}$$

$$F'(\infty) = 0, \tag{2.85}$$

and

$$F'(t) \to C_2 - \frac{z_k}{f_\infty} \ln(z_k t), \tag{2.86}$$

as $t \to 0$. As can be seen, the substitution for f has the advantage of yielding an extra boundary condition at infinity, at the expense of one at $t = 0$. This

means that we have one less unknown condition at infinity on which to iterate as part of the solution. The transformation $z = z_k t$ is convenient in that it fixes the junction position at $t = 1$, although this does not lead to fewer variables to iterate on: the junction position now reappears as a parameter within the equation. Instead, the main motivation for the substitution is to determine z_k accurately. Since a Runge-Kutta-Fehlberg (RKF) algorithm is being employed, the height is discretized and thus z_k can only be determined approximately. To produce an accurate value of z_k then requires the use of a very small step length, which would obviously impact on the running time and efficiency of our method and the earlier substitution allows us to determine z_k in a far more efficient manner, as is seen later.

In keeping with the nature of the RKF algorithm being used (2.81) is restated as the following three first-order equations by introducing $a = F, b = F'$ and $c = F''$:

$$\frac{da}{dt} = b, \tag{2.87}$$

$$\frac{db}{dt} = c, \tag{2.88}$$

$$\frac{dc}{dt} = \frac{(Ja - tc)}{t^2}, \tag{2.89}$$

with the relevant boundary conditions, from (2.82) and (2.86),

$$a(t_0) = 0, \tag{2.90}$$

$$b(t_0) = -\frac{z_k}{f_\infty} \ln t_0 z_k + C_2, \tag{2.91}$$

$$c(t_0) = -\frac{z_k}{f_\infty t_0}, \tag{2.92}$$

for the range $t_0 \leq t \leq 1$, with $t_0 \ll 1$ and with $J = \frac{z_k}{2}$. In addition

$$\frac{da}{dt} = b, \tag{2.93}$$

$$\frac{db}{dt} = c, \tag{2.94}$$

$$\frac{dc}{dt} = -Kac, \tag{2.95}$$

with the relevant boundary conditions

$$a(\infty) = 1, \tag{2.96}$$

$$b(\infty) = 0, \tag{2.97}$$

$$c(\infty) = c_\infty, \tag{2.98}$$

for the range $t \geq 1$, with $K = \frac{z_k}{k_3}$ and c_∞ to be determined numerically. We also require continuity of a, b and c at $t = 1$, as well as

$$k_3 = -c(1) \tag{2.99}$$

which represents continuity of the eddy viscosity at $z = z_k$. Both of the above sets of equations are now in a form suitable for solution by means of an RKF algorithm, the details of which are included in Appendix A.

Whilst the problem can be separated into two halves corresponding to $0 \leq t \leq 1$ and $1 \leq t < \infty$, there are insufficient boundary conditions for each half to be solved independently. The problem is solved by finding a solution to each half such that each solution gives the same result at the junction $t = 1$. Hence the RKF algorithm is first applied to (2.93) - (2.98), corresponding to $t \geq 1$. The algorithm is then run from infinity to $t = 1$, using the conditions at infinity (for practical purposes it is obviously necessary for a finite number t_∞ to be used instead of infinity) as the initial conditions and varying the parameters K and c_∞, until the condition

$$k_3 = -c(1) \tag{2.100}$$

is satisfied to within an acceptable level of accuracy. In this case we stop the iteration when

$$|k_3 + c(1)| < 10^{-6}. \tag{2.101}$$

This approach generates a set of values at $t = 1$ which are dependent on the choice of K and c_∞ and these values are then used as the initial conditions for (2.87) - (2.92), corresponding to $t \leq 1$. The algorithm is then run on these equations to calculate the values of a, b and c at the plate. The whole process is repeated until a pair of values for K and c_∞ are found which give $a(0) = 0$ (in practice we solve for $|a(0)| < 10^{-5}$) and $c(1) = -k_3$. Once we have determined K we can calculate z_k through the simple relation $K = \frac{z_k}{k_3}$ and then use the values generated by the algorithm for $b(t_0)$ and $c(t_0)$ to work out the values of f_∞ and C_2, from (2.91) and (2.92) for some value $t_0 \ll 1$. With this approach, the accuracy with which we can determine z_k is controlled not by our step length but by the accuracy to which we can determine the parameter K. Since we calculate K using an iterative procedure, specifically a Newton iteration, we can easily determine K and hence z_k to a high degree of accuracy.

The numerical method employed here is both fast and reliable and produces the solutions for different values of t_∞, t_0 and step length d illustrated in Figure 2.4. The figure shows that the choice of step length, once sufficiently small to be accurate, and t_∞, once sufficiently large, appear to have no appreciable effect on the outcome of the algorithm, so from now on the step length is taken to be $d = 10^{-3}$ and $t_\infty = 30$.

Taking the solution described above we then calculate the unknown parameters for differing values of t_0. Table 2.1 illustrates the fact that when t_0 is sufficiently small the solution is approximately unchanged by taking different values of t_∞, t_0 and d. Taking $f_\infty = 0.469$ and $C_2 = -0.08$ we therefore have

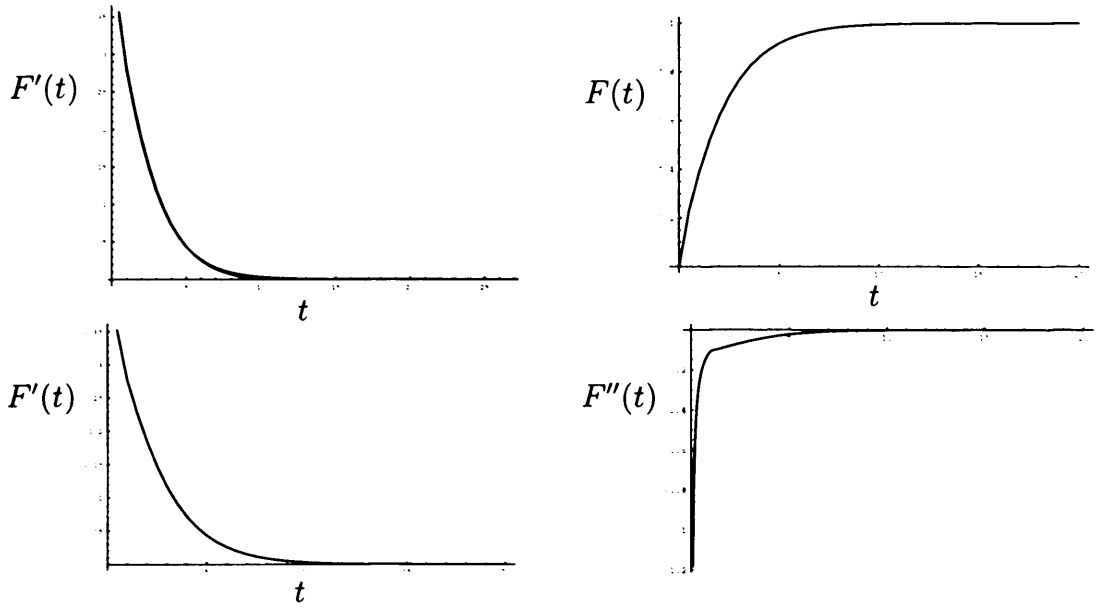

Figure 2.4: *Left top: Numerical results for* $F'(t)$ *with* $t_\infty = 30$, 20 *and* 10. *Right top: Numerical results for* $F(t)$ *with step length* $d = -10^{-3}$, -10^{-4} *and* -10^{-5}. *Left bottom: Numerical results for* $F'(t)$ *with step length* $d = -10^{-3}$, -10^{-4} *and* -10^{-5}. *Right bottom: Numerical results for* $F''(t)$ *with step length* $d = -10^{-3}$, -10^{-4} *and* -10^{-5}. *In all cases the horizontal axis measures the height* t *and at* $t = 1$ *(corresponding to the junction position of the Cebeci-Smith eddy viscosity) a change in the behaviour of the numerical results is apparent.*

the following asymptotic form for F',

$$F' \to -0.08 - 0.119 \ln (0.0559t) \tag{2.102}$$

as $t \to 0$.

t_∞	t_0	d	z_k	f_∞	C_2
10	0.001	−0.001	0.05309	0.4483	−0.082
20	0.001	−0.001	0.05584	0.4692	−0.083
30	0.001	−0.001	0.05586	0.4693	−0.077
20	0.0001	−0.0001	0.05584	0.4690	−0.083
20	0.00001	−0.00001	0.05584	0.4690	−0.083
20	0.001	−0.0001	0.05584	0.4692	−0.083
20	0.001	−0.00001	0.05584	0.4692	−0.083

Table 2.1: *Value of Flow Parameters for Varying Values of* t_∞, t_0 *and* d.

2.7.1 An Alternative Formulation for Flat Plate Flow

In order to validate the numerical method described (and hence the results subsequently presented) we now wish to compare our work with that of other authors. In particular we will compare our results with those of Afzal, Sakiadis and Tsou et al. for a continuous flat plate with a moving surface (since it is supposed that at any point on the plate the flow is only affected by upstream influences and so at any point the velocity profile, say, should be the same regardless of whether the plate is finite or semi-infinite).

For such comparisons to be made one slight difficulty has to be overcome. Afzal, Sakiadis and Tsou et al. examined continuous surfaces and so were not able to non-dimensionalize their length scales against the plate length (leading to the Reynolds number $Re = \frac{Ul}{\nu}$) as we have. Instead they introduced a similarity-type solution immediately (leading to the Reynolds number $R_x = \frac{Ux_D}{\nu}$). Hence the results produced here are given in terms of Re whilst the work of those authors with which we seek to compare is given in terms of R_x. Fortunately these two Reynolds numbers can, in some senses, be treated as equivalent. Indeed, if a similarity solution of the type $z = \frac{y_D}{x_D}$ is introduced initially (i.e. before the Reynolds equations are non-dimensionalized in §2.4)

then the resultant system of equations would be identical, except that they would be given in terms of R_x rather than Re.

Hence, all the results shown here can be reproduced identically using R_x and so a direct comparison with Afzal, Sakiadis and Tsou et al. is then possible. Moreover, since in all our results Re only appears implicitly through the presence of factors of ϵ and

$$\frac{R_x}{Re} = O(1) \tag{2.103}$$

then $\ln R_x \approx \ln Re$ as Re (and hence R_x) $\rightarrow \infty$. Thus instead of reworking our results in terms of R_x, we are simply able to equate the two different choices of Reynolds numbers when making comparisons with other authors.

Since the authors with which we compare our results all use R_x, and as some significance has been placed on being able to make such comparisons, it is reasonable to wonder why we have chosen to non-dimensionalize this problem with respect to the plate length and not just introduce a similarity-type solution immediately. The reason for this is two-fold.

First, when examining finite surfaces, it is 'natural' to non-dimensionalize with respect to the surface length and indeed this was how the problem was initially solved. It would of course have been easy simply to present the alternative formulation outlined above instead of our initial approach but then the reader may reasonably ask why did we not non-dimensionalize with respect to the plate length since it is, to some extent, the obvious thing to do?

Second, and most importantly, the formulation used here allows us to pose the current problem in precisely the same terms as Neish & Smith for the flow of a uniform stream past a stationary flat plate. In particular the parameter ϵ is defined in precisely the same way in both contexts (i.e. based on the Reynolds number $Re = \frac{Ul}{\nu}$). Crucially this removes any possible ambiguity

when discussing the boundary layer thickness here and that determined by Neish & Smith (so when we say that an $O(\epsilon)$ boundary layer thickness is not suitable for the current problem, yet does hold for the flow considered by Neish & Smith, the fact that the parameter ϵ is the same in both cases highlights the point that the two boundary layer thicknesses are not the same). This is important as the enhanced boundary layer thickness invoked here is a significant finding of this chapter.

Having shown the equivalence of the two formulations we now proceed to compare our results with existing research.

2.7.2 Velocity Profiles

It is now possible to convert the earlier numerical results into the actual non-dimensional velocity profile for the boundary layer. Initially though, a comparison is made between our results and those of other authors. Afzal[2] and Tsou et al[77] plot values of $\frac{U-u_D}{u_{\tau D}}$ against $\frac{y_D u_{\tau D}}{\nu}$ to verify the 'law of the wall' for the behaviour of the velocity near the plate, so now we calculate $\frac{U-u_D}{u_{\tau D}}$ at varying values of $\frac{y_D u_{\tau D}}{\nu}$ first noting that

$$\frac{U-u_D}{u_{\tau D}} = \frac{1-\frac{\epsilon f_\infty F'(t)}{z_k}}{k_1 \epsilon} \tag{2.104}$$

and

$$\frac{y_D u_{\tau D}}{\nu} = k_1^3 \epsilon R_x z_k t, \tag{2.105}$$

where $R_x = xRe = \frac{U x_D}{\nu}$. Taking Re and $R_x = 600,000$ the above quantities are calculated at varying heights t and our predictions for $\frac{U-u_D}{u_{\tau D}}$ compared with those of Tsou. The choice of $R_x = 600,000$ is made as Tsou used this particular value whilst the choice $Re = 600,000$ follows from §2.7.1 where we

showed that these two Reynolds numbers can in some sense be taken to be equivalent.

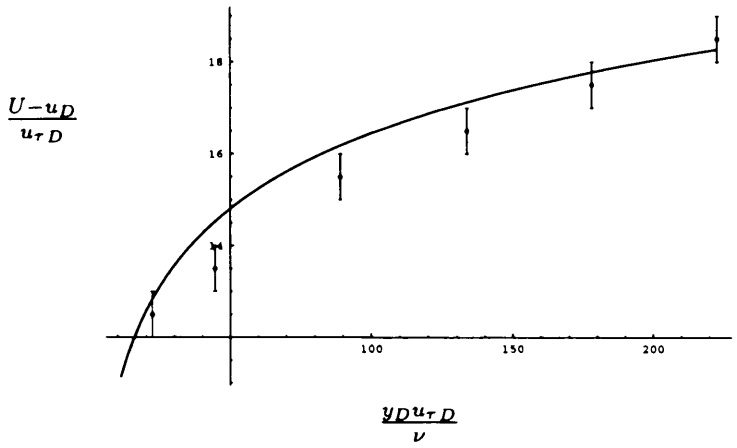

Figure 2.5: *Velocity profile for the law of the wall compared with Tsou et al.*[7]. *The curve represents the present predictions whilst the error bars are an approximate representation of the results of Tsou et al.at various points.* The results of Tsou et al. are experimental results.

t	$\frac{y_D u_{\tau D}}{\nu}$	$\frac{U-u_D}{u_{\tau D}}$	Tsou
0.1	22.27	12.84	12 – 13
0.2	44.54	14.53	13 – 14
0.4	89.07	16.18	15 – 16
0.6	133.61	17.13	16 – 17
0.8	178.14	17.78	17 – 18
1.0	222.68	18.28	18 – 19

Table 2.2: *Comparison with the 'Law of the Wall' Profile of Tsou et al.*[7].

As can be seen from Table 2.2 and Figure 2.5, our results correspond well with those of Tsou et al. Next we plot our results for the velocity profile, noting that the velocity has the asymptotic form

$$f' \sim -0.65 - \ln z, \tag{2.106}$$

as $z \to 0$.

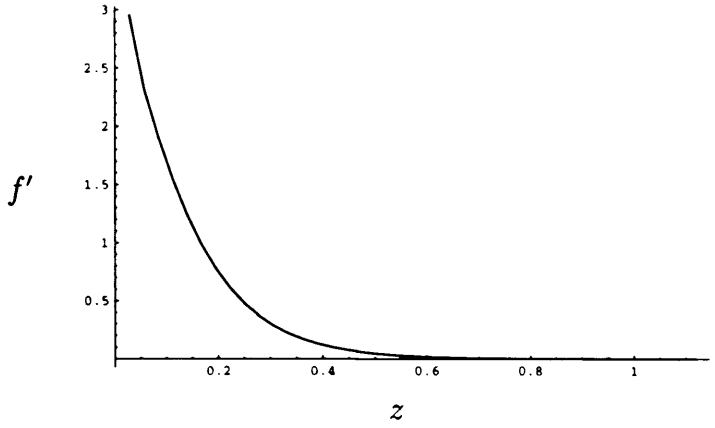

Figure 2.6: *Velocity profile for* $f'(z)$.

Our numerical results can also be used to calculate the normal velocity profile, as shown in Figure 2.7.

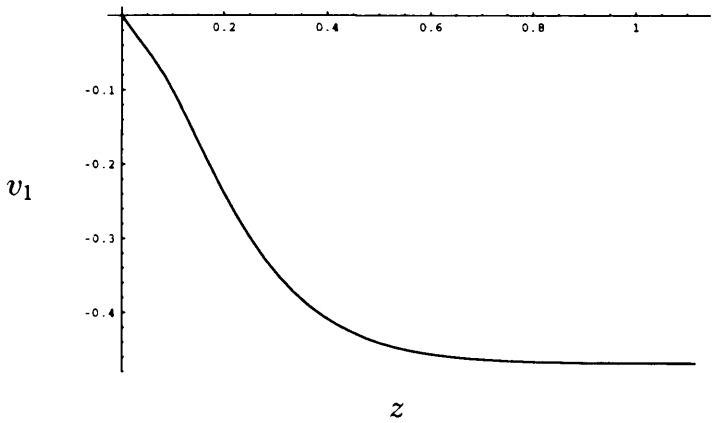

Figure 2.7: *Normal velocity profile for* $v_1 = zf' - f$.

The present approach has produced numerical results for the velocity profile which appear to be in good agreement with previous authors' work. The general agreement seems to vindicate the approach which we have taken here and in particular the current assumption that the boundary layer height is $O(k_1^2)$. Further verification regarding the accuracy of the earlier results is now sought by calculating the displacement thickness and skin friction on the plate

and comparing our predictions with those of other authors. The displacement thickness is considered first.

2.7.3 Displacement Thickness

The displacement thickness δ_D^* can be determined from the numerical results of §2.7. Since

$$\delta_D^* = \int_0^\infty \frac{u_D}{U} dy_D, \tag{2.107}$$

(2.25) and (2.38) gives

$$\delta_D^* = k_1^2 \epsilon f_\infty x_D, \tag{2.108}$$

the values for which are shown in Figure 2.8. We also compare the present

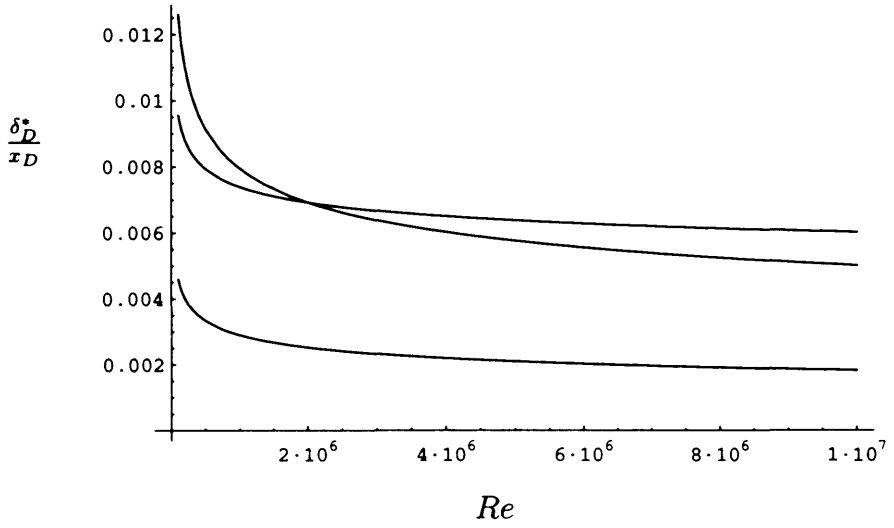

Figure 2.8: *Comparison of our predictions (top curve on right hand side) for the displacement thickness with those of Sakiadis*[62] *for a continuous flat plate with a moving surface (middle) and a finite plate in a moving stream (bottom).*

work with the results of Sakiadis[62] for a continuous flat plate with a moving surface and a moving finite flat plate where the displacement thicknesses are

given by

$$\delta_D^* = 0.126 R_x^{\frac{1}{5}}, \tag{2.109}$$

$$\delta_D^* = 0.046 R_x^{\frac{1}{5}}, \tag{2.110}$$

respectively, where $R_x = \frac{Ux}{\nu}$ as before and again we are taking Re and R_x to be equivalent.

Re	δ_D^*	Sakiadis
500,000	0.008	0.009(0.003)
10^6	0.007	0.008(0.003)
10^7	0.006	0.005(0.002)

Table 2.3: *Comparison of the present prediction for displacement thickness on a flat plate with the results of Sakiadis*[62] *for a flat plate with a moving surface and (in brackets) those for a flat plate in a uniform stream.*

Our results compare well with those for a continuous flat plate with a moving surface but are markedly different from those for a finite flat plate moving at constant velocity through a fluid at rest. This is consistent with the work of Neish & Smith[50] for a finite flat plate in a uniform stream, the approach of whom has been adopted here. The turbulent boundary layer examined here is taken to be significantly larger than the turbulent boundary layer on a finite flat plate from Neish & Smith. Thus not only might we expect our results to differ but it would seem, since the displacement thickness is a measure of the overall boundary layer thickness, that our prediction would be greater than that for a finite flat plate.

2.8 Skin Friction

It is also possible to make analytic predictions for the skin friction. Since $C_1 = -1$, (2.55) becomes

$$\frac{\partial u_2}{\partial y_2} - y_2^2[1 - \exp(-\frac{y_2 u_\tau}{26\epsilon})]^2(\frac{\partial u_2}{\partial y_2})^2 = -1 \tag{2.111}$$

and so as $y_2 \rightarrow 0$

$$\frac{\partial u_2}{\partial y_2} \rightarrow -1. \tag{2.112}$$

Now since $u_D = U(1 + \epsilon u_1)$ and $y_D = k_1^2 l \epsilon^{-1} R^{-1} y_1$,

$$\frac{\partial u_D}{\partial y_D} \rightarrow -\frac{U\epsilon^2 R}{k_1^2 l}. \tag{2.113}$$

Hence this leads to the following form for the skin friction c_f,

$$c_f = 2k_1^2\epsilon^2, \tag{2.114}$$

as illustrated in Figure 2.9, where the skin friction coefficient is defined as

$$c_f = \frac{2\tau_{WD}}{\rho U^2}, \tag{2.115}$$

and where the shear stress on the plate τ_{DW} is defined as

$$\tau_{WD} = \mu(|\frac{\partial u_D}{\partial y_D}|)_{y_D=0}. \tag{2.116}$$

In the above derivation of the skin friction τ_{WD} is defined by (2.116) and here the modulus of the shear stress is used. This is not found in all definitions of the shear stress (such as Afzal[2] and Cooper[20]) but is necessary here as otherwise τ_{WD} would be negative and so the friction velocity $u_{\tau D} = (\frac{\tau_{WD}}{\rho})^{\frac{1}{2}}$ would be a meaningless quantity in this context. Hence the shear stress is defined so that it is always positive.

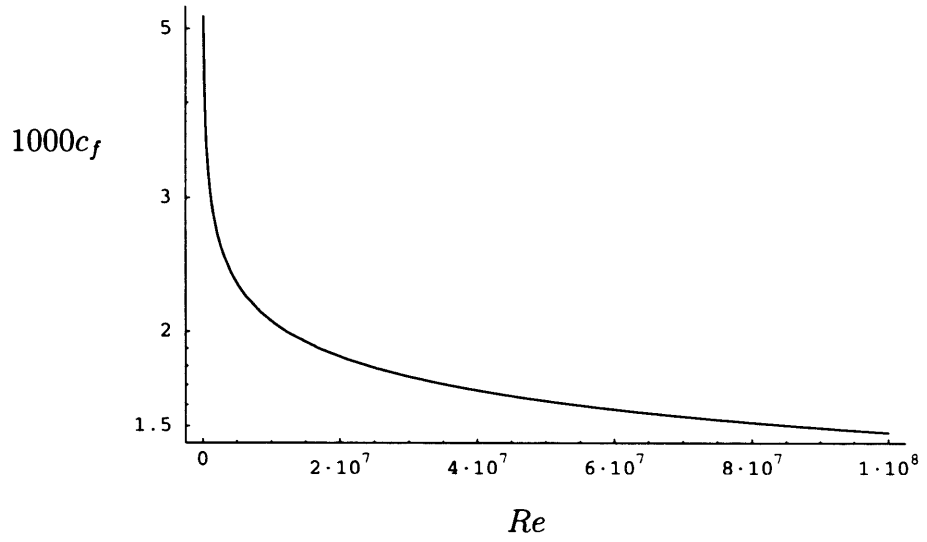

Figure 2.9: *Skin friction on a flat plate with a moving surface, based on* (2.114).

With c_f given as above we can now tabulate predictions for the skin friction coefficient against Reynolds number and compare with the work of Afzal[2] (as read from the graphs in his paper) on a continuous flat plate and the results from Tsou et al.[77] for a finite flat plate. As can be seen from the table above

Re	$\mathbf{c_f}$	**Afzal**	**Tsou**
10^5	0.0052	0.0048 – 0.0050	0.0059 – 0.0061
10^6	0.0031	0.0031 – 0.0033	0.0033 – 0.0040
10^7	0.0021	0.0022 – 0.0023	0.0026 – 0.0028
10^8	0.0015	0.0014 – 0.0016	0.0019 – 0.0021

Table 2.4: *Comparison of Skin Friction on a Flat Plate with Afzal[2] & Tsou et al.[77].*

our present predictions compare well with Afzal's for a continuous flat plate. Tsou's results for a finite flat plate are included to illustrate the difference between the flow examined here (and those of Afzal & Sakiadis) and that of a finite flat plate (either stationary in a uniform stream or moving at a constant speed in a stationary fluid). Finally it is noted that this work leads to the

following forms for the dimensional and non-dimensional friction velocities as claimed earlier,

$$u_{\tau D} = k_1 U \epsilon \tag{2.117}$$

$$u_\tau = \frac{\epsilon}{k_1} \tag{2.118}$$

where

$$u_{\tau D}^2 = \frac{\tau_{W D}}{\rho} \tag{2.119}$$

$$= \frac{U^2 c_f}{2} \tag{2.120}$$

2.9 Summary

Overall it appears then that the current approach is successful in determining the velocity profile, displacement thickness and skin friction on a flat plate with a moving surface. Since the current results emerge with apparent accuracy and efficiency it is felt that we can, with some confidence, apply the same method to more complicated flows.

Chapter 3

Rotating Flat Disc

3.1 Introduction

Having applied the approach outlined in Chapter 2 to the relatively simple problem of the 2DTBL, it is now possible to ask whether this technique works for more complicated flows, specifically three-dimensional flows with system rotation. Hence we now investigate the flow generated by a disc rotating in an otherwise stationary and unbounded fluid, as shown in Figure 3.1. Aside from

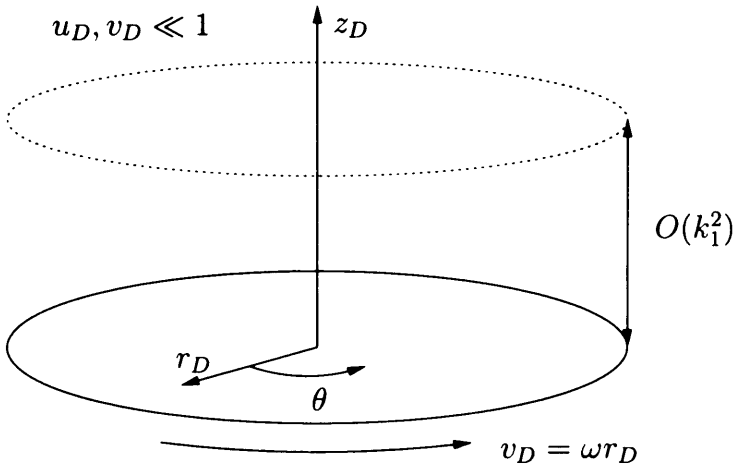

Figure 3.1: *Diagram of a rotating flat disc and the flow thickness produced.*

being an interesting and classical problem, the flow past a rotating disc is one which has many industrial and mechanical applications, including industrial sanders and chemical centrifuges. It might also be expected that the flow past a rotating disc would share some characteristics with the flow past a set of rotors. In fact Smith & Timoshin[68] have shown that for laminar flow the far-field fluid response of a slender rotating body, which is finite in radial extent, is independent of the actual configuration of that body; hence a rotating disc and a rotating cut-disc, say, would appear indistinguishable at a sufficient radial distance away. This suggests that an investigation of the flow past a rotating disc may reveal some preliminary insight into that past a set of rotors. Indeed it is shown later that the turbulent boundary layer on a rotating disc is the same as a significant portion of the turbulent boundary layer on a cut-disc (the latter being related to that on a rotor). Moreover a rotating disc can be considered to be a special example of a rotor, namely one consisting of just one blade and no wakes, or as the limit as the number of blades in a rotor configuration increases to the point that the wake regions are negligible. Hence an examination of this present flow represents a logical stage in the modelling of a rotor.

The solution of the laminar flow case for a rotating disc has been determined by von Karman[79], a description of which is also contained in Schlichting[64], and Cochran[16]. Other authors have contributed further valuable insight into this particular problem, in particular Purvis[58] who investigated the problem of a horizontal rotating disc near the ground. The turbulent case, which is of interest here, has also been examined, and, as would be expected of such an obvious and practically relevant problem, has been investigated widely, although not as comprehensively as in the laminar case. Of particular relevance and interest

here are the works of, amongst others, Cebeci & Abbott[11] and Cooper[20], both of which produced numerical results using an eddy viscosity model; Cham & Head[14] who used a momentum-integral method as well as conducting experimental measurements; Erian & Tong[29] and Littell & Eaton[45], who also undertook experimental investigations; and Wu & Squires[81] who conducted a large-eddy simulation. Whilst these authors' works are particularly pertinent to the present investigation - either because they produce results with which the present work can be compared or because some aspect of their approach is similar to ours - there is also a large amount of research to which we shall not refer. This is, in part at least, due to the prohibitively large range of work on rotating disc flow. Furthermore, certain aspects of the flow on a rotating disc, such as stability (see Lingwood[44]) and transition to turbulence, will not be considered herein.

As with the flow past a flat plate with a moving surface the approach to be used considers the turbulent boundary layer which is again taken to have height $O(k_1^2)$. Our approach to this problem proceeds as follows. The Reynolds equations for the 3DTBL are taken as the relevant governing equations (§3.2) and the phenomenon of turbulent intermittency is discussed in §3.3. Next a two-layer structure is applied to the boundary layer (§3.4). An analytical solution to the LS is then derived in §3.5, followed by a numerical solution to the flow in the ITL (including velocity profiles and displacement thickness) in §3.6. Finally an analytical prediction for the skin friction is produced (§3.7).

3.2 Governing Equations and Problem Formulation

As in Chapter 2 the Reynolds equations and the Cebeci-Smith eddy viscosity model are used. The appropriate Reynolds equations are not derived here as the derivation is simply an extension of that for the 2DTBL case shown earlier and so instead they are simply quoted. For convenience cylindrical polar co-ordinates r_D, θ and z_D are used, as in Figure 3.1, where u_D,v_D, and w_D are the velocity components in the radial, azimuthal and normal directions respectively. Assuming that the flow is steady and independent of θ we then have the following Reynolds equations

$$u_D\frac{\partial u_D}{\partial r_D} - \frac{v_D^2}{r_D} + w_D\frac{\partial u_D}{\partial z_D} = \nu\frac{\partial^2 u_D}{\partial {z_D}^2} + \frac{\partial}{\partial z_D}(\nu_{tD}\frac{\partial u_D}{\partial z_D}), \tag{3.1}$$

$$u_D\frac{\partial v_D}{\partial r_D} + \frac{u_D v_D}{r_D} + w_D\frac{\partial v_D}{\partial z_D} = \nu\frac{\partial^2 v_D}{\partial {z_D}^2} + \frac{\partial}{\partial z_D}(\nu_{tD}\frac{\partial v_D}{\partial z_D}) \tag{3.2}$$

and continuity equation

$$\frac{1}{r_D}\frac{\partial(u_D r_D)}{\partial r_D} + \frac{\partial w_D}{\partial z_D} = 0. \tag{3.3}$$

Now the eddy viscosity is defined as

$$\nu_{tD} = \begin{cases} k_2\omega r_D\delta_D^* & \text{for } z_D \geq z_{Dk}, \\ k_1^2 z_D^2[1-\exp(-\frac{z_D}{26\nu}|\frac{\tau_{WD}}{\rho}|^{\frac{1}{2}})]^2|\frac{\partial u_D}{\partial z_D}+\frac{\partial v_D}{\partial z_D}| & \text{for } z_D \leq z_{Dk}, \end{cases} \tag{3.4}$$

where ω is the angular velocity at which the disc rotates, the constants k_1 and k_2 are the same as in Chapter 2, namely 0.4 and 0.0168 respectively, the displacement thickness δ_D^* is

$$\delta_D^* = \int_0^\infty \frac{v_D}{\omega r_D} dz_D, \tag{3.5}$$

and the shear stress on the disc, τ_{WD}, is given by

$$\tau_{WD} = \mu(\frac{\partial v_D}{\partial z_D})_{z_D=0}. \tag{3.6}$$

The boundary conditions are $u_D = 0, v_D = \omega r_D$ at $z_D = 0$ (due to the disc rotation) and $u_D, v_D \to 0$ as $z_D \to \infty$ (due to the far-field fluid being at rest). The current problem is approached in a way similar to that for the flat plate flow of the previous chapter by treating the boundary layer being as comprised of two coupled layers linked through logarithmic matching, and then proceeding to generate results for the skin friction, velocity profiles and displacement thickness. First a similarity solution for the whole of the turbulent boundary layer is sought by introducing the substitutions

$$u_D = \omega r_D u = \omega r_D f'(\frac{z_D}{k_1^2 r_D^n}), \tag{3.7}$$

$$v_D = \omega r_D v = \omega r_D g'(\frac{z_D}{k_1^2 r_D^n}), \tag{3.8}$$

which, from the continuity equation, lead to the following form for the normal velocity w_D

$$w_D = -\omega k_1^2[(n+2)r_D^n f - n r_D^n \eta f']. \tag{3.9}$$

Here $f(0) = g(0) = 0$ can be taken without loss of generality. As with the flow on a flat plate the factor k_1^2 is absorbed in the transformation. This highlights the notion that the ratio of the z_D-scale to the r_D-scale is proportional to k_1^2 and thus small. One might suppose that, as in Chapter 2, we could try a similarity substitution

$$u_D = \omega r_D^m u = \omega r_D^m f'(\frac{z_D}{k_1^2 r_D^n}), \tag{3.10}$$

$$v_D = \omega r_D^m v = \omega r_D^m g'(\frac{z_D}{k_1^2 r_D^n}), \tag{3.11}$$

where u and v are the non-dimensional radial and azimuthal velocities, but, as was found in the previous chapter, the value of m is determined by the necessary matching with the velocity of the surface, which requires in this case

$m = 1$. Upon substitution of (3.7) and (3.8) into (3.1) - (3.4) we have

$$\omega^2 r_D(f'^2 - (n+2)ff'' - g'^2) = \frac{\omega\nu}{k_1^4 r_D^{2n-1}} f''' + \tag{3.12}$$

$$\omega^2 {r_D}^{2-n} \frac{\partial}{\partial\eta} \begin{cases} k_3 g_\infty f'' & \text{for } \eta \geq \eta_k \\ \eta^2[1 - \exp(-\frac{k_1^2 \eta r_D^n}{26\nu} u_{\tau D})]^2 (f''^2 + g''^2)^{\frac{1}{2}} f'' & \text{for } \eta \leq \eta_k \end{cases}$$

and

$$\omega^2 r_D(2f'g' - (n+2)fg'') = \frac{\omega\nu}{k_1^4 r_D^{2n-1}} g''' + \tag{3.13}$$

$$\omega^2 {r_D}^{2-n} \frac{\partial}{\partial\eta} \begin{cases} k_3 g_\infty g'' & \text{for } \eta \geq \eta_k \\ \eta^2[1 - \exp(-\frac{k_1^2 \eta r_D^n}{26\nu} u_{\tau D})]^2 (f''^2 + g''^2)^{\frac{1}{2}} g'' & \text{for } \eta \leq \eta_k \end{cases}$$

where $\eta = \frac{z_D}{k_1^2 r_D^n}$ and $'$ denotes differentiation with respect to η. Since the system has now been reduced to a pair of ordinary differential equations the transformed junction position η_k must be constant and thus the real junction position z_k grows proportionally with radius. In order to balance the inertial terms and Reynolds stresses we must take $n = 1$; thus the equations become

$$f'^2 - 3ff'' - g'^2 = \frac{1}{R} f''' + \tag{3.14}$$

$$\frac{\partial}{\partial\eta} \begin{cases} k_3 g_\infty f'' & \text{for } \eta \geq \eta_k \\ \eta^2[1 - \exp(-\frac{\eta R}{26} u_\tau)]^2 (f''^2 + g''^2)^{\frac{1}{2}} f'' & \text{for } \eta \leq \eta_k \end{cases}$$

and

$$2f'g' - 3fg'' = \frac{1}{R} g''' + \tag{3.15}$$

$$\frac{\partial}{\partial\eta} \begin{cases} k_3 g_\infty g'' & \text{for } \eta \geq \eta_k \\ \eta^2[1 - \exp(-\frac{\eta R}{26} u_\tau)]^2 (f''^2 + g''^2)^{\frac{1}{2}} g'' & \text{for } \eta \leq \eta_k \end{cases}$$

where

$$u_{\tau D} = k_1^2 \omega r_D u_\tau, \tag{3.16}$$

$$R = k_1^4 R_r, \tag{3.17}$$

$$R_r = \frac{\omega r_D^2}{\nu}. \tag{3.18}$$

Here R andR_r are the normalized rotational and the rotational Reynolds numbers respectively. We also have

$$w = \frac{w_D}{k_1^2 \omega r_D} = -3f + \eta f' \tag{3.19}$$

where w is the non-dimensional normal velocity component.

Note that when the powers of r_D are balanced in (3.13) and (3.14) the power of r_D in the viscous term does not balance those in the inertial and turbulent terms but instead a factor r_D^2 is absorbed into the Reynolds number.

3.3 Intermittency

In their respective studies of the flow generated by a rotating disc Cebeci & Abbott[11] and Cooper [20] include an intermittency factor $\gamma(z_D)$ as an additional multiplicative factor in the upper tier form of the eddy viscosity. The form for $\gamma(z_D)$ used by Cooper is

$$\gamma(z_D) = (1 + 5.5(\frac{z_D}{\delta_{D0.995}}))^{-1} \tag{3.20}$$

where $\delta_{D0.995}$ represents the value of z_D at which $v_D = 0.005\omega r_D$. However this factor is not found universally within studies using the Cebeci-Smith model. For instance it is not used for instance by Afzal[2] and Neish & Smith[50], although it is included by Smith & Cebeci[66]. Cooper & Reshotko[22] also use an intermittency factor in their investigation of the flow between a rotating and a stationary disc but note that where it is used it does not affect the results significantly. Further, in some of the calculations of Cooper & Reshotko, $\gamma(z_D)$ is only negligibly different from unity and hence is neglected altogether. The intermittency factor is used to account for regions of laminar flow (and transition from laminar to turbulent motion) which exist within the turbulent

boundary layer and which arise due to the inherent uncertainty of turbulent flow. We simply assume that the turbulent boundary layer is fully turbulent and so these regions do not occur. Therefore it is not necessary to include an intermittency factor here or dwell on the increased complexity that arises from the inclusion of $\gamma(z)$. It is worth noting nonetheless that the eddy viscosity model used by Cebeci & Abbott is a modified Cebeci-Smith model which is further designed to encompass intermittency, although these modifications are again omitted from the current work for the same reasons as apply to the intermittency factor.

3.4 Boundary Layer Structure

In essence the appropriate boundary layer structure applicable to the 3DTBL on a rotating disc is the same as that for the 2DTBL on a flat plate with a moving surface. Thus it is taken to consist of an inertial-turbulent layer (ITL) and a laminar sublayer (LS). This is true when the boundary layer is turbulent, although an important characteristic of the boundary layer on a rotating disc is that at low radii the flow is laminar. Turbulence is generally taken to set in when the Reynolds number $R_r \geq 10^5$ (Cooper) and, since $R_r \sim r_D^2$, at sufficiently low radii R_r lies below 10^5 and hence the flow is laminar. Therefore there exists a radial structure to the boundary layer where essentially there is laminar flow up to some radius, then turbulent flow at all larger radii. In reality this transition to turbulence does not take place abruptly at a particular radius but is spread over a radial range. The problem of transition from laminar to turbulent flow in this context has been considered, by amongst others, Cooper who takes the flow to be laminar up to a specified radius then uses the laminar velocity profile as a starting condition for the turbulent flow region holding at

all radii greater than the transition radius. For the purposes of the present study we are only concerned with the three-dimensional turbulent boundary layer (3DTBL) and thus the laminar and transitional regions are not considered (see also §3.3). This is in part due to the fact that the laminar flow case is already well understood and in part to pose a basic simple problem first. It is supposed then that our work only applies to the flow at radii beyond a transition radius, which Cooper takes to correspond to $R_\tau = 304,000$. Again the turbulent boundary layer is regarded as being composed of two distinct parts - the ITL and the LS - with heights $O(1)$ and $O(\epsilon^{-1}R^{-1})$ respectively, which are logarithmically matched. Moreover, as the continued use of the terms inertial-turbulent layer and laminar sublayer suggests, the ITL involves an inertial-turbulent balance where the velocity is given by the free stream plus a small perturbation, whilst the LS has a viscous-turbulent balance and the velocity scale is given by the velocity of the surface - in this case the rotation rate of the disc - plus a small perturbation.

3.4.1 Inertial-Turbulent Layer

In the ITL we take u_D, v_D, w_D to be $O(\epsilon)$, where we define $\epsilon = (\ln R)^{-1}$ as previously, so that $u = f' = \epsilon f_1' + ...$ and $v = g' = \epsilon g_1' + ...$ As in the previous chapter the ITL is larger than might be expected since if we suppose that $\eta = \epsilon\eta_1$ then the governing equations reduce to

$$0 = \frac{\partial}{\partial \eta_1} \begin{cases} k_3 g_{1\infty} f_1'' & \text{for } \eta_1 \geq \eta_{1k}, \\ \eta_1^2 (f_1''^2 + g_1''^2)^{\frac{1}{2}} f_1'' & \text{for } \eta_1 \leq \eta_{1k}, \end{cases} \tag{3.21}$$

and

$$0 = \frac{\partial}{\partial t} \begin{cases} k_3 g_{1\infty} g_1'' & \text{for } \eta_1 \geq \eta_{1k}, \\ {\eta_1}^2 (f_1''^2 + g_1''^2)^{\frac{1}{2}} g_1'' & \text{for } \eta_1 \leq \eta_{1k}. \end{cases} \tag{3.22}$$

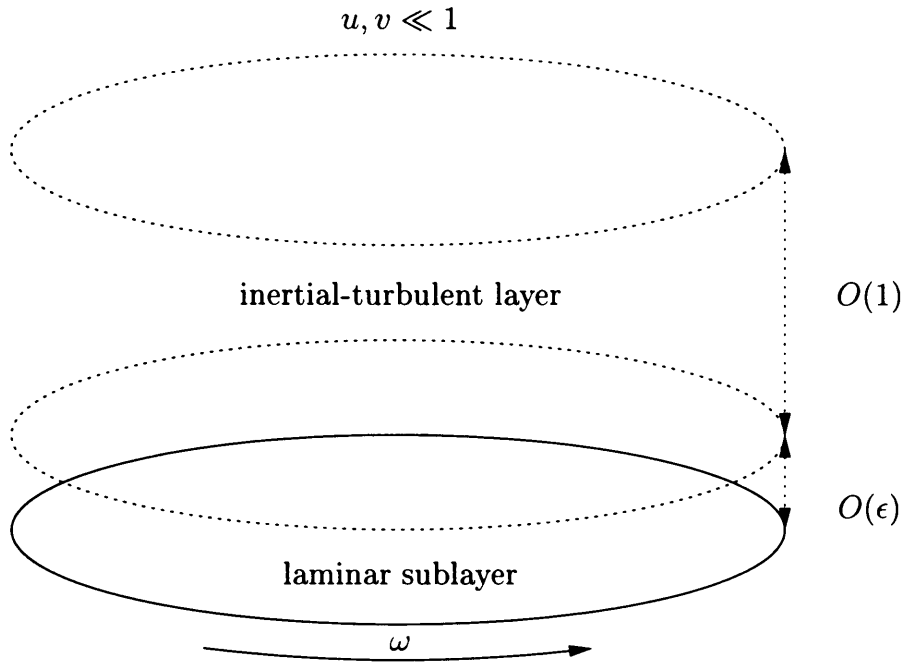

Figure 3.2: *Diagram of the structure of the 3DTBL on a rotating disc. For ease the laminar sublayer and inertial-turbulent layer are not drawn to scale.*

This then leads to the same contradiction as before, namely a zero flow in the ITL which then cannot match with the velocity in the LS. Instead we take η to be $O(1)$ which subsequently reduces (3.13) and (3.14) to

$$f_1'^2 - 3f_1f_1'' - g_1'^2 = \frac{\partial}{\partial\eta}\begin{cases} k_3 g_{1\infty} f_1'' & \text{for } \eta \geq \eta_k, \\ \eta^2(f_1''^2 + g_1''^2)^{\frac{1}{2}} f_1'' & \text{for } \eta \leq \eta_k, \end{cases} \tag{3.23}$$

and

$$2f_1'g_1' - 3f_1g_1'' = \frac{\partial}{\partial\eta}\begin{cases} k_3 g_{1\infty} g_1'' & \text{for } \eta \geq \eta_k, \\ \eta^2(f_1''^2 + g_1''^2)^{\frac{1}{2}} g_1'' & \text{for } \eta \leq \eta_k. \end{cases} \tag{3.24}$$

The viscous term is now negligible and since $\eta = O(1)$ the exponential term in the lower form of the eddy viscosity is sufficiently small to be neglected.

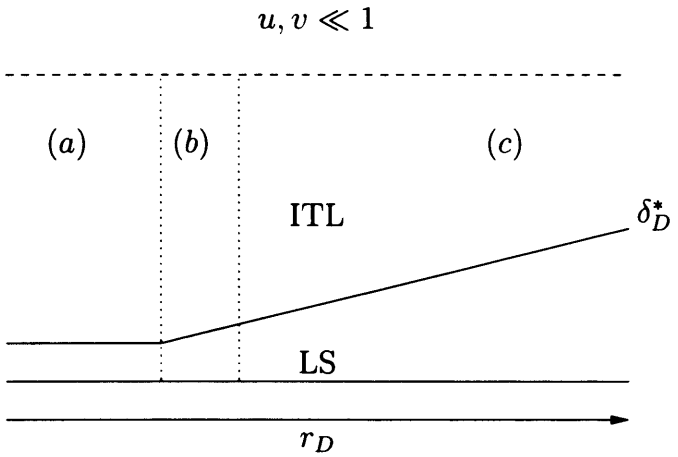

Figure 3.3: *Diagram of the radial structure of the 3DTBL on a rotating disc. The regions labelled (a), (b) and (c) are respectively the areas where laminar flow, transition-to-turbulence and turbulent flow occur. The individual regions are drawn schematically and no inference should be drawn from the relative extent of each area. The displacement thickness δ_D^* is included as an illustration of the different behaviour which occurs in the laminar and turbulent flow regimes.*

3.4.2 Laminar Sublayer and Matching

In the LS, $v = g' = 1 + \epsilon g_2' + ...$ to match with the ITL and to satisfy the boundary condition on the surface, while the scaling $\eta = \epsilon^{-1}R^{-1}\eta_2$ is required to ensure a balance between the viscous and turbulent terms. Finally here we take $u = f' = \epsilon^{-2}R^{-1}f_2' + ...$ in order to retain an inertial effect in the radial momentum balance. This is necessary to avoid a zero radial flow as $\eta_2 \to \infty$ which cannot match with the radial velocity in the ITL. The above transforms (3.13) and (3.14) into

$$\epsilon^{-4}R^{-2}(f_2'^2 - 3f_2f_2'') - 1 - 2\epsilon g_2' - \epsilon^2 g_2'^2 \qquad (3.25)$$
$$= f_2''' - \frac{\partial}{\partial \eta_2}(\eta_2^2[1 - \exp(-\frac{\eta_2}{26\epsilon}u_\tau)]^2 g_2''f_2'')$$

and

$$2\epsilon^{-2}R^{-1}f_2' + 2\epsilon^{-1}R^{-1}f_2'g_2' - 3\epsilon^{-1}R^{-1}f_2g_2'' \tag{3.26}$$
$$= \epsilon^3 Rg_2''' - \epsilon^3 R\frac{\partial}{\partial\eta_2}(\eta_2^2[1-\exp(-\frac{\eta_2}{26\epsilon}u_\tau)]^2 g_2''^2),$$

Since $|g''| \gg |f''|$, assuming monotonic decay in the azimuthal velocity, so that $g'' < 0$, enables us to take $(f''^2 + g''^2)^{\frac{1}{2}} = -g''$, to leading order.

Neglecting higher order terms thus leads to

$$-1 = f_2''' - \frac{\partial}{\partial\eta_2}(\eta_2^2[1-\exp(-\frac{\eta_2}{26\epsilon}u_\tau)]^2 g_2''f_2'') \tag{3.27}$$

and

$$0 = g_2''' - \frac{\partial}{\partial\eta_2}(\eta_2^2[1-\exp(-\frac{\eta_2}{26\epsilon}u_\tau)]^2 g_2''^2). \tag{3.28}$$

Equation (3.28) suggests logarithmic behaviour as $\eta_2 \to \infty$ as with the flat plate problem of Chapter 2, and again it is necessary to match the solutions for the ITL and the LS:

$$u = f'(\eta) = \epsilon f_1(\eta \to 0) \sim \epsilon A\eta(\ln\eta)^2, \tag{3.29}$$
$$= \epsilon^{-2}R^{-1}f_2'(\eta_2 \to \infty) \sim \epsilon^{-2}R^{-1}B\eta_2, \tag{3.30}$$
$$v = g'(\eta) = \epsilon g_1'(\eta \to 0) \sim \epsilon C\ln\eta, \tag{3.31}$$
$$= 1 + \epsilon g_2'(\eta_2) \sim 1 + \epsilon D\eta_2, \tag{3.32}$$

where u and v are the non-dimensional radial and azimuthal velocity components respectively.

Now we consider the magnitude of the term $\ln\eta$ as $\eta \to 0$. As the LS is approached $\eta = O(\epsilon^{-1}R^{-1})$ and so

$$\ln\eta \sim \ln(\epsilon^{-1}R^{-1}) \tag{3.33}$$
$$\approx \ln(R^{-1}) \tag{3.34}$$
$$= -\epsilon^{-1} \tag{3.35}$$

as the flow approaches the laminar sublayer. Hence from (3.29) - (3.32)

$$\epsilon A\eta(\ln\eta)^2 = \epsilon^{-1}A\eta \tag{3.36}$$

$$= \epsilon^{-2}R^{-1}B\eta_2 \tag{3.37}$$

$$= \epsilon^{-1}B\eta, \tag{3.38}$$

$$\epsilon C\ln\eta = 1+\epsilon D\ln\eta_2 \tag{3.39}$$

$$= 1+\epsilon D(\ln\eta+\ln R+\ln\epsilon). \tag{3.40}$$

By definition of ϵ, equation (3.40) leads then to $C = D = -1$, and $A = B$ and consideration of (3.23) as $\eta \to 0$ yields $A = B = -1$. Thus for the ITL we have the solution

$$u = \epsilon f_1'(\eta), \tag{3.41}$$

$$v = \epsilon g_1'(\eta), \tag{3.42}$$

$$\eta = \frac{z_D}{k_1^2 r_D}, \tag{3.43}$$

$$f_1'(\eta\to 0) \sim -\eta(\ln\eta)^2, \tag{3.44}$$

$$g_1'(\eta\to 0) \sim -\ln\eta, \tag{3.45}$$

and for the LS

$$u = \epsilon^{-2}R^{-1}f_2'(\eta_2), \tag{3.46}$$

$$v = 1+\epsilon g_2'(\eta_2), \tag{3.47}$$

$$\eta = \frac{z_D}{k_1^2 r_D}, \tag{3.48}$$

$$\eta_2 = \epsilon R\eta, \tag{3.49}$$

$$f_2'(\eta_2\to\infty) \sim -\eta_2, \tag{3.50}$$

$$g_2'(\eta_2\to\infty) \sim -\ln\eta_2. \tag{3.51}$$

The full asymptotic forms here are actually

$$f_1'(\eta \to 0) \sim C_1 - \eta(\ln \eta)^2, \tag{3.52}$$

$$g_1'(\eta \to 0) \sim C_2 - \ln \eta, \tag{3.53}$$

$$f_2'(\eta_2 \to \infty) \sim C_3 - \eta_2, \tag{3.54}$$

$$g_2'(\eta_2 \to \infty) \sim C_4 - \ln \eta_2, \tag{3.55}$$

and that as in §2.5.2, it is supposed that the presence of $O(\epsilon^2)$ logarithmic asymptotes means it is not necessary to have $C_1 = C_3$ and $C_2 = C_4$.

3.5 Analytical Solution in the Laminar Sublayer

Integrating (3.28), and noting that $g_2' \sim -\ln \eta_2$ as $\eta_2 \to \infty$, leads to

$$-1 = g_2'' - \eta_2^2[1 - \exp(-\frac{\eta_2}{26\epsilon} u_\tau)]^2 g_2''^2 \tag{3.56}$$

which is the same as (2.72). Hence there is now the same solution for g_2' as for u_2 before. This is illustrated in Figure 3.4 and again suggests the asymptotic

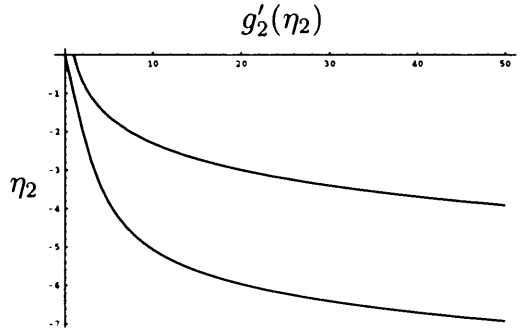

Figure 3.4: *Lower curve: Analytical solution in the laminar sublayer. Upper curve: Plot of* $\ln \eta_2$. *This is essentially a reproduction of Figure* 2.3 *but is included here for the convenience of the reader.*

form

$$g_2' \sim -\ln \eta_2 - 3.001. \tag{3.57}$$

As mentioned previously it is supposed that there exists an $O(\epsilon^2)$ term in the expansion for f' in the LS and this $O(\epsilon^2)$ term is likely to dominate the radial velocity in the LS, and so it seems unnecessary to determine f_2', which is $O(\epsilon^{-1}R^{-1})$. Instead we now proceed to a numerical solution for the ITL.

3.6 Numerical Solution in the Inertial-Turbulent Layer

As with the problem of the flat plate, it is possible to numerically solve for the velocity components on a rotating disc using a Runge-Kutta-Fehlberg (RKF) algorithm. Again the LS is ignored and a numerical solution is only considered for the equations valid in the ITL. These are

$$f_1'^2 - 3f_1f_1'' - g_1'^2 = \frac{\partial}{\partial\eta}\begin{cases} k_3 g_{1\infty} f_1'' & \text{for } \eta \geq \eta_k \\ \eta^2(f_1''^2 + g_1''^2)^{\frac{1}{2}} f_1'' & \text{for } \eta \leq \eta_k \end{cases} \tag{3.58}$$

and

$$2f_1'g_1' - 3f_1g_1'' = \frac{\partial}{\partial\eta}\begin{cases} k_3 g_{1\infty} g_1'' & \text{for } \eta \geq \eta_k \\ \eta^2(f_1''^2 + g_1''^2)^{\frac{1}{2}} g_1'' & \text{for } \eta \leq \eta_k. \end{cases} \tag{3.59}$$

Now we make the substitutions

$$\eta = \eta_k t, \tag{3.60}$$

$$f_1 = g_{1\infty} F, \tag{3.61}$$

$$g_1 = g_{1\infty} G, \tag{3.62}$$

and obtain

$$\eta_k(F'^2 - 3FF'' - G'^2) = \frac{\partial}{\partial t}\begin{cases} k_3 F'' & \text{for } t \geq 1 \\ t^2(F''^2 + G''^2)^{\frac{1}{2}} F'' & \text{for } t \leq 1 \end{cases} \tag{3.63}$$

and

$$\eta_k(2F'G' - 3FG'') = \frac{\partial}{\partial t}\begin{cases} k_3 G'' & \text{for } t \geq 1 \\ t^2(F''^2 + G''^2)^{\frac{1}{2}} G'' & \text{for } t \leq 1 \end{cases} \tag{3.64}$$

with boundary conditions

$$F(0) = 0, \tag{3.65}$$

$$F'(\infty) = 0, \tag{3.66}$$

$$G(0) = 0, \tag{3.67}$$

$$G(\infty) = 1, \tag{3.68}$$

$$G'(\infty) = 0, \tag{3.69}$$

$$F''(1)^2 + G''(1)^2 = k_3^2, \tag{3.70}$$

where (3.70) arises from continuity of eddy viscosity at $t=1$,
and asymptotes

$$F' \rightarrow C_1^* - \frac{\eta_k^2 t_0}{g_{1\infty}}(\ln(t_0\eta_k))^2, \tag{3.71}$$

$$G' \rightarrow C_2^* - \frac{\eta_k}{g_{1\infty}}\ln(t_0\eta_k), \tag{3.72}$$

where $t_0 \ll 1$. These can be solved using an RKF algorithm. As before, the substitutions (3.60) - (3.62) are made for convenience, determining an extra boundary condition at infinity and helping to calculate the junction position η_k efficiently and accurately.

Equations (3.63) and (3.64) are rewritten as a set of first-order equations

by defining

$$s_1 = F(t), \tag{3.73}$$

$$s_2 = F'(t), \tag{3.74}$$

$$s_3 = F''(t), \tag{3.75}$$

$$s_4 = G(t), \tag{3.76}$$

$$s_5 = G'(t), \tag{3.77}$$

$$s_6 = G''(t). \tag{3.78}$$

The problem then separates into two sets of equations, one set of which corresponds to $t \leq 1$,

$$\frac{ds_1}{dt} = s_2, \tag{3.79}$$

$$\frac{ds_2}{dt} = s_3, \tag{3.80}$$

$$\begin{aligned}\frac{ds_3}{dt} = {} & [(\eta_k(s_2^2 - s_5^2 - 3s_1s_3) - 2t|s_3 + s_6|s_3)(t^2(|s_3 + s_6|)^{-1}s_6^2 + \\ & t^2|s_3 + s_6|) - (t^2(|s_3 + s_6|)^{-1}s_3s_6)(\eta_k(2s_2s_5 - 3s_1s_6) - \\ & 2t|s_3 + s_6|s_6)]/[(t^2(|s_3 + s_6|)^{-1}s_6^2 + t^2|s_3 + s_6|) \\ & (t^2(|s_3 + s_6|)^{-1}s_3^2 + t^2|s_3 + s_6|) - (t^2(|s_3 + s_6|)^{-1}s_3s_6)^2],\end{aligned} \tag{3.81}$$

$$\frac{ds_4}{dt} = s_5,$$

$$\frac{ds_5}{dt} = s_6, \tag{3.82}$$

$$\begin{aligned}\frac{ds_6}{dt} = {} & [(\eta_k(2s_2s_5 - 3s_1s_6) - 2t|s_3 + s_6|s_6)(t^2(|s_3 + s_6|)^{-1}s_3^2 + \\ & t^2|s_3 + s_6|) - (t^2(|s_3 + s_6|)^{-1}s_3s_6)(\eta_k(s_2^2 - s_5^2 - 3s_1s_3) - \\ & 2t|s_3 + s_6|s_3)]/[(t^2(|s_3 + s_6|)^{-1}s_6^2 + t^2|s_3 + s_6|) \\ & (t^2(|s_3 + s_6|)^{-1}s_3^2 + t^2|s_3 + s_6|) - (t^2(|s_3 + s_6|)^{-1}s_3s_6)^2],\end{aligned} \tag{3.83}$$

with boundary conditions

$$s_1(t_0) = 0, \tag{3.84}$$

$$s_2(t_0) = C_1^* - \frac{\eta_k^2 t_0}{g_{1\infty}}[\ln(t_0\eta_k)]^2, \tag{3.85}$$

$$s_3(t_0) = -\frac{\eta_k^2}{g_{1\infty}}[\ln(t_0\eta_k)]^2 - \frac{2\eta_k^2}{g_{1\infty}}\ln(t_0\eta_k), \tag{3.86}$$

$$s_4(t_0) = 0, \tag{3.87}$$

$$s_5(t_0) = C_2^* - \frac{\eta_k}{g_{1\infty}}\ln(t_0\eta_k), \tag{3.88}$$

$$s_6(t_0) = -\frac{\eta_k}{g_{1\infty}t_0}, \tag{3.89}$$

where $J = \eta_k$ (the use of the notation J is designed to draw analogy with the equivalent numerical method used for the flat plate problem of Chapter 2). The second set, corresponding to $t \geq 1$, is

$$\frac{ds_1}{dt} = s_2, \tag{3.90}$$

$$\frac{ds_2}{dt} = s_3, \tag{3.91}$$

$$\frac{ds_3}{dt} = K(s_2^2 - s_5^2 - 3s_1s_3), \tag{3.92}$$

$$\frac{ds_4}{dt} = s_5, \tag{3.93}$$

$$\frac{ds_5}{dt} = s_6, \tag{3.94}$$

$$\frac{ds_6}{dt} = K(2s_2s_5 - 3s_1s_6), \tag{3.95}$$

with boundary conditions

$$s_1(\infty) = s_{1\infty}, \tag{3.96}$$

$$s_2(\infty) = 0, \tag{3.97}$$

$$s_3(\infty) = s_{3\infty}, \tag{3.98}$$

$$s_4(\infty) = 1, \tag{3.99}$$

$$s_5(\infty) = 0, \tag{3.100}$$

$$s_6(\infty) = s_{6\infty}, \tag{3.101}$$

with $K = \frac{\eta_k}{k_3}$. We also require

$$k_3^2 = s_3(1)^2 + s_6(1)^2 \tag{3.102}$$

to satisfy continuity of the eddy viscosity. Note here that given K and $s_6(t_0)$ we can automatically determine the correct asymptotic value of $s_3(t_0)$. Thus the condition that

$$s_3(t_0) = -s_6(t_0)t_0Kk_3\ln(t_0Kk_3)(\ln(t_0Kk_3) + 2) \tag{3.103}$$

must also be applied. The RKF algorithm is then run on the second set of equations, (3.79) - (3.89), using the conditions at infinity as the starting values. As before, 'infinity' is taken to be a suitably large but finite number, t_∞, with the values of K and $s_{i\infty}$ (where $i = 1, 3$ or 6) varied. This scheme produces a set of values at $t = 1$ which are used as the initial conditions for the first set of equations, (3.90) - (3.101). The RKF algorithm then runs on these equations to produce a set of values at t_0. These values at t_0 depend on the values of K and $s_{i\infty}$ chosen, and so the process can be repeated until a set of values for K and $s_{i\infty}$ is found which yields $s_1(t_0) = s_4(t_0) = 0$, $s_3(1)^2 + s_6(1)^2 = k_3^2$ and which satisfies (3.103). Here it is assumed that, as $s_1(0) = s_4(0) = 0$, if

t_0 is sufficiently small then $s_1(t_0) \approx s_4(t_0) \approx 0$. In practice these boundary conditions are judged to be satisfied when

$$|s_1(t_0)| < 10^{-3}, \tag{3.104}$$

$$|s_4(t_0)| < 10^{-3}, \tag{3.105}$$

$$|s_3(1)^2 + s_6(1)^2 - k_3^2| < 10^{-6}, \tag{3.106}$$

$$|s_3(t_0) + s_6(t_0)t_0Kk_3 \ln(t_0Kk_3)(\ln(t_0Kk_3) + 2)| < 10^{-6}. \tag{3.107}$$

Thus the solutions illustrated in Figure 3.5 and Figure 3.6 are obtained for different values of t_∞, t_0 and step length d.

As in §2.7 the results are virtually unaffected by changes in t_∞, t_0 and step length d. These results can now be used to find the unknown parameters as shown in Table 3.1.

t_∞	t_0	d	η_k	$g_{1\infty}$	C_1^*	C_1	C_2^*	C_2
20	10^{-3}	-10^{-3}	0.0271	0.2175	0.1958	1.5722	−0.2165	−1.7384
20	10^{-4}	-10^{-4}	0.0271	0.2170	0.1956	1.5671	−0.2194	−1.7576
20	10^{-5}	-10^{-5}	0.0271	0.2169	0.1957	1.5659	−0.2208	−1.7672
18	10^{-3}	-10^{-3}	0.0271	0.2178	0.1958	1.5740	−0.2155	−1.7320
15	10^{-3}	-10^{-3}	0.0269	0.2166	0.1960	1.5799	−0.2133	−1.7189

Table 3.1: *Calculation of Flow Parameters.*

This problem has proven to be significantly harder to solve numerically than the flow past a flat plate, as there are several more variables and unknown parameters to contend with. As such the algorithm used is slower and the iterations necessary to determine the values of K and $g_{1\infty}$ are more complicated.

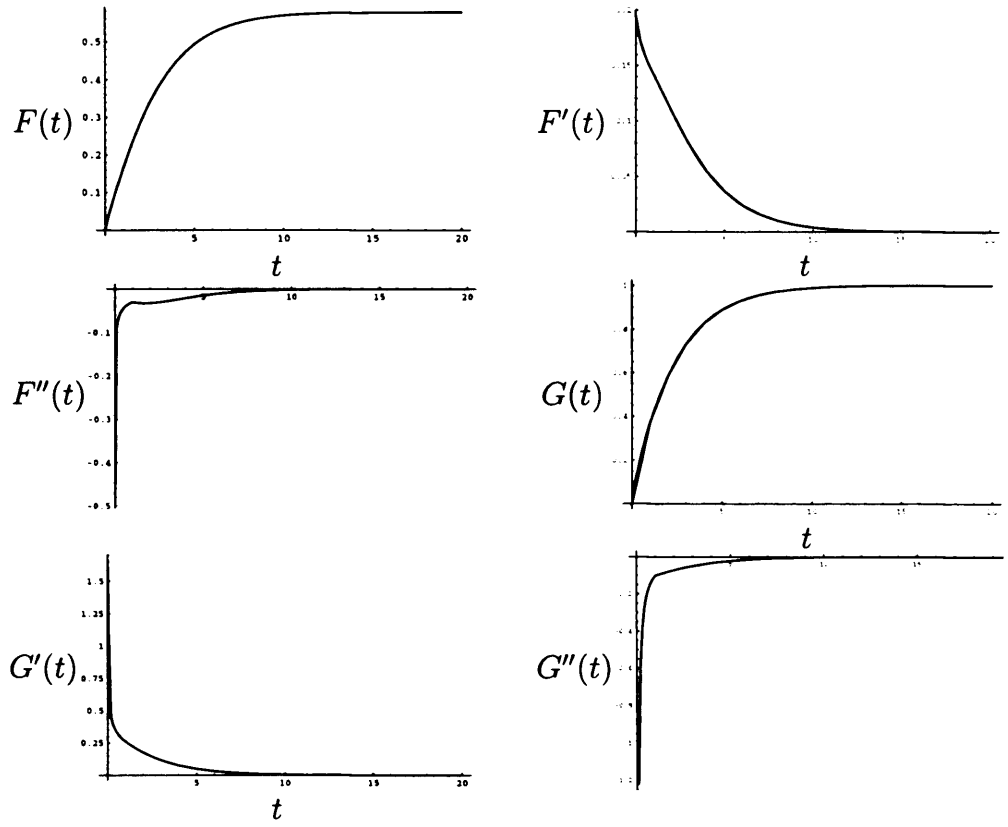

Figure 3.5: *Numerical results for a rotating disc with step length* $d = -0.001$, $d = -0.0001$ *and* $d = -0.00001$. *In all cases the horizontal axis denotes the height* t. *As with the numerical results for the flat plate problem of Chapter 2, there is a noticeable change in the behaviour of the results at* $t = 1$.

3.6.1 Velocity Profiles

We now compare the current prediction for the radial velocity profile with that of Erian & Tong[29], who plot $\frac{u_D}{\omega r_D}$ against $z_D(\frac{\omega}{\nu})^{\frac{1}{2}}$. Noting that

$$\frac{u_D}{\omega r_D} = \frac{\epsilon g_{1\infty} F'(t)}{\eta_k} \tag{3.108}$$

and

$$z_D(\frac{\omega}{\nu})^{\frac{1}{2}} = k_1^2 \eta_k (R_r)^{\frac{1}{2}} t, \tag{3.109}$$

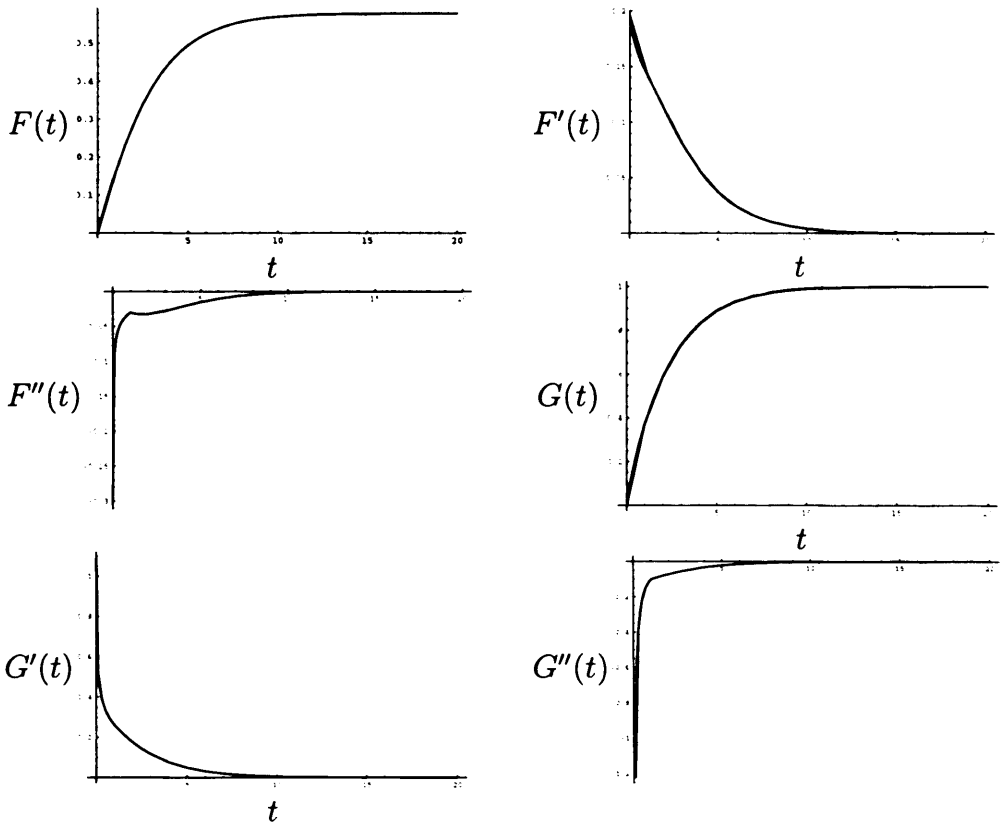

Figure 3.6: *Numerical results for a rotating disc with* $t_\infty = 20$, $t_\infty = 18$ *and* $t_\infty = 15$. *Again the height t is measured along the horizontal axis throughout.*

we tabulate our results for $\frac{u_D}{\omega r_D}$ with those of Erian & Tong for different values of t. Table 3.2 and Figure 3.7 demonstrate that the current results are in good agreement with the work of Erian & Tong. Finally Figure 3.8 and Figure 3.9 show the non-dimensional velocity profiles, f_1', g_1' and w_1 (where $w = \epsilon w_1 = -3\epsilon f_1 + \epsilon\eta f_1'$) which appear to be similar to the results of, amongst others, Cooper.

t	$z_D(\frac{\omega}{\nu})^{\frac{1}{2}}$	$\frac{u_D}{\omega r_D}$	Erian&Tong
1	4.32	0.112	0.105 – 0.115
2	8.64	0.086	0.085 – 0.095
3	12.96	0.062	0.065 – 0.075
4	17.28	0.043	0.045 – 0.055
5	21.60	0.029	0.025 – 0.035

Table 3.2: *Comparison of Velocity Profiles with Erian & Tong*[29].

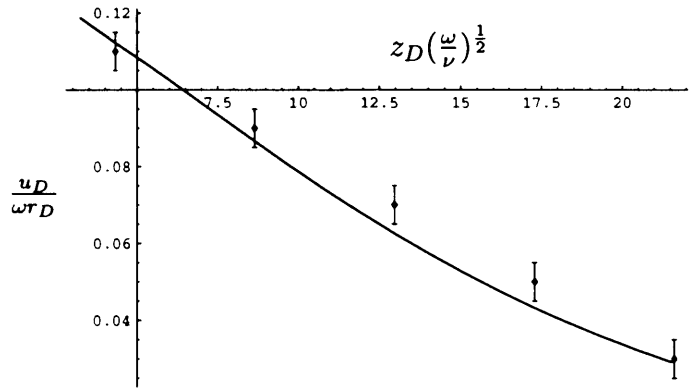

Figure 3.7: *Radial velocity profile on a rotating disc compared with the work of Erian & Tong*[29]. *The current predictions are shown as a curve whilst the results of Erian & Tong at various points are included as error bars, indicating the range in which their results lie as accurately as is possible.*

3.6.2 Displacement Thickness

Using the numerical results of §3.6 it is possible to determine the displacement thickness δ_D^*, which is found to be

$$\delta_D^* = \epsilon g_{1\infty} k_1^2 r_D = 0.0347 \epsilon r_D \tag{3.110}$$

and is shown in Figure 3.10. Our calculations for the displacement thickness can then be compared with Cooper[20] for different values of the rotational Reynolds number R_r. Cooper's form for δ_D^* is actually

$$\delta_D^* = 0.0700 (\frac{\nu}{\omega})^{\frac{1}{5}} r_D^{\frac{3}{5}}. \tag{3.111}$$

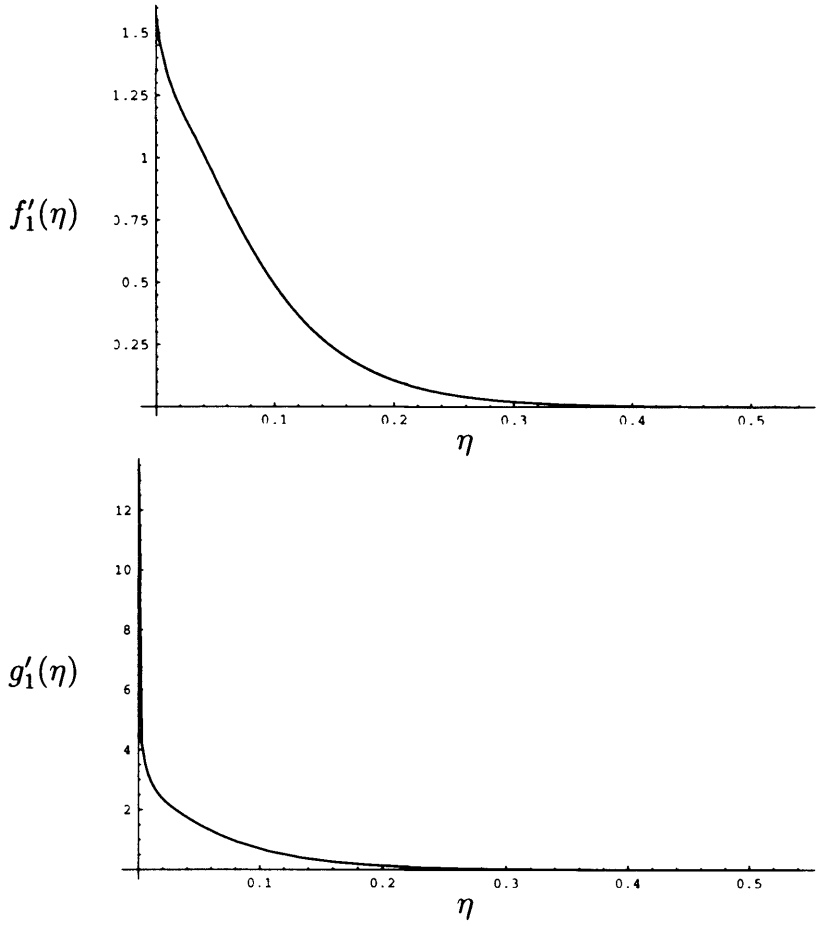

Figure 3.8: *Top: Radial velocity profile for* $f_1'(\eta)$. *Bottom: Azimuthal velocity profile for* $g_1'(\eta)$.

Hence Cooper has $\delta_D^* \sim r_D^{\frac{3}{5}}$ whilst our work suggests that $\delta_D^* \sim \frac{r_D}{\ln r_D}$; thus the current results could never coincide exactly with those of Cooper. This discrepancy may arise from the omission of the intermittency factor in the present work, else it may be necessary to extend our analysis to include higher order terms to derive a more accurate prediction for δ_D^* or it may be the use of a similarity solution which leads to this discrepancy. This latter case is, in the author's belief, most likely to be the crucial factor.

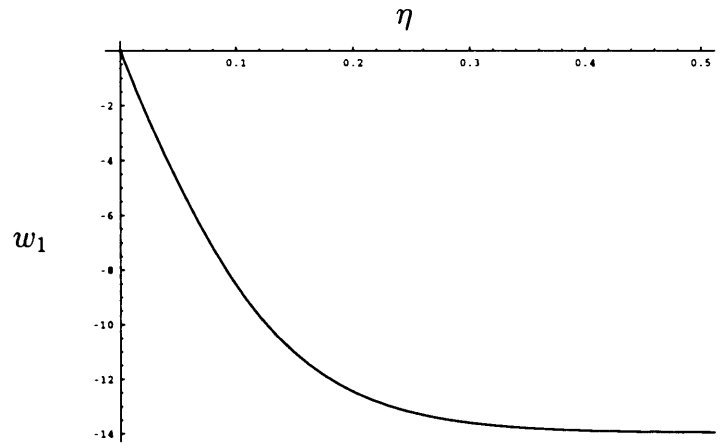

Figure 3.9: *Non-dimensional normal velocity,* $w_1 = -3f_1 + \eta f_1'$, *on a rotating disc.*

Re	δ_D^*	Cooper
600,000	$0.0036r_D$	$0.0050r_D$
10^7	$0.0028r_D$	$0.0028r_D$
10^{10}	$0.0018r_D$	$0.0007r_D$

Table 3.3: *Comparison of Displacement Thickness with Cooper*[20].

3.7 Skin Friction

The skin friction on the surface is now sought. For this purpose, from §3.4.2, the following equation is used

$$0 = g_2''' - \frac{\partial}{\partial \eta_2}(\eta_2^2[1 - \exp(-\frac{\eta_2}{26\epsilon}u_\tau)]^2 g_2''^2), \tag{3.112}$$

which upon integration yields

$$-1 = g_2'' - \eta_2^2[1 - \exp(-\frac{\eta_2}{26\epsilon}u_\tau)]^2 g_2''^2 \tag{3.113}$$

since $g_2' \sim -\ln \eta_2$ as $\eta_2 \to \infty$. Therefore, as $\eta_2 \to 0$,

$$g_2'' \to -1. \tag{3.114}$$

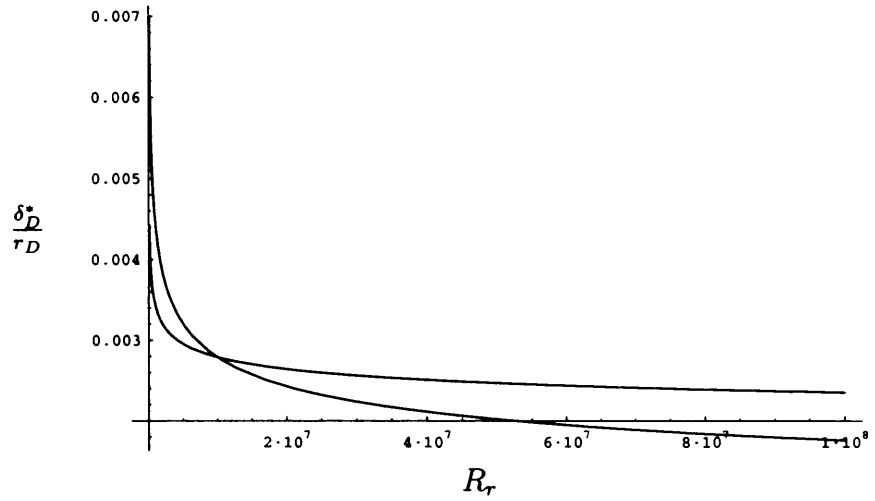

Figure 3.10: *Comparison of the values predicted for the displacement thickness on a rotating disc between the present work (upper curve on right hand side) and that of Cooper*[20] *(lower curve on right hand side).*

As $v_D = \omega r_D(1 + \epsilon g_2')$ and $\eta_2 = \frac{\epsilon R z_D}{k_1^2 r_D}$, it follows that as $z_D \to 0$

$$\frac{\partial v_D}{\partial z_D} \to -\frac{\omega \epsilon^2 R}{k_1^2}. \tag{3.115}$$

The circumferential skin friction coefficient is defined as

$$c_{f\theta} = \frac{2\tau_{W D\theta}}{\rho(\omega r_D)^2} \tag{3.116}$$

where

$$\tau_{W D\theta} = \mu(|\frac{\partial v_D}{\partial z_D}|)_{z_D=0}. \tag{3.117}$$

Hence

$$c_{f\theta} = 2k_1^2\epsilon^2, \tag{3.118}$$

as illustrated in Figure 3.11. This is the same as for the skin friction coefficient on a flat plate, and again we can compare with previous work, this time Cebeci & Abbott[11].

As can be seen from the Table 3.4, the present results are in good general agreement with those of Cebeci & Abbott, although our results are consistently

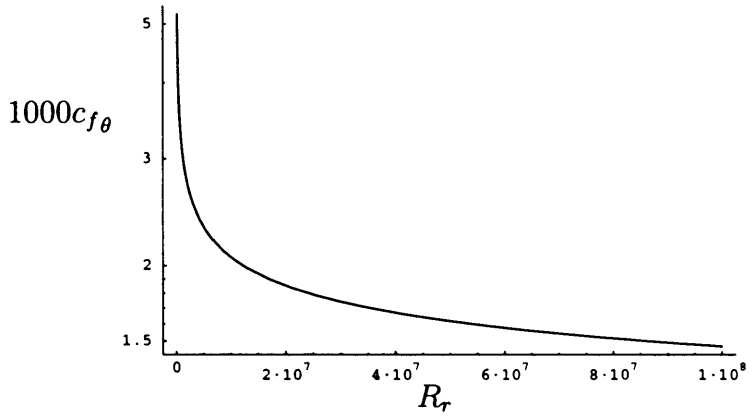

Figure 3.11: *Skin friction on a rotating disc, from* (3.118).

Re	$\mathbf{c_{f\theta}}$	**Cebeci&Abbott**
600,000	0.0036	0.0037 – 0.0040
800,000	0.0032	0.0035 – 0.0038
1,000,000	0.0031	0.0034 – 0.0037
2,000,000	0.0027	0.0030 – 0.0032

Table 3.4: *Comparison of Skin Friction on a Rotating Disc with Cebeci & Abbott*[11].

lower. This discrepancy may arise from the slightly different forms of the Cebeci-Smith eddy viscosity model used. Now we also mention that since in the LS $|g''| \gg |f''|$, to leading order

$$\tau_{WD} = \tau_{WD\theta}; \tag{3.119}$$

hence

$$u_{\tau D} = k_1 U\epsilon, \tag{3.120}$$

$$u_\tau = \frac{\epsilon}{k_1}, \tag{3.121}$$

where

$$u_{\tau D}^2 = \frac{\tau_{WD}}{\rho} \tag{3.122}$$

$$= \frac{U^2 c_{f\theta}}{2}, \tag{3.123}$$

as used earlier.

3.8 Summary

The approach used here has successfully generated predictions for the skin friction and velocity profile which are in good broad agreement with existing work on a rotating disc. The results here for the displacement thickness are not so good, insofar as they suggest that this measure of the boundary layer thickness grows more rapidly than is seen by von Karman or Cooper. This discrepancy may arise as a result of the similarity solution used here.

Generally speaking, we can conclude that the success of the present approach in modelling the flows on a flat plate and a rotating disc demonstrate the reasonable overall validity of the model being used and the assumptions made, notably that the boundary layer height scales like k_1^2.

Chapter 4

Turbulent Boundary Layers with Azimuthal Dependence

4.1 Introduction

One of the major simplifications which arises when examining the flow past a rotating disc is that the flow may be symmetric about the axis of rotation (axisymmetry). This reduces the complexity of the system greatly, enabling the boundary layer to be taken as quasi two-dimensional, in the sense of depending only on radius and height: and ultimately allows the rotating disc problem to be posed simply in terms of one similarity variable. In the case of a [illegible] rotor, however, the flow is clearly not axisymmetric (non-axisymmetric) and as a result this problem is fully three-dimensional and far more complicated. Further, a potentially important feature of the flow past a set of rotors is that the wake from one rotor can interact with the next oncoming blade (see Purvis[58] and Smith & Timoshin[68,69]). This means that the system cannot entirely be treated as a set of isolated blades and wakes (and so the flow on the

blades cannot be taken to be the same as disc flow, although it is subsequently shown that there are significant similarities). Instead it is necessary, or at least desirable, to model the system in such a way that enables us to deal with both blades and wakes, and the interactions that arise between them.

The present chapter considers turbulent boundary layers with azimuthal dependence, or, as they are subsequently referred, non-axisymmetric turbulent boundary layers (NATBL). The aim here is to understand how non-axisymmetry influences the turbulent system and then proceed to examine flows which do not exhibit axisymmetry. Furthermore, and particularly for the case of a set of rotors or, as is examined subsequently, a cut-disc, we also need to account for the inherent physical periodicity of the flow.

When considering the problem of the NATBL several key questions come to mind. Firstly, what are the appropriate Reynolds equations? Next, can the 3DTBL structure applied to the rotating disc be used for the NATBL? And finally, if the three-dimensional turbulent boundary layer (3DTBL) structure is unsatisfactory, what is the appropriate structure? With respect to the Reynolds equations, the author's background research has failed to reveal any previous studies of the NATBL and certainly none have been found which use fully 3D Reynolds equations in a non-axisymmetric flow in cylindrical polar co-ordinates. Instead then these equations are derived from the boundary layer equations, using the principles of Smith & Cebeci[66] and following (as closely as possible) their derivation of the 2D Reynolds equations in Cartesian co-ordinates, as outlined in §2.2.

The requirement of θ-dependency in the NATBL means that the boundary layer here clearly cannot be exactly the same as that on a rotating disc. We also later show that, whilst many similarities exist, some major modifications

to the boundary layer structure are necessary to examine the flow generated by a rotating non-axisymmetric surface. As mentioned above, the lack of any earlier related work means that (to the author's knowledge at least) no existing structure for the NATBL has been described and so, as with the Reynolds equations, one is derived herein. Fortunately it is possible to draw upon previous research into flows which, whilst not directly applicable to the NATBL, do share some important characteristics.

It is worth noting here that one of the most basic examples of a non-axisymmetric body is that of a cut-disc (this is described and illustrated in more detail in Chapter 5, but for our purposes it is sufficient to consider a cut disc to be a flat disc which has had segments removed - or 'cut' - leaving an alternate sequence of areas of disc and wakes). Understanding this cut-disc flow is our main motivation in investigating the NATBL since this flow can be related to that caused by a cut rotor, as we shall see in more detail later. The notion of a cut-disc is used to help determine the flow characteristics of the NATBL as intuitively it is expected that this flow will have some similarities with the flow past a complete rotating disc and with the flow past a flat plate in a moving stream, these flows representing two extreme cases of a cut-disc. Hence it is anticipated that the NATBL is similar to the 2DTBL on a flat plate and the 3DTBL on a rotating disc. This turns out to be true but there are several difficulties which need to be addressed. Most notably, the 2DTBL on a flat plate is much thinner than the 3DTBL on a rotating disc and, in addition the displacement thickness on a flat plate grows linearly on the surface and remains constant in the wake; if the latter were also true for a cut-disc that would violate the requirement of periodicity. We are also able to draw guidance from the work of Neish & Smith who, following others, examined the turbulent

flow past a flat plate and subsequent wake and used a model for the boundary layer structure which involved an inertial-turbulent layer for the whole flow, and different laminar sublayers for the plate and the wake. This forms the basis of our model for the NATBL but with significant modifications to cope with the difficulties discussed above, as well as others which arise.

We also mention here that although our chief interest is in rotor blade flow (and as a precursor, cut-disc flow), the NATBL structure and equations used here can be applied to other flows without axisymmetry. Such azimuthal variations could include a cut or gap in the body surface or a deformation, such as a bump. Indeed it transpires that for the greater part of the NATBL the exact form of the non-axisymmetric surface is unimportant and instead it is the body (or disc) solidity which matters. The solidity is denoted $\hat{a}$ throughout and is defined as the ratio of the surface area of the body to the total area of surfaces and wakes.

Now we proceed to examine turbulent boundary layers with azimuthal dependence and for the purposes of understanding the flow produced by a rotating body without axisymmetry the following strategy is adopted. The appropriate Reynolds equations for the flow are determined (§4.2) and the particular model used for the NATBL structure is described (§4.3). This description of the NATBL is then used to examine those regions which are not dependent on the exact non-axisymmetric body involved and these are examined in §4.4 before (Chapter 5) a specific NATBL is considered, namely the problem of a rotating cut-disc. Finally, in §4.5, the nature of the θ-dependency in the NATBL is examined.

4.2 The Non-Axisymmetric Reynolds Equations in Cylindrical Polar Co-ordinates

As mentioned in §4.1 the modelling of the turbulent boundary layer on a rotor requires consideration of azimuthal dependence. In order to understand such flows we need the Reynolds equations applicable to a non-axisymmetric flow and a model for the structure of a non-axisymmetric boundary layer. First the Reynolds equations for this current problem are derived in a suitable co-ordinate system - namely cylindrical polar co-ordinates. For completeness, time-derivatives and pressure gradient terms are retained in this derivation, even though the flows to which these equations are applied here are taken to be steady and the pressure gradient often zero.

The approach used here will follow that of Smith & Cebeci in deriving the 2D Reynolds equations in cartesian co-ordinates. This involves the following key stages:

1. separating the velocity components into mean and turbulent fluctuating parts;

2. taking a time-average over a sufficiently large time interval;

3. rewriting the turbulent fluctuation terms so that they are written as the derivative of a time-averaged quantity; and

4. the omission of some terms as being negligibly small.

Since this process has been used to determine the appropriate Reynolds equations for a variety of flows previously, and can be found in many references, including Smith & Cebeci[66], Schlichting[64] and Cebeci & Abbott[12], the justi-

fication and reasoning for this approach is not included here and instead the reader is referred to those authors listed above.

To begin we take the three-dimensional boundary layer equations in cylindrical polar co-ordinates,

$$\frac{\partial \overline{u}}{\partial t} + \overline{u}\frac{\partial \overline{u}}{\partial r_D} - \frac{\overline{v}^2}{r_D} + \frac{\overline{v}}{r_D}\frac{\partial \overline{u}}{\partial \theta} + \overline{w}\frac{\partial \overline{u}}{\partial z_D} = -\frac{1}{\rho}\frac{\partial \overline{p}}{\partial r_D} + \nu\frac{\partial^2 \overline{u}}{\partial z_D^2} \tag{4.1}$$

and

$$\frac{\partial \overline{v}}{\partial t} + \overline{u}\frac{\partial \overline{v}}{\partial r_D} + \frac{\overline{u}\overline{v}}{r_D} + \frac{\overline{v}}{r_D}\frac{\partial \overline{v}}{\partial \theta} + \overline{w}\frac{\partial \overline{v}}{\partial z_D} = -\frac{1}{\rho r_D}\frac{\partial \overline{p}}{\partial \theta} + \nu\frac{\partial^2 \overline{v}}{\partial z_D^2}, \tag{4.2}$$

with continuity equation

$$\frac{1}{r_D}\frac{\partial(\overline{u}r_D)}{\partial r_D} + \frac{1}{r_D}\frac{\partial \overline{v}}{\partial \theta} + \frac{\partial \overline{w}}{\partial z_D} = 0. \tag{4.3}$$

As in §2.2 we separate the velocity components, and now also the pressure, into mean and turbulent fluctuating terms and hence introduce the substitutions

$$\overline{u} = u_D + u^*, \tag{4.4}$$

$$\overline{v} = v_D + v^*, \tag{4.5}$$

$$\overline{w} = w_D + w^*, \tag{4.6}$$

$$\overline{p} = p_D + p^*. \tag{4.7}$$

Taking the time-average, where the time-average of a quantity s is denoted $< s >$, we obtain

$$\frac{\partial u_D}{\partial t} + u_D\frac{\partial u_D}{\partial r_D} - \frac{v_D^2}{r_D} + \frac{v_D}{r_D}\frac{\partial u_D}{\partial \theta} + w_D\frac{\partial u_D}{\partial z_D} = -\frac{1}{\rho}\frac{\partial p_D}{\partial r_D} + \nu\frac{\partial^2 u_D}{\partial z_D^2} \tag{4.8}$$
$$-[\frac{1}{2}\frac{\partial(< u^{*2} >)}{\partial r_D} - \frac{(< v^{*2} >)}{r} + < (w^*\frac{\partial u^*}{\partial z_D}) > + \frac{1}{r_D} < (v^*\frac{\partial u^*}{\partial \theta}) >]$$

and

$$\frac{\partial v_D}{\partial t} + u_D\frac{\partial v_D}{\partial r_D} + \frac{u_D v_D}{r_D} + \frac{v_D}{r_D}\frac{\partial v_D}{\partial \theta} + w_D\frac{\partial v_D}{\partial z_D} = -\frac{1}{\rho r_D}\frac{\partial p}{\partial \theta} + \nu\frac{\partial^2 v_D}{\partial z_D^2} \tag{4.9}$$
$$-[< (u^*\frac{\partial v^*}{\partial r_D}) > + \frac{< (u^*v^*) >}{r_D} + < (w^*\frac{\partial v^*}{\partial z_D}) > + \frac{1}{2r_D}\frac{\partial(< (v^{*2}) >)}{\partial \theta}].$$

Equations (4.8) and (4.9) can now be rewritten using the continuity equation so that all the terms involving turbulent fluctuations can, where appropriate, be expressed as derivatives of time-averaged quantities. Hence

$$\frac{\partial u_D}{\partial t}+u_D\frac{\partial u_D}{\partial r_D}-\frac{v_D^2}{r_D}+\frac{v_D}{r_D}\frac{\partial u_D}{\partial \theta}+w_D\frac{\partial u_D}{\partial z_D}=-\frac{1}{\rho}\frac{\partial p_D}{\partial r_D} \qquad (4.10)$$
$$+\nu\frac{\partial^2 u_D}{\partial z_D^2}-[\frac{\partial(<u^{*2}>)}{\partial r_D}+\frac{<(u^{*2})>}{r_D}-\frac{<(v^{*2})>}{r_D}$$
$$+\frac{\partial <(u^*w^*)>}{\partial z_D}+\frac{1}{r_D}\frac{\partial <(u^*v^*)>}{\partial \theta}]$$

and

$$\frac{\partial v_D}{\partial t}+u_D\frac{\partial v_D}{\partial r_D}+\frac{u_Dv_D}{r_D}+\frac{v_D}{r_D}\frac{\partial v_D}{\partial \theta}+w_D\frac{\partial v_D}{\partial z_D}= \qquad (4.11)$$
$$-\frac{1}{\rho r_D}\frac{\partial p_D}{\partial \theta}+\nu\frac{\partial^2 v_D}{\partial z_D^2}-[\frac{\partial <(u^*v^*)>}{\partial r_D}$$
$$+\frac{<(2u^*v^*)>}{r_D}+\frac{\partial <(v^*w^*)>}{\partial z_D}+\frac{1}{r_D}\frac{\partial <(v^{*2})>}{\partial \theta}].$$

As in Smith & Cebeci[66] terms including u^{*2} are taken to be negligibly small and omitted, and we extend this now to include terms such as v^{*2} and u^*v^*[1] (which do not occur in the 2D case derived by Smith & Cebeci). This reduces the equations to

$$\frac{\partial u_D}{\partial t}+u_D\frac{\partial u_D}{\partial r_D}-\frac{v_D^2}{r_D}+\frac{v_D}{r_D}\frac{\partial u_D}{\partial \theta}+w_D\frac{\partial u_D}{\partial z_D}=$$
$$-\frac{1}{\rho}\frac{\partial p_D}{\partial r_D}+\nu\frac{\partial^2 u_D}{\partial z_D^2}-\frac{\partial <(u^*w^*)>}{\partial z_D} \qquad (4.12)$$

and

$$\frac{\partial v_D}{\partial t}+u_D\frac{\partial v_D}{\partial r_D}+\frac{u_Dv_D}{r_D}+\frac{v_D}{r_D}\frac{\partial v_D}{\partial \theta}+w_D\frac{\partial v_D}{\partial z_D}=$$
$$-\frac{1}{\rho r_D}\frac{\partial p_D}{\partial \theta}+\nu\frac{\partial^2 v_D}{\partial z_D^2}-\frac{\partial <(v^*w^*)>}{\partial z_D}. \qquad (4.13)$$

If an eddy viscosity term is now introduced so that

$$<u^*w^*> = -\nu_{tD}\frac{\partial u_D}{\partial z_D}, \qquad (4.14)$$

$$<v^*w^*> = -\nu_{tD}\frac{\partial v_D}{\partial z_D}, \qquad (4.15)$$

1. This is as a result of the assumption used by Cebeci & Smith, and herein, that the normal turbulent fluctuations dominate those in the direction of the free stream or surface velocity, as relevant. The extension of this idea to the current problem is an initial attempt to simplify (4.10) and (4.11).

we arrive at the Reynolds equations for a three-dimensional boundary layer in cylindrical polar co-ordinates without symmetry in θ,

$$\frac{\partial u_D}{\partial t} + u_D\frac{\partial u_D}{\partial r_D} - \frac{v_D^2}{r_D} + \frac{v_D}{r_D}\frac{\partial u_D}{\partial \theta} + w_D\frac{\partial u_D}{\partial z_D} = -\frac{1}{\rho}\frac{\partial p_D}{\partial r_D} + \nu\frac{\partial^2 u_D}{\partial z_D^2} + \frac{\partial}{\partial z_D}(\nu_{tD}\frac{\partial u_D}{\partial z_D}) \tag{4.16}$$

and

$$\frac{\partial v_D}{\partial t} + u_D\frac{\partial v_D}{\partial r_D} + \frac{u_D v_D}{r_D} + \frac{v_D}{r_D}\frac{\partial v_D}{\partial \theta} + w_D\frac{\partial v_D}{\partial z_D} = -\frac{1}{\rho r_D}\frac{\partial p_D}{\partial \theta} + \nu\frac{\partial^2 v_D}{\partial z_D^2} + \frac{\partial}{\partial z_D}(\nu_{tD}\frac{\partial v_D}{\partial z_D}). \tag{4.17}$$

The eddy viscosity is defined as in §3.2 for an axisymmetric surface and hence

$$\nu_{tD} = \begin{cases} k_2\omega r_D\delta_D^* & \text{for } z_D \geq z_{Dk}, \\ k_1^2 z_D^2[1-\exp(-\frac{z_D}{26\nu}(\frac{\tau_{WD}}{\rho})^{\frac{1}{2}})]^2|\frac{\partial u_D}{\partial z_D} + \frac{\partial v_D}{\partial z_D}| & \text{for } z_D \leq z_{Dk}, \end{cases} \tag{4.18}$$

where the displacement thickness is given by

$$\delta_D^* = \int_0^\infty \frac{v_D}{\omega r_D} dz_D. \tag{4.19}$$

Since these Reynolds equations will be applied to the flow generated by a rotor, it is convenient to transform them into the equivalent equations for the 3DTBL in cylindrical polar co-ordinates in a frame of reference which is rotating at angular velocity ω:

$$\frac{\partial u_D}{\partial t} + u_D\frac{\partial u_D}{\partial r_D} - \frac{v_D^2}{r_D} + \frac{v_D}{r_D}\frac{\partial u_D}{\partial \theta} + w_D\frac{\partial u_D}{\partial z_D} - 2\omega v_D - \omega^2 r_D = -\frac{1}{\rho}\frac{\partial p_D}{\partial r_D} + \nu\frac{\partial^2 u_D}{\partial z_D^2} + \frac{\partial}{\partial z_D}(\nu_{tD}\frac{\partial u_D}{\partial z_D}) \tag{4.20}$$

and

$$\frac{\partial v_D}{\partial t} + u_D\frac{\partial v_D}{\partial r_D} + \frac{u_D v_D}{r_D} + \frac{v_D}{r_D}\frac{\partial v_D}{\partial \theta} + w_D\frac{\partial v_D}{\partial z_D} + 2\omega u_D = -\frac{1}{\rho r_D}\frac{\partial p_D}{\partial \theta} + \nu\frac{\partial^2 v_D}{\partial z_D^2} + \frac{\partial}{\partial z_D}(\nu_{tD}\frac{\partial v_D}{\partial z_D}), \tag{4.21}$$

with the eddy viscosity defined as in (4.18), and continuity equation

$$\frac{1}{r_D}\frac{\partial(u_D r_D)}{\partial r_D} + \frac{1}{r_D}\frac{\partial v_D}{\partial \theta} + \frac{\partial w_D}{\partial z_D} = 0. \tag{4.22}$$

The displacement thickness δ_D^* is now defined as

$$\delta_D^* = \int_0^\infty \frac{\omega r_D + v_D}{\omega r_D} dz_D. \tag{4.23}$$

For convenience, and since we now only work in a rotating frame, we have used the same notation as for the stationary reference frame.

For the special case of a radially-defined surface, such as a cut-disc where the leading and trailing edges of each rotor are given by a constant value of θ, a similarity solution is applied and the transformation used earlier for the rotating disc problem is extended to the non-axisymmetric case by defining

$$\eta = \frac{z_D}{k_1^2 r_D}, \tag{4.24}$$

$$u_D = \omega r_D u = \omega r_D f'(\eta, \theta), \tag{4.25}$$

$$v_D = \omega r_D v = \omega r_D g'(\eta, \theta). \tag{4.26}$$

Here $'$ denotes partial differentiation with respect to η. Upon substitution into the continuity equation, this leads to the following form for the normal velocity

$$w_D = -\omega k_1^2 r_D (3f - \eta f' + \frac{\partial g}{\partial \theta}). \tag{4.27}$$

As before, the pressure gradient is taken to be zero, which is subsequently justified, and the Reynolds equations, assuming steadiness, now transform to

$$f'^2 - 3ff'' - g'^2 + g'\frac{\partial f'}{\partial \theta} - f''\frac{\partial g}{\partial \theta} - 2g' - 1 = \frac{1}{R}f''' + \tag{4.28}$$

$$\frac{\partial}{\partial \eta}\begin{cases} k_3 \delta^* f'' & \eta \geq \eta_k \\ \eta^2[1 - \exp(-\frac{R\eta u_\tau}{26})]^2 (f''^2 + g''^2)^{\frac{1}{2}} f'' & \eta \leq \eta_k \end{cases}$$

and

$$2f'g' - 3fg'' + g'\frac{\partial g'}{\partial \theta} - g''\frac{\partial g}{\partial \theta} + 2f' = \frac{1}{R}g''' + \tag{4.29}$$
$$\frac{\partial}{\partial \eta}\begin{cases} k_3\delta^* g'' & \eta \geq \eta_k \\ \eta^2[1-\exp(-\frac{R\eta u_\tau}{26})]^2(f''^2+g''^2)^{\frac{1}{2}}g'' & \eta \leq \eta_k \end{cases}$$

where

$$\delta^* = \int_0^\infty [1 + g'(\eta,\theta)]d\eta \tag{4.30}$$

and $R = k_1^4 R_r$ is the normalized rotational Reynolds number, $R_r = \frac{\omega r_D^2}{\nu}$ is the rotational Reynolds number and $u_{\tau D} = k_1^2 \omega r_D u_\tau$.

4.3 Boundary Layer Structure

Having determined the appropriate governing equations for the NATBL we now seek a model for its structure. As previously mentioned, we use the idea of a cut-disc, and its similarities with other, more well-established flows, in order to identify a suitable system for this current flow problem. It is assumed that a model can be devised which applies to a variety of surfaces (not just one specific to a cut-disc say) and which in particular works for a cut-disc regardless of its configuration. This means that the model must in some way at least resemble the two extreme cases of a cut-disc - the 2DTBL on a flat plate and the 3DTBL on a rotating disc. This in effect suggests two different height scales, namely $O(\epsilon)$ and $O(1)$, the heights of the two turbulent boundary layers mentioned above, and hence perhaps two different 'outer' layers (here outer layer is used to refer to any region of the boundary layer where viscosity is negligible). Further, Neish & Smith proposed two different laminar sublayers for the flat plate and the wake which is a requirement of the change in boundary conditions (and hence asymptotic behaviour) between the blade and the wake.

Combining these two notions we arrive at the key elements of the structure for the turbulent boundary layer on a non-axisymmetric body. The laminar sublayer on the surface is assumed to be the same as that on the rotating disc, except of course that θ-dependence must now be allowed, whilst in the wake this sublayer is no longer valid and it turns out that a larger sublayer is induced. An important feature which arises from having two different sublayers is that the asymptotic behaviour of each one as the outer layer is approached is different, and hence there must exist θ-dependence in the outer layer also, in order to match with the asymptotic forms in the two sublayers. However, in simply trying to extend the inertial-turbulent layer that exists on the rotating disc to the present scenario, it is found that this layer must be independent of θ, contradicting the necessary matching conditions with the two sublayers. Alternatively we could take the outer layer to be the same as that on a flat plate, but now the displacement thickness is found to grow monotonically with θ which is clearly not possible for a periodic solution to exist.

The resolution of these two contradictions lies in taking two different outer layers. Firstly we have an $O(1)$ outermost layer which is independent of θ and secondly a 'buffer' layer with height $O(\epsilon)$ which is located between the outermost region and the laminar sublayer. This buffer layer has θ dependence and is able to match with the two different sublayers, but in the overlap region with the outer layer, the asymptotic behaviour of the velocities in the buffer layer is independent of θ; hence there is no contradiction with the need to have an $O(1)$ thickness outer layer which is θ-independent. Thus we model the NATBL as being composed of three layers: the outer inertial-turbulent layer, the inner inertial-turbulent layer and the laminar sublayer, as can be seen in Figure 4.1, stressing that although there exists separate laminar sublayers in

the wake and on the surface, the two outer layers, in structure at least, are the same throughout the boundary layer.

This section now proceeds to examine each region in more detail, noting that in the outer and inner inertial-turbulent layers $\eta = O(1)$ and $O(\epsilon)$ respectively and so the exponential term in the lower form of the eddy viscosity is negligibly small.

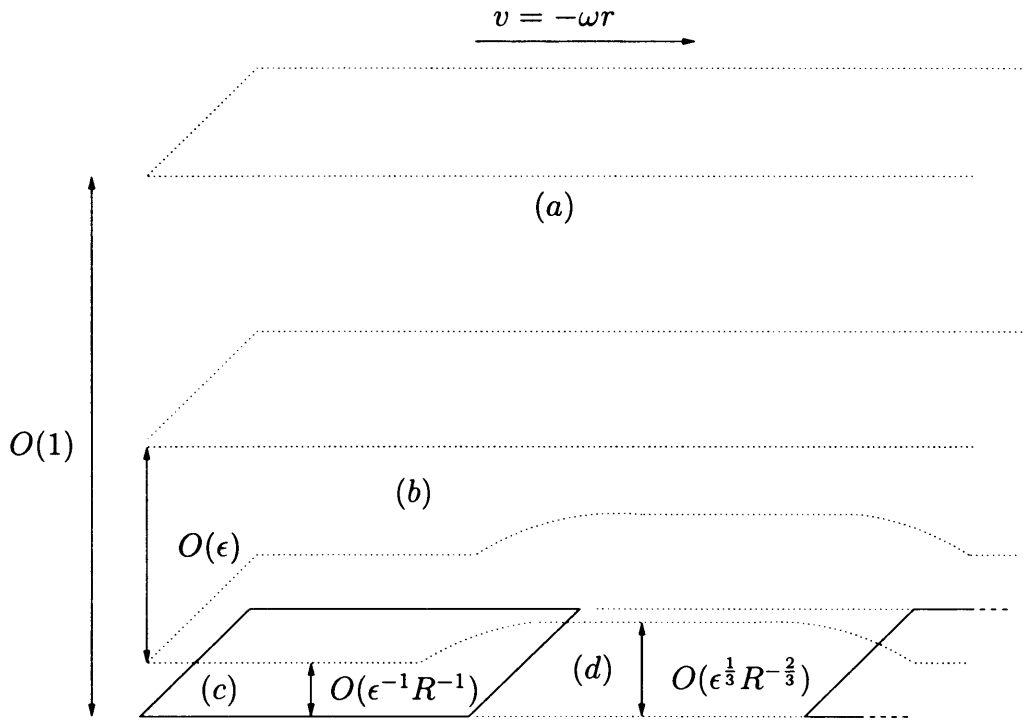

Figure 4.1: *The structure of the non-axisymmetric turbulent boundary layer with wakes. Again the relative heights of the four regions - the OITL, the IITL, the LSB and the LSW, which are labelled* $(a) - (d)$ *respectively - are not drawn to scale for clarity.* The specific details of each region are described subsequently.

4.3.1 Outer Inertial-Turbulent Layer

As with the ITL on the rotating disc, in the outer inertial-turbulent layer (OITL) we take $\eta = \eta_1 + ...$ and suppose that the velocities differ from the free stream value by only a small amount - $O(\epsilon)$. Since η_1 and θ are $O(1)$ we thus take $f' = \epsilon f_1'(\eta) + ...$ and $g' = -1 + \epsilon g_1'(\eta) + ...$ and to leading order we therefore have

$$\frac{\partial f_1'}{\partial \theta} = \frac{\partial g_1'}{\partial \theta} = 0. \tag{4.31}$$

Hence to this order the flow is independent of θ as previously stated. At the next order we have

$$f_1'^2 - 3f_1 f_1'' - g_1'^2 = \frac{\partial}{\partial \eta_1}(\nu_{t1} f_1'') \tag{4.32}$$

and

$$2f_1' g_1' - 3f_1 g_1'' = \frac{\partial}{\partial \eta_1}(\nu_{t1} g_1''), \tag{4.33}$$

where the eddy viscosity is now

$$\nu_{t1} = \begin{cases} k_3 g_{1\infty} & \text{for } \eta \geq \eta_{1k}, \\ \eta_1^2 (f_1''^2 + g_1''^2)^{\frac{1}{2}} & \text{for } \eta \leq \eta_{1k}. \end{cases} \tag{4.34}$$

As might be expected, these equations are the same as those for the ITL on a rotating disc. Thus, as $\eta_1 \to 0$, the asymptote $g_1' \sim \ln \eta_1$ holds again. In fact we have

$$f_1' \sim C_1 + A_1 \eta_1 (\ln \eta_1)^2 \tag{4.35}$$

$$g_1' \sim C_2 + A_2 \ln \eta_1 \tag{4.36}$$

as $\eta_1 \to 0$, where C_1, C_2, A_1 and A_2 are constants.

4.3.2 Inner Inertial-Turbulent Layer

In the inner inertial-turbulent layer (IITL) we take $\eta = \epsilon\eta_2 + \ldots$. The asymptotic behaviour in the OITL as $\eta_1 \to 0$ implies that, as the two inertial-turbulent layers overlap, $f' \approx \epsilon C_1 + O(\epsilon^2(\ln\epsilon)^2)$ and $g' \approx -1 + O(\epsilon\ln\epsilon)$. Thus in the IITL the expansions

$$f' = \epsilon C_1 + \epsilon^2(\ln\epsilon)^2 f_2' + \epsilon^2 F_2' + \ldots, \tag{4.37}$$

$$g' = -1 - a^{\frac{1}{2}}\epsilon\ln\epsilon - \epsilon g_2' + \ldots, \tag{4.38}$$

apply (for convenience the perturbation expansion for g' defined above is designed to ensure that $g_2'' \geq 0$ so that $|g_2''| = g_2''$) and from (4.29) and (4.30) lead to

$$-a - \frac{\partial f_2'}{\partial\theta} = \frac{\partial}{\partial\eta_2}(\eta_2^2 g_2'' f_2'') \tag{4.39}$$

and

$$-\frac{\partial g_2'}{\partial\theta} = \frac{\partial}{\partial\eta_2}(\eta_2^2 g_2''^2). \tag{4.40}$$

Here a is the solidity of the surface (defined to be the ratio of the area of all the blades to the total blade and wake area) and the coefficient of the $O(\epsilon\ln\epsilon)$ term in the expansion for g' comes from consideration of the matching conditions in §4.3.5. It is worth mentioning in passing that, if only the IITL is present, then $f_2' \to 0$ and $g_2' \to 0$ as $\eta_2 \to \infty$ and hence, if we still have $f_2' \sim -\eta_2$ and $g_2' \sim \ln\eta_2$ as $\eta_2 \to 0$, (4.40) yields

$$\frac{\partial\delta^*}{\partial\theta} = a \tag{4.41}$$

on the blade surface, and

$$\frac{\partial\delta^*}{\partial\theta} = 0 \tag{4.42}$$

in the wakes. Hence on the surface $\delta^* = a\theta$, which implies that the displacement thickness grows on the surface yet remains constant in the wakes. This

is the same as Neish & Smith found for the displacement thickness on a flat plate, and leads to an ever-increasing displacement thickness; that, as discussed earlier, cannot be correct physically and necessitates the existence of the OITL.

We have also included an $O(\epsilon^2)$ perturbation in the form of the radial velocity. This is required to balance the $O(\epsilon)$ constant term in the expansion for f' which is itself necessary because the constant term in the asymptotic form for $f_1'(\eta_1)$ in the OITL needs to be matched with the velocity in the IITL, yet cannot be allowed to persist throughout the boundary layer as it would violate the requirement that u, and hence f', be zero at the surface. Thus higher order asymptotic logarithmic behaviour is required to balance the constant term ϵC_1 and this also necessitates an $O(\epsilon^2)$ perturbation to the radial velocity in both the laminar sublayers. We now have

$$f_2' \sim C_3 + A_3\eta_2, \tag{4.43}$$

$$g_2' \sim C_4 + A_4 \ln \eta_2, \tag{4.44}$$

as $\eta_2 \to \infty$, while

$$f_2' \sim C_5 + A_5\eta_2, \tag{4.45}$$

$$g_2' \sim C_5 + A_6 \ln \eta_2, \tag{4.46}$$

as $\eta_2 \to 0$ over the blade and

$$f_2' \sim \overline{f_4} + A_9(\theta)\eta_2{}^{\frac{1}{2}}, \tag{4.47}$$

$$g_2' \sim -\overline{g_4} + A_{10}(\theta)\eta_2{}^{\frac{1}{2}}, \tag{4.48}$$

in the wake, where $\overline{f_4}$ and $\overline{g_4}$ are arbitrary functions of θ.

The asymptotic form in the wake is based on the work of Neish & Smith and comes from consideration of the laminar sublayer in the wake, which we

examine in §4.3.4. Finally, and in light of the logarithmic matching of §2.5.2 and §3.4.2, we also require

$$F_2' \sim B_1 + C_1 \ln \eta_2 \tag{4.49}$$

and

$$F_2' \sim B_2 + \frac{3C_1}{2} \ln \eta_2 \tag{4.50}$$

as $\eta_2 \longrightarrow 0$ over the blade and wake respectively.

4.3.3 Laminar Sublayer on the Blade

The laminar sublayer on the blade (LSB) is taken to be the same as that on the rotating disc, and hence the vertical length scale has $\eta = \epsilon^{-1}R^{-1}\eta_3 + ...$, with

$$f' = \epsilon^2 F_3' + \epsilon^{-2}R^{-1} f_3' + ..., \tag{4.51}$$

$$g' = \epsilon g_3' + ..., \tag{4.52}$$

and as a consequence, the governing equations are now

$$-1 = f_3''' - \frac{\partial}{\partial \eta_3}(\eta_3^2[1 - \exp(-\frac{\eta_3}{26\epsilon}u_\tau)]^2 g_3'' f_3'') \tag{4.53}$$

and

$$0 = g_3''' - \frac{\partial}{\partial \eta_3}(\eta_3^2[1 - \exp(-\frac{\eta_3}{26\epsilon}u_\tau)]^2 g_3''^2). \tag{4.54}$$

These equations are the same as (3.27) and (3.28) for the LS on a rotating disc and hence we have the following asymptotic forms

$$f_3' \sim C_7 + A_7\eta_3, \tag{4.55}$$

$$g_3' \sim C_8 + A_8 \ln \eta_3, \tag{4.56}$$

$$F_3' \sim B_2 + C_1 \ln \eta_3, \tag{4.57}$$

as $\eta_3 \rightarrow \infty$. Before proceeding to examine the laminar sublayer in the wake, we note that (4.53) is not the leading order radial momentum equation, which is actually

$$0 = F_3''' - \frac{\partial}{\partial \eta_3}(\eta_3^2[1 - \exp(-\frac{\eta_3}{26\epsilon}u_\tau)]^2 g_3'' F_3'') \tag{4.58}$$

but that since in the overlap region with the IITL, f_3' dominates over F_3' (which is only required in order to balance the term ϵC_1 in the expansion for f' in the IITL) and since f_3' matches with the leading order perturbation of f' in the IITL, it is the behaviour of f_3' which is ultimately of most importance to us.

4.3.4 Laminar Sublayer in the Wake

Now the work of Neish & Smith, concerning the wake behind a flat plate in a uniform stream, is extended to the present case. Thus in the IITL we take the wake boundary condition to be of the form

$$g_2' \propto \eta_2^{\frac{1}{2}} \tag{4.59}$$

as $\eta_2 \rightarrow 0$. The boundary condition (4.59) is necessary for a zero shear stress condition to be achieved within the laminar sublayer in the wake (LSW), and ensuring the turbulent-viscous balance,

$$\frac{\partial v_D}{\partial z_D} \sim z_D^2 (\frac{\partial v_D}{\partial z_D})^2 \tag{4.60}$$

as $z_D \rightarrow 0$, (4.59) requires the following height scaling for the LSW; $\eta = \epsilon^{-\frac{1}{3}} R^{-\frac{2}{3}} \eta_4$. Hence, to satisfy the asymptotic behaviour indicated in (4.59) and to balance the Reynolds equations, we must take

$$f' = \epsilon^2 F_4' + \epsilon^2 (\ln \epsilon)^2 \overline{f_4}(\theta) + \epsilon^{\frac{4}{3}} R^{-\frac{1}{3}} (\ln \epsilon)^2 f_4' + ..., \tag{4.61}$$

$$g' = -1 - a^{\frac{1}{2}} \epsilon \ln \epsilon + \epsilon \overline{g_4}(\theta) + \epsilon^{\frac{1}{3}} R^{-\frac{1}{3}} g_4' + ..., \tag{4.62}$$

leading to the resultant governing equations,

$$-a - \frac{\partial \overline{f_4}}{\partial \theta} = f_4''' + \frac{\partial}{\partial \eta_4}(\eta_4{}^2[1 - \exp(-\frac{\eta_4 R^{\frac{1}{3}}}{26\epsilon^{\frac{1}{3}}}u_\tau)]^2 g_4'' f_4'') \tag{4.63}$$

and

$$-\frac{\partial \overline{g_4}}{\partial \theta} = g_4''' + \frac{\partial}{\partial \eta_4}(\eta_4{}^2[1 - \exp(-\frac{\eta_4 R^{\frac{1}{3}}}{26\epsilon^{\frac{1}{3}}}u_\tau)]^2 g_4''^2) \tag{4.64}$$

with the matching conditions

$$f_4' \sim C_{11} + A_{11}(\theta)\eta_4{}^{\frac{1}{2}}, \tag{4.65}$$

$$g_4' \sim C_{12} + A_{12}(\theta)\eta_4{}^{\frac{1}{2}}, \tag{4.66}$$

$$F_2' \sim B_3 + \frac{3C_1}{2}\ln \eta_4, \tag{4.67}$$

as $\eta_4 \to \infty$.

4.3.5 Matching

In the matching of the asymptotic forms described above we limit consideration to leading order terms only and hence do not always check the matching of some small terms between layers. This is done for both clarity and expediency, as to completely match every term in each asymptotic expansion would require a myriad of terms included in the perturbation expansions for each layer. Instead, only the leading order terms and those higher order terms which are important in the expansions are shown to be matched and it is understood that other higher order terms can be matched by the inclusion of additional small terms in the expansions described previously for each layer.

Due to the complexities which arise in matching between the four layers the exact details of the matching process is somewhat laborious and so is included in Appendix B for convenience. Instead we now simply present the

main product of the matching process, namely the constant coefficients of the following asymptotic forms:

$$f_1' \sim -a^{\frac{1}{2}}\eta_1(\ln\eta_1)^2, \tag{4.68}$$

$$g_1' \sim -a^{\frac{1}{2}}\ln\eta_1, \tag{4.69}$$

as $\eta_1 \to 0$;

$$f_2' \sim -a^{\frac{1}{2}}\eta_2, \tag{4.70}$$

$$g_2' \sim a^{\frac{1}{2}}\ln\eta_2, \tag{4.71}$$

as $\eta_2 \to \infty$;

$$f_2' \sim -a\eta_2, \tag{4.72}$$

$$g_2' \sim \ln\eta_2, \tag{4.73}$$

as $\eta_2 \to 0$ over the blade;

$$f_2' \sim \overline{f_4} + A_9(\theta)\eta_2{}^{\frac{1}{2}}, \tag{4.74}$$

$$g_2' \sim -\overline{g_4} + A_{10}(\theta)\eta_2{}^{\frac{1}{2}}. \tag{4.75}$$

as $\eta_2 \to 0$ in the wake;

$$f_3' \sim -\eta_3, \tag{4.76}$$

$$g_3' \sim -\ln\eta_3, \tag{4.77}$$

as $\eta_3 \to \infty$; and

$$f_4' \sim A_{11}(\theta)\eta_4{}^{\frac{1}{2}}, \tag{4.78}$$

$$g_4' \sim A_{12}(\theta)\eta_4{}^{\frac{1}{2}}, \tag{4.79}$$

as $\eta_4 \to \infty$. The functions A_i, with $i = 9, 10, 11$ or 12, are given by the, as yet, unknown wake functions $\overline{f_4}$ and $\overline{g_4}$, by means of $(B.11)$ and $(B.14)$. We now

note an important aspect of the matching which is that we have not imposed the condition $A_5 = A_7$. Instead our matching analysis implies that $A_5 = -a$ and $A_7 = -1$. This discrepancy arises because the forcing inertial terms in the radial momentum equations for the IITL and the LSB are $-a$ and -1 respectively, whilst the coefficient of the asymptotic (logarithmic) form for g_2' and g_3' is fixed equal to unity in order to match with the free stream velocity. We now suppose that in the two layers the asymptotic behaviour is as we have determined but that in reality, where the layers overlap, the coefficient of the asymptotic form varies smoothly from -1 to $-a$. This comes from consideration of the forcing inertial terms.

In the LSB, to leading order, the inertial terms reduce to -1 since all the velocity components are taken to be small. However as $\eta_3 \to \infty$ the azimuthal velocity increases and eventually $g' = O(1)$ and since, to leading order in the IITL, $g' = -1$ we might suppose that in the overlap between the two regions $g' = \gamma + O(\epsilon)$ where γ varies continuously between 0 and -1 as we pass from the LSB into the IITL. This then leads to the following radial momentum equation for this overlap region

$$-\gamma^2 - 2\gamma - 1 = f_3''' - \frac{\partial}{\partial \eta_3}(\eta_3^2[1 - \exp(-\frac{\eta_3}{26\epsilon}u_\tau)]^2 g_3'' f_3'') \tag{4.80}$$

and hence the asymptotic form

$$f_3' \sim -(\gamma + 1)^2 \eta_3. \tag{4.81}$$

Thus the coefficient of the asymptotic form increases where the layers overlap. Note that as $(\gamma + 1)^2$ becomes small, as $\gamma \to -1$, eventually the inertial terms in the radial momentum equation for the LSB become negligible in comparison to the viscous and turbulent terms and so a new structure is required, namely that of the IITL. Hence $\gamma \neq -1$ in the LSB and so the coefficient of the

asymptote in (4.81) cannot become zero. Instead the asymptote eventually matches that of the IITL, namely

$$f_3' \sim -a\eta_2. \tag{4.82}$$

The structure of the NATBL outlined above is consistent and satisfies the two main conditions referred to earlier - that the boundary layer should in some way resemble that on a rotating disc, and that a periodic solution is possible. It also allows for an examination of the NATBL where the entire boundary layer can be modelled together and not just as a set of isolated blades.

Obviously it is necessary to have more than just a consistent structure - for instance, there may exist a range of alternative boundary layer structures which are valid - so it is also important that this model can be successfully applied to solving physical systems. To that end it is applied to the problem of the flow generated by a cut-disc (Chapter 5) and in Appendix B a linear solution to the flow in the IITL is examined. First though a general solution to the flow in the NATBL is considered.

4.4 General Flow Solution in the NATBL

We take the boundary layer structure to be as described previously, with a θ-independent outer inertial-turbulent layer, a thinner inner inertial-turbulent layer and different laminar sublayers over the blade and in the wake, as indicated in Figure 4.1. Each of these layers can be considered in turn for a specific flow problem but we first note that the LSB on a cut-disc is the same as that on a rotating disc (regardless of the precise details of the NATBL) and hence the analytical solution derived in §3.5 holds here also. For this reason no further consideration is given to the LSB on a non-axisymmetric surface.

In contrast, the LSW is unlike any boundary layer region we have examined so far, and whereas in the LSB a simple analytical solution is possible, in the LSW it is not, due to the presence of the unknown wake functions $\overline{f}_4(\theta)$ and $\overline{g}_4(\theta)$. These functions can be determined from the asymptotic behaviour of the velocity in the IITL through (4.47) and (4.48) but since $\overline{f}_4(\theta)$ and $\overline{g}_4(\theta)$ are expected to vary with each non-axisymmetric body, such calculations would need to be repeated for each configuration of interest. Accurate determination of $\overline{f}_4(\theta)$ and $\overline{g}_4(\theta)$, and hence the velocity in the sublayer, is possible but since the LSW is comparatively small relative to the two inertial-turbulent layers, it is not considered necessary to determine the detailed LSW solution and instead we proceed to examine the two thicker inertial-turbulent layers.

Since the flow in the IITL is dependent on the exact configuration of the rotating surface involved, no general solution can be obtained and instead a solution specific to the problem of a rotating cut-disc is considered in Chapter 5. In contrast, however, the OITL can be classified simply in terms of the disc solidity and so we are now able to provide a solution for the flow in the OITL for any given surface simply with knowledge of its solidity.

4.4.1 Solution in the Outer Inertial-Turbulent Layer on a Body without Axisymmetry

In this region $\eta = \eta_1 + ...$, $u = f' = \epsilon f_1'(\eta) + ...$ and $v = g' = -1 + \epsilon g_1'(\eta) + ...$, so we have

$$f_1'^2 - 3f_1 f_1'' - g_1'^2 = \frac{\partial}{\partial \eta_1}(\nu_{t1} f_1'') \tag{4.83}$$

and

$$2f_1' g_1' - 3f_1 g_1'' = \frac{\partial}{\partial \eta_1}(\nu_{t1} g_1''), \tag{4.84}$$

as before, with the eddy viscosity given by

$$\nu_{t1} = \begin{cases} k_3 g_{1\infty} & \text{for } \eta \geq \eta_{1k}, \\ \eta_1^2 (f_1''^2 + g_1''^2)^{\frac{1}{2}} & \text{for } \eta \leq \eta_{1k}, \end{cases} \tag{4.85}$$

and boundary conditions

$$f_1'(\infty) = 0, \tag{4.86}$$

$$g_1'(\infty) = 0, \tag{4.87}$$

$$f_1(0) = 0, \tag{4.88}$$

$$g_1(0) = 0, \tag{4.89}$$

$$f_1'(\eta_1 \to 0) \sim C_1 - a^{\frac{1}{2}} \eta_1 (\ln \eta_1)^2, \tag{4.90}$$

$$g_1'(\eta_1 \to 0) \sim C_2 - a^{\frac{1}{2}} \ln \eta_1, \tag{4.91}$$

along with the requirement of continuity of $f_1, f_1', f_1'', g_1, g_1', g_1''$ and ν_{t1} at $\eta_1 = \eta_{1k}$.

This is the same numerical problem as for the ITL on the rotating disc but with slightly different coefficients for the asymptotic conditions. Hence we might expect the unknown parameters, $g_{1\infty}, C_1$ and C_2 to differ from the rotating disc case, as well as for varying values of a. In fact, we find that $(g_{1\infty}, C_1, C_2) = a^{\frac{1}{2}}(g_{1\infty rot}, C_{1rot}, C_{2rot})$, where s_{rot} denotes the already known value of a parameter s in the rotating disc problem. Further, we find that if we define

$$f_1 = a^{\frac{1}{2}} g_{1\infty} F, \tag{4.92}$$

$$g_1 = a^{\frac{1}{2}} g_{1\infty} G, \tag{4.93}$$

$$\eta_1 = \eta_{1k} t, \tag{4.94}$$

we have exactly the same formulation (including the asymptotic conditions)

as in the rotating disc problem, (3.63) and (3.64), and so we have the potentially useful result

$$\underline{\mathbf{u}} = \mathbf{a}^{\frac{1}{2}}\underline{\mathbf{u}}_{\mathbf{rot}} \tag{4.95}$$

where $\underline{\mathbf{u}}$ is the velocity in the OITL and $\underline{\mathbf{u}}_{\mathbf{rot}}$ is the equivalent velocity in the ITL on the rotating disc. This means that the previous results for a rotating disc can be used to determine the following velocity profiles for various values of the parameter a.

Figure 4.2 shows the radial, azimuthal and normal velocities for selected values of a. (4.95) shows how, as we might expect, the velocities in the OITL decrease as $a \to 0$, and this is also apparent from Figure 4.2. Effectively the OITL has been reduced, to leading order at least, to the ITL on a rotating disc with a reduced rate of rotation (now only $a^{\frac{1}{2}}\omega$). An interesting feature of these results is that the magnitude of the normal velocity is significantly larger than that of the radial velocity. This is an occurrence which is noted by QinetiQ in their practical work on helicopters.

Whilst it is fortunate that the OITL solution, to leading order at least, is expressible purely in terms of the disc solidity and the solution to the rotating disc problem, this poses an interesting question: how does the inherent θ-dependence of the physical surface permeate (if indeed it does) the θ-independent OITL and even the outer inviscid region? This question is now considered.

4.5 θ-dependence in the Boundary Layer

Since the outer inertial-turbulent layer is independent of θ we now consider how the inherent θ-dependence of the non-axisymmetric body passes from the inner inertial-turbulent layer (IITL) through the OITL and into the outer inviscid

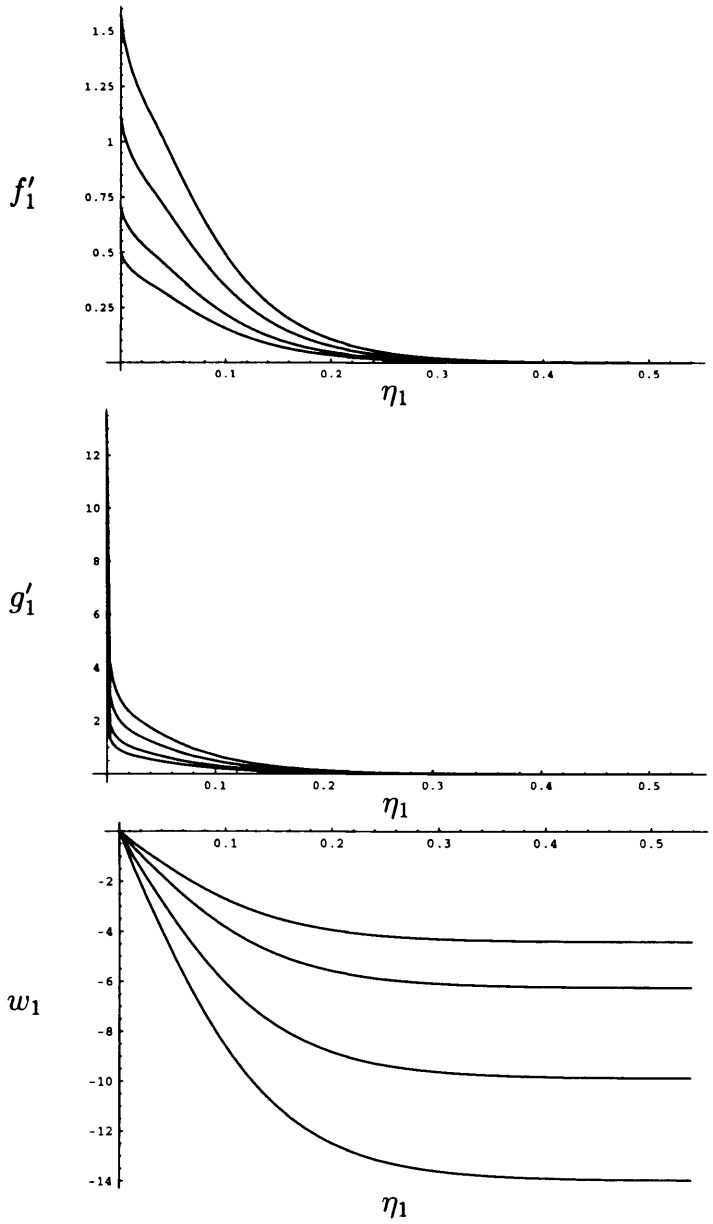

Figure 4.2: *Radial velocity profile for* $f_1'(\eta)$ *(top), azimuthal velocity profile for* $g_1'(\eta)$ *(middle) and normal velocity profile for* w_1 *(bottom) in the OITL for varying values of the disc solidity* a*. For the radial and azimuthal velocities, from top to bottom the curves correspond to* $a = 1; 0.5; 0.2;$ *and* 0.1*. For the normal velocity this order is reversed.*

region. We recall that in the IITL as $z_2 \to \infty$ we have

$$v_2 \sim a^{\frac{1}{2}} \ln z_2. \tag{4.96}$$

Now let w_2 denote the non-dimensional normal velocity component in the IITL. Then in the IITL we have quasi 2D flow with continuity equation

$$\frac{1}{r}\frac{\partial v_2}{\partial \theta} + \frac{\partial w_2}{\partial z_2} = 0, \tag{4.97}$$

since it is possible to consider the radius to be just a parameter of the flow (as it only appears explicitly and not as a derivative); hence a stream function can be defined by

$$\frac{\partial \varphi}{\partial z_2} = v_2 \tag{4.98}$$

and, from (4.96),

$$\varphi \sim a^{\frac{1}{2}}(z_2 \ln z_2 - z_2) + B(\theta) \tag{4.99}$$

as $z_2 \to \infty$, where $B(\theta)$ is an unknown function of θ. This then implies, from the continuity equation, the following form for the normal velocity,

$$w_2 \sim -\frac{dB}{d\theta}, \tag{4.100}$$

as $z_2 \to \infty$, since by definition of the stream function

$$w_2 = -\frac{\partial \varphi}{\partial \theta}. \tag{4.101}$$

Now considering the relative magnitudes of the terms on the right hand side of (4.99), the ratio of the two terms on entry to the OITL is approximately

$$\frac{B}{z_2} \sim O(\epsilon), \tag{4.102}$$

since $z_2 \to O(\epsilon^{-1})$. The terms in the IITL which are dependent on θ and which continue into the OITL are therefore smaller in order of magnitude by a factor

ϵ. Accordingly we suppose that in the OITL the flow is only independent of θ to leading order and that, to understand how the physical dependence on θ appears and is linked to the outer inviscid region, we need to consider these higher order terms. As such we consider the flow in the OITL to be of the form

$$\underline{\mathbf{u}} = \underline{\mathbf{u}}_{freestream} + \epsilon\underline{\mathbf{u}}_{disc1} + \epsilon^2\underline{\mathbf{u}}_{disc2} + \epsilon^2\underline{\mathbf{u}}_{\theta} + ... \tag{4.103}$$

where $\underline{\mathbf{u}}_{freestream}$, $\underline{\mathbf{u}}_{disc1}$, $\underline{\mathbf{u}}_{disc2}$ and $\underline{\mathbf{u}}_{\theta}$ are respectively the free stream velocity, the leading and second-order solutions for a free rotating disc, and the θ-dependent perturbations, and next we must examine how this expansion works in the Reynolds equations.

4.5.1 Outer Inertial-Turbulent Layer

First, from §4.2, the appropriate steady dimensional Reynolds equations with pressure gradients are recalled:

$$u\frac{\partial u}{\partial r} - \frac{v^2}{r} + \frac{v}{r}\frac{\partial u}{\partial \theta} + w\frac{\partial u}{\partial z} - 2\omega v - \omega^2 r = -\frac{1}{\rho}\frac{\partial p}{\partial r} + \frac{\partial}{\partial z}(\nu_t\frac{\partial u}{\partial z}) \tag{4.104}$$

and

$$u\frac{\partial v}{\partial r} + \frac{uv}{r} + \frac{v}{r}\frac{\partial v}{\partial \theta} + w\frac{\partial v}{\partial z} + 2\omega u = -\frac{1}{\rho r}\frac{\partial p}{\partial \theta} + \frac{\partial}{\partial z}(\nu_t\frac{\partial v}{\partial z}), \tag{4.105}$$

with

$$\nu_t = \begin{cases} k_2\omega r\delta^* & \text{for } z \geq z_k, \\ k_1^2 z^2[(\frac{\partial u}{\partial z})^2 + (\frac{\partial v}{\partial z})^2]^{\frac{1}{2}} & \text{for } z \leq z_k, \end{cases} \tag{4.106}$$

and continuity equation

$$\frac{1}{r}\frac{\partial (ur)}{\partial r} + \frac{1}{r}\frac{\partial v}{\partial \theta} + \frac{\partial w}{\partial z} = 0. \tag{4.107}$$

The subscript D has been dropped for convenience, whilst the viscous term is negligible here and so is omitted. Despite stating in §4.2 that we can take

the (leading order) pressure term to be zero pressure gradient terms are now retained; they are balanced consistently by θ-dependent terms and do not alter the governing equations derived in §4.2 (and so they were omitted for convenience). This is explained in further detail in §4.5.3. Taking

$$u = \epsilon u_1 + \epsilon^2 u_2 + \epsilon^2 u_2^* + \epsilon^3 u_3 + ..., \tag{4.108}$$

$$v = -\omega r + \epsilon v_1 + \epsilon^2 v_2 + \epsilon^2 v_2^* + \epsilon^3 v_3 + ..., \tag{4.109}$$

$$w = \epsilon w_1 + \epsilon^2 w_2 + \epsilon^2 w_2^* + \epsilon^3 w_3 + ..., \tag{4.110}$$

$$p = \epsilon^2 p_1 + \epsilon^3 p_2 + ..., \tag{4.111}$$

$$\delta^* = \epsilon \delta_1^* + \epsilon^2 \delta_2^* + \epsilon^3 \delta_3^* + ..., \tag{4.112}$$

where velocity terms denoted with an asterisk correspond to the θ-dependent potential terms whilst all other terms are independent of θ. Substitution into (4.104) - (4.106) yields

$$u_1 \frac{\partial u_1}{\partial r} - \omega \frac{\partial u_2^*}{\partial \theta} + w_1 \frac{\partial u_1}{\partial z} - \frac{v_1^2}{r} = -\frac{1}{\rho}\frac{\partial p_1}{\partial r} + \frac{\partial}{\partial z}\begin{cases} k_3 \omega r \delta_1^* \frac{\partial u_1}{\partial z} \\ z^2 \left|\frac{\partial u_1}{\partial z} + \frac{\partial v_1}{\partial z}\right| \frac{\partial u_1}{\partial z} \end{cases} \tag{4.113}$$

and

$$u_1 \frac{\partial v_1}{\partial r} - \omega \frac{\partial v_2^*}{\partial \theta} + w_1 \frac{\partial v_1}{\partial z} + \frac{u_1 v_1}{r} = -\frac{1}{\rho r}\frac{\partial p_1}{\partial \theta} + \frac{\partial}{\partial z}\begin{cases} k_3 \omega r \delta_1^* \frac{\partial v_1}{\partial z} \\ z^2 \left|\frac{\partial u_1}{\partial z} + \frac{\partial v_1}{\partial z}\right| \frac{\partial v_1}{\partial z} \end{cases} \tag{4.114}$$

Since u_1, v_1 and w_1 are independent of θ these equations can be separated into two sets: one consisting of terms which are independent of θ - the leading order equations for the OITL - and the other consisting of those terms which involve θ, namely

$$-\omega \frac{\partial u_2^*}{\partial \theta} = -\frac{1}{\rho}\frac{\partial p_1}{\partial r}, \tag{4.115}$$

and

$$-\omega \frac{\partial v_2^*}{\partial \theta} = -\frac{1}{\rho r}\frac{\partial p_1}{\partial \theta}. \tag{4.116}$$

Since the pressure is independent of z, p_1 is independent of z and so from (4.115) and (4.116), we have

$$\frac{\partial u_2^*}{\partial z} = \frac{\partial v_2^*}{\partial z} = 0, \tag{4.117}$$

which is to be expected for the potential terms in line with (4.100). Thus to the next lowest order we have

$$\begin{aligned} &w_2\frac{\partial u_1}{\partial z} + u_1\frac{\partial u_2}{\partial r} + u_2\frac{\partial u_1}{\partial r} + \frac{v_1}{r}\frac{\partial u_2}{\partial \theta} - \frac{2v_1v_2}{r} \\ &+(w_2^*\frac{\partial u_1}{\partial z} - \omega\frac{\partial u_3}{\partial \theta} + u_1\frac{\partial u_2^*}{\partial r} + u_2^*\frac{\partial u_1}{\partial r} + \frac{v_1}{r}\frac{\partial u_2^*}{\partial \theta} - \frac{2v_1v_2^*}{r}) = -\frac{1}{\rho}\frac{\partial p_2}{\partial r} + \\ &\frac{\partial}{\partial z}\begin{cases} k_3\omega r\delta_1^*\frac{\partial u_2}{\partial z} + k_3\omega r\delta_2^*\frac{\partial u_1}{\partial z} & \text{for } z \geq z_k \\ k_1^2z^2[|\frac{\partial u_1}{\partial z} + \frac{\partial v_1}{\partial z}|\frac{\partial u_2}{\partial z} + \frac{[\frac{\partial u_1}{\partial z}\frac{\partial u_2}{\partial z} + \frac{\partial v_1}{\partial z}\frac{\partial v_2}{\partial z}]}{|\frac{\partial u_1}{\partial z} + \frac{\partial v_1}{\partial z}|}\frac{\partial u_1}{\partial z}] & \text{for } z \leq z_k \end{cases} \end{aligned} \tag{4.118}$$

and

$$\begin{aligned} &w_2\frac{\partial v_1}{\partial z} + u_1\frac{\partial v_2}{\partial r} + u_2\frac{\partial v_1}{\partial r} + \frac{v_1}{r}\frac{\partial v_2}{\partial \theta} + \frac{v_1u_2}{r} + \frac{v_2u_1}{r} \\ &+(w_2^*\frac{\partial v_1}{\partial z} - \omega\frac{\partial v_3}{\partial \theta} + u_1\frac{\partial v_2^*}{\partial r} + u_2^*\frac{\partial v_1}{\partial r} + \frac{v_1}{r}\frac{\partial v_2^*}{\partial \theta} + \frac{v_1u_2^*}{r} + \frac{v_2^*u_1}{r}) \\ &= -\frac{1}{\rho r}\frac{\partial p_2}{\partial \theta} + \\ &\frac{\partial}{\partial z}\begin{cases} k_3\omega r\delta_2^*\frac{\partial v_1}{\partial z} + k_3\omega r\delta_1^*\frac{\partial v_2}{\partial z} & \text{for } z \geq z_k \\ k_1^2z^2[|\frac{\partial u_1}{\partial z} + \frac{\partial v_1}{\partial z}|\frac{\partial v_2}{\partial z} + \frac{[\frac{\partial u_1}{\partial z}\frac{\partial u_2}{\partial z} + \frac{\partial v_1}{\partial z}\frac{\partial v_2}{\partial z}]}{|\frac{\partial u_1}{\partial z} + \frac{\partial v_1}{\partial z}|}\frac{\partial v_1}{\partial z}] & \text{for } z \leq z_k. \end{cases} \end{aligned} \tag{4.119}$$

The bracketed terms are those which involve θ and balance the pressure gradient term and hence both (4.118) and (4.119) can be considered as being composed of two parts - an equation for the potential-pressure balance and one for the second order free disc equation. Also, since (4.100) implies that

$$\frac{\partial w_2^*}{\partial z} = 0, \tag{4.120}$$

we have the following form for the velocity perturbations

$$u = \epsilon u_1(r,z) + \epsilon^2 u_2(r,z) + \epsilon^2 u_2^*(r,\theta) + \epsilon^3 u_3(r,\theta,z) + ..., \quad (4.121)$$

$$v = -\omega r + \epsilon v_1(r,z) + \epsilon^2 v_2(r,z) + \epsilon^2 v_2^*(r,\theta) \quad (4.122)$$

$$+\epsilon^3 v_3(r,\theta,z) + ...,$$

$$w = \epsilon w_1(r,z) + \epsilon^2 w_2(r,z) + \epsilon^2 w_2^*(r,\theta) + \epsilon^3 w_3(r,\theta,z) + ..., \quad (4.123)$$

for the flow in the OITL.

4.5.2 Inner Inertial-Turbulent Layer

The extra perturbations necessary to include θ-dependence in the OITL also necessitate additional terms in the expansions for the velocities in the IITL in order that the velocities can be matched. Hence we take (4.104) - (4.106) and let

$$u = \epsilon\omega r C + \epsilon^2(\ln\epsilon)^2 u_1 + \epsilon^2(\ln\epsilon)u_2 + \epsilon^2 u_3 + ..., \quad (4.124)$$

$$v = -\omega r - a^{\frac{1}{2}}\epsilon(\ln\epsilon)\omega r - \epsilon v_1 + \epsilon^2(\ln\epsilon)^2 v_2 + \epsilon^2 \ln\epsilon v_3 \quad (4.125)$$

$$+\epsilon^2 v_4 + ...,$$

$$w = \epsilon^2(\ln\epsilon)^2 w_1 + \epsilon^2(\ln\epsilon)w_2 + \epsilon^2 w_3 + ..., \quad (4.126)$$

$$z = \epsilon z_1 + ..., \quad (4.127)$$

leading to the following equations at leading order:

$$-a\omega^2 r - \omega\frac{\partial u_1}{\partial\theta} = \frac{\partial}{\partial z_1}(z_1^2|\frac{\partial v_1}{\partial z_1}|\frac{\partial u_1}{\partial z_1}) \quad (4.128)$$

and

$$-\omega\frac{\partial v_1}{\partial\theta} = \frac{\partial}{\partial z_1}(z_1^2|\frac{\partial v_1}{\partial z_1}|\frac{\partial v_1}{\partial z_1}). \quad (4.129)$$

These are equivalent to the equations for the IITL as derived in §4.3.2 so inclusion of these extra potential terms does not alter the earlier equations.

To the next order then

$$-2a^{\frac{1}{2}}\omega v_1 - \omega\frac{\partial u_2}{\partial\theta} = \frac{\partial}{\partial z_1}(z_1^2|\frac{\partial v_1}{\partial z_1}|\frac{\partial u_2}{\partial z_1}) \tag{4.130}$$

and

$$-\omega\frac{\partial v_2}{\partial\theta} = \frac{\partial}{\partial z_1}(z_1^2|\frac{\partial v_1}{\partial z_1}|\frac{\partial v_2}{\partial z_1} - z_1^2|\frac{\partial v_2}{\partial z_1}|\frac{\partial v_1}{\partial z_1}). \tag{4.131}$$

No solution to these higher order terms will be attempted; they are shown only so that we can explain how the θ-dependence behaves. Instead we now proceed to examine the pressure gradient in the NATBL.

4.5.3 Non-Zero Pressure Gradients

Assuming a non-zero radial pressure gradient on a rotating disc, from §3.2 we would have, in a stationary frame of reference,

$$u_D\frac{\partial u_D}{\partial r_D} - \frac{v_D^2}{r_D} + w_D\frac{\partial u_D}{\partial z_D} = -\frac{1}{\rho}\frac{\partial p_D}{\partial r_D} + \nu\frac{\partial^2 u_D}{\partial z_D^2} + \frac{\partial}{\partial z_D}(\nu_{tD}\frac{\partial u_D}{\partial z_D}) \tag{4.132}$$

but since

$$\frac{\partial p_D}{\partial z_D} = 0 \tag{4.133}$$

and

$$u_D = u_D(r_D, z_D), \tag{4.134}$$

$$v_D = v_D(r_D, z_D), \tag{4.135}$$

$$w_D = w_D(r_D, z_D), \tag{4.136}$$

we must have $\frac{\partial p_D}{\partial r_D} = 0$. Thus the assumption that we have a non-zero pressure gradient is not correct. This arises because the velocity components on a rotating disc are functions of the height z_D whereas the pressure is not and hence there is no term to balance a non-zero pressure gradient. If there existed a velocity component which was independent of z_D then it would necessarily

be zero due to the matching with the stationary flow outside of the boundary layer. However, in the case of the NATBL we have shown in §4.4 that non-zero potential velocity components exist which are independent of z_D and which can balance pressure terms. We are therefore able to ignore the pressure when we consider the leading order velocity components as it is cancelled out by second order velocity terms and so the earlier assertion that the pressure can be taken to be zero, whilst being a simplification used for convenience, does not affect the solution structure outlined. Finally we note that in the OITL the potential velocity components are $O(\epsilon^2)$ and hence so is the pressure. Thus there is no $O(\epsilon)$ pressure term to balance the θ derivatives in (4.31) and so the earlier demonstration that f_1' and g_1' are independent of θ is still valid.

4.6 Summary

In this chapter the appropriate governing equations for the NATBL have been derived along with a three-tiered model for the turbulent boundary layer structure. This model allows for the inherent periodicity and θ-dependence of the flow and can, potentially, be applied to a range of non-axisymmetric systems.

One of the major features of this solution is the close correspondence to the rotating disc problem of Chapter 3 since most of the NATBL can be treated as being essentially the same as the 3DTBL on a rotating disc. Also, the importance of the disc solidity to the flow is revealed.

Finally it has been shown how the θ-dependence of this system is carried as a higher order perturbation throughout the NATBL.

Chapter 5

Rotating Cut-Disc

5.1 Introduction

Having determined the appropriate Reynolds equations and a structure for the non-axisymmetric turbulent boundary layer (NATBL) in the previous chapter, we are now able to examine turbulent boundary layers on rotating bodies which do not have axisymmetry. In particular it is possible to consider flows which are more relevant to the application to helicopter dynamics. Many suitable problems could now be investigated but, as with the analogous laminar flow problem which has been examined by amongst others Smith & Timoshin[68,69], Bowles & Smith[5,6] and Purvis[58], we start by considering the flow generated by a rotating cut-disc. This is taken to be a disc which has had radial segments removed and thus consists of alternate disc portions, which are referred to as 'blades', and 'wakes' as illustrated in Figure 5.1.

The cut-disc problem is of interest as it is a simple non-axisymmetric rotating flow and bears some (if only a little) resemblance to the related problem of the flow produced by a set of rotors, whilst omitting many of the more

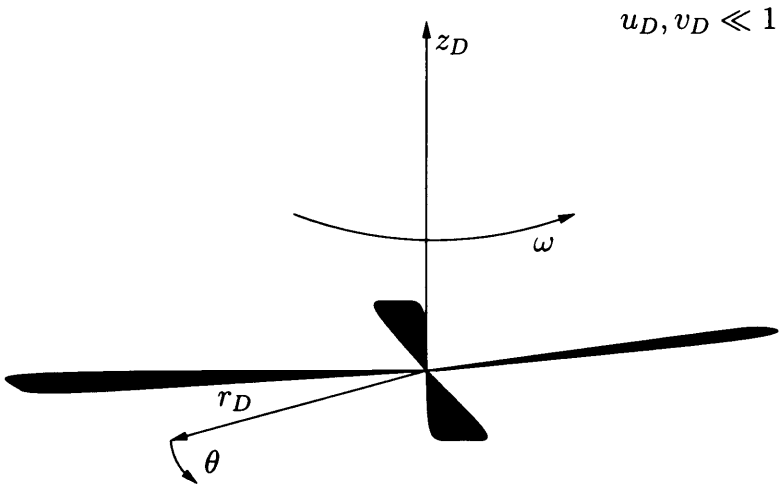

Figure 5.1: *Diagram of a rotating cut-disc.*

complicated aspects inherent in the latter flow. In particular, the lack of blade camber and thickness, and hence the vertical symmetry of the system, means that it is unnecessary to consider the pressure outside the boundary layer, and so the cut-disc flow is much easier to understand than would be the case for a rotor.

The laminar flow problem of a rotating cut-disc has been examined (numerically and analytically) by Smith & Timoshin[68] but in general it does not appear to have been studied commonly in engineering, and as such there appears to be a lack of previous research of any kind, for laminar or turbulent flows of this nature. This is to be expected since the blades on the cut-disc are taken to be (theoretically) infinitesimally thin, which is somewhat unrealistic for practical applications. Instead, where configurations similar to cut-discs arise they tend to involve blade thickness (shape) or inclination, features which are often too important to be neglected. In this case the configuration is likely to be considered a rotor, and not a cut-disc which is admittedly rather a model system.

Nonetheless there are several similarities between this cut-disc flow and that generated by a set of rotor blades. Firstly a cut-disc can be considered to be an approximation to a set of rotors with thin, radial blades. Also, as we shall see later, it is possible to reduce the turbulent boundary layer on a set of radial rotors to that on a cut-disc. Hence, once we are able to understand the present flow, we will be able to determine the turbulent boundary layer on any set of radial rotors (subject, as is discussed in future chapters, to knowledge of the wake shape and the pressure in an outer inviscid region). We also note that it is the similarity solution introduced in the previous chapter which limits the present consideration to radially defined blades only. Obviously many engineering applications involve blades which are not radial. To consider such flows would however involve solving the fully three-dimensional Reynolds equations. This is possible but represents a much more complicated numerical problem, and one that is not considered here. Moreover it has been shown in tests by Smith & Timoshin[68] that for a finite cut-disc, in the laminar case at least, the flow at large radii beyond the blades is unaffected by introducing radial variations in the shape of the blades. It would be desirable to make such tests for turbulent flow also but as mentioned that would require a fully 3D numerical solution. Instead it is assumed that we can reasonably first model a set of rotors by assuming the blades to be radial.

As discussed previously, the Reynolds equations and boundary layer structure derived in §4.2 and §4.3 respectively form the basis of our model for the NATBL on a cut disc and that work is now applied to the present flow. As has been previously shown, the solution to the flow in the outer inertial-turbulent layer (OITL), to leading order at least, can be derived simply from the earlier numerical work for a rotating disc in §3.6 whilst the solution for the laminar

sublayer on the blade (LSB) is identical to that in §3.5. In contrast the inner inertial-turbulent layer (IITL) in the cut-disc context is found to be sensitive to, and the results produced dependent on, the configuration of the cut-disc chosen. In all cases shown, only cut-discs with evenly spaced identical blades are used. Thus each configuration can be classified in terms of the number of blades (N) and the disc solidity (a). The values of N and a used are generally chosen to be as illustrative as possible.

For real helicopter rotor blades typically $0.1 \leq a \leq 0.15$ (Gent et al[32]). In the present study numerical results will largely be presented with $a = 0.1$ and $a = 0.2$. Large values of a, corresponding to $0.2 < a < 1$, are also of interest to illustrate the behaviour of the flow as the solidity decreases from $a = 1$ (a rotating disc) to $a \approx 0.1$ (a realistic helicopter solidity) while in §5.4 the interesting case of $a \ll 1$ is examined.

Modern helicopters not only differ from one another in terms of their blade solidity. The number of rotor blades also varies (usually two, three, four or five) depending on the type of helicopter in question. Whilst it is possible to produce theoretical results for any such (positive integer) number of blades, for clarity, only the cases $N = 1$ and $N = 2$ are shown, although of course the case $N = 1$ has no practical relevance[1] for helicopter dynamics beyond the rotating disc problem considered in Chapter 3.

The examination of the cut-disc flow proceeds as follows. Since the flow in the OITL has been reduced to one which is already understood, this chapter is concerned with the IITL, which is examined here in three parts. **First** (§5.2) a numerical solution is derived for the case of a flat cut-disc (one without inclination) and then **second** the work is extended to the problem of a cut-disc where each blade is inclined to the horizontal (§5.3). In the general inclined

1. Although there does exist a type of helicopter with only one blade.

case the vertical asymmetry of the system means that the wake shape (plus also the external pressure) needs to be determined. Instead here the inclined case is simplified by a specification of the wake shape (or more accurately, the wake shift - the vertical distance from the leading edge of one blade and the trailing wake of the previous blade). This is because the determination of the wake shape is very difficult. Assuming a fixed wake shape enables a simple solution to be derived which allows us to develop some understanding of a key aspect of asymmetric blade flow - the interaction of the flow above and below the blades. In practice this involves specifying the wake shift (rather than a particular value of inclination angle). **Third** and finally (§5.4) the extreme as the disc solidity decreases towards zero is investigated to see whether the flow past a cut-disc reduces then to that past an isolated blade.

5.2 Cut-Disc without Inclination

5.2.1 Governing Equations

As derived in §4.2, the governing equations for non-axisymmetric flow in a frame which rotates with the cut-disc are

$$f'^2 - 3ff'' - g'^2 + g'\frac{\partial f'}{\partial \theta} - f''\frac{\partial g}{\partial \theta} - 2g' - 1 = \frac{1}{R}f''' + \frac{\partial}{\partial \eta}\begin{cases} k_3\delta^* f'' & \text{for } \eta \geq \eta_k \\ \eta^2[1-\exp(-\frac{R\eta}{26}u_\tau)]^2(f''^2+g''^2)^{\frac{1}{2}}f'' & \text{for } \eta \leq \eta_k \end{cases} \tag{5.1}$$

and

$$2f'g' - 3fg'' + g'\frac{\partial g'}{\partial \theta} - g''\frac{\partial g}{\partial \theta} + 2f' = \frac{1}{R}g''' + \frac{\partial}{\partial \eta}\begin{cases} k_3\delta^* g'' & \text{for } \eta \geq \eta_k \\ \eta^2[1-\exp(-\frac{R\eta}{26}u_\tau)]^2(f''^2+g''^2)^{\frac{1}{2}}g'' & \text{for } \eta \leq \eta_k \end{cases} \tag{5.2}$$

where $R = k_1^4 R_\tau$ is the normalized rotational Reynolds number, $R_\tau = \frac{\omega r_D^2}{\nu}$ is the rotational Reynolds number and $u_{\tau D} = k_1^2 \omega r_D u_\tau$. The boundary conditions for this system are

$$f(0,\theta) = 0, \tag{5.3}$$

$$g(0,\theta) = 0, \tag{5.4}$$

$$f'(0,\theta) = 0, \tag{5.5}$$

$$g'(0,\theta) = 0, \tag{5.6}$$

$$f'(\infty,\theta) = 0, \tag{5.7}$$

$$g'(\infty,\theta) = -1. \tag{5.8}$$

Thus (5.1) - (5.8) form the relevant nonlinear system for the flow generated by a cut-disc and are used to determine, numerically, the velocity profiles generated by various blade configurations and, analytically in the limit as the blades become much narrower than the gaps, the blade region and near-wake behaviour. For the purposes of a numerical solution only the OITL and the IITL will be considered since these two regions comprise almost all of the total boundary layer. We take the solution in the OITL to be that derived in §4.4.1 for the appropriate value of the disc solidity and so now proceed to examine the solution in the IITL.

5.2.2 Inner Inertial-Turbulent Layer on a Cut-Disc

Since the flow in the OITL is comparatively easy to determine, and as we have θ-dependence at leading order in the IITL, this region is, to some extent, the more interesting of the two inertial-turbulent layers. In the IITL $\eta = \epsilon\eta_2 + ...$, $u = f' = \epsilon C_1 + \epsilon^2(\ln\epsilon)^2 f_2' + \epsilon^2 F_2' + ...$ and $v = g' = -1 - a^{\frac{1}{2}}\epsilon\ln\epsilon - \epsilon g_2' + ...$,

which lead to the reduced equations

$$-a - \frac{\partial f_2'}{\partial \theta} = \frac{\partial}{\partial \eta_2}(\eta_2^2 g_2'' f_2'') \tag{5.9}$$

and

$$-\frac{\partial g_2'}{\partial \theta} = \frac{\partial}{\partial \eta_2}(\eta_2^2 g_2''^2). \tag{5.10}$$

As in §4.3.2, the presence of the constant term ϵC_1 in the expansion of f' is required to match the asymptotic behaviour of f' in the OITL as $\eta_1 \to 0$. Thus the value of C_1 is determined from the numerical results for the OITL and is $O(a^{\frac{1}{2}})$. In this region, the actual blade configuration does have an impact on the overall flow (as shall be shown subsequently) and so we now need to consider the total proportion of the blade area, a, and the number of blades, N. Since the azimuthal momentum equation has been decoupled from the radial momentum equation, and is thus now just an equation for one unknown, g_2', it is simpler to solve and so we first concentrate on solving (5.10) for the azimuthal velocity, by means of a finite-difference method.

Defining S by

$$S = \eta_2^2 g_2''^2, \tag{5.11}$$

Equation (5.10) becomes

$$-\frac{\partial S}{\partial \theta} = 2\eta_2 S^{\frac{1}{2}} \frac{\partial^2 S}{\partial \eta_2^2}, \tag{5.12}$$

with $S(\infty, \theta) = a$, $S(0, \theta) = 1$ on the blade and $S(0, \theta) = 0$ in the wake. Now (5.12) is suitable for solution using a finite-difference technique. Replacing differentials with finite differences, we obtain

$$-\frac{1}{2S_{i-1,j}^{\frac{1}{2}}}\left[\frac{S_{i,j} - S_{i-1,j}}{d}\right] = \eta_2\left[\frac{S_{i-1,j+1} - 2S_{i-1,j} + S_{i-1,j-1}}{h^2}\right], \tag{5.13}$$

and hence,

$$S_{i,j} = -2S_{i-1,j}^{\frac{1}{2}}\eta_2 d\left[\frac{S_{i-1,j+1} - 2S_{i-1,j} + S_{i-1,j-1}}{h^2}\right] + S_{i-1,j}, \tag{5.14}$$

where d is the azimuthal step length, h is the vertical step length and (i, j) represents the i^{th} azimuthal station and j^{th} vertical station. (5.14) is now solved numerically. An initial profile, corresponding to a position just before the leading edge of the first blade,

$$S_{0,j} = a\frac{(1 - \exp(-\eta_{2\infty} - jh))}{(1 - \exp(-\eta_{2\infty}))} \tag{5.15}$$

is guessed, and is then used to determine $S_{1,j}$ from (5.14). Here a finite number, $\eta_{2\infty}$, is used instead of infinity. The forward-marching procedure is continued in $\pm\theta$ (see below) until a θ-periodic solution is obtained. In practice $S_{i,j}$ is recorded every time the program has marched a distance $\frac{2\pi}{N}$ (the period of the configuration) and the results are judged to be periodic when

$$|S_{i_k,j} - S_{i_{k+1},j}| < 10^{-6}, \tag{5.16}$$

where $S_{i_k,j}$ and $S_{i_{k+1},j}$ are the vertical profiles after the program has marched a distance $\frac{2\pi k}{N}$ and $\frac{2\pi(k+1)}{N}$ respectively (a suitable value of $\frac{k}{N}$ is typically about ten). The boundary conditions for S become

$$S_{i,0} = 1 \quad \text{on the blade,} \tag{5.17}$$

$$S_{i,0} = 0 \quad \text{in the wake,} \tag{5.18}$$

$$S_{i,j_{max}} = a, \tag{5.19}$$

where j_{max} corresponds to the height $\eta_2 = \eta_{2\infty}$. An important feature of the numerical procedure is that a solution can only be determined if we march 'backwards'. The reason for this is because θ acts like a negative time variable in the effective nonlinear diffusion equation (5.12). In other words, we must take $d < 0$ and hence, defining the starting azimuthal station to be $\theta = 0$, $\theta < 0$ throughout also. In addition we march downwards from $\eta_{2\infty}$ to zero and so h is negative as well. Different values of $\eta_{2\infty}$ are chosen until a value is found

which when increased produces a negligible variation in the numerical results. Finally we note that (5.13) implies that $|d| \approx \frac{1}{2}h^2$ is required, and in practice we find that if approximately $O(|d|) > O(h^2)$ then our finite difference method fails. This has serious repercussions for the efficiency of the numerical solution since even a small decrease in the vertical step length can lead to a significant increase in the number of calculations necessary; in particular it is problematic for some aspects of the flow which we discuss subsequently. We are nonetheless able to produce sufficiently many results, albeit sometimes slowly. Faster finite difference methods are possible but were not judged necessary for the present purpose. Now we proceed to examine the numerical results produced.

5.2.3 Numerical Results for the Azimuthal Momentum Equation

Equation (5.12) has been solved for a variety of blade configurations. Although only the case of evenly spaced, identical blades is considered, the method used is capable of solving for configurations consisting of any number of blades, of varying size and distance apart.

Initially we examine the impact on the numerical results of varying the horizontal and vertical step lengths used. As can be seen from Figure 5.2, the results are virtually independent of step length for sufficiently small values of h and d (the vertical and horizontal step lengths respectively). Hence for the purposes of the following numerical work the values $h = -0.02\pi$ and $d = -0.000002\pi$ are used, these choices ensuring a balance between achieving numerical accuracy and computational efficiency. Next the choice of η_{2_∞} used is varied and compared with results generated by Smith[67] using $\eta_{2_\infty} = 40$. As can be seen from Figure 5.3, our numerical results are in good agreement with

those of Smith. There are some noticeable differences between the two sets of data but these are felt to be due to the somewhat coarse vertical step length ($|d| = 0.2$) used by Smith. Consideration of the results shown in Figure 5.3 leads us to take $\eta_{2\infty} = 10\pi$, again for accuracy and computational efficiency (the specific choice of $\eta_{2\infty} = 10\pi$ was also chosen so that a factor π could be scaled out of both the horizontal and vertical step lengths for convenience).

Now that all the necessary parameters have been determined, we present our numerical results for S for a variety of blade configurations. Since there exists a wide variety of possible results which we could present (notwithstanding the possible values of a and N from which we can choose), we limit ourselves to those included in Figure 5.4, where the numerical profiles at the trailing and leading edges are illustrated and also show how S varies with θ at different heights for several formations. For the purposes of the comparison of the θ variations at different heights we examine the numerical results at $\eta_2 = 0.02\pi$ and $\eta_2 = 5\pi$, corresponding to a height just above the blade and the numerical midpoint of the IITL respectively. Figure 5.4 shows that S varies significantly more at a low height just off the blade than it does at a greater height where the flow approaches the (θ-independent) OITL, as we might intuitively expect.

Two further interesting features are also apparent. Close to $\eta_2 = 0$ the results for the case where $a = 0.1$ and $N = 1$ in the vicinity of the blade are virtually indistinguishable from the equivalent results when $a = 0.2$ and $N = 2$ at the first blade (in fact one of the reasons for producing these particular results was to examine whether this was indeed true). Also, as η_2 increases, it appears that there is a lag in the response of the flow to the change from blade to wake.

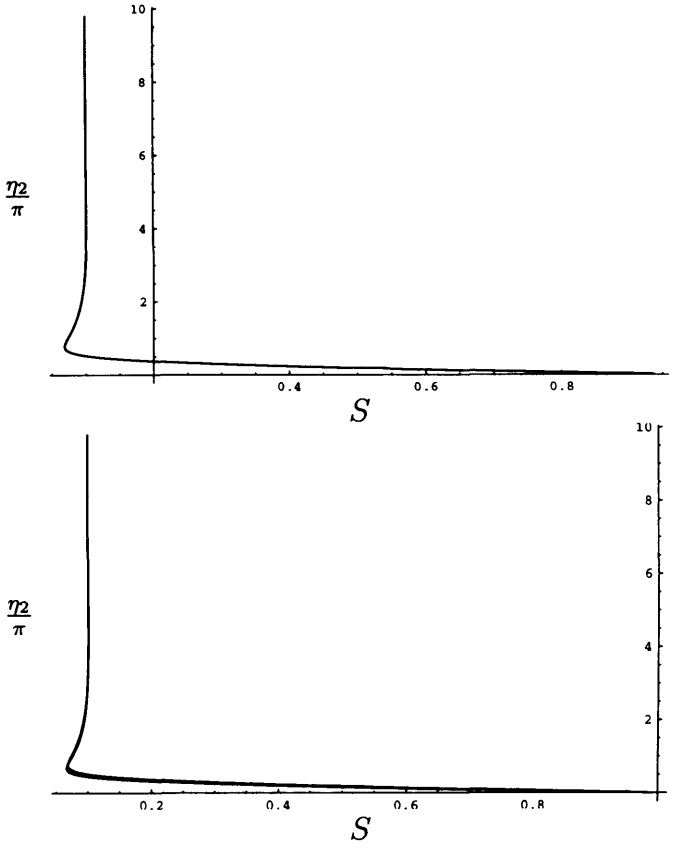

Figure 5.2: *Top: Numerical results at the trailing edge with varying horizontal step length* $d = -0.00001\pi$; -0.000002π; -0.000001π; -0.0000005π *and* -0.0000002π. *Bottom: Numerical results with vertical step length* $h = -0.02\pi$; -0.004π; *and* -0.002π. *In all cases the disc solidity is* $a = 0.1$ *and there is one blade.*

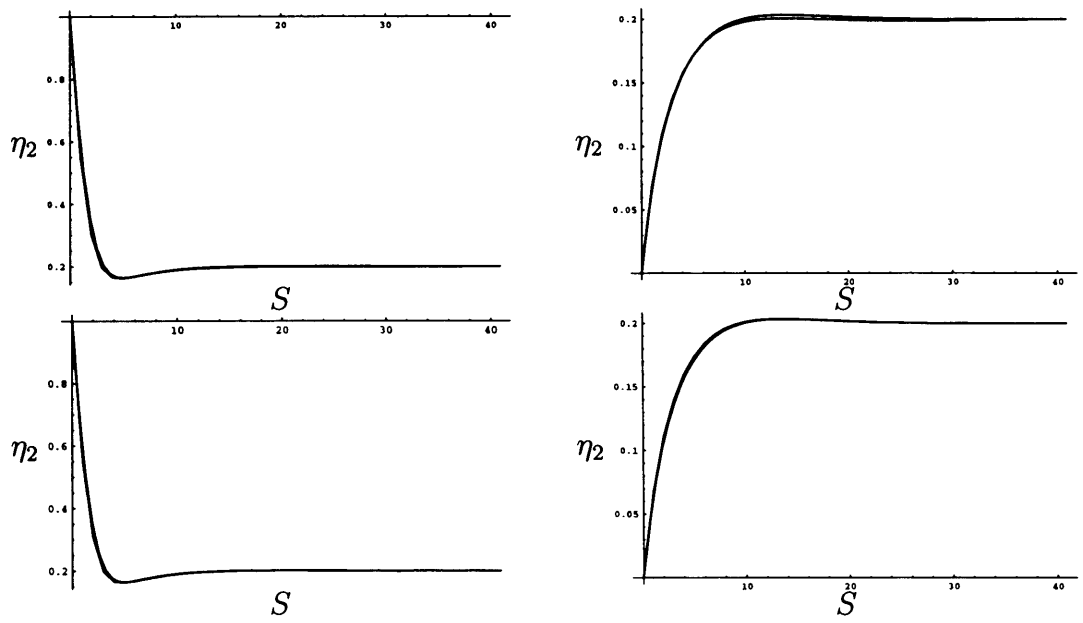

Figure 5.3: *Left top: Comparison of our numerical results with those of Smith*[67] *at the trailing edge with* $\eta_{2\infty} = 40$. *Right top: Comparison of our numerical results with those of Smith at the leading edge with* $\eta_{2\infty} = 40$. *Left bottom: Numerical results at trailing edge with* $\eta_{2\infty} = 30; 10\pi;$ *and* 13π. *Right bottom: Numerical results at leading edge with* $\eta_{2\infty} = 30; 10\pi;$ *and* 13π. *Due to the coarse grid used by Smith in his calculations these results are not smooth curves. Nonetheless they provide generally good agreement with the present work.*

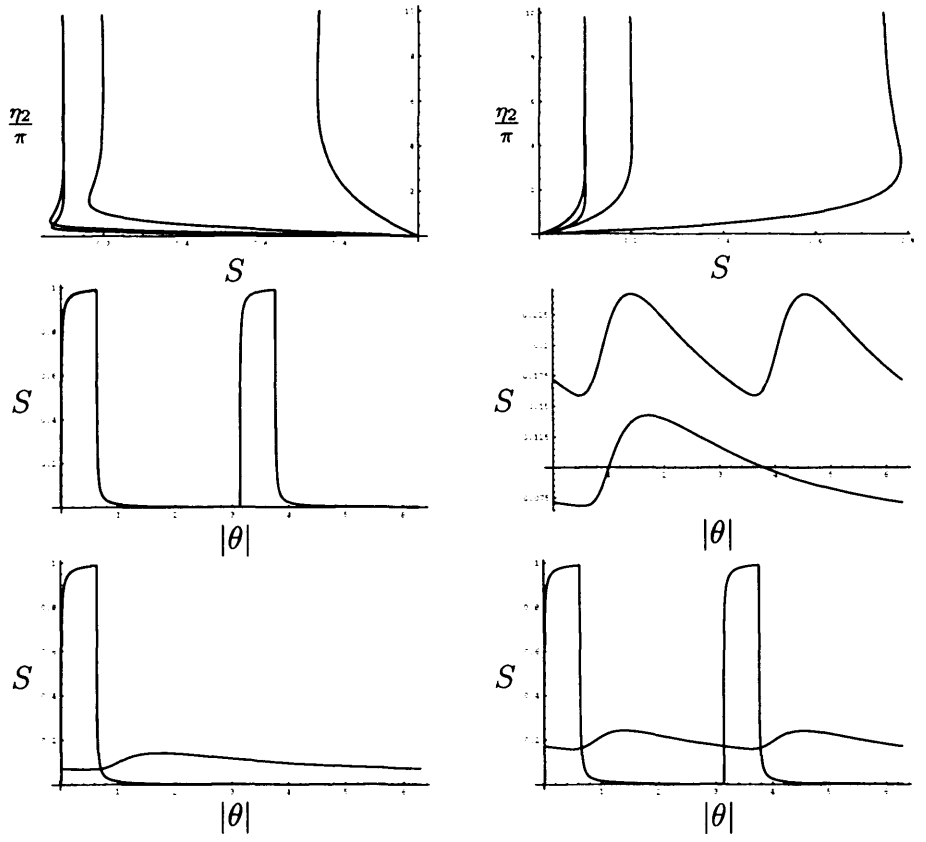

Figure 5.4: *Left top: Numerical results for S at trailing edge. From right to left;* $a = 0.75$ *and* $N = 1$*;* $a = 0.2$ *and* $N = 1$*;* $a = 0.1$ *and* $N = 1$*; and* $a = 0.1$ *and* $N = 2$*. Right top: Numerical results for S at leading edge. From right to left;* $a = 0.75$ *and* $N = 1$*;* $a = 0.2$ *and* $N = 1$*;* $a = 0.1$ *and* $N = 1$*; and* $a = 0.1$ *and* $N = 2$*. Left middle: Numerical results for S at height* $\eta_2 = 0.02\pi$ *for two different configurations:* $a = 0.1$ *and* $N = 1$ *and* $a = 0.2$ *and* $N = 2$*. Right middle: Numerical results for S at height* $\eta_2 = 5\pi$ *for two different configurations:* $a = 0.1$ *and* $N = 1$ *(lower curve) and* $a = 0.2$ *and* $N = 2$ *(upper curve). Left bottom: Numerical results for S at heights* $\eta_2 = 0.02\pi$ *and* $\eta_2 = 5\pi$ *with one blade* $(N = 1)$ *and disc solidity* $a = 0.1$*. Right bottom: Numerical results for S at heights* $\eta_2 = 0.02\pi$ *and* $\eta_2 = 5\pi$ *with two blades* $(N = 2)$ *and disc solidity* $a = 0.2$*.*

5.2.4 Azimuthal Velocity Profiles

Whilst for the purposes of a numerical solution it is convenient to solve (5.10) in terms of the quantity S, it is desirable and of more practical value to interpret the results in terms of the actual velocity. Hence we now convert the numerical results for S into scaled azimuthal velocity profiles for $g_2'(\eta_2)$. The relation

$$S = \eta_2^2 g_2''^2 \tag{5.20}$$

can be rearranged to express g_2'' as a function of the numerical results for S, with appropriate choice of sign,

$$g_2'' = \frac{S^{\frac{1}{2}}}{\eta_2}, \tag{5.21}$$

which can be integrated numerically using Simpson's Rule to determine g_2', for all values of η_2. In practice (5.21) is integrated from $\eta_{2\infty}$ to η_2 for all values of η_2 in the range $0 \leq \eta_2 < \eta_{2\infty}$. This produces values for $g_2'(\eta_2) - g_2'(\eta_{2\infty})$ and the asymptotic form

$$g_2'(\eta_{2\infty}) = a^{\frac{1}{2}} \ln(\eta_{2\infty}) \tag{5.22}$$

is then used to determine $g_2'(\eta_2)$. Actually the fuller asymptotic form is

$$g_2'(\eta_{2\infty}) = C_4 + a^{\frac{1}{2}} \ln(\eta_{2\infty}) \tag{5.23}$$

but it is assumed here that $\eta_{2\infty}$ is sufficiently large that (5.22) is an adequate approximation. Profiles of $g_2'(\eta_2)$ were calculated for a range of cut-disc configurations and these are illustrated in Figure 5.5. As can be seen, the results for a given blade solidity are approximately unchanged by varying the number of blades in these instances.

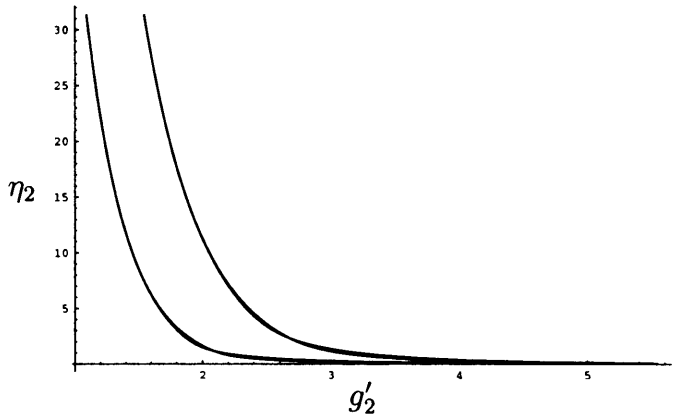

Figure 5.5: *Scaled azimuthal velocity profiles for varying values of the disc solidity and the number of blades. From right to left:* $a = 0.2$ *and* $N = 1$*;* $a = 0.2$ *and* $N = 2$*;* $a = 0.1$ *and* $N = 1$*; and* $a = 0.1$ *and* $N = 2$*. The four sets of data seem to correspond to two general curves, corresponding to the two different blade solidities considered.*

5.2.5 Numerical Solution to the Radial Momentum Equation

Whilst the azimuthal velocity is the dominant part of the velocity in the IITL, the radial component is also important, in particular with respect to the application to helicopter dynamics since, for instance, radial outflow may contribute to the influence that side structures have on the overall flow dynamics of a helicopter. Moreover it is worth noting that in practice the radial outflow from a set of rotors is considered negligible (Gent et al.[32]) when compared to the normal velocity generated (and this certainly appears to be the case in Figure 4.2 for the results in the OITL), and that the typical relative magnitude of the radial and normal velocity components is an important issue we wish to consider here. In particular, the question of whether the relative weakness of the radial outflow is due to helicopter design, or is an inherent feature of

non-axisymmetric rotating flows, is a point of interest.

Thus having determined the numerical solution for g_2' we turn to the radial momentum equation in the IITL, namely

$$-a - \frac{\partial f_2'}{\partial \theta} = \frac{\partial}{\partial \eta_2}(\eta_2^2 g_2'' f_2''), \tag{5.24}$$

and attempt to do likewise for f_2', also by means of a finite difference solution. As before, $S = (\eta_2 g_2'')^2$. Now we also let $T = -\eta_2 f_2''$. Differentiating (5.24), we have

$$-\frac{\partial T}{\partial \theta} = \eta_2 \frac{\partial^2}{\partial \eta_2^2}(S^{\frac{1}{2}} T) \tag{5.25}$$

with $S(\infty, \theta) = a$ and $S(0, \theta) = 1$ on the blade and $S(0, \theta) = 0$ in the wake again, and now also $T \sim a^{\frac{1}{2}}\eta_2$ as $\eta_2 \to \infty$ and $T(0, \theta) = 0$. Using a finite difference method leads to

$$\begin{aligned} T_{i,j} = \quad & T_{i-1,j} - \frac{\eta_2 d}{h^2}[T_{i-1,j}(S^{\frac{1}{2}}_{i-1,j+1} - 2S^{\frac{1}{2}}_{i-1,j} + S^{\frac{1}{2}}_{i-1,j-1}) \\ & +2(S^{\frac{1}{2}}_{i-1,j} - S^{\frac{1}{2}}_{i-1,j-1})(T_{i-1,j} - T_{i-1,j-1}) \\ & +S^{\frac{1}{2}}_{i-1,j}(T_{i-1,j+1} - 2T_{i-1,j} + T_{i-1,j-1})], \end{aligned} \tag{5.26}$$

with h, d, i and j defined as in the azimuthal problem. Again we guess an initial starting profile for $T_{0,j}$. Here we take

$$T_{0,j} = a^{\frac{1}{2}}(\eta_{2\infty} - jh + j_{max}h) \tag{5.27}$$

with j_{max} defined as previously. This profile is used to calculate $T_{1,j}$ from the given $T_{0,j}$ and $S_{1,j}$ (which has already been determined), and so on, until a periodic solution is achieved. Again, this is deemed to have occurred when

$$|T_{i_k,j} - T_{i_{k+1},j}| < 10^{-6} \tag{5.28}$$

with $T_{i_k,j}$ and $T_{i_{k+1},j}$ defined in an analogous way to $S_{i_k,j}$ and $S_{i_{k+1},j}$ in §5.2.2. This leads to the following numerical results (Figure 5.7) for the cases $a = 0.1$

and $a = 0.2$, but first to verify these results, in Figure 5.6 we compare our numerical results for varying vertical and horizontal step lengths. Again the results are largely unaltered by decreasing the step length further than $h = -0.02\pi$ and $d = -0.000002\pi$, and so these values are used for all subsequent work (as presented in Figure 5.7). Since the radial outflow is driven by the azimuthal velocity, and $\eta_{2\infty} = 10\pi$ is a sufficient height for determining $g_2'(\eta_2)$, it is assumed that this choice of $\eta_{2\infty}$ is satisfactory for calculating $f_2'(\eta_2)$ also.

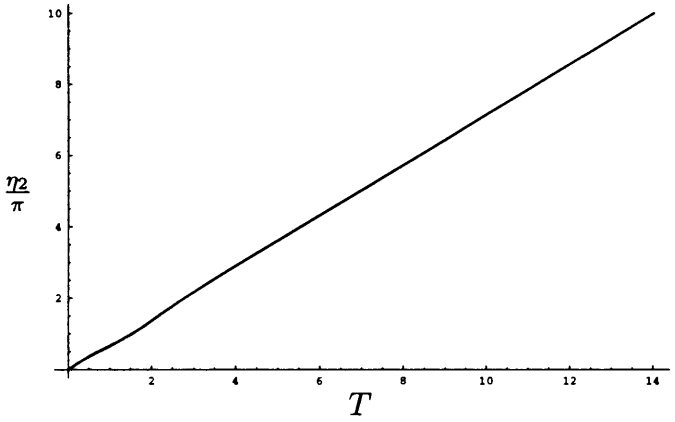

Figure 5.6: *Radial numerical results at the trailing edge with disc solidity* $a = 0.2$, *number of blades* $N = 1$, *varying horizontal step length* $d = -0.0001\pi$; -0.00001π; *and* -0.000001π, *and varying vertical step length* $h = -0.02\pi$; *and* -0.04π.

In Figure 5.7 we also illustrate the numerical results at low height, between 0.02π and 2π. Only the values at the trailing edge are shown as it is really only the magnitude of the radial results which is of interest here.

5.2.6 Radial Velocity Profiles

As for the azimuthal numerical results the above radial numerical results are converted into radial velocity profiles for the IITL at the trailing edge, using

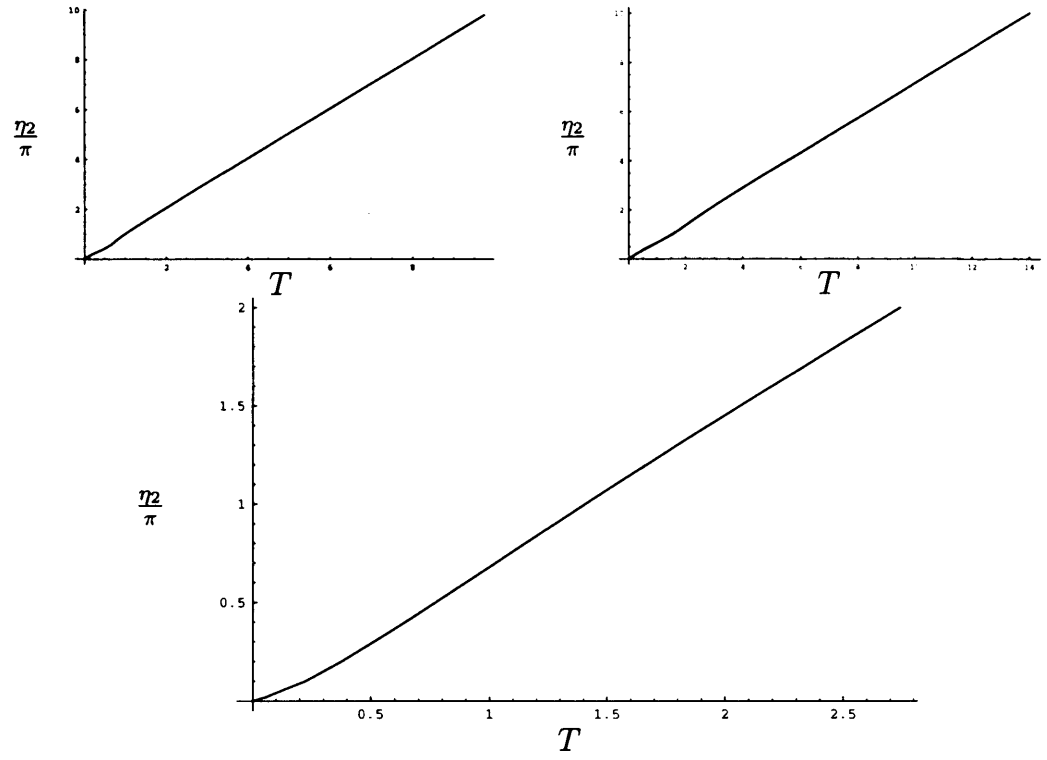

Figure 5.7: *Left top: Radial numerical results for T at trailing edge for disc solidity $a = 0.1$ and $N = 1$. Right top: Radial numerical results for T at trailing edge for $a = 0.2$ and $N = 1$. Bottom: Close-up of the radial numerical results for T at trailing edge for $a = 0.2$ and $N = 1$ at low height.*

a similar method as that in §5.2.4. Now we have $T = -\eta_2 f_2''$, so that

$$f_2'' = -\frac{T}{\eta_2}, \tag{5.29}$$

which can then be integrated using Simpson's Rule again, to determine f_2' using an (approximate) asymptotic form. In this case the asymptotic form is

$$f_2' \sim -a^{\frac{1}{2}}\eta_2 \tag{5.30}$$

as $\eta_2 \to \infty$. This leads to the velocity profile shown in Figure 5.8 for the case where $a = 0.1$ and there is only one blade.

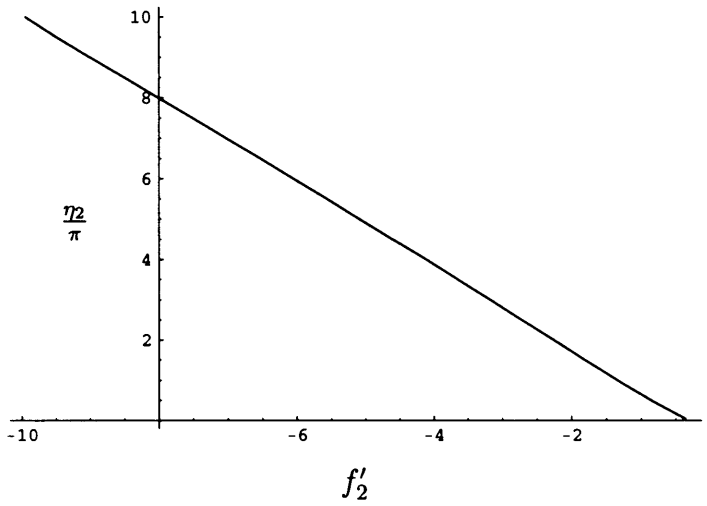

Figure 5.8: *Profile of the radial velocity component f_2' at trailing edge with disc solidity $a = 0.1$ and $N = 1$.*

As mentioned previously, an important area of interest is the relative magnitudes of the radial and normal velocity components and so we now proceed to use our numerical results to calculate the normal velocity in the IITL.

5.2.7 Normal Velocity Profile

In the NATBL the normal velocity is given by

$$w_D = -\omega k_1^2 r_D (3f - \eta f' + \frac{\partial g}{\partial \theta}), \tag{5.31}$$

which to leading order in the IITL becomes

$$w_2 = -(2C_1\eta_2 + \frac{\partial g_2}{\partial \theta}) \tag{5.32}$$

from the expansions for the radial and azimuthal velocity components described in §4.3.2. The constant term C_1 is determined from consideration of the OITL and the rotating disc problem of Chapter 3 and it is found that $C_1 = 1.57a^{\frac{1}{2}}$. We are able to repeat the numerical integration performed in

§5.2.4 to determine $g_2(\eta_2, \theta)$ at the required θ position and then approximate the term $\frac{\partial g_2}{\partial \theta}$ by calculating $g_2(\eta_2, \theta)$ and $g_2(\eta_2, \theta + \delta)$ (where $\delta \ll 1$) and then using the simple formula

$$\frac{\partial g_2}{\partial \theta} \approx \frac{g(\eta_2, \theta + \delta) - g(\eta_2, \theta)}{\delta}. \tag{5.33}$$

The normal velocity at the trailing edge induced by a rotating cut-disc consisting of one blade with disc solidity $a = 0.1$ is presented in Figure 5.9.

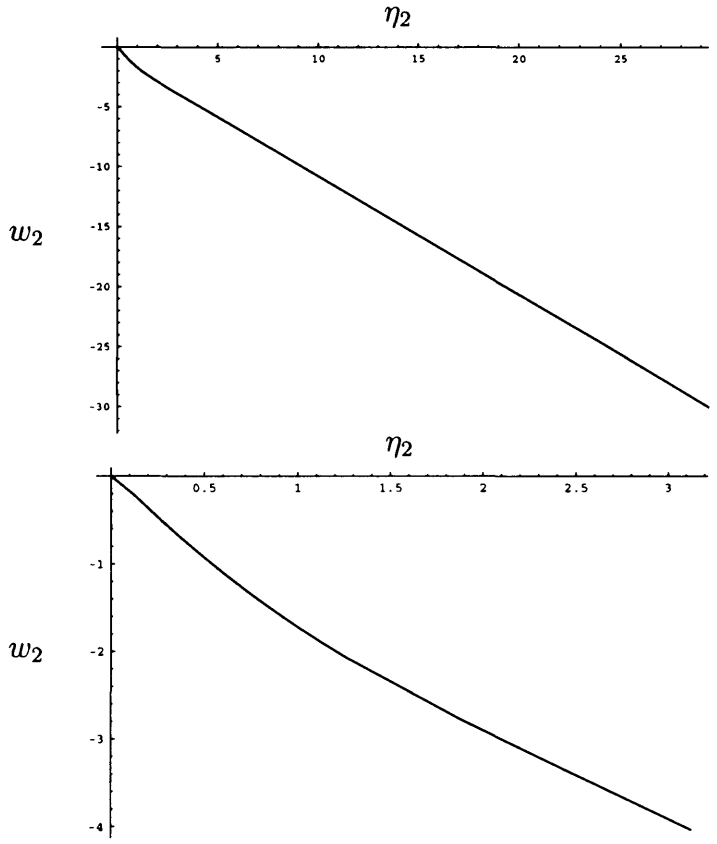

Figure 5.9: *Top: Normal velocity component at the trailing edge in the IITL for a cut-disc with one blade ($N = 1$) and disc solidity $a = 0.1$. Bottom: Close-up view of the normal velocity component at low height.*

Figure 5.8 and Figure 5.9 show that the magnitude of the normal velocity is much greater than that of the radial velocity, as noted by Gent et al. Now we

consider extending the analysis of this cut-disc flow to include the case where the blades have inclination.

5.3 Cut-Disc with Inclination

5.3.1 Introduction

As has been discussed, the flow generated by a rotating disc is one which is of some significance in terms of helping to understand the flow created by a set of rotors. Nonetheless this is a highly simplified and idealized situation and one which needs to be developed further in order to gain more realistic understanding of rotor blade dynamics. To that end we now consider the problem of a cut-disc where each of the blades is inclined at a fixed angle to the horizontal plane in which they rotate, as shown in Figure 5.10.

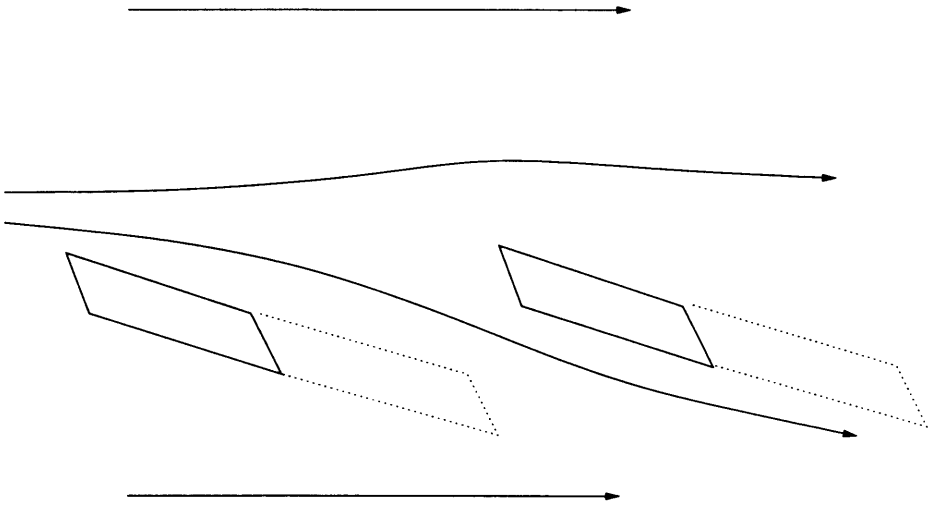

Figure 5.10: *Radial view of a cut-disc with inclined blades.*

This problem is of interest primarily for two reasons: first because helicopter rotor blades are usually inclined and second because the problem involves interaction between the flow above and below the blade, a feature which

does not occur in the cut-disc flow without inclination. We take the blades to have a fixed inclination to the horizontal, although in practise this may vary for helicopter rotors as the blades rotate. This variation occurs because, in forward helicopter flight, advancing blades moving in the direction of the helicopter's motion would generate more lift than the receding blades - those moving away from the direction of the helicopter's motion - if all blades had the same inclination. Thus, in reality, to ensure that each blade generates the same amount of lift (to minimize strain on the helicopter and provide more stable flight) the blade inclination is continuously varied. Since the present theoretical work is not considering forward flight it therefore seems appropriate to restrict this investigation to blades with fixed inclination. For simplicity we consider the inclination to be the same for all the blades (although this assumption is not strictly necessary since the numerical approach involved can include differing blade inclinations).

The current problem is taken to be an approximation to the flow generated by a set of inclined rotor blades but is also of some potential practical interest in other engineering applications since this configuration also occurs in, for example, engine components. Despite these practical applications and the relevance to helicopter dynamics, as with the cut-disc flow without inclination there appears to have been little previous research into the current problem.

5.3.2 Problem Formulation and Numerical Method

For simplification a fixed wake shape is imposed on the system. In reality the wake shape should be determined as part of the overall solution but here we prescribe a wake shape and attempt to find a periodic solution. The free (as opposed to fixed) wake problem is discussed in more detail in §5.3.6. It is

found that, for the purposes of numerical evaluation, the actual imposed wake shape is unimportant - all that matters is the vertical position of the wake line, defined in this instance to be the line along which $S = 0$ (where $S = \eta_2^2 g_2''^2$ again, as in §5.2) as the wake reaches the next blade, as illustrated in Figure 5.10. The distance from the leading edge of a blade to the point on the wake at the same value of θ is known as the wake shift.

In practice we guess that the wake shape is almost linear, with gradient equal to that of the blade, from the trailing edge. Hence the wake shift is approximately given by the gap between two blades, $2(1-a)\pi$,[1] multiplied by the inclination. Since in helicopter flight typical blade inclination is small (7-8 degrees to the horizontal) and because large angles of inclination may interact with the boundary layer structure proposed, we assume that the inclinations involved are suitably small and hence so is the wake shift. As such the wake shift is typically taken to be -0.02π and -0.2π, although results are shown for wake shift $-\pi$ also, as an illustration (the specific choices for the wake shift value are also limited by the vertical step length of the numerical marching method used). Consideration is restricted to negative values of the wake shift as this is generally the case in helicopter dynamics (Seddon[65]).

Performing a Prandtl shift (see Appendix C) transforms the problem to one of a cut-disc which can be solved as in §5.4 and §5.5, although the added complication of the wake shift still needs to be accounted for. In practice the only additional complication arises from having to shift the oncoming profile to reflect where the wake now meets the next oncoming blade, hence affirming the importance of the vertical position of the wake shape as the wake reaches the next blade (the wake shift). This complication arises for the following reason. With a typical wake shape, part of the upper wake from one blade will

1. Based on the flow at unit radius and there being only one blade.

actually become part of the oncoming profile for the lower wake of the next blade, as illustrated in Figure 5.10. Thus for the purposes of the following numerical procedure, the wake shape is not directly important. Nonetheless it still influences the flow through the pressure outside the boundary layer (which in turn also influences the wake shape) and of course to relate the numerical results to the real velocity profiles requires the 'undoing' of the Prandtl shift; however these are not issues which need be considered here (although the outer pressure problem is considered in Chapter 6).

5.3.3 Numerical Results for the Azimuthal Momentum Equation

Since the azimuthal momentum equation is still uncoupled in the current problem, we again determine the azimuthal solution first. Using the method described in §5.3.2 we produced the following numerical results for vertical shift values of -0.2π and $-\pi$ respectively, as illustrated in Figure 5.11 and Figure 5.12.

It is immediately evident that these results are somewhat curious. First it is surprising that, even for a small wake shift, the results above and below the blade should differ so significantly, but second, and of greater concern, the results for $\eta_2 < 0$ have not achieved periodicity yet, and appear unlikely to even be approaching a periodic solution. There also seems to exist a region directly below the blade where, relative to the values of S above and further below the blade, the numerical results are very small. Not only does this seem unrealistic, but the region actually grows after each successive revolution, thus contributing to (if not actually causing) the lack of periodicity already highlighted. Consideration of the numerical method used here explains the

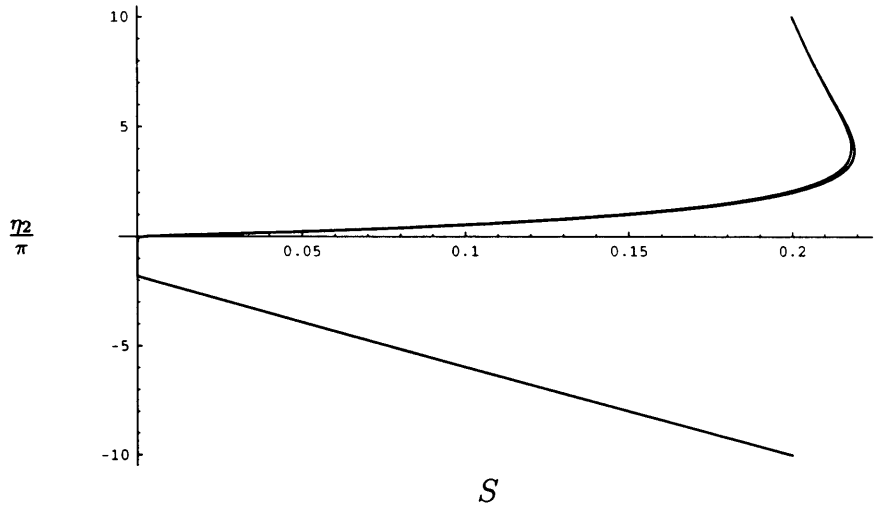

Figure 5.11: *Numerical results for S at the leading edge with wake shift -0.2π, $a = 0.2$, $N = 1$ and varying step lengths $d = 0.02\pi$ and 0.01π.*

occurrence of this region.

In each wake, $S = 0$ is the boundary condition applied across the wake centre line. When the S-profile is shifted at the onset of the next blade, the point at which $S = 0$ is shifted down to a vertical station below the blade. As the finite difference method is advanced all the subsequent points at this vertical station retain the zero value of S (since if S is zero at any point, S must remain zero at all future points according to (5.14)). Hence a curve along which $S = 0$ persists throughout the boundary layer, and since, at the start of each wake, there exists a new point at which the value of S is set to zero, this leads to yet another $S = 0$ curve created at the next leading edge and so on.

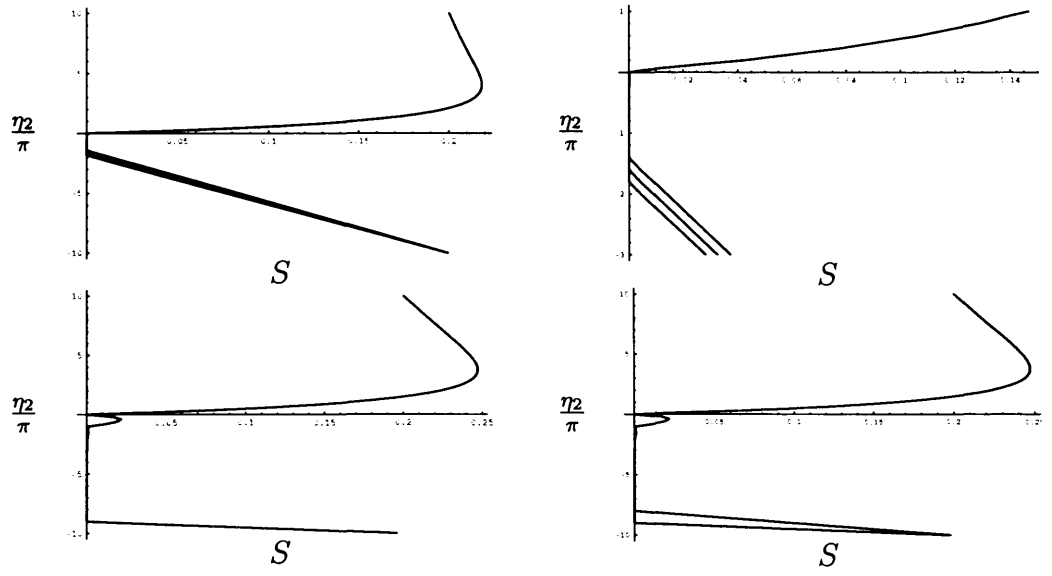

Figure 5.12: *Left top: Numerical results after successive revolutions with wake shift* -0.2π. *From bottom to top; 10 program revolutions; 9 program revolutions; 8 program revolutions. Right top: Numerical results after successive revolutions with wake shift* -0.2π *at small heights. From bottom to top; 10 program revolutions; 9 program revolutions; 8 program revolutions. Left bottom: Numerical results with wake shift* $-\pi$ *after 10 program revolutions. Right bottom: Numerical results after successive revolutions with wake shift* $-\pi$. *From bottom to top; 11 program revolutions; 10 program revolutions; 9 program revolutions. All numerical results presented here are at the leading edge with* $a = 0.2$ *and* $N = 1$.

This explains the lack of periodicity in the flow results (at each blade a new $S = 0$ curve is created) and the constraint that S is zero at so many points immediately below the blade confines S to small values in this region. This also helps to explain the surprisingly marked difference in the numerical results above and below the blade. Of course it should be noted that the problems which occur below the blade arise precisely because we take a negative shift value - the S-profile is shifted downward - if we took a positive value of the wake shift, the same problems would arise in the upper half of the boundary layer instead.

Physically the above discussion seems to correspond to a lack of dissipation of the wake by the numerical scheme. Since it seems unrealistic, or at least questionable, for the wakes to last perpetually and not decay, we are led to modify the numerical procedure used in §5.2.2.

Consider the S-profile shifted downward at each new blade. At the point at which $S = 0$ (which in future is termed a 'corner' due to its geometry), S is now taken to be the average of the values of S at the two most closely adjacent vertical stations. This leads to the numerical results of Figure 5.13 which appear more correct physically.

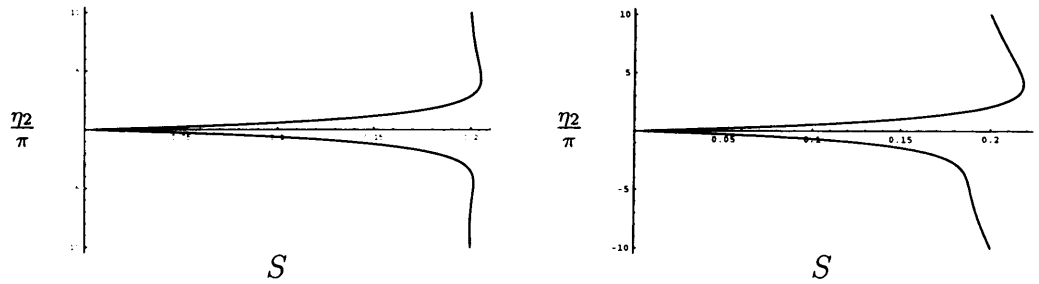

Figure 5.13: *Left: Numerical results for S with wake shift -0.02π. Right: Numerical results for S with wake shift -0.2π. In both cases results are presented for $a = 0.2$ and $N = 1$ at the leading edge.*

Figure 5.13 shows that, as might be expected, where the wake shift is increased the results above and below the blade vary more considerably, and indeed for small values of the wake shift the two halves are quite similar. Having thus modified our numerical method to introduce dissipation of the corners, we now try to examine the development of a corner analytically.

5.3.4 The Corner Problem

Using our numerical results we can examine how these corners progress as we march round in θ. Figure 5.14 shows the numerical profiles for S at a variety of θ positions. As $|\theta|$ gradually increases, the corner begins to 'smooth' out and becomes less dramatic.

This behaviour is now addressed analytically by taking (5.12) and examining the solution locally about a corner, η_0. Letting $\eta_2 = \eta_0 + \theta^m \xi$ and $S = \theta^m U(\xi)$ we find that a balance of terms requires $m = \frac{2}{3}$. Hence (5.12) yields the nonlinear ordinary differential equation

$$U''(\xi) = \frac{(U - \xi U')}{3\eta_0 \xi U^{\frac{1}{2}}} \tag{5.34}$$

for $U(\xi)$ with $U(0) = 0$ and $U \sim \mu|\xi|$ as $|\xi| \to \infty$, in keeping with the 'corner' geometry, for some unknown constant μ. The value of μ is assumed to depend on the particular disc solidity and configuration involved. For a particular corner position η_0, (5.34) can be solved for a given value of μ, using an RKF algorithm say.

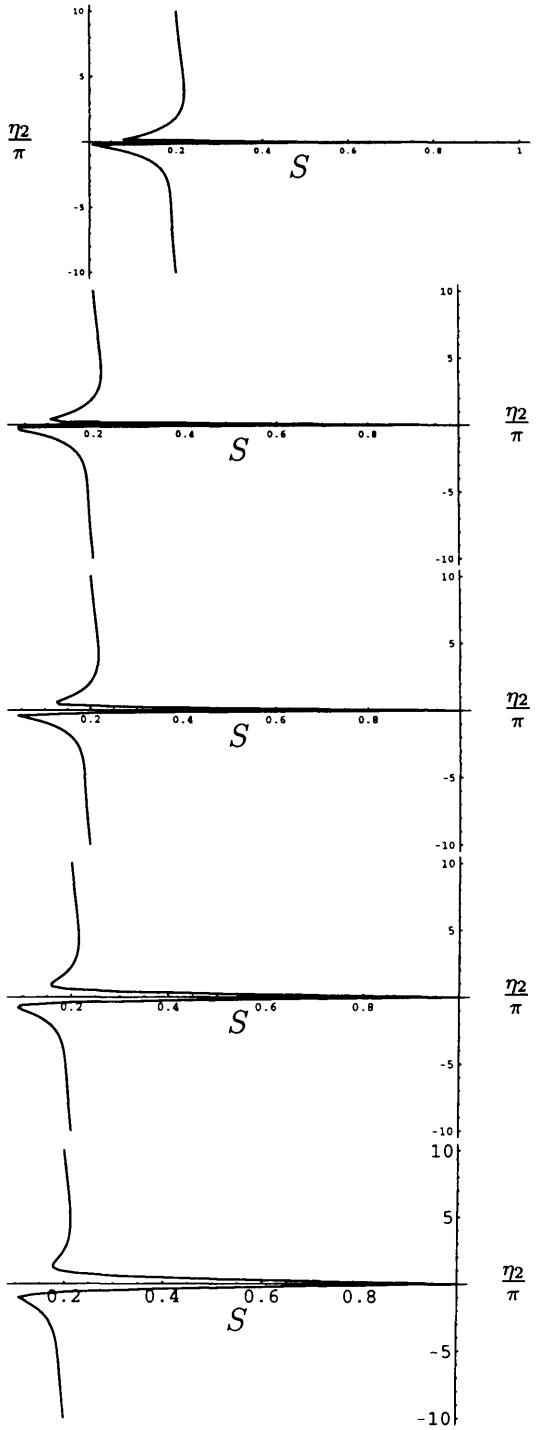

Figure 5.14: *Numerical results showing corner development at* $\theta = -0.01\pi$ *(top),* $\theta = -0.05\pi$, $\theta = -0.1\pi$, $\theta = -0.2\pi$ *and* $\theta = -0.3\pi$ *(bottom). Results are for* $a = 0.2$ *and* $N = 1$.

Since we are only interested in the general behaviour of the corner it is sufficient to consider a more generic case only and hence we set $U(0) = \gamma$ and let $t = \gamma U$, so that

$$\gamma t''(\xi) = \sqrt{\gamma}\frac{(t - \xi t')}{3\xi t^{\frac{1}{2}}}. \tag{5.35}$$

Now defining $\xi = \sqrt{\gamma}s$ we have a marching equation

$$t''(s) = \frac{(t - st')}{3st^{\frac{1}{2}}} \tag{5.36}$$

for $t(s)$, given $t(0) = 1$ and $t'(0) = 0$.

Equation (5.36) can then be solved using an RKF algorithm and produces the solution illustrated in Figure 5.15.

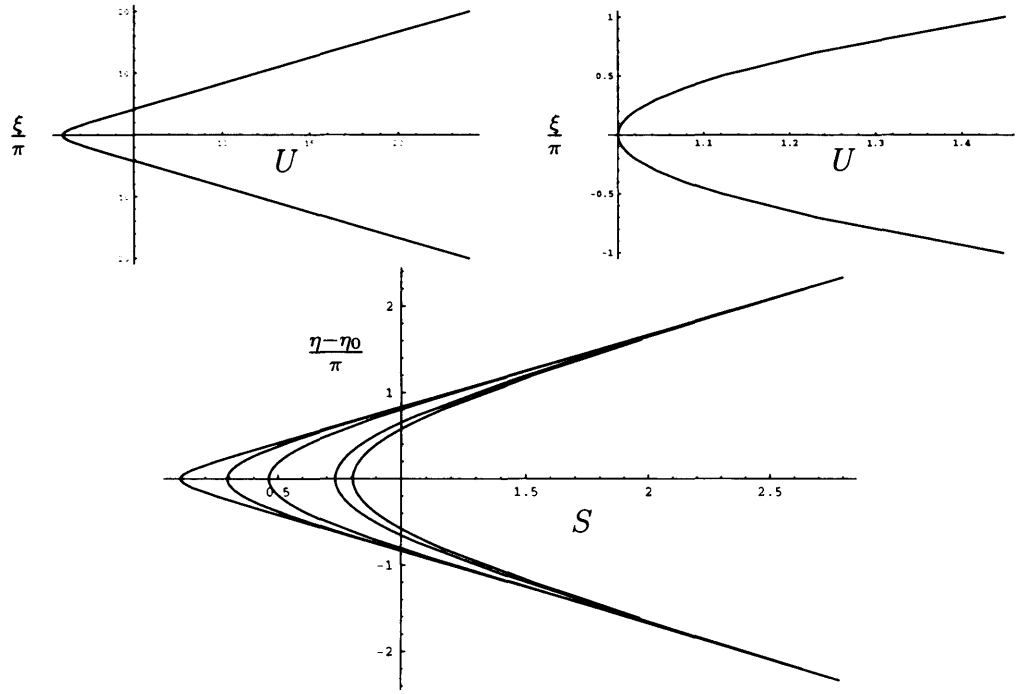

Figure 5.15: *Left Top: Solution to the corner problem* (5.36). *Right Top: Near corner behaviour, i.e. close-up of left top. Bottom: S-profiles near corner for* $\theta = -0.01\pi$; -0.05π; -0.1π; -0.2π *and* -0.3π.

Figure 5.15 shows that as $|\theta|$ increases the analytical solution for this corner

effect 'smoothes out' as evidenced by our earlier numerical results.

5.3.5 Numerical Solution to the Radial Momentum Equation

The solution for the radial momentum equation for the cut-disc can also be extended to examine the radial results in the inclined case. Again, this just requires shifting our numerical results at each leading edge. This produces the following results presented in Figure 5.16.

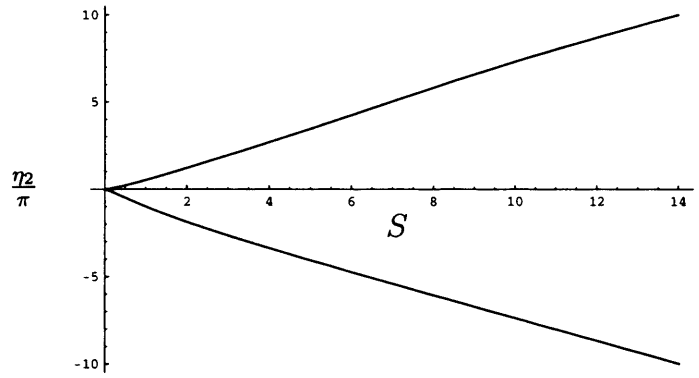

Figure 5.16: *Radial numerical results for S at leading edge with wake shift $= -0.2\pi, N = 1$ and disc solidity $a = 0.2$.*

5.3.6 The Free Wake Problem

In the examination of the inclined blade problem above, we made the simplification of imposing a fixed shape rather than actually calculating the wake shape which would be generated by the flow past a series of thin inclined blades. This was done as a primary step, to lessen the numerical task, and because even this simpler problem allowed us to examine the impact of wake shifts and the interaction of the upper and lower parts of the flow. The free

wake case is not investigated in detail in the present study since, in three-dimensional flows at least, it requires a complicated numerical solution which is prohibitively long. Instead it is briefly discussed.

In the fully free wake case the pressure perturbations outside the boundary layer have to be considered, which in the ordinary cut-disc problem can be taken to be zero. In particular we have to consider the difference in the pressure above and below the cut disc, specifically in the wake where the free wake shape is in essence determined by the condition that the pressure difference across the wake shape is zero. Since the boundary layer pressure is independent of height, this condition is equivalent to having a zero pressure difference at the edge of the boundary layer. However as we shall discuss in more detail in Chapter 7, the pressure outside the boundary layer cannot be determined without knowledge of the wake shape and the boundary layer thickness. This coupling of the wake shape, boundary layer thickness and the inviscid-region pressure, i.e. inner-outer interaction, is what makes the determination of the free wake shape (and the pressure) so difficult to achieve (and so is not attempted here). Instead we move on to another important aspect of the flow, namely the low solidity limit ($a \ll 1$).

5.4 Low Solidity

Having solved (5.10) numerically, with a method which allows $\hat{a}$ solution for any blade configuration and for any value of the disc solidity, the special case where a is small is now considered analytically. This extreme is of interest for several reasons, not least because the assumption $a \ll 1$ enables analytical solutions to (5.12) to be derived. These analytical results can then be compared with the appropriate numerical results from §5.2.3 which not only serves to validate

the low-solidity analysis but is useful in supporting the numerical findings.

Low solidity is also an important regime to consider given that with a view to industrial applications, a typical helicopter rotor has a solidity of approximately $a = 0.1 - 0.15$, which is quite small. Another motivation behind our examination of this problem is to see how a cut-disc flow is related to the flow past an isolated blade (or flat plate) such as was studied by Neish & Smith amongst others. This is particularly useful as in Chapter 7 we will model 3D asymmetric blade flow by assuming the blades to be 2D and seeking a periodic solution. Hence it is important to relate the low solidity 3D cut-disc behaviour to that of a 2D blade. That then leads to another significant question. If in the limit as $a \to 0$ the cut-disc can be approximated by a set of 2D isolated blades, how then can this approximation incorporate periodicity, given that the flow past a set of isolated blades is not periodic?

The low solidity limit is clearly a useful point to examine and will be considered in three parts. In §5.4.1 we examine our numerical results for decreasing a to test if a limit is discernible. Then in §5.4.2 we consider the flow in a region near the blade and compare our numerical results with an analytical low solidity solution. Similarly we also examine the flow behaviour in the near wake in §5.4.3 , a region of the wake in which the distance from the nearest blade is large compared to the typical blade length yet small compared to the overall wake size. Again a (mostly) analytical solution is derived and compared with numerical solutions.

5.4.1 Low Solidity Limit

Here the behaviour of our results as $a \to 0$ is examined to test if a limit might reasonably exist. From (5.12) we find that

$$\frac{S}{\theta} \sim \frac{S^{\frac{3}{2}}}{\eta_2} \tag{5.37}$$

and hence, considering the region where θ is $O(1)$ say,

$$O(\eta_2) = O(S^{\frac{1}{2}}). \tag{5.38}$$

Since $S(\infty, \theta) = a$, in the wake we suppose that S is $O(a)$ (this may not be possible over the blade since then $S(0, \theta) = 1$) and hence the vertical scale has thickness $\eta_2 = O(a^{\frac{1}{2}})$.

The numerical results of §5.2.3 are now examined for varying values of a at different values of θ in the wake to see how they behave as a decreases towards zero. In this case it is found that, as a decreases, it is necessary to take smaller values of d to produce accurate results and hence we now take $d = -0.02\pi a^{\frac{1}{2}}$. Fortunately, since $\eta_2 = O(a^{\frac{1}{2}})$, it is possible to take $\eta_{2\infty} = 10\pi a^{\frac{1}{2}}$ and so the number of vertical steps required remains the same as a is varied. Unfortunately though, it is also necessary to take h to be smaller for the numerical method of §5.2.2 to work. Hence the value $h = -0.000002\pi a$ is selected.

This means that as a is decreased the number of iterations required increases by a factor a^{-1}. Thus for low values of a the computations required become increasingly long and, ultimately, prohibitively impractical. For this reason the numerical work is limited here to values of a no smaller than 0.01. Moreover the increasingly large number of horizontal steps required results in large amounts of data being generated by the numerical scheme. For issues of

capacity, data was only initially retained at a limited number of vertical stations and hence the lack of 'smoothness' in the graphs shown. It is possible to reproduce these results retaining numerical results at a greater number of grid points but as such a task would be quite computationally intensive, and since these results are only required to illustrate the existence of a limit, this is not deemed necessary (in practice, on the initial run to produce this data, results were retained at a large number of horizontal points so that it would be possible to examine the behaviour as θ varies. It was then intended to re-run the program, retaining data at selected horizontal stations and with a fine vertical resolution to produce smooth curves of the results. Unfortunately, unforeseen technical difficulties have meant that this calculation is now considerably less efficient than was originally the case and so for the reasons detailed above, a second run has not been attempted).

The results are shown in Figure 5.17 at different θ positions. Since θ is taken to be $O(1)$, and we are considering the flow in the wake, results are presented at $\theta = -\pi$ and $\theta = -\frac{3\pi}{2}$. Also, guided by the scalings described above, the results shown are for $\frac{S(\frac{\eta_2}{\sqrt{a}})}{a}$.

These results seem to indicate that the numerical solutions tend towards a limit as the solidity becomes smaller. It is possible to continue to produce numerical results for smaller values of a to demonstrate the possible existence of the limit more conclusively but as discussed we are restricted by computational efficiency.

5.4.2 Blade Region Analysis

Next we consider the low solidity behaviour in a region close to the blade and initially derive an analytical solution for the low solidity blade flow which

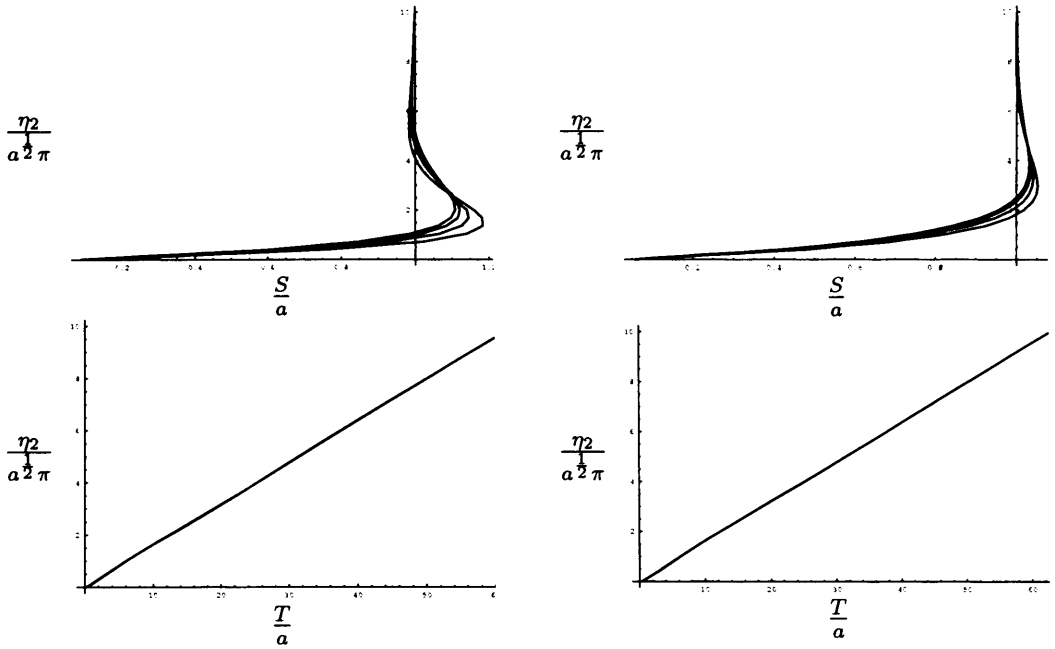

Figure 5.17: *Low disc solidity azimuthal numerical results at* $\theta = \pi$ *(left top); and at* $\theta = \frac{3\pi}{2}$ *(right top). In both cases from right to left,* $a = 0.16; 0.09, 0.04;$ *and* 0.01. *Low disc solidity radial numerical results at* $\theta = \pi$ *(left bottom); and at* $\theta = \frac{3\pi}{2}$ *(right bottom) with* $a = 0.09$ *and* 0.04. *The lack of smoothness to the graphs here is a result of the restriction of the number of vertical stations at which data was retained as part of the numerical process.*

can then be compared with our previous numerical results. In the IITL the equation for the azimuthal velocity, $v_2 = g_2'$, is

$$-\frac{\partial g_2'}{\partial \theta} = \frac{\partial}{\partial \eta_2}(\eta_2^2 g_2''^2), \tag{5.39}$$

from (5.10) and hence

$$-\frac{\partial \tau_2}{\partial \theta} = \frac{\partial^2}{\partial \eta_2^2}(\eta_2^2 \tau_2^2), \tag{5.40}$$

where $\tau_2 = g_2''$. Close to the blade, θ and η_2 are taken to scale with a, so that

$$\theta = a\bar{\theta}, \tag{5.41}$$

$$\eta_2 = a\bar{\eta}, \tag{5.42}$$

which leads to the scaling $\tau_2 = O(a^{-1})$, and so we define $\tau_2 = a^{-1}\overline{\tau}$. Now if $T = \overline{\eta}^2\overline{\tau}^2$ we have the partial differential equation

$$T^{-\frac{1}{2}}\frac{\partial T}{\partial \overline{\theta}} = -2\overline{\eta}\frac{\partial^2 T}{\partial \overline{\eta}^2}. \tag{5.43}$$

The relevant solution is of similarity type. Letting $s = \frac{\overline{\eta}}{-\overline{\theta}}$ and trying $T = H(s)$, (5.43) requires H to satisfy the ordinary differential equation

$$H^{\frac{1}{2}}H' = 2H'', \tag{5.44}$$

which, subject to the appropriate boundary conditions $H(\infty) = a$ and $H(0) = 1$, has the solution (expressing s as a function of H)

$$s = 2H^{\frac{1}{2}} + 2a^{\frac{1}{2}}\ln|(H^{\frac{1}{2}} - a^{\frac{1}{2}})| - 2 - 2a^{\frac{1}{2}}\ln|(1 - a^{\frac{1}{2}})|. \tag{5.45}$$

The solution is illustrated in Figure 5.18 for $a = 0.2$. We now compare our numerical results with (5.45) at the trailing edge of the blade and examine these results for $a = 0.2$ and $a = 0.1$, in the latter case with both one and two blade configurations. As can be seen, the numerical results are reasonably approximated by the analytical solution.

Having determined the low solidity solution close to the blade we consider how it compares to that of an isolated flat plate. One major difference between these two flows is that it has been assumed here that the junction between the two tiers of the Cebeci-Smith model lies within the OITL, leaving only the lower form within the IITL, and so in the subsequent comparison with the results of Neish & Smith the present work in the IITL is compared with the lower form of their solution on the blade. This comparison is shown in Figure 5.19.

On consideration of the solution found by Neish & Smith, the close agreement between the present work (with $a \ll 1$) and that for a flat plate is to be

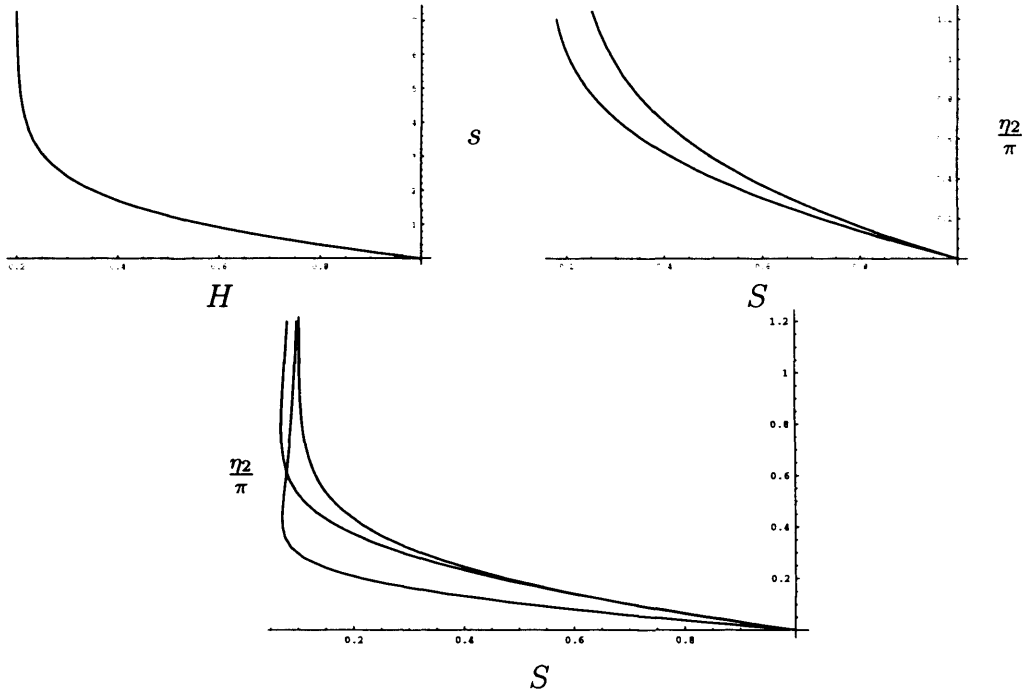

Figure 5.18: *Left top: Plot of blade region analytical solution for disc solidity* $a = 0.2$, *from* (5.45). *Right top: Comparison of numerical (lower curve on far right) and analytical blade region results at trailing edge of the blade for* $a = 0.2$ *and* $N = 1$. *Bottom: Comparison of numerical and analytical (upper curve on far right) results at trailing edge for* $a = 0.1$ *and* $N = 1$ *(lower curve on far right) and* 2 *(middle curve on far right).*

expected. On the blade, and still considering the lower tier of the Cebeci-Smith model only, they have the solution

$$u_1 = \ln \eta + 0.307 - \frac{\eta}{2} \tag{5.46}$$

for the range $0 \leq \eta \leq 1.889$, where u_1 is the perturbation from the free stream velocity (equivalent to the present g_2') and η is the same as the similarity variable s used here. Rearranging (5.46) so that it is of the same form as (5.45) we find that

$$\eta = 2H^{\frac{1}{2}} - 2, \tag{5.47}$$

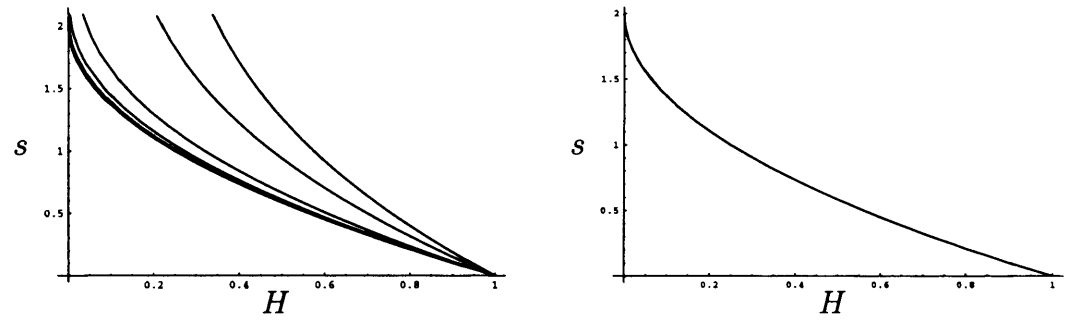

Figure 5.19: *Left: Comparison of the present work in the low solidity limit on the blade with the work of Neish & Smith for a flat plate (curve on far left). The values of the blade solidity shown are (from right to left)* $a = 0.2$*;* 0.1*;* 0.01*;* 0.001 *and* 0.0001*. Right: Comparison of present work with disc solidity* $a = 10^{-10}$ *and the work of Neish & Smith. Note that as we are presenting analytical results here it is possible to include values of the blade solidity as low as necessary, i.e. we are not restricted by numerical efficiency as in numerical solutions.*

where $H = \eta^2 u_1'^2 = s^2 g_2''^2$. Our solution (5.45) clearly reduces to that of Neish & Smith, (5.47), when $a \to 0$.

5.4.3 Near Wake Analysis

Finally we examine the near wake region of the flow. Here again θ is $O(a)$ and we define $\overline{\theta}$ and $\overline{\eta}$ as in (5.41) and (5.42), but now $|\overline{\theta}| \gg 1$ whilst still having $|\theta| \ll 1$. Then, from (5.43), making the similarity transformation $T = \frac{I(\omega)}{-\overline{\theta}}$, where $\omega = \frac{\overline{\eta}}{(-\overline{\theta})^{\frac{1}{2}}}$, yields

$$2\omega I^{\frac{1}{2}} I'' = -I - \frac{1}{2}\omega I', \tag{5.48}$$

subject to $I(0) = I(\infty) = 0$. The boundary condition at $\omega = 0$ follows immediately from the boundary condition on $T(\overline{\eta} = 0, \theta)$, whilst the condition

at infinity comes from the corresponding boundary condition, $T(\overline{\eta} = \infty, \theta) = a$ and taking $a \ll 1$. (5.48) can be solved using an RKF algorithm, which produces the solution illustrated in Figure 5.20 although this is just one of an infinite number of solutions since, from (5.48) and the corresponding boundary conditions, if $I(\omega)$ is a solution, then so is $j^2 I(j\omega)$, for any value of j.

The unique solution required can be found by consideration of the integral

$$Q = \int_0^\infty I(\omega)^{\frac{1}{2}} d\omega \tag{5.49}$$

which, by definition of $I(\omega)$ and through integration by parts, is equivalent to

$$Q = a^{-1} \int_0^\infty (v_\infty - v) dz, \tag{5.50}$$

where v_∞ is the azimuthal velocity in the IITL as $\eta_2 \rightarrow \infty$. From (5.10) in the wake, it can be shown that, with $a \ll 1$,

$$\frac{\partial Q}{\partial \theta} = 0 \tag{5.51}$$

and hence Q is conserved throughout the wake, whilst on the blade

$$\frac{\partial Q}{\partial \theta} = \frac{1}{a}. \tag{5.52}$$

Since the blade occupies an angle $2\pi a$, we have, taking $Q = 0$ at the start of the blade (which comes from the definition of $I(\omega)$),

$$Q = 2\pi \tag{5.53}$$

in the near-wake as $a \rightarrow 0$, and so

$$\int_0^\infty I(\omega)^{\frac{1}{2}} d\omega = 2\pi, \tag{5.54}$$

which determines the unique solution as required. This solution can then be compared with our numerical results for different values of a.

Bearing in mind that the wake region of interest is where $|\bar{\theta}| \gg 1$ and $|\theta| \ll 1$, we choose the values of θ at which to make comparisons accordingly, taking $6\pi a \leq -\theta \leq 36\pi a$. Again the choice of disc solidity, and hence the results available, is restricted by numerical efficiency when it comes to making comparisons. However, notwithstanding numerical efficiency, it is possible to produce results for lower values of a if necessary.

As with the low solidity results of §5.4.1, since large amounts of data are generated by the numerical method used (since the gridsizes involved are so small) only a limited amount of data can be stored. This means that output is stored at a small number of vertical stations and so the curves shown are slightly jagged. It is possible to reproduce these results, recording data at more vertical stations but at these values of the disc solidity, this would be very inefficient and since our numerical results already show good agreement with the near-wake analytical solution, it is not deemed necessary to produce more data here (the technical difficulties which applied in §5.4.1 also occur here).

Crucially, this near-wake solution only applies when $|\theta| \ll 1$ and when $\bar{\theta}$ becomes sufficiently large the condition $I(\infty) = 0$ becomes invalid and eventually the effect of the overall cut-disc structure reasserts itself on the flow through the boundary condition $I(\infty) = -a\bar{\theta}$.

5.5 Summary

We have obtained the theoretical velocity profiles within the NATBL on a cut-disc. Not only is this perhaps important as an initial model for a set of rotors but also part of the value in understanding the cut-disc case is that, within strict limits, any set of rotor blades can be reduced by use of the Prandtl shift

to a cut-disc with or without inclination. Hence knowledge of the cut-disc flow can be applied to solve the boundary layer problem, in principle, for any set of rotor blades subject to knowledge of the wake shape. This reduces the problem of the flow produced by a set of rotors to one in which we have to solve instead for the pressure outside the boundary layer, and hence the pressure on the blades and the as-yet-unknown wake shape as discussed in more detail in Chapters 6 and 7. We have also produced results which, qualitatively at least, agree with the observations of Gent et al that the normal velocity on a set of rotors is significantly greater than the radial velocity component.

Consideration of the inclined flow problem was restricted to a simplified and unrealistic scenario. That however allowed us to examine the effect of interaction between the flow just above and just below the rotating body, a feature which is of some significance when asymmetrical blade shape is involved.

In the extreme of low solidity we have found that the numerical results do appear to reduce to a limit as a tends to zero and that locally on the blade this low solidity solution is ultimately the same as the solution found by Neish & Smith for the flow past an isolated flat plate. This shows that the case where a is small can be modelled by treating the cut-disc flow as approximately that of a set of isolated blades. Although the value of a required for this approximation to be very accurate may be too low for practical helicopter configurations, nonetheless even when a is about 0.1 the present work is in reasonable agreement with that of Neish & Smith. This finding is particularly relevant to the subsequent work in Chapter 7 on the flow past asymmetric blades where we take the flow to be 2D and treat it as consisting of aligned flat plates. Finally it has also been shown that the overall (global) cut-disc response reasserts itself on the motion through the global-wake behaviour when

θ is order unity.

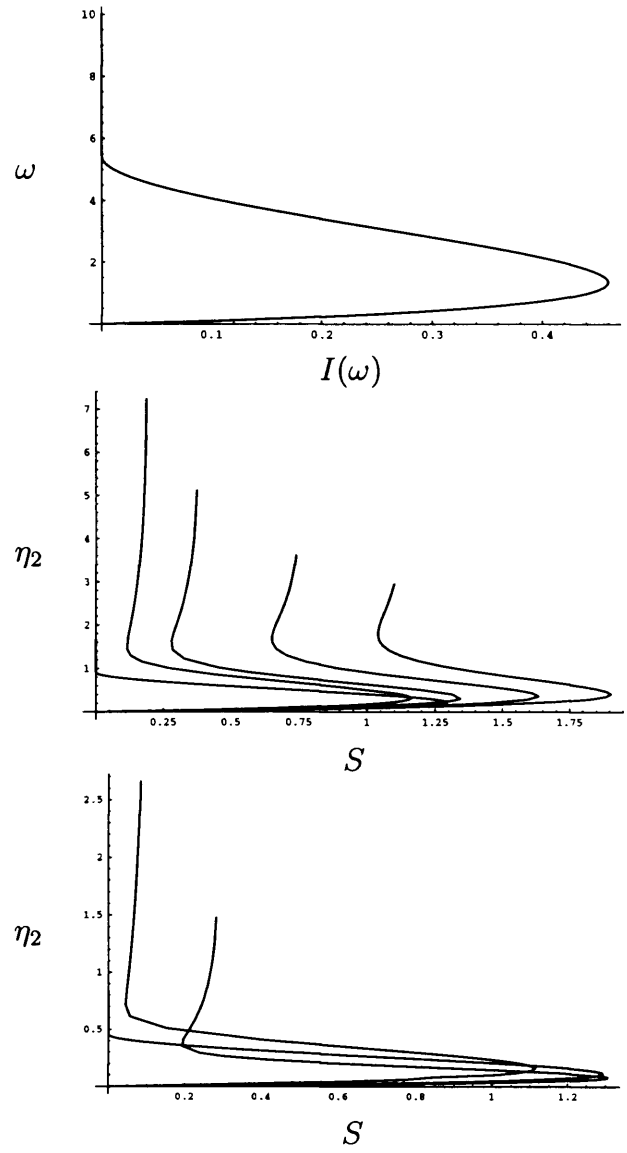

Figure 5.20: *Top: Near wake numerical solution. Middle: Comparison of near wake numerical solution and our full numerical results for* $a = 0.01$ *at varying values of* θ*. From right to left,* $\theta = -0.36\pi; -0.24\pi; -0.12\pi; -0.06\pi;$ *and* I *from numerical solution to* (5.48)*. Bottom: Comparison of near wake numerical solution and our full numerical results for* $a = 0.0025$ *at varying values of* θ*. From right to left,* $\theta = -0.36\pi; -0.12\pi;$ *and* I *from numerical solution to* (5.48)*.*

Chapter 6

On Rotors with Vertically Symmetric Blade Shape

6.1 Introduction

Until now the present investigation has been restricted to flat, although possibly inclined, surfaces as a simplification. In practice though a set of rotors will have blades with shape (thickness), an important aspect to consider. Obviously in the two solid-surface flows which have been examined (those of a flat plate with a moving surface and a rotating disc) it might be expected that constant body thickness has no impact on the flow except perhaps as an edge effect, which is an influence that is ignored here. In contrast, blade thickness could be expected to significantly affect the flow generated by a rotating cut-disc. It is possible to extend the analysis of the cut-disc flow of Chapter 5 to include blades with thickness: in an initial step we now consider the flow produced by a cut-disc with symmetric blade shape, where this is taken to mean that the thickness of the blade at all points is the same above and below

the plane in which the body is rotating, as illustrated in Figure 6.1.

$$u_D \ll 1, v_D \ll 1$$

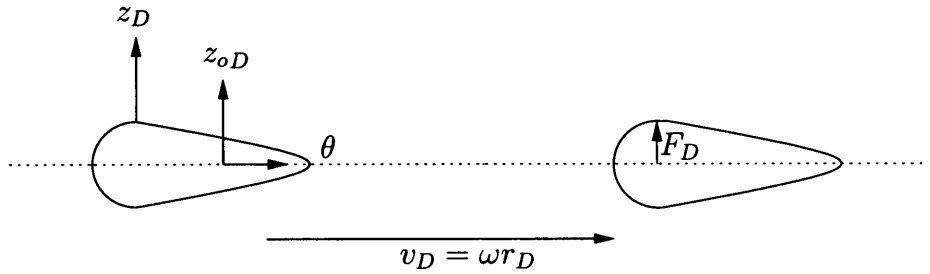

Figure 6.1: *Radial view of a cut-disc with symmetric blade thickness denoted F_D. The actual height z_{oD} and the Prandtl shift height z_D are both included for guidance and the upper dashed line denotes the junction of the boundary layer and the outer inviscid region.*

In truth, symmetric blade flow is of little direct interest here - symmetric blades do not generate lift and so are of no practical use in helicopter design - instead it is asymmetric blades which, ideally, we want to model. Unfortunately the latter case is extremely complicated and so initially the blade shapes are taken to be symmetric as a simplification (asymmetry is considered in Chapter 7). Importantly the symmetric flow is much easier to solve than the more realistic and practically more useful one of flow past blades with asymmetric shape, yet it incorporates several of the features of the asymmetric flow system, and it is therefore a useful problem to consider. This chapter is concerned with those important aspects of the asymmetric case which are shared with the symmetric problem using the latter flow as a vehicle for exam-

ining these features without having to contend with some of the more difficult elements of asymmetric blades.

The key similarities between the symmetric and asymmetric flows which are of interest to the present investigation are as follows:

1. the use of the Prandtl shift (see Appendix C) to reduce the boundary layer to that on a cut-disc;

2. the subsequent applicability of the Reynolds equations and NATBL structure of Chapter 4 and hence the cut-disc results of Chapter 5;

3. the formulation of Laplace's equation as the governing equation for the pressure outside the NATBL;

4. and the influence of the blade shape on the outer pressure problem through a boundary condition at the edge of the NATBL.

The symmetric case involves a considerable simplification over the asymmetric flow in that the blade symmetry means we do not have to determine the wake shape (a complicated part of the asymmetric problem). This symmetric problem is thus used as a means of investigating those features described, without having to deal with the wake shape. In particular this is done by examining a highly idealized symmetric flow problem where the following restrictions are made. Firstly, for the previous work of Chapters 4 and 5 to apply, a similarity solution must again be used within the turbulent boundary layer, and then also outside the NATBL to simplify the numerical problem. Crucially, as it turns out, this means that the blade thickness must grow linearly with the radius. Secondly, only rotor configurations consisting of three or more blades are considered, each of which has shape satisfying

$$\int_0^L \frac{\partial^2 F_D}{\partial \theta^2} d\theta = 0, \tag{6.1}$$

where L is the period of the configuration and F_D is the dimensional blade shape. These conditions on the rotor configuration and blade shape are required to ensure a solution, of the form subsequently used in §6.3, which decays at infinity, is possible. Finally the typical thickness of the blades is assumed to be sufficiently small that it has no qualitative impact on the general structure of the turbulent boundary layer. Again it is noted that these restrictions render this problem to be very unrealistic but that our key objective is to illustrate those points enumerated above, not to derive a general solution to the symmetric blade problem.

The laminar version of this flow has been examined analytically and numerically by Smith & Timoshin[68,69] who firstly reduced the system to that on a cut-disc (using the Prandtl shift) and then solved the resulting boundary layer problem. They then considered the 2D outer potential flow past aligned blades with symmetric (and also asymmetric) blade shape. In particular their approach of reducing the flow to that on a cut-disc is adopted here.

In contrast however the turbulent flow past a set of symmetric rotors does not appear to have been examined in any great detail to date. This is probably in large part due to the relative unimportance of symmetric blade flow when compared with the equivalent asymmetric problem which has been studied in far more depth (see Smith & Timoshin[68,69], Nakayama[49] and Riley & Brotherhood[60]). Nonetheless, although blades with symmetric shape are of little interest with respect to helicopters, indirectly the present problem may be more relevant in other industrial applications such as engine components, food mixers, etc, where rotor blade configurations are used for purposes other than for generating lift.

This chapter will proceed as follows. In §6.2 the governing equations for

this symmetric case will be set out and the system posed as two problems - that of the flow in the turbulent boundary layer and that of the pressure outside the NATBL. Each of the key aspects of this present problem (the Prandtl shift, the application to the cut-disc flow, the formulation of the outer pressure problem and the influence of the blade shape) will be discussed in turn. Then, subject to the restrictions mentioned above, in §6.3 a numerical procedure for solving for the pressure on the blade is described and results produced for a given, albeit unrealistic, blade shape.

As shown later, for any given blade shape the results of §4.4 and §5.2 can readily be used to determine the velocity components within the NATBL, but this will not be included here as the symmetric case is of limited direct interest. Instead we concentrate on the solution for the pressure at the edge of the boundary layer and hence the pressure on the blades.

6.2 Governing Equations and Problem Formulation

As mentioned above, it is assumed that the NATBL structure described in §4.3 applies here. Taking the dimensional blade shape to be given by $F_D(r_D, \theta)$, this then leads to the following non-axisymmetric dimensional Reynolds equations

$$\frac{\partial u_D}{\partial t_D} + u_D\frac{\partial u_D}{\partial r_D} - \frac{v_D^2}{r_D} + \frac{v_D}{r_D}\frac{\partial u_D}{\partial \theta} + w_D\frac{\partial u_D}{\partial z_D} - 2\omega v_D - \omega^2 r_D = -\frac{1}{\rho}\frac{\partial p_D}{\partial r_D} + \nu\frac{\partial^2 u_D}{\partial z_D^2} + \frac{\partial}{\partial z_D}(\nu_{tD}\frac{\partial u_D}{\partial z_D}) \tag{6.2}$$

and

$$\frac{\partial v_D}{\partial t_D} + u_D\frac{\partial v_D}{\partial r_D} + \frac{u_D v_D}{r_D} + \frac{v_D}{r_D}\frac{\partial v_D}{\partial \theta} + w_D\frac{\partial v_D}{\partial z_D} + 2\omega u_D = -\frac{1}{\rho r_D}\frac{\partial p_D}{\partial \theta} + \nu\frac{\partial^2 v_D}{\partial z_D^2} + \frac{\partial}{\partial z_D}(\nu_{tD}\frac{\partial v_D}{\partial z_D}), \tag{6.3}$$

with

$$\nu_{tD} = \begin{cases} k_2\omega r_D\delta_D^*, \\ k_1^2(z_D - F_D)^2[1 - \exp(-\frac{z_D}{26\nu}(\frac{\tau_{WD}}{\rho})^{\frac{1}{2}})]^2[(\frac{\partial u_D}{\partial z_D})^2 + (\frac{\partial v_D}{\partial z_D})^2]^{\frac{1}{2}}, \end{cases} \tag{6.4}$$

and continuity equation

$$\frac{1}{r_D}\frac{\partial(u_D r_D)}{\partial r_D} + \frac{1}{r_D}\frac{\partial v_D}{\partial \theta} + \frac{\partial w_D}{\partial z_D} = 0. \tag{6.5}$$

The boundary conditions at infinity are,

$$u_D = v_D = w_D = 0, \tag{6.6}$$

and those at $z_D = F_D$ are,

$$u_D = w_D = 0, \tag{6.7}$$

$$v_D = \omega r_D. \tag{6.8}$$

This system can now be conveniently split into two, coupled problems. As with the flows previously considered there is the question of the velocity profiles within the NATBL and secondly there is a new element, that of the pressure in the inviscid flow region - the outer pressure problem. In order to understand both these aspects of the flow it is now convenient to reduce the symmetric blades to flat surfaces through use of the Prandtl transformation.

6.2.1 The Prandtl Shift and Transformation to the Cut-Disc Flow

After the Prandtl transformation ($C.1$) and ($C.2$) is performed, (6.2) and (6.3) remain unchanged whilst (6.4), (6.6) - (6.8) reduce to the eddy viscosity and

boundary conditions pertinent to a rotating cut-disc. Then if the similarity solution (4.24) - (4.26) is applied, the governing equations for the flow within the turbulent boundary layer are taken to be (4.29) and (4.30). Hence the results of §4.4 and §5.2 now hold for this flow too except that here we are using the transformed Prandtl co-ordinate system ($C.1$) and ($C.2$) rather than the actual normal velocity and height.

The radial and azimuthal velocities illustrated in Figures 4.2, 5.5 and 5.8 are valid here, except that the heights used, η_1 and η_2, should be interpreted as the normal distance from the cut-disc, rather than the actual height above the plane of rotation as they were taken in Chapters 4 and 5. All that is then required to solve for the boundary layer part of the problem is to transform the cut-disc results of Chapter 5 to yield the real normal velocity component for a given $F_D(r_D, \theta)$. As discussed above we instead consider the second aspect of this flow, that of the pressure response in the inviscid flow region.

6.2.2 The Outer Pressure Problem and the Influence of the Blade Shape

Since it is the pressure, or more specifically the pressure difference, exerted on a rotor blade which generates lift, making helicopter flight possible, it is vital to understand how blade shape affects the pressure experienced by a rotor blade. Within the NATBL it is possible to work in the Prandtl shifted co-ordinates and hence to dispense with the precise blade thickness for the purposes of determining the velocity in the transformed system. The influence of the blade shape reasserts itself on the flow through the modified normal velocity, and hence through a continuity condition at the edge of the boundary layer. The pressure outside the NATBL must then satisfy this condition.

We seek to calculate the pressure at the edge of the boundary layer, which, since the pressure is taken to be independent of height within the NATBL, yields the pressure on the blade. The system is taken to be suitably non-dimensionalized and outside the boundary layer the viscous and Reynolds stresses are negligible and the fluid velocity is small, so that nonlinear inertial terms can be ignored. Thus we have the governing equations

$$\frac{\partial u}{\partial t} = -\frac{\partial p}{\partial r}, \tag{6.9}$$

$$\frac{\partial v}{\partial t} = -\frac{1}{r}\frac{\partial p}{\partial \theta}, \tag{6.10}$$

$$\frac{\partial w}{\partial t} = -\frac{\partial p}{\partial z}. \tag{6.11}$$

Here cylindrical polar co-ordinates in a fixed frame are used, with continuity equation

$$\frac{\partial u}{\partial r} + \frac{u}{r} + \frac{1}{r}\frac{\partial v}{\partial \theta} + \frac{\partial w}{\partial z} = 0. \tag{6.12}$$

Combining (6.9) - (6.12) yields Laplace's equation for the pressure outside the boundary layer,

$$\frac{\partial^2 p}{\partial r^2} + \frac{1}{r}\frac{\partial p}{\partial r} + \frac{1}{r^2}\frac{\partial^2 p}{\partial \theta^2} + \frac{\partial^2 p}{\partial z^2} = 0. \tag{6.13}$$

Now the co-ordinate system is transformed to one which rotates with the set of rotors by defining $\bar{\theta} = \theta - t$ so that, assuming the flow to be steady in this new reference frame, (6.13) becomes

$$\frac{\partial^2 p}{\partial r^2} + \frac{1}{r}\frac{\partial p}{\partial r} + \frac{1}{r^2}\frac{\partial^2 p}{\partial \bar{\theta}^2} + \frac{\partial^2 p}{\partial z^2} = 0, \tag{6.14}$$

while (6.11) now transforms to

$$\frac{\partial w}{\partial \bar{\theta}} = \frac{\partial p}{\partial z}. \tag{6.15}$$

Here, after consideration of the Prandtl shift transformations ($C.1$) and ($C.2$), (6.15) yields the following condition at the edge of the boundary layer,

$$\frac{\partial^2 F}{\partial \bar{\theta}^2} = \frac{\partial p}{\partial z}\Big|_{z=0}, \tag{6.16}$$

where $F(r,\theta)$ is the non-dimensional blade shape. This condition arises since the normal velocity w at the edge is independent of θ and since $u \to 0$ and $v \to -r$ here. Actually the full condition is, from Smith & Timoshin,

$$\frac{\partial^2}{\partial\bar{\theta}^2}(F+\delta) = \frac{\partial p}{\partial z}|_{z=0}, \tag{6.17}$$

where δ is the boundary layer thickness. Here we take the size of the blade shape to dominate over the boundary layer thickness and so δ is ignored for convenience.

Therefore given any particular blade shape F we have a boundary condition, (6.16), for the normal pressure gradient which we can apply at the edge of the NATBL and thus to the flow in the outer inviscid region. We are now in a position to solve for the pressure outside the boundary layer and do so in the next section by first describing a method of solution for this highly idealized symmetric flow then illustrating the method with a simple (and unrealistic) blade shape.

6.3 Method of Solution to the Outer Pressure Problem

The system (6.14) is to be solved subject to (6.16), as well as $p(r,\infty,\bar{\theta}) = 0$. A solution is attempted by means of a similarity transformation, first noting that from now on we use θ rather than $\bar{\theta}$ for convenience. Supposing that $p = r^n P(\eta,\theta)$, where $\eta = \frac{z^q}{r^m}$, and substituting this into (6.14), we find that for the powers of r in each term to balance it is necessary to take $q = m = 1$. This yields

$$\frac{\partial^2 P}{\partial\theta^2} + (1+\eta^2)P'' - (2n-1)\eta P' + n^2 P = 0, \tag{6.18}$$

where $'$ denotes partial differentiation with respect to η. This then suggests the following form for $F(r,\theta)$

$$F(r,\theta) = r\overline{F}(\theta). \tag{6.19}$$

It is worth repeating at this stage that the assumption of this similarity substitution is a sizeable restriction on the particular flow which is examined here, especially since the blade shape is required to grow with the radius.

Consideration of (6.16) then yields $n = 2$ and hence

$$\frac{\partial^2 P}{\partial\theta^2} + (1+\eta^2)P'' - 3\eta P' + 4P = 0. \tag{6.20}$$

Next a solution of the following form is attempted:

$$P = Re[\sum_{k=0}^{\infty} A_k \exp(ikN\theta)\phi_k(\eta)], \tag{6.21}$$

where N is the number of blades, and which upon substitution transforms (6.20) into the following equation for ϕ_k,

$$(1+\eta^2)\phi_k'' - 3\eta\phi_k' + (4 - k^2N^2)\phi_k = 0. \tag{6.22}$$

Equation (6.22) is suitable for solution with an RKF algorithm but first we should check to see if (6.22) yields solutions which satisfy the boundary conditions at infinity and at the edge of the boundary layer. To this end we begin by examining the boundary condition at $\eta = 0$ and here it is useful to rewrite (6.16) as

$$a_0 + \sum_{k=1}^{\infty}[a_k \cos(\frac{2k\pi\theta}{L}) + b_k \sin(\frac{2k\pi\theta}{L})] = Re[\sum_{k=0}^{\infty} A_k \exp(ikN\theta)\phi_k'(0)], \tag{6.23}$$

where

$$\frac{\partial^2\overline{F}}{\partial\theta^2} = a_0 + \sum_{k=1}^{\infty}[a_k \cos(\frac{2k\pi\theta}{L}) + b_k \sin(\frac{2k\pi\theta}{L})] \tag{6.24}$$

is the Fourier Series for $\frac{\partial^2 \overline{F}}{\partial \theta^2}$ with Fourier coefficients given by the formulae

$$a_0 = \frac{1}{L}\int_0^L \frac{\partial^2 \overline{F}}{\partial \theta^2} d\theta, \tag{6.25}$$

$$a_k = \frac{2}{L}\int_0^L \frac{\partial^2 \overline{F}}{\partial \theta^2} \cos\left(\frac{2k\pi\theta}{L}\right) d\theta, \tag{6.26}$$

$$b_k = \frac{2}{L}\int_0^L \frac{\partial^2 \overline{F}}{\partial \theta^2} \sin\left(\frac{2k\pi\theta}{L}\right) d\theta. \tag{6.27}$$

Here L is the period of the configuration and so $N = \frac{2\pi}{L}$. Defining $\phi_k'(0) = 1$ for convenience, (6.23) then reduces to the condition

$$A_k = a_k - ib_k \tag{6.28}$$

which can be calculated from (6.25) - (6.27). Hence defining A_k by (6.28) ensures that (6.16) holds.

It is worth noting that in most cases we are at liberty to normalize ϕ_k such that $\phi_k'(0) = 1$ since it is possible to scale A_k appropriately to ensure this. A difficulty may arise if we need to take $\phi_k'(0) = 0$ for some value of k. In this case $a_k = b_k = 0$ from (6.23), for some k, and this may then mean that there are terms in the expansion for the pressure which are non-zero at the edge of the boundary layer but which have zero normal pressure gradients and hence are not determined here. It is easy to verify for any given blade shape whether there may be a difficulty with the definition of ϕ_k used here, simply by examining the Fourier coefficients involved and this needs to be checked for any particular blade shape studied.

We also need to ensure that the condition $p \to 0$ at infinity holds. This is now equivalent to $\phi_k(\infty) = 0$ for all k. Examining the limit as $\eta \to \infty$, (6.22) becomes

$$\eta^2 \phi_k'' - 3\eta\phi_k' + (4 - k^2N^2)\phi_k = 0, \tag{6.29}$$

which has the solutions $\phi_k = \eta^{2+kN}$ and $\phi_k = \eta^{2-kN}$. Unless $k = 0$ we have

therefore determined the behaviour of both solutions at infinity. From (6.25), the restriction on blade shape, (6.1), now implies that $A_0 = 0$ and so the behaviour of $\phi_0(\infty)$ is irrelevant for this flow since ϕ_0 makes no contribution to the pressure and so the case $k = 0$ is of no concern and can be ignored. Further, since from §6.1 we are only considering the case where $N \geq 3$, for all $k \geq 1$ there is a solution to (6.22) which decays at infinity (the restrictions imposed on the blade shape and the number of blades are included precisely to avoid any problems with the flow at infinity).

Having ensured that there exists solutions to (6.22), and hence (6.20), which satisfy the appropriate boundary conditions, it is now possible to solve this problem for any given blade shape. Firstly the Fourier series for $\frac{\partial^2 \overline{F}}{\partial \theta^2}$ is determined and the Fourier coefficients used to determine A_k. (6.22) is then solved using an RKF algorithm using the boundary conditions $\phi_k'(0) = 1$ and $\phi_k(\infty) = 0$. From this solution $\phi_k(0)$, and hence the pressure on the blades, is determined. In this case a finite height of twenty is used instead of infinity and (6.22) solved for all values of $k \leq k_{max}$ where k_{max} is increased until a converged solution is found. This method is now illustrated by solving for the pressure given a known blade shape.

6.3.1 Solution with $\overline{F}(\theta) = \theta^3(1 - \frac{\theta}{\theta_0})^3$ and Four Blades

We now determine the pressure on a set of blades each of which has identical shape given by $\overline{F}(\theta) = \theta^3(1-\frac{\theta}{\theta_0})^3$ as illustrated in Figure 6.2 where, in the case presented $\theta_0 = \frac{\pi}{5}$ and the number of blades is taken to be four, corresponding to disc solidity $a = 0.4$. This choice of blade shape is chosen to ensure that (6.1) holds and to aid the calculation of the Fourier coefficients and it must be noted that this is a wholly unrealistic choice, which is immediately apparent when

compared with a realistic helicopter rotor blade (for example see Nakayama[49] or Riley & Brotherhood[60].

Mathematica was used to determine the Fourier coefficients and hence A_k for all values $k \leq k_{max}$ where k_{max} is taken, in turn, to be twelve, twenty-five and fifty, and the results are presented in Figure 6.2. As can be seen the solution for the pressure seems to converge well before fifty terms and hence it is not deemed necessary to include further terms in the expansion for $P(\eta, \theta)$. Figure 6.2 also shows that the pressure is largely constant in each wake which might be expected as the wake shape is flat in this symmetric case.

6.4 Summary

We have shown how the problem of the flow generated by a set of rotor blades with symmetric blade shape can be reduced to that of the NATBL on a cut-disc and to solving Laplace's equation for the pressure outside the NATBL. This is important as the same process is involved in determining the solution to a system with asymmetric blade shape (except that there is the added complication of the unknown wake shape to be determined). In particular we have shown how the velocity profiles within the turbulent boundary layer can be found from knowledge of the blade shapes and the results of the cut-disc flow. This is also partially true for the asymmetric case where the velocity profiles within the NATBL can be determined on the blade. For the solution in the wake however it is necessary for the wake shape to be determined.

The actual method of solution used here, and hence the results for the pressure exerted on the blade, is highly restricted and only applies to very limited cases. Nonetheless there is an important aspect which can be drawn from this idealized problem. The derivations of the blade shape-dependent bound-

ary condition and Laplace's equation for the pressure hold for more general flows. Hence for a given blade shape the outer pressure problem requires the solution of Laplace's equation subject to a known boundary condition for the pressure gradient. Again this also holds for the asymmetric case except that the condition on the pressure gradient now involves the unknown wake shape as well.

It may be possible to extend this work to the case of more realistic rotor blade configurations but since the problem of symmetric blades is of limited interest beyond those aspects which it shares with the asymmetric case, it is not judged necessary to do so here. In particular, one of the most severe limitations is the similarity solution introduced in §6.3 but avoiding this necessitates a solution to the fully 3D system (6.14) subject to (6.16). Instead we proceed to examine the case of asymmetric blade shape.

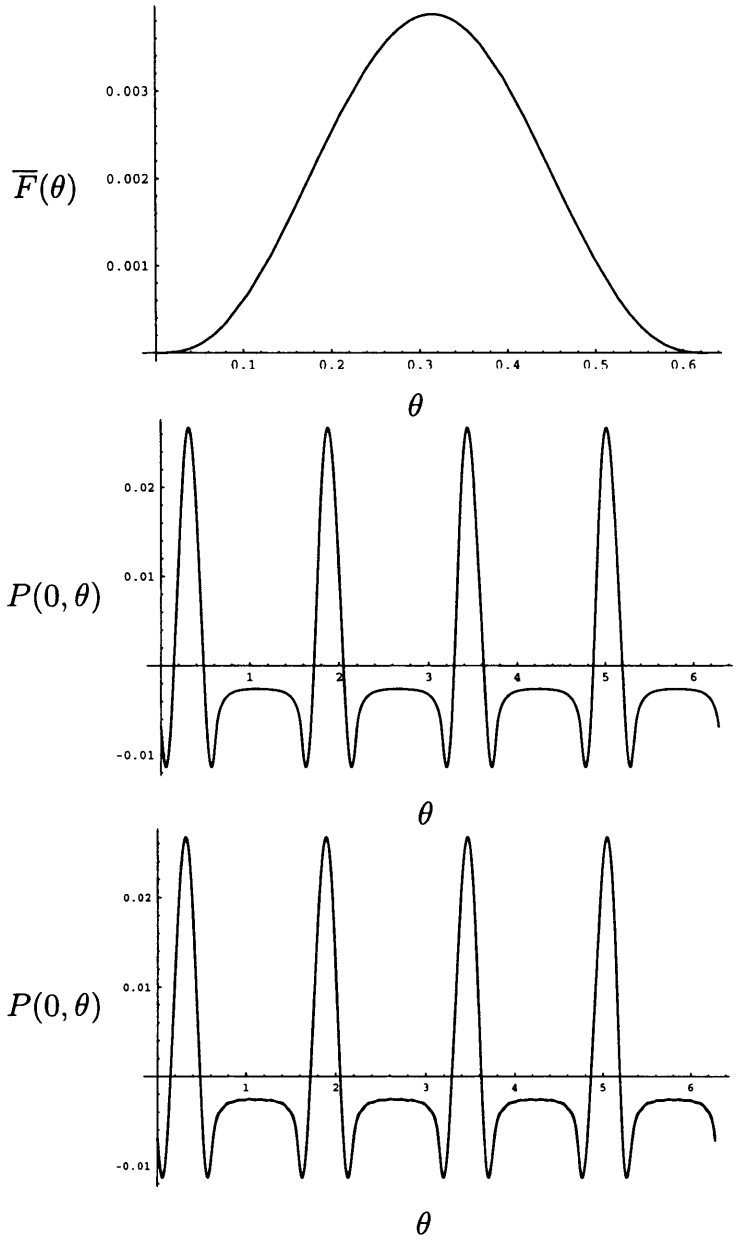

Figure 6.2: *Top: The blade thickness,* $\overline{F}(\theta) = \theta^3(1 - \frac{\theta}{\theta_0})^3$ *with* $\theta_0 = \frac{\pi}{5}$. *Middle: The pressure on each blade and wake of a cut-disc with symmetric blade shape given by* $\overline{F}(\theta) = \theta^3(1 - \frac{\theta}{\theta_0})^3$ *with* $\theta_0 = \frac{\pi}{5}$, $a = 0.4$ *and* $N = 4$. *Bottom: Comparison of results for pressure* $P(\theta, 0)$ *with twelve, twenty-five and fifty terms of* (6.21).

Chapter 7

On Rotors with Vertically Asymmetric Blade Shape and the Influence of Ground Effect

7.1 Introduction

In helicopter dynamics, the properties of flow past blades with asymmetric shape are more significant than the earlier studied symmetric cases since it is this asymmetry which, in creating a pressure difference across the surface of the blades, allows the rotor to generate lift, enabling helicopters to fly. Thus whilst several aspects of rotor blade flow (the non-axisymmetry, interaction of the flow above and below the blade, and variable external pressure) have already been considered, asymmetry is such a fundamental feature that we now investigate the flow past a set of rotors with asymmetric blade shape.

The general problem of three-dimensional (3D) flow past asymmetric blades is very complicated and although the principles of flight are the same for both

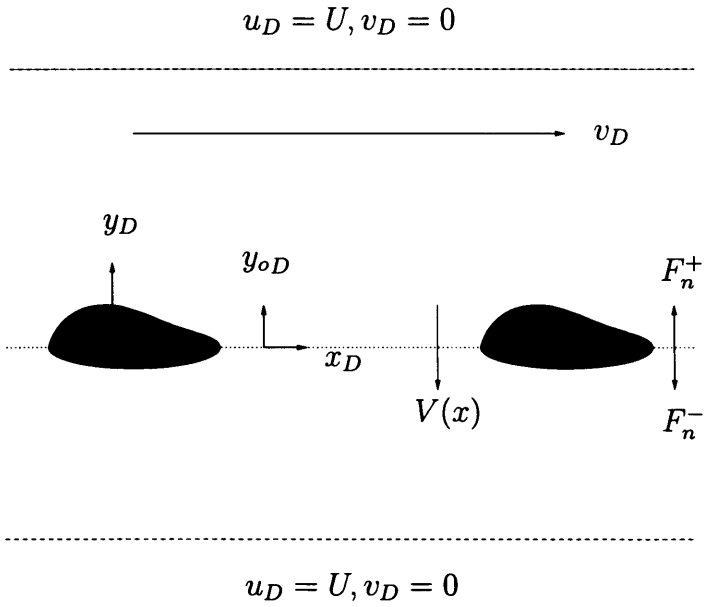

Figure 7.1: *Diagram of a set of adjacent airfoils in a free stream. The actual height, y_{oD}, and the Prandtl shift height, y_D, are shown for comparison, as are the upper and lower blade shapes F_n^+ and F_n^- respectively. The upper and lower dashed lines represent the edges of the turbulent boundary layer outside of which the flow is that of the free stream velocity.*

rotary-wing aircraft (such as helicopters) and fixed-wing vehicles (such as airplanes), in the former case the wake generated at the trailing edge of one blade is likely to interact with the next blade (see Purvis[58] and Smith & Timoshin[68,69]), creating a complicated flow regime. Thus for a set of realistic rotors it is judged important to not only consider flow past an isolated blade, but also that past many blades. The latter configuration presents many difficulties. It can be reduced to the problem of the flow around a cut-disc (possibly with inclination) through use of the Prandtl shift but then one must solve for the pressure outside the boundary layer, which is determined by the as yet unknown wake shape and boundary layer thickness, which cannot be

calculated without knowledge of the external pressure. This is the documented phenomenon of inner-outer interaction (Smith & Timoshin) where the outer pressure problem and the inner wake shape need to be resolved simultaneously.

The above complexity is somewhat prohibitive when it comes to studying the asymmetric flow problem and so, whilst there is an extensive amount of existing research on the flow past asymmetric blades, much of this work takes the case where they are isolated, such as in the experimental work conducted by Nakayama[49], and so is of little direct interest here. Of more relevance are CFD based numerical models of helicopter rotor blade flow such as Yihua, Zhiqiang & Yuan[82] [1] and existing experimental work on actual helicopter rotors including cases where sensors have been fitted to the rotor blades and have been able to measure the pressure and velocities which occur (see Riley & Brotherhood[60]).

The laminar case of flow generated by a [illegible] rotor with asymmetric blade shape has been studied by Smith & Timoshin[68,69] who, as with the case of blade symmetry, used the Prandtl shift to reduce the boundary layer to that on a cut-disc (which for symmetric flow they subsequently solved numerically and analytically). In the particular case of blade asymmetry the cut-disc problem has to be solved with vertical shifts in the velocity profiles at each leading edge (as was the case when a cut-disc with inclination was considered in Chapter 5). This is to take account of the fact that the wake centre line no longer necessarily runs from the trailing edge of one blade to the leading edge of the next one. Smith & Timoshin then considered the 2D inviscid potential flow problem outside the boundary layer. In the latter part, Smith & Timoshin[69] were able to derive a solution for the unknown pressure difference on the blades and normal velocity jump across the wakes which is determinable

1. Also see Strawn & Ahmad[83].

from knowledge of the blade shapes, boundary layer thicknesses and vertical wake shifts. Crucially, their work on the outer pressure problem immediately applies to the configuration of interest here since turbulent stress is taken to be negligible outside the boundary layer.

Vertical flow asymmetry is of course not just confined to blade shape. Another important aspect of helicopter dynamics is the significant influence that the ground (or indeed any such surface) has on the flow regime. This ground effect is important for several reasons. One is the sheer scale of the influence - it is believed (see Bramwell[8]) that early helicopter flight was only made possible due to ground effect as there is a sizeable reduction in, say, the power required to sustain a helicopter in hover when the ground is near compared with when the distance to the ground is large. Another reason is that helicopters will obviously experience ground effect regularly (at least during take-off and landing for every flight) and so this phenomenon occurs extensively. Hence the influence of the ground (which is taken to be a solid impermeable wall horizontal to and directly below the rotor blades) is examined here.

Purvis[58] examined the laminar system of a rotating disc, and that of a body (an under-carriage) attached to a rotating disc, both at various distances from the ground. Similarly, the problem of the flow (laminar and turbulent) between a rotating and a stationary disc has been investigated by many preceding authors. This will be discussed in more detail in Chapter 8, although it is noted here that these two-disc flows are not directly relevant to the present problem as they involve ground effect acting on a viscous height scale, which is much shorter than the height scales considered in the present chapter.

Now we consider one particular aspect of the asymmetric flow: the inviscid potential flow past a succession of asymmetric blades and the influence of the

ground over a (quite) large vertical length scale. Essentially this means that the effect of the ground is felt on the whole system and does not interact with individual blades (whereas in Chapter 8 the influence of the ground is examined on a viscous length scale so that interaction between the ground and the turbulent boundary layer is considered). In particular here the study is restricted to 2D flow and the blades are taken to be sufficiently small that on a global scale they appear only as points, corresponding to the surface solidity a being small. Following the work in Chapter 5 on the low disc solidity limit on a cut-disc, we anticipate that this 2D system will be a reasonable approximation to the desired 3D case when the disc solidity a is small. As with the symmetric blade configurations of the previous chapter, the boundary layer thicknesses are considered negligible in comparison to the blade shape and are therefore omitted.

The current problem is of interest for the following reasons. As mentioned above, asymmetry is highly important in realistic helicopter dynamics and so we now want to examine the impact this has on the pressure and the fluid downwash, and how particular blade shapes (or rather, the difference in the upper and lower blade shapes) affect these two quantities. Moreover, as we are considering 2D potential flow it is relatively straightforward to extend this system to one which incorporates ground effect, which is another substantial feature of many practical rotor blade flows. The restriction to 2D is designed to simplify the problem and allows the existing results of Smith & Timoshin to be applied here (the difficulties inherent in the analogous 3D flow are discussed in §7.5). The non-axisymmetric turbulent boundary layer (NATBL) is not considered here since our earlier work on a cut-disc now applies, albeit in terms of the Prandtl co-ordinates. Crucially the assumption here that the

boundary layer thicknesses are negligible compared to the blade shape allows us to divorce the inner and outer aspects of this problem and allows a solution to be derived more readily.

We begin (in §7.2) by describing the flow which Smith & Timoshin examined and include those results which are relevant to the present system. In §7.3 we then set out the specific flow problem that is to be examined and proceed to build on these previous results to derive solutions on two different length scales. First the pressure on a blade and the downwash in the wake in a region close to the blade are derived (§7.3.1); this local solution is then illustrated for a simple blade shape (§7.3.2) and compared with a numerical solution to a truncated version of the full result of Smith & Timoshin (§7.3.3). Then the global form of the downwash (also known as the induced velocity) is determined, where the distance to the nearest blade is large (§7.3.4), and the two solutions are matched. This global solution is then extended to form a complex potential (§7.3.5) on the global scale before the influence of ground effect is incorporated through the use of an image potential (§7.4). Finally, as mentioned above, in §7.5 the 3D flow problem is briefly discussed.

7.2 Problem Formulation and Governing Equations

Here we seek to use the work of Smith & Timoshin[69] to see if a periodic 2D solution exists for the inviscid potential flow past a set of asymmetric blades. Since their results form the basis of the subsequent work in this chapter, the flow which they examined is now briefly discussed before a solution pertinent to the present investigation is produced.

The (non-dimensional) flow which Smith & Timoshin considered was for the physical system of a uniform stream of unit magnitude past an array of N aligned blades each of which runs from a_n (the leading edge) to b_n (the trailing edge), where $1 \leq n \leq N$ and where all the leading and trailing edges lie along the line $y = 0$ as indicated in Figure 7.1. This classification of the leading and trailing edges leads to the obvious description of each blade as $a_n b_n$ which is now used throughout. The analysis of Smith & Timoshin applies equally whether N is finite or not but since they considered viscous flow there exists boundary layers on all the blades. Since each boundary layer grows monotonically, Smith & Timoshin were restricted to a finite number of blades. With the present flow the boundary layers are taken to be so negligibly small that even in the limit as N approaches infinity they can still be ignored and so we are able to apply the results of Smith & Timoshin for any value of N, including infinity.

Each blade is taken to have asymmetric thickness and hence the upper and lower blade shapes F_n^+ and F_n^- are taken to apply in the regions $y \geq 0$ and $y \leq 0$ respectively whilst the wake shape (or alternatively the wake centre line) is denoted W_n for the wake running from b_n to a_{n+1}. These blade and wake shapes are then combined into two global shape functions, f_+ and f_-, corresponding to the upper and lower halves of the flow respectively. f_+ is defined piecewise as

$$f_+(x) = \begin{cases} F_n^+(x) & \text{for } a_n \leq x \leq b_n \\ W_n(x) & \text{for } b_n \leq x \leq a_{n+1} \end{cases} \tag{7.1}$$

for $a_n \leq x \leq a_{n+1}$, with a similar definition applying to f_-. These shape functions are then used by Smith & Timoshin when defining the Prandtl shift (Appendix C), thereby reducing the problem to that of a cut-disc where there

is a pressure difference across the blades and a nonzero downwash[1] in the wakes. In this description the blade shapes are measured as the distance from the line $y = 0$ (as illustrated in Figure 7.1) and so in the wake $f_+ - f_- = 2W_n$.

The outer potential flow here is the same as that in Chapter 6. However in the case where the blades have symmetric thickness we were only concerned with the pressure perturbations outside the NATBL which by symmetry were the same above and below the blade. Now with asymmetry introduced it is necessary to consider the pressure in both the upper and lower halves of the flow, denoted p_+ and p_- respectively, both of which satisfy Laplace's equation following the analogous result (6.13) of §6.2.2. Since ultimately the actual pressures exerted on the upper and lower surfaces of the blade matter only in terms of the difference in the pressure, it is now more practical to deal with the pressure difference

$$p = p_+ - p_-. \tag{7.2}$$

Due to the linearity of the Laplace operator the pressure difference also satisfies Laplace's equation and hence

$$\nabla^2 p = 0. \tag{7.3}$$

From Smith & Timoshin the boundary conditions for p are

$$p(x,0) = 0 \quad \text{for } b_n \leq x \leq a_{n+1}, \tag{7.4}$$

$$\frac{\partial p}{\partial y}(x,0) = -V'(x) \quad \text{for } a_n, \leq x \leq b_n, \tag{7.5}$$

where $V(x) = (f_+ + \delta_n^+ - f_- - \delta_n^-)'$ on the blades, and which, from the definition of the Prandtl shift, is equivalent to the difference in the normal velocities above and below the line $y = 0$, denoted v_+ and v_- respectively. It is important to note that as with the blade shapes, the normal velocity in each half of the flow is measured in opposite directions. Hence in the wakes $v_+ - v_- = 2v_+$

1. i.e. Here is a nonzero normal velocity across the wake line.

and so $V(x)$ is equivalent to twice the downwash. Here δ_n^+ and δ_n^- are the boundary layer thicknesses on the upper and lower sides of the blade. Smith & Timoshin then use the work of Muskhelishvili[48] for mixed boundary value problems to derive the following solution for $V(x)$ in the wakes:

$$\pi V(x) = \prod_{\iota=1}^{N} \left|\frac{x-b_\iota}{x-a_\iota}\right|^{\frac{1}{2}} \sum_{i=1}^{N} \int_{a_i}^{b_i} \frac{V(\xi)}{(x-\xi)} \prod_{j=1}^{N} \left|\frac{\xi-a_j}{\xi-b_j}\right|^{\frac{1}{2}} d\xi, \tag{7.6}$$

and for the pressure difference on the blades:

$$\pi p(x,0) = -\prod_{\iota=1}^{N} \left|\frac{x-b_\iota}{x-a_\iota}\right|^{\frac{1}{2}} \sum_{i=1}^{N} \mathcal{PV}\int_{a_i}^{b_i} \frac{V(\xi)}{(x-\xi)} \prod_{j=1}^{N} \left|\frac{\xi-a_j}{\xi-b_j}\right|^{\frac{1}{2}} d\xi. \tag{7.7}$$

These results are significant as they form the governing equations used throughout the remainder of the chapter and are applied to the particular flow of present concern which is to be discussed in more detail in the next section. In the case of the flow considered by Smith & Timoshin, these inviscid-region equations had to be coupled with the boundary layer flows to provide a solution as it is necessary to know the boundary layer thicknesses (δ_n^+ and δ_n^-) in order to solve (7.6) and (7.7). In the current setting however, as the boundary layers are considered negligible, this coupling does not arise and so (7.6) and (7.7) can be solved directly. Finally, $\mathcal{PV}$ denotes a Cauchy principal value integral.

7.3 A Periodic Flow Past 2D Blades

As described above, the work of Smith & Timoshin applies to any array of aligned blades but since the present 2D system is taken as an approximation to the 3D flow generated by a [illegible] rotor we are interested only in a periodic solution. Equations (7.6) and (7.7) could be solved numerically for a finite number of blades or, in the case where $N = \infty$, the summations could be truncated to provide an approximate solution. Since such numerical solutions

have been obtained by Smith & Timoshin this is not repeated here (except for a simple solution to the flow local to a blade in §7.3.3). Instead (7.6) and (7.7) are examined analytically in two different regimes. Firstly a solution is derived in an area local to a given blade, $a_k b_k$ say, to see how the flow behaves in this region. The problem is then illustrated for a given blade shape before solving (7.6) numerically to verify the accuracy of the local form. Then in the far-wake region (where the distance to the nearest blade is large) a global solution is obtained to test if a periodic flow is possible. In order to relate these two solutions, they are then matched before finally the impact of ground effect on the current flow is considered through the use of image potentials.

7.3.1 Local Solution

To begin we now consider the local flow form, namely the flow in a region close to a blade. This enables the pressure difference on the blade to be ascertained and also allows us to examine whether the flow here behaves like that past an isolated blade. Since we are interested in the flow where $x \approx a_k$, the substitution $x = a_k + a\overline{x}$, is used with $x = b_k$ corresponding to $\overline{x} = 1$, and $\xi = a_i + a\overline{\xi}$ for $a_i \leq \xi \leq b_i$, remembering that for the present purpose $a \ll 1$. Initially the velocity difference $V(x)$ is considered. Introducing the notation

$$V(x) = \frac{df_+}{dx} - \frac{df_-}{dx} = \frac{df}{dx}, \tag{7.8}$$

so that f is the difference in the shape functions, we have the following solution for $V(\overline{x})$ in the wakes close to a blade

$$a\pi V(\overline{x}) = \pi \frac{\partial f}{\partial \overline{x}} = \left|\frac{\overline{x}-1}{\overline{x}}\right|^{\frac{1}{2}} \int_0^1 \frac{\frac{\partial f}{\partial \overline{\xi}}}{(\overline{x}-\overline{\xi})} \left|\frac{\overline{\xi}}{\overline{\xi}-1}\right|^{\frac{1}{2}} d\overline{\xi} + O(a). \tag{7.9}$$

This solution is the same as that for an isolated blade plus a small, $O(a)$, correction and so if $a \ll 1$ the flow close to $a_k b_k$ is approximately that of the

flow past an isolated blade.

It is possible to calculate (7.9) for a particular blade shape but initially, and with a view to the required matching with the global solution that is subsequently derived, we examine how the local solution (7.9) behaves as the distance from the blade increases, corresponding to the region where $\overline{x} \gg 1$. Letting $\overline{x} \to \infty$, (7.9) becomes

$$\pi \frac{\partial f}{\partial \overline{x}} \sim \frac{I}{\overline{x}} \tag{7.10}$$

and hence

$$f \sim \frac{I \ln(\overline{x})}{\pi} + C_1, \tag{7.11}$$

where

$$I = \int_0^1 \frac{\partial f}{\partial \overline{\xi}} \left| \frac{\overline{\xi}}{\overline{\xi} - 1} \right|^{\frac{1}{2}} d\overline{\xi}. \tag{7.12}$$

Having determined the local behaviour of $V(x)$ we now consider the pressure difference on the blade. In this case (7.7) is evaluated, noting that here the integral has to be treated as a Cauchy principal value (PV) integral[1] due to the presence of the factor $\frac{1}{x-\xi}$ (since $x = \xi$ at some point within the range of integration there is a possible singularity). Following the same derivation as for $V(x)$, we then have

$$a\pi p(\overline{x}, 0) = -\left| \frac{\overline{x} - 1}{\overline{x}} \right|^{\frac{1}{2}} PV \int_0^1 \frac{\frac{\partial f}{\partial \overline{\xi}}}{(\overline{x} - \overline{\xi})} \left| \frac{\overline{\xi}}{\overline{\xi} - 1} \right|^{\frac{1}{2}} d\overline{\xi} + O(a). \tag{7.13}$$

Equations (7.9) and (7.13) show that the blade shape is vitally important here in determining $p(\overline{x}, 0)$ and $V(\overline{x})$ and that changes in the blade shape can dramatically affect the nature of, say, the pressure difference on the blade.

Thus we have derived the local form of the pressure difference and although recognizing that on this length scale the specific blade shape involved can dramatically alter the resulting solution (and so solving (7.9) for a given

1. see Carrier, Krook and Pearson[10].

blade shape is only of limited value), a specific solution is now shown as an illustration.

7.3.2 Solution with $f(\overline{x}) = (f_+ - f_-)(\overline{x}) = \overline{x}^{\frac{1}{2}}(1-\overline{x})^{\frac{3}{2}}$

Equation (7.9) is now examined by choosing the blade shapes such that

$$f(\overline{x}) = (f_+ - f_-)(\overline{x}) = \overline{x}^{\frac{1}{2}}(1-\overline{x})^{\frac{3}{2}} \tag{7.14}$$

as illustrated in Figure 7.2. Although this choice of blade shape is essentially chosen for convenience only, consideration is given to choose a blade shape which is at least loosely realistic. As with the subsequent global solution of §7.3.4 the blades are taken to be identical and evenly separated. Therefore

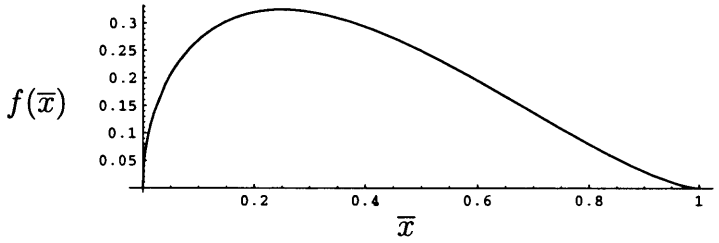

Figure 7.2: *Plot of blade shape difference* $f(\overline{x}) = \overline{x}^{\frac{1}{2}}(1-\overline{x})^{\frac{3}{2}}$.

$V(\overline{x})$ on the blades is given by

$$V(\overline{x}) = \frac{1}{2}\overline{x}^{-\frac{1}{2}}(1-\overline{x})^{\frac{3}{2}} - \frac{3}{2}\overline{x}^{\frac{1}{2}}(1-\overline{x})^{\frac{1}{2}} \tag{7.15}$$

and so in the wake regions close to the blades we now have the solution from (7.9) and (7.15),

$$V(\overline{x}) = \frac{1}{2a\pi}\left|\frac{\overline{x}-1}{\overline{x}}\right|^{\frac{1}{2}}\left[4 + (4\overline{x}-1)\ln\left[\left(\left|\frac{\overline{x}-1}{\overline{x}}\right|\right)\right]\right] \tag{7.16}$$

as illustrated in Figure 7.3. It is likewise possible to calculate the pressure difference on the blade as

$$p(\overline{x}) = -\frac{1}{2a\pi}\left|\frac{\overline{x}-1}{\overline{x}}\right|^{\frac{1}{2}}\left[4 + (4\overline{x}-1)\ln\left[\left(\left|\frac{\overline{x}-1}{\overline{x}}\right|\right)\right]\right], \tag{7.17}$$

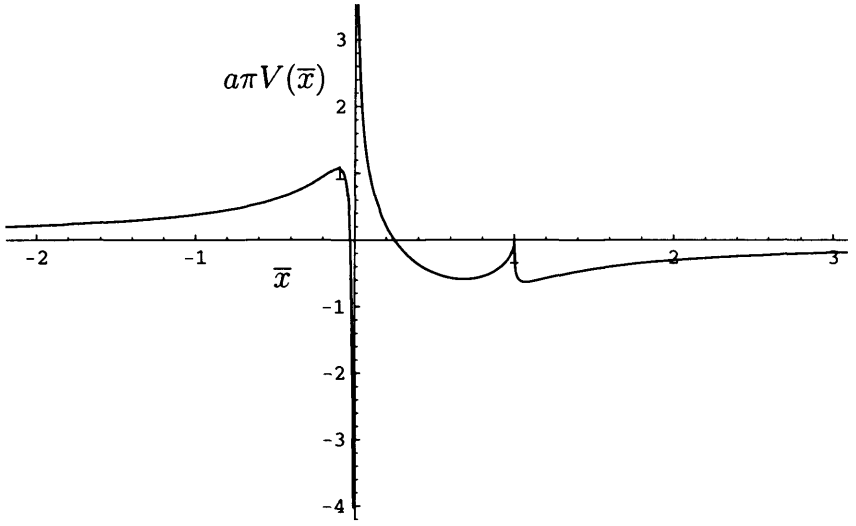

Figure 7.3: *Local Solution of* $V(\overline{x})$ *where* $f(\overline{x}) = (f_+ - f_-)(\overline{x}) = \overline{x}^{\frac{1}{2}}(1-\overline{x})^{\frac{3}{2}}$ *on the blade.* The blade runs from $\overline{x}=0$ to $\overline{x}=1$.

which is illustrated in Figure 7.4, remembering that the integral in (7.13) is a Cauchy principal value due to the existence of a possible singularity.

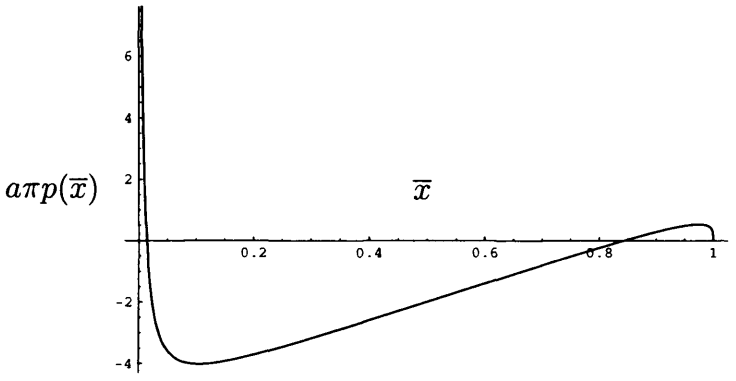

Figure 7.4: *Pressure difference* $p(\overline{x})$ *on the blade where the blade shape is given by* $f(\overline{x}) = \overline{x}^{\frac{1}{2}}(1-\overline{x})^{\frac{3}{2}}$.

Equation (7.17) can be integrated along the blade to calculate the total

pressure difference (P) which turns out to be

$$\begin{aligned} P &= \int_{a_n}^{b_n} p(x)dx \\ &= a\int_0^1 p(\overline{x})d\overline{x} \\ &= -\frac{a\pi}{2}. \end{aligned} \tag{7.18}$$

This shows how despite the singularity which occurs at $\overline{x} = 0$, the total pressure difference on the blade is finite.

7.3.3 Numerical Solution

Next (7.6) is evaluated numerically and compared with the analytical local solution derived above, (7.9), to see how accurate the local approximation is. For this purpose we take $a = 0.1$ and examine the region close to the blade which runs from $x = 0$ to $x = 0.2\pi$ (known as a_0b_0). Next the two summations in (7.6) are truncated, corresponding to the twenty-five blades before and after a_0b_0 instead of allowing N to be infinite. This is a reasonable approximation since if $x \approx 0$, then $\frac{|x-0.2\pi-50\pi|}{|x-50\pi|} \approx 1$. This truncated form of (7.6) is now evaluated using Mathematica to produce the following solutions presented in Figure 7.5.

As can be seen, the numerical results are in very good agreement with the analytical solutions, particularly so for regions close to the blade ($\overline{x} \approx 0$ and $\overline{x} \approx 1$) and that as $|\overline{x}|$ increases the two solutions begin to differ more widely. This is anticipated since the local analytical solution applies only to the flow close to the blade. Interestingly, the numerical results also show how close the flow in a region near the blade is to an isolated blade. The use of Mathematica to solve this problem, whilst being convenient and efficient, has the drawback that it is unable to produce results for $\overline{x} \approx 1+$ and so results are only shown

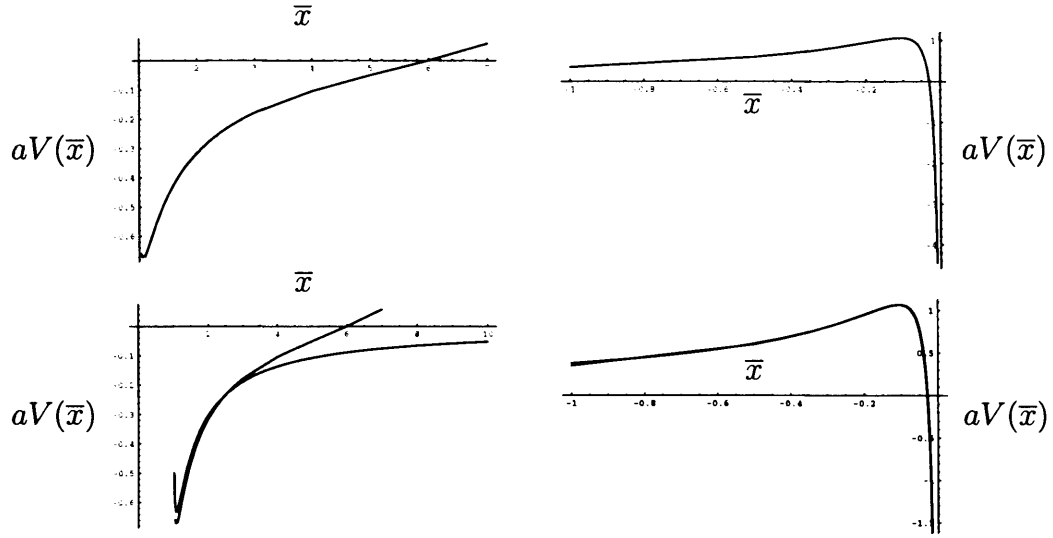

Figure 7.5: *Local Solution of* $V(\overline{x})$ *where* $f(\overline{x}) = \overline{x}^{\frac{1}{2}}(1-\overline{x})^{\frac{3}{2}}$ *on the blade. Left top: Numerical solution to* (7.6) *in the (downstream) range* $\overline{x} \leq 0$. *Right top: Numerical solution to* (7.6) *in the range* $\overline{x} \geq 1.035$ *(upstream). Left bottom: Numerical solution compared with analytical local solution* (7.9) *in the range* $\overline{x} \leq 0$ *(downstream). Right bottom: Numerical solution compared with analytical local solution* (7.9) *in the range* $\overline{x} \geq 1$ *(upstream). The increasing disparity between the analytical and numerical local solutions as* $|\overline{x}|$ *increases is to be expected since the analytical solution is only valid in a region close to the blade.*

for $\overline{x} \geq 1.035$. It may be possible to calculate the truncated form of (7.6) for $1 \leq \overline{x} \leq 1.035$ using Simpson's rule but this is not performed here.

Next the nature of the flow in regions where there is a large distance to the nearest blade is examined. This is denoted the 'global solution'.

7.3.4 Global Solution

With a local solution now determined, it is timely to check whether (7.6) permits a periodic solution, by means of considering the global behaviour of the flow. To this end, (7.6) is examined here on a length scale much greater than a typical blade length and in particular where $x - a_i \approx x - \xi_i$ for all leading edges a_i and where ξ_i is an arbitrary point on the blade $a_i b_i$. This means that the distance from each blade is large. Letting $\xi = a_i + a\bar{\xi}$ for $a_i \leq \xi \leq b_i$ as before, leads to the following global solution to (7.6),

$$\pi \frac{\partial f}{\partial x} = \sum_{i=1}^{n} \frac{I}{x - a_i}, \tag{7.19}$$

which in 3D is the equation for a sum of line vortices at a_n. Here I is defined, as in the local case, by

$$I = \int_0^1 \frac{\partial f}{\partial \bar{\xi}} \left| \frac{\bar{\xi}}{\bar{\xi} - 1} \right|^{\frac{1}{2}} d\bar{\xi}. \tag{7.20}$$

Note that this only holds if all the blade differences f are the same (and for the blade difference used in §7.3.2 it is found that $I = \frac{\pi}{2}$). Otherwise a different integral, I_i say, would exist for each blade. The simplification that each blade is identical and evenly separated has a little validity since in practice most helicopter rotor blades are approximately the same and evenly spaced. Blade inclination does vary as the blades rotate, so the blades are not truly the same at any given moment, but as discussed previously in Chapter 5 this is not a feature with which we are concerned here.

This leads to the following form for f,

$$f \to \frac{I}{\pi} \sum_{i=1}^{n} \ln |x - a_i| + C_2. \tag{7.21}$$

Thus close to a blade we have the isolated blade solution with a small correction term, whilst in the wake the flow 'feels' all the blades. In this global solution

if x is allowed to approach a_i say, so that this solution can be examined as the flow nears the blade $a_i b_i$, then the term $\ln|x - a_i|$ in (7.21) becomes much greater than all the other terms and so the influence of the blade $a_i b_i$ comes to dominate the flow, as was found with the local solution, and which seems intuitively correct.

In the case of an infinite number of blades, each of which is identical and evenly separated, it is possible to scale the horizontal lengths appropriately so that $a_n = \pi n + \frac{\pi}{2}$, for all integer values of n, so that the global solution becomes

$$\pi V(x) = \sum_{i=-\infty}^{\infty} \frac{I}{x - (\pi i + \frac{\pi}{2})}. \tag{7.22}$$

This solution is clearly 2π-periodic since, if we now consider $V(x + 2\pi)$,

$$\begin{aligned} \pi V(x + 2\pi) &= \sum_{i=-\infty}^{\infty} \frac{I}{x + 2\pi - (\pi i + \frac{\pi}{2})} \\ &= \sum_{i=-\infty}^{\infty} \frac{I}{x - (\pi(i-2) + \frac{\pi}{2})} \\ &= \sum_{i=-\infty}^{\infty} \frac{I}{x - (\pi i + \frac{\pi}{2})} \\ &= \pi V(x). \end{aligned} \tag{7.23}$$

In particular (7.22), from Carrier, Krook & Pearson[10], is equivalent to

$$V(x) = -\frac{I}{\pi} \tan(x). \tag{7.24}$$

This known result is important as we have shown that a periodic solution exists on this global length scale which is necessary if this 2D flow is to have any relevance to the practical 3D flows which are of interest.

7.3.5 Complex Potential

It is now possible to extend the global solution for the normal downwash (7.24) to a description for the entire problem. Since we have potential flow, the Cauchy-Riemann equations apply to $-p(x)$ and $V(x)$ and so there exists a complex potential $\overline{\omega}(z)$ where $z = x + iy$ and

$$\frac{d\overline{\omega}}{dz} = -p + i(v_+ - v_-). \tag{7.25}$$

Hence given (7.24) we take this complex potential to be given by

$$\frac{d\overline{\omega}}{dz} = -\frac{iI}{\pi}\tan(z) \tag{7.26}$$

and so

$$\overline{\omega} = \frac{iI}{\pi}\ln(\cos z). \tag{7.27}$$

The pressure difference p is therefore given by

$$p = Re[\frac{iI}{\pi}\tan(x + iy)], \tag{7.28}$$

and examining this solution as $y \to \infty$ we find that

$$p \to -\frac{I}{\pi} \tag{7.29}$$

since, as $y \to \infty$, $\tan(z) \to i$ and the complex potential tends to

$$\frac{\partial\overline{\omega}}{\partial z}(z) \to \frac{I}{\pi}, \tag{7.30}$$

with I being real, by definition.

Thus it seems that, on this global scale, the blade shape only affects the magnitude of the normal velocity across the wake and not the direction at any point. Similarly the blade shape only affects the magnitude of the pressure difference at infinity. This is in contrast to the local behaviour where the blade

shape influences the entire nature of these two quantities. The diminishing impact of the blade shape as the distance to the nearest blade increases seems natural, especially as on this global scale the distance to the nearest blade is taken to be very large. We have therefore shown that, in the limit of $a \ll 1$, in a region close to a given blade we have a flow approximately the same as that past an isolated blade yet nonetheless the global solution is periodic. This is important as one of the problems in modelling a [illegible] rotor as a series of 2D isolated blades is reconciling the fact that such a flow is not periodic (see Neish & Smith[50]). In this case we have shown how, on a global scale, the influence of all the blades can 'combine' to ensure periodicity but that on a local scale only the nearest blade is important (to leading order) and the impact of all the other blades is reduced to a higher order effect. In some respects this mirrors the findings of Chapter 5 when we found that when the disc solidity becomes small the cut-disc flow close to a blade and in the near-wake resembles that of an isolated flat plate and wake. However, as the distance from the blade increases, this near-wake solution breaks down and the influence of the other blades reasserts itself on the flow.

7.4 Ground Effect

As mentioned previously the influence of the ground is an important and interesting aspect of rotor dynamics and one which we now seek to examine. Supposing that each blade is at a height h above the ground, we can incorporate ground effect by including an image potential at a height $-h$. Thus (7.26) becomes

$$\frac{d\overline{\omega}}{dz}(z) = -\frac{iI}{\pi}(\tan(z+ih) + \tan(z-ih)), \tag{7.31}$$

which is equivalent to

$$\frac{d\overline{\omega}}{dz}(z) = -\frac{2iI}{\pi}\tan(z)\frac{(1-\tanh(h)^2)}{(1+\tan(z)^2\tanh(h)^2)}. \tag{7.32}$$

For small values of h this yields

$$\frac{d\overline{\omega}}{dz}(z) = -\frac{2iI}{\pi}\tan(z)\frac{(1-h^2)}{(1+h^2\tan(z)^2)}, \tag{7.33}$$

as illustrated in Figure 7.6, and ultimately reduces to

$$V(x) = -\frac{2I}{\pi}\tan(x) \tag{7.34}$$

at $y = 0$ as $h \to 0$,[1] as shown in Figure 7.6 also.

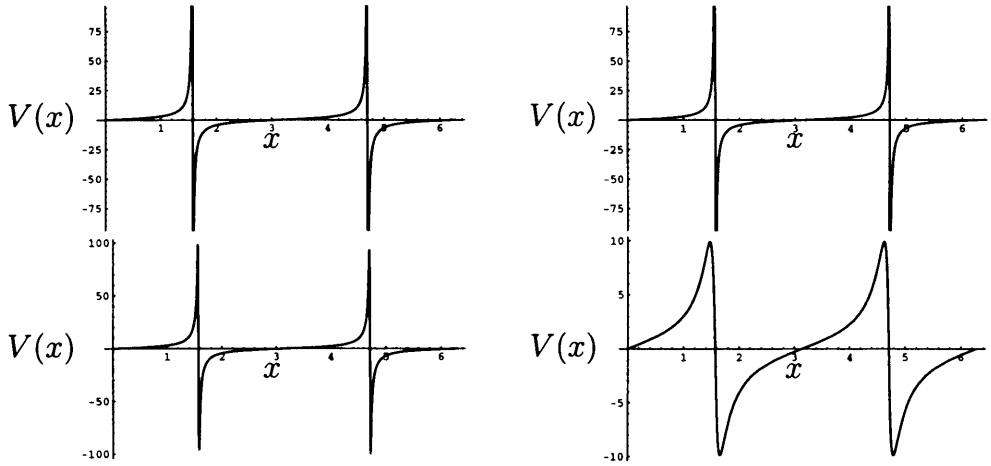

Figure 7.6: *Plot of $V(x)$ in ground effect, as given by* (7.32)*, with distance from the ground $h = 0$ (left top), $h = 0.001$ (right top), $h = 0.01$ (left bottom) and $h = 0.1$ (right bottom).*

As can clearly be seen from (7.34), when $h \to 0$ the normal velocity across the $y = 0$ line doubles when the blades are very close to the ground.

This is interesting as in helicopter rotors the downwash through the rotor blades is related to the power required to sustain a vehicle in hover. In particular, a simple modelling of a helicopter rotor as an actuator disc (see

1. It should be noted here that even as $h \to 0$, h is taken to be greater than the typical boundary layer thickness, and of course for a real helicopter $h \not\to 0$ due to the presence of the helicopter itself.

Bramwell[8], Stepniewski & Keys[73], Seddon[65] and Spalart[72]) suggests that the induced power is related to the downwash (Seddon) and so in the limit as the ground becomes infinitesimally close to the blades, the induced power would be expected to increase and means that the power required to maintain a helicopter in hover is greatly reduced by the presence of the ground. In practice it is found that when the distance from the ground is approximately 30% of the rotor length then the induced power required to maintain hover is reduced by 50% (Seddon).

Similarly we can now also derive the local behaviour of the flow with ground effect by examining

$$V(\overline{x}+ih)+V(\overline{x}-ih)=|\frac{\overline{x}-1+ih}{\overline{x}+ih}|\int_0^1\frac{\partial f}{\partial\xi}|\frac{\xi}{\xi-1}|\frac{(2\overline{x}-2\xi)}{(\overline{x}-\xi)^2-h^2}d\xi, \quad (7.35)$$

which approaches $2V(\overline{x})$ as $h \rightarrow 0$. Thus on the local scale, the magnitude of the induced velocity at any point is again doubled. A similar result can be shown for the pressure difference, so that p also doubles when ground effect is included and the distance to the ground decreases to zero.

7.5 On Three-Dimensional Rotors with Asymmetric Blade Shape

Finally we now discuss the problem of a set of 3D rotors with asymmetric blade shape. The solution to this 3D flow can be considered as consisting of three parts. First the boundary layer problem can be reduced to that on a cut-disc, possibly with inclination, through use of the Prandtl shift, which is solved in Chapter 5. Second there is the outer pressure problem which essentially requires the solution of Laplace's equation subject to a boundary

condition dependent on the (known) blade shape and the (generally unknown) wake shape. In Chapter 6 this was shown for a highly simplified flow with the wake shape determined by the symmetry of the region. The final aspect of the problem is then the determination of the unknown wake shape itself. As discussed previously, this part of the problem is intimately connected to the solution for the outer pressure problem (viscous-inviscid interaction) and the determination of the wake shape presents several well-known difficulties.

The wake shape cannot be calculated pointwise as the requirement of periodicity means that at any point in the wake the flow must be affected by the downstream behaviour. This can be seen from our numerical solution to the symmetric blade shape problem where we use the whole blade and wake shape to calculate the pressure in the outer inviscid region. Moreover the sheer range of possible wake shapes which are feasible prohibit a trial-and-error method of solution. In the 2D case it is possible to derive the Muskhelishvili equation governing the wake shape (as well as the pressure difference) and in particular, the assumption that the boundary layer thickness is minuscule in comparison to the blade shape, allows us to either directly calculate the wake shape for a given rotor or, as previously in this chapter, derive local and global solutions for the downwash and pressure difference. Unfortunately in the 3D version of the problem there appears to be no such succinct equations to describe the flow and hence calculate the solution.

7.6 Summary

In this chapter it has been possible to consider vertical flow asymmetry in two different contexts (blade shape and ground effect). In particular we have shown that for the 2D inviscid flow past a set of aligned blades, if a is small

then in a region close to a blade the flow is approximately that of an isolated blade whilst on a global far-wake length scale the flow is periodic. The implied splitting of scales is important in terms of modelling the flow past a set of rotor. Moreover it has been shown how, intuitively, the blade shape is crucial in determining the nature of the pressure difference and normal velocity across the wake, local to a blade, whereas on a global scale only the magnitudes of these quantities are affected by the blade shape.

When ground effect is included, the pressure difference and downwash double in magnitude as the distance between the blade and the ground decreases to zero. That leads to a change in the magnitude of the power required to sustain lift, a feature which is noted by amongst others Seddon[65] and Gent et al[32].

Chapter 8

The Flow Between a Stationary and a Rotating Disc

8.1 Introduction

Thus far in this thesis, with the exception of the inclusion of ground effect at the end of the previous chapter, only unbounded flows have been considered. This has meant that in most of the preceding work, the flows have been treated as if they occur in an infinite or semi-infinite fluid domain. Whilst this is often a reasonable assumption to make, in numerous practical scenarios some form of obstacle or barrier exists. As such, a bounded flow system is now considered, namely the turbulent flow between two discs at a fixed distance s_D (the gap-width) apart, one of which is rotating at constant angular velocity ω (the rotor) and the other one stationary (the stator).

As well as being an intriguing flow in its own right, this particular problem is of interest for the following reasons. Firstly it is an obvious extension to the free disc system investigated in Chapter 3 and allows for the possibility

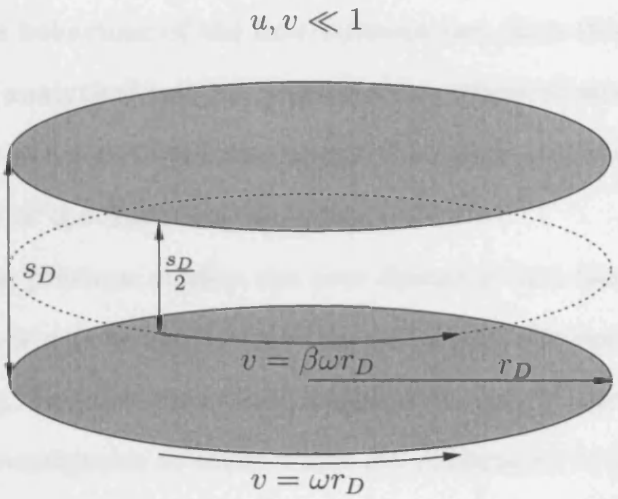

Figure 8.1: *Diagram of a rotating disc and a stationary disc.*

of comparing the velocity profiles between the current and free disc flows. Moreover, as already stated, rotating discs occur commonly in engineering and here it is sometimes unreasonable to assume an infinite fluid domain.

In addition to these motivations the primary reason for considering this flow is its application to helicopter dynamics and for the present purpose the benefit in understanding the current problem is two-fold. Crucially ground effect can now be considered on a viscous length scale so that interaction between the ground and the turbulent boundary layer can be examined. Further, since the current flow is three-dimensional, a cylindrical enclosure can also be introduced to the system as a simple model for the presence of a side structure. This is briefly considered here although for the most part the only surfaces involved are those of the two discs.

In light of the relevance of this two-disc system in engineering applications, it is not surprising that the present flow and several related ones have been studied extensively by many different authors, with much of this work involving experiments or numerical solutions. Whilst providing substantial quantitative

knowledge of the behaviour of the flow between two discs this nonetheless results in a lack of analytical insight. In particular, where theoretical treatments have been performed significant assumptions are often made or results limited to certain values of the Reynolds number.

Some of these previous studies are now discussed but this is by no means meant to be taken as a comprehensive review as the relevant literature is far too wide-ranging. Instead, only those works which are of particular relevance to the present investigation or those which are illustrative of the types of flows possible, are mentioned.

Perhaps the most relevant to the present study is the work of Cooper & Reshotko[22] who also modelled the three-dimensional turbulent boundary layer (3DTBL) between a rotating and a stationary disc. Their work consists of a numerical solution to the Reynolds equations (for a 'narrow' and a 'wide' gap-width) using the Cebeci-Smith model for the eddy viscosity. Crucially, the form of the Cebeci-Smith model used by Cooper & Reshotko is important here as it forms the basis of the one which is used in this chapter. Unfortunately, their study was limited to turbulent boundary layers with a Reynolds number up to 10^7. Bayley & Owen[3] also used the boundary layer approximation and a simple effective viscosity model to produce numerical data for the case where there is an applied radial outflow. They then compared these results with their own experimental work.

Daily & Nece[25] examined both laminar and turbulent two-disc flow experimentally, with some theoretical work based on a $\frac{1}{7}$-th power law for the velocity. This work provides a clear description of the different types of boundary layers which can occur between two discs: an issue which is considered in more detail later when the nature of the turbulent boundary layer looked at

here is discussed. A further related problem is that of 2D turbulent Couette flow which has been examined analytically by Afzal[1]. Not only does this flow share certain similarities with the flow between a rotating and a stationary disc but Cooper & Reshotko also suggest that such flows actually approach turbulent Couette flow at sufficiently large radii. Finally it should be noted that the cases of co- and counter-rotating discs and of the inclusion of cylindrical enclosures around the two discs have been examined by, amongst others, Bhattacharyya & Pal[4], Daniels, Johnson & Graber[26], Dijkstra & van Heist[27], Gan, Kilic & Owen[31] and Szeri, Schneider & Labbe[75].

There appears to have been very little analytical discussion of this problem, in particular involving the use of an eddy viscosity approach to modelling the turbulent stresses. Moreover where the Cebeci-Smith model has been used, it only applies for a limited radial range. Here we seek to address the apparent lack of analytical investigations into this system. As such our aim is to develop some analytical understanding of the flow between two discs (including some simple discussions about the appropriate nature of the form of the eddy viscosity relevant here). The subsequent work is therefore intended to be a tentative first step towards understanding this system and is not a comprehensive solution. As such, and as a simplification, the following assumptions are made:

1. Only the flow at large radii (relative to the gap-width) is considered;

2. It is (initially at least) assumed that the flow is antisymmetric about the centre of the gap between the two discs; and

3. The appropriate eddy viscosity model to use corresponds to the lower tier of the Cebeci-Smith model, as used by Cooper & Reshotko, only.

These assumptions are discussed in more detail throughout this chapter and unfortunately restrict the direct application of the present work to helicopter dynamics. In particular, as rotor blades are obviously finite in extent and as the presence of a helicopter body means that there is always a significant clearance between the rotors and the ground (or any other surface beneath the helicopter), it is unlikely in practical situations that flow at the radii considered here could occur. Moreover, much of the existing experimental and numerical work does not directly relate to the present problem as such research generally applies to the flow at lower radii (although often at large enough radii for turbulence to occur). This is a hinderance insofar as there is then very little previous research with which to compare our own results.

It is hoped that the work here is still important to helicopter dynamics as there exists the possibility of extending the analytical features discussed to include flows at lower radii. More generally this work is still directly valid to any engineering application where two discs are in very close proximity.

Based on the assumptions mentioned above, this chapter adheres to the following structure. The appropriate governing equations are described, although this is done without specifying the precise details of the Cebeci-Smith model immediately (§8.2). A structure for the turbulent boundary layer is then set out in §8.3. An analytical solution at large radii (§8.4.1) and a numerical method (§8.4.2) are derived and the subsequent predictions compared in §8.4.3. A test case using a speculative form of the eddy viscosity is described in §8.4.4 followed by a further analytical solution (§8.4.5) based on this choice of the eddy viscosity. In §8.4.6 these results are contrasted with those for a free rotating disc based on the results of Chapter 3. The skin friction on the two discs is then calculated analytically and compared with the asymptotic

behaviour of the skin friction as found by Cooper & Reshotko (§8.4.7). Finally three possible extensions of this model are briefly considered, namely asymmetry about the gap centre line (§8.5.1), the addition of an enclosure around the two discs as a means of modelling the impact of side-structures on the flow (§8.5.2) and the flow between a rotating cut-disc and a stationary disc (§8.5.3).

8.2 Problem Formulation

As with the rotating disc flow in Chapter 3, the Reynolds equations, taken with a suitable eddy viscosity model, are considered the governing equations of the current problem. From Cooper & Reshotko, these are (using the same notation, where appropriate, as in Chapter 3),

$$u_D\frac{\partial u_D}{\partial r_D} - \frac{{v_D}^2}{r_D} + w_D\frac{\partial u_D}{\partial z_D} = -\frac{1}{\rho}\frac{\partial p_D}{\partial r_D} + \nu\frac{\partial^2 u_D}{\partial {z_D}^2} + \frac{\partial}{\partial z_D}(\nu_{tD}\frac{\partial u_D}{\partial z_D}), \tag{8.1}$$

$$u_D\frac{\partial v_D}{\partial r_D} + \frac{u_D v_D}{r_D} + w_D\frac{\partial v_D}{\partial z_D} = -\frac{1}{\rho r_D}\frac{\partial p_D}{\partial \theta} + \nu\frac{\partial^2 v_D}{\partial {z_D}^2} + \frac{\partial}{\partial z_D}(\nu_{tD}\frac{\partial v_D}{\partial z_D}) \tag{8.2}$$

and

$$\frac{1}{r_D}\frac{\partial(u_D r_D)}{\partial r_D} + \frac{\partial w_D}{\partial z_D} = 0. \tag{8.3}$$

The eddy viscosity used by Cooper & Reshotko is

$$\nu_{tD} = \begin{cases} \overline{k_4}(\frac{\tau_{\theta d}}{\rho})^{\frac{1}{2}}\delta_m^* & \text{for } \overline{z}_D \geq \overline{z}_{Dk} \\ k_1^2\overline{z}_D^2[1-\exp(-\frac{z_D}{26\nu}(\frac{\tau_{WD}}{\rho})^{\frac{1}{2}})]^2|\frac{\partial u_D}{\partial z_D}+\frac{\partial v_D}{\partial z_D}| & \text{for } \overline{z}_D \leq \overline{z}_{Dk}. \end{cases} \tag{8.4}$$

The quantity $\overline{z}_D$ represents the distance from the nearest disc, hence the lower tier of the Cebeci-Smith model occurs in a layer on both discs (possibly) separated by the upper tier. In general the junction position $\overline{z}_{Dk}$ can take two different values (corresponding to the two junction positions) but in the anti-symmetric case, $\overline{z}_{Dk}$ is obviously a unique value.

This modified form of the Cebeci-Smith model contains several differences from that of the free disc case. In particular, the outer form contains several modifications including a new constant $\overline{k_4} = 0.057$ and the expression $(\frac{\tau_{\theta d}}{\rho})^{\frac{1}{2}}$ whilst the z_D^2 term in the inner part has been replaced by $\overline{z}_D^2$.

There is also the as yet unspecified quantity δ_m^*, which is a measure of the boundary layer thickness and which arises from the fact that in a merged boundary layer the notion of the displacement thickness is no longer appropriate. Cooper & Reshotko define δ_m^* for $R_r \leq 10^7$, based on the displacement thickness terms which they derived for a free rotating disc and a rotating disc with an applied pressure gradient, and is given in terms of R_r, the radial Reynolds number as defined previously. Cooper & Reshotko use the form

$$\begin{aligned} \delta_m^* &= 5.5 + 0.503 R_r^{\frac{3}{20}} + 0.0131 R_r^{\frac{1}{2}} \\ &\quad + (1 - 2\beta_p)(0.6 - 0.503 R_r^{\frac{3}{20}} + 0.0097 R_r^{\frac{1}{2}}) \end{aligned} \tag{8.5}$$

and treat β_p as an unknown to be determined, where β_p is termed the local radial pressure gradient and defined as

$$\beta_p^2 = \frac{1}{\rho \omega^2 r_D} \frac{\partial p}{\partial r}. \tag{8.6}$$

Note that as the flow approaches an antisymmetric state, then $\beta_p \rightarrow \beta$ (the non-dimensional centre line velocity) and hence $\beta_p \rightarrow \frac{1}{2}$ as $R_r \rightarrow \infty$.

Since this particular choice for the eddy viscosity is only defined for a Reynolds number no greater than 10^7, there is some ambiguity about the appropriate form to use at large values of R_r. This is now discussed.

8.2.1 Eddy Viscosity

Due to the limited range of validity of (8.4) it is important to consider the eddy viscosity in more detail. Equation (8.4) is not the only form of the Cebeci-

Smith model which could be considered here. Wilson[80] uses a further different form for the viscosity in a confined region, albeit for the merged turbulent boundary layer in a curved duct. This involves a quasi-displacement thickness and for the present purpose is defined as

$$\overline{\delta}^* = \int_0^{0.5} (\frac{2v_D}{\omega r_D} - 1) dz_D, \tag{8.7}$$

but is otherwise identical to the form used in Chapter 3.

Since most of the previous research into this problem has consisted of numerical solutions not involving the Cebeci-Smith eddy viscosity, or experimental work, and since the δ_m^* used by Cooper & Reshotko is only defined on a limited range of values of R_r, the appropriate choice of δ_m^* for the whole flow, and hence the numerical system to be solved, is not well established. Moreover, in light of the fact that Cooper & Reshotko only define δ_m^* on a finite range of Reynolds numbers it is reasonable to wonder whether the outer tier of the eddy viscosity need be used throughout the 3DTBL or if for some radial range only the inner tier (which must be present for logarithmic matching with the laminar sublayers to be possible) applies. Attention is thus turned to the choice of $\nu_{\tau D}$ appropriate here. Four options seem possible:

1. Only the inner tier of the Cebeci-Smith model occurs at radii this large;

2. The appropriate Cebeci-Smith model used should be the same as that of Wilson;

3. Consideration could be limited to the same radial range as Cooper & Reshotko;

4. An as yet unknown form for $\nu_{\tau D}$ could be applied for values of the Reynolds number greater than those considered by Cooper & Reshotko.

Since we are assuming antisymmetry here it is not acceptable to restrict our investigations to relatively low Reynolds numbers and so we cannot simply limit this present problem to the range which Cooper & Reshotko examined. Moreover it is shown subsequently that the form used by Wilson is not suitable for this flow. Hence either a new, as yet undetermined value for $\nu_{\tau D}$, or only the inner tier of the Cebeci-Smith model, must be used.

The simplest choice is therefore that the outer tier is not present at all (and that the lower tier is simply the same as that of Cooper & Reshotko) and this is what is now assumed to hold. In practice a somewhat speculative alternative formulation (by no means based on any first principals or on Prandtl's mixing length hypotheses) involving both tiers of the Cebeci-Smith model is also used as it provides a means to compare the subsequent analytical and numerical results produced (this is not really possible using only the inner tier as in this case it has not been possible to produce numerical results at a sufficiently large radius). Hence having decided on the eddy viscosity to use here, we proceed to examine the Reynolds equations further.

8.2.2 Governing Equations

As previously stated (8.1) – (8.3) with the eddy viscosity term given by the inner tier of (8.4) are taken as the basis of the governing equations used here. The lengths r_D and z_D are now non-dimensionalized against the gap-width s_D,

and the velocities against ωr_D. Hence

$$r_D = \frac{s_D}{k_1^2} r, \tag{8.8}$$

$$z_D = s_D z, \tag{8.9}$$

$$u_D = \omega r_D f'(r,z), \tag{8.10}$$

$$v_D = \omega r_D g'(r,z), \tag{8.11}$$

$$p_D = \rho \omega^2 r_D^2 P(r), \tag{8.12}$$

where $'$ denotes differentiation with respect to z, and where the radius is scaled against k_1^2 for convenience. The above equations yield the following form for the normal velocity w_D,

$$w_D = -2\omega s_D f - \omega s_D r \frac{\partial f}{\partial r}. \tag{8.13}$$

Thus the distance between the two discs is now taken to be unity and the Reynolds equations for this problem have become

$$f'^2 + rf'\frac{\partial f'}{\partial r} - g'^2 - 2ff'' - rf''\frac{\partial f}{\partial r} = -r\frac{\partial P}{\partial r} - 2P + \frac{1}{R_s} f''' \tag{8.14}$$
$$+r\frac{\partial}{\partial z}(\overline{z}^2[1-\exp(-\frac{zRu_\tau}{26})]^2(f''^2+g''^2)^{\frac{1}{2}}f'')$$

and

$$2f'g' + rf'\frac{\partial g'}{\partial r} - 2fg'' - rg''\frac{\partial f}{\partial r} = \frac{1}{R_s} g''' \tag{8.15}$$
$$+r\frac{\partial}{\partial z}(\overline{z}^2[1-\exp(-\frac{zRu_\tau}{26})]^2(f''^2+g''^2)^{\frac{1}{2}}g'')$$

with $R_s = \frac{\omega s_D^2}{\nu}$, the gap-width Reynolds number which is considered large, and $\overline{z}$ measuring the (non-dimensional) distance from the nearest disc.

We now consider the pressure gradient terms involved here. When the flow is antisymmetric, along the line $z = \frac{1}{2}$, $f' = 0$ and $g' = \frac{1}{2}$. Consideration of

the inertial-turbulent layer subsequently reveals that $P = \frac{1}{8}$ so that the $O(1)$ terms in the perturbation expansions balance. This yields

$$\frac{\partial p_D}{\partial r_D} = \frac{\rho \omega^2 r_D}{4}, \tag{8.16}$$

and appears to be in agreement with the calculations of Cooper & Reshotko which indicate that in the limit as $r \to \infty$,

$$\frac{\partial p}{\partial r} \to \frac{\rho \omega^2 r_D}{4}. \tag{8.17}$$

Since the main area of focus here is when the turbulent boundary layers are fully merged, in particular when the flow is sufficiently developed for antisymmetry to occur, the regime of interest corresponds to $r \gg 1$ and so the governing equations (8.14) and (8.15) are considered as the radius r becomes large. (8.14) and (8.15) certainly seem to suggest that as this occurs the turbulent terms come to dominate the inertial ones, particularly in the azimuthal momentum equation so that eventually only the turbulent stresses will remain. This raises the important question of the appropriate choice of radial length scale for this problem. This is discussed subsequently in conjunction with the appropriate boundary layer structure to use.

8.3 Boundary Layer Structure

As with the rotating disc considered in Chapter 3, when the radius r is small the flow is actually laminar, and turbulence is only taken to occur after some transitional radius onwards. This can be seen when the different boundary layers which occur between two discs are considered. Daily & Nece[25] actually identify four distinct flow regimes: separate laminar boundary layers; merged laminar boundary layers; separate turbulent boundary layers; and merged turbulent boundary layers. The flow between two such discs can include one or

more of these different regimes depending on the gap-width and disc radii. In particular, if the gap-width is sufficiently large then all four regimes, except for that of merged laminar boundary layers, can exist within one configuration. For our purposes and since this chapter is concerned with the solution at large radii only, it is assumed that the boundary layers on each disc have merged and the flow between the two discs can in effect be taken to be a single turbulent boundary layer (and since the issue of transition to turbulence has been dealt with in Chapter 3, no additional consideration of transition is deemed necessary).

At small values of the radius it is expected that the flow in the vicinity of the rotating disc is the same as for the free disc case. As r, and hence the displacement thickness δ^* (and more generally the overall boundary layer thickness) increases, eventually the boundary layer on the rotating disc will become so large that it interacts with the stationary disc. This interaction leads on to a new flow developing at large radii where the boundary layer thickness no longer varies with radius and instead fills the entire gap between the discs. Since the free disc case has already been examined, attention is now devoted to the region of the flow where the stationary disc cannot be ignored. As suggested by the existing numerical and experimental data, here the fluid velocity in the gap is order unity and along the centre line appears to increase from zero up to half that of the rotating disc, at which stage the flow appears to be antisymmetric.

This chapter considers this apparent antisymmetric phase of the flow as a first step (the 'logical' next step - allowing asymmetry about the gap centre-line - is discussed later but is otherwise not undertaken here) to modelling the entire problem. Crucially, the restriction to antisymmetry allows us to make

the considerable simplification of only having to solve for one half of the gap. The antisymmetric solution produced can be treated as either an approximation to the actual asymmetric flow or more properly, as a solution which is only applicable at very large radii (or equivalently, very large Reynolds numbers). This limited range of validity is acceptable here for two reasons. First Cooper & Reshotko have already used the Cebeci-Smith model to produce numerical results for the radial range up to the point where antisymmetry appears to occur and secondly because many of the analytical features considered here, including the structure of the turbulent boundary layer, can be readily extended to the asymmetric flow range.

Therefore for the purposes of this chapter the boundary layers are deemed to be turbulent and to have merged completely and, initially at least, the flow is taken to be antisymmetric about the midpoint of the gap between the two discs.

The three-dimensional turbulent boundary layer (3DTBL) is again modelled as consisting of two layers, the outer, inertial-turbulent layer and the inner, laminar sublayer. There also exists a second laminar sublayer which occurs on the stationary disc and which is created by the presence of non-zero flow in the gap. It is assumed that at sufficiently large values of r the two laminar sublayers have the same structure and that a symmetry argument suggests that the azimuthal velocity in the greater, central part of the 3DTBL, known as the core, is approximately $\frac{1}{2}$.

8.3.1 Inertial-Turbulent Layer

The region of interest is taken to occur when $r = O(\epsilon^{-1})$, as this choice of radial scale ensures a balance between the inertial and turbulent terms, and

so the following scalings are introduced

$$r = \epsilon^{-1} r_1, \tag{8.18}$$

$$z = z_1, \tag{8.19}$$

$$f' = \epsilon f_1', \tag{8.20}$$

$$g' = \frac{1}{2} + \epsilon g_1', \tag{8.21}$$

for the inertial-turbulent layer (ITL), which reduces (8.14) and (8.15) to

$$-g_1' = r_1 \frac{\partial}{\partial z_1} (\overline{z}_1^2 (f_1''^2 + g_1''^2)^{\frac{1}{2}} f_1'') \tag{8.22}$$

and

$$f_1' = r_1 \frac{\partial}{\partial z_1} (\overline{z}_1^2 (f_1''^2 + g_1''^2)^{\frac{1}{2}} g_1''). \tag{8.23}$$

These equations suggest that unless $f_1' \to 0$ as $r_1 \to \infty$ then, in this limit, the turbulent stresses will dominate the flow. This means that the solution $f_1' \equiv 0$ is possible and so $f_1' \to 0$ after all. Therefore, and supported by the work of Cooper & Reshotko, it is assumed that $f_1' \to 0$ as the radius increases.

8.3.2 Laminar Sublayer on the Rotating Disc

In the laminar sublayer on the rotating disc (RLS), it is now supposed that we can still employ a similarity solution, as in the free disc case, and define

$$r = \epsilon^{-1} r_2, \tag{8.24}$$

$$\eta_2 = R \frac{\overline{z}}{r}, \tag{8.25}$$

$$f' = \epsilon^{-2} R^{-1} f_2'(\eta_2), \tag{8.26}$$

$$g' = 1 + \epsilon g_2'(\eta_2), \tag{8.27}$$

which leads to the following equations for the RLS,

$$-\frac{3}{4} = f_2''' + \frac{\partial}{\partial \eta_2} (\eta_2^2 |g_2''| f_2'') \tag{8.28}$$

and

$$0 = g_2''' + \frac{\partial}{\partial \eta_2}(\eta_2^2 | g_2'' | g_2''). \tag{8.29}$$

The assumption of a similarity solution applying in the laminar sublayer is acceptable here (whilst not in the ITL) as the height of the RLS is taken to behave like $\frac{r_D}{R}$ and since the Reynolds number is itself proportional to r_D^2, this implies that within the RLS, $z_D \sim \frac{1}{r_D}$, and so actually decays with the radius.

8.3.3 Laminar Sublayer on the Stationary Disc

As mentioned previously, the two laminar sublayers are considered to have the same structure. Thus it is supposed that in the laminar sublayer on the stationary disc (SLS);

$$r = \epsilon^{-1} r_3; \tag{8.30}$$

$$\eta_3 = R\frac{\overline{z}}{r}; \tag{8.31}$$

$$f' = \epsilon^{-2} R^{-1} f_3'(\eta_3); \tag{8.32}$$

$$g' = \epsilon g_3'(\eta_3); \tag{8.33}$$

leading to the following equations for the SLS

$$\frac{1}{4} = f_3'''' + \frac{\partial}{\partial \eta_3}(\eta_3^2 | g_3'' | f_3'') \tag{8.34}$$

and

$$0 = g_3''' + \frac{\partial}{\partial \eta_3}(\eta_3^2 | g_3'' | g_3''). \tag{8.35}$$

Consideration is now given to the matching of the asymptotic behaviour in the overlap regions of these three layers.

8.3.4 Matching

Equation (8.29) implies that as $\eta_2 \to \infty$, then $g_2' \sim \ln \eta_2$ and since in the inertial-turbulent layer and the laminar sublayer on the rotating disc,

$$g' = \frac{1}{2} + \epsilon g_1', \tag{8.36}$$

$$g' = 1 + \epsilon g_2', \tag{8.37}$$

respectively, as $z_1 \to 0$

$$g_1' \sim -\frac{1}{2} \ln z_1. \tag{8.38}$$

Similarly, as $z_1 \to 1$

$$g_1' \sim \frac{1}{2} \ln (1 - z_1). \tag{8.39}$$

Also

$$g_2' \sim -\frac{1}{2} \ln \eta_2, \tag{8.40}$$

$$g_3' \sim \frac{1}{2} \ln (1 - \eta_3), \tag{8.41}$$

as $\eta_2 \to \infty$ and as $\eta_3 \to \infty$ respectively (incidentally this asymptotic behaviour is comparable to that in turbulent Couette flow, see Appendix *D*). Equations (8.22) and (8.23) can now be used to establish the asymptotic nature of f_1' as

$$f_1' \sim \frac{z_1}{r_1} \ln z_1 \tag{8.42}$$

as $z_1 \to 0$, and

$$f_1' \sim \frac{(1 - z_1)}{r_1} \ln (1 - z_1) \tag{8.43}$$

as $z_1 \to 1$. In contrast (8.28) implies that

$$f_2' \sim -\frac{3}{2} \eta_2 \tag{8.44}$$

as $\eta_2 \to \infty$, whilst (8.34) yields

$$f_3' \sim \frac{1}{2} (1 - \eta_3) \tag{8.45}$$

as $\eta_3 \to \infty$. As in Chapter 4, the coefficients of the radial velocity asymptotes are not the same for each layer. This arises for the same reason as in §4.3.5, namely that in each layer the forcing inertial term is different but that as the layers overlap these inertial terms tend toward each other and hence so do the coefficients of the radial velocities in each layer. Similarly, as in Chapter 3, the presence of logarithmic terms in the radial asymptotic behaviour leads to additional factors of ϵ arising as $z_1 \to 0$ and $z_1 \to 1$. These extra factors ensure the asymptotic forms of the radial velocity have the same order in the overlap regions.

8.4 Antisymmetric Flow between Two Discs

Having determined the appropriate governing equations and boundary layer structure for the current system we now seek to determine a solution. As stated the flow is taken to be antisymmetric about the midpoint of the gap. We can feel justified in using this simplification by examining the numerical results of Cooper & Reshotko which appear to be at least close to antisymmetry at a finite, albeit large, radius and as Afzal has shown that in turbulent Couette flow the centre line velocity tends to one half that of the moving wall. The assumption of antisymmetry has the advantage of meaning that the flow need only be determined for one half of the total gap, and in practice this will mean the flow is generally determined for the range $0 \leq z \leq \frac{1}{2}$.

The relevant boundary conditions are

$$f(\frac{1}{2}) = 0, \tag{8.46}$$

$$f'(\frac{1}{2}) = 0, \tag{8.47}$$

$$f'(0) = 0, \tag{8.48}$$

$$g(\frac{1}{2}) = 0, \tag{8.49}$$

$$g'(\frac{1}{2}) = \frac{1}{2}, \tag{8.50}$$

$$g'(0) = 1, \tag{8.51}$$

where the rotating disc is at $z = 0$ and the stationary disc, $z = 1$. The conditions on $f(\frac{1}{2})$ and $g(\frac{1}{2})$ are arbitrary and are chosen to simplify the numerical method used later.

The governing equations derived in §8.3.1 for the ITL appear to be solvable as a fourth-order system as now neither f_1 or g_1 appear explicitly. However, f_1 is required to determine the normal velocity component and although this is not of immediate concern here, g_1 may occur explicitly if an eddy viscosity similar to that used by Wilson is considered. For these reasons the current problem is treated as a sixth-order system. Actually, when calculating the appropriate form of the normal velocity, (8.13), the condition $f(0) = 0$ was used but since f does not occur explicitly in (8.22) and (8.23), it is possible to now use the condition $f(\frac{1}{2}) = 0$ (i.e. in this case f is redefined as $f - f(\frac{1}{2})$) as this is particularly convenient with respect to the subsequent numerical scheme. Hence we have all the necessary conditions to enable a solution to be determined.

8.4.1 Large Radii Limit

We first examine (8.22) and (8.23) in the limit as $r_1 \to \infty$ and as previously stated, in order for (8.22) to balance, it is assumed that $f' \to 0$ (as noted by Cooper & Reshotko). The equation for the azimuthal velocity therefore reduces to

$$0 = r_1 \frac{\partial}{\partial z_1}(z_1^2 |g_1''| g_1'') \tag{8.52}$$

and thus

$$-\frac{1}{4} = z_1^2 |g_1''| g_1'' \tag{8.53}$$

from use of the asymptotic behaviour as $z_1 \to 0$ (or as $z_1 \to 1$). From (8.53):

$$g_1' = -\frac{1}{2} \ln z_1 + C_1, \tag{8.54}$$

where the unknown constant C_1 needs to be determined from the boundary condition $g_1'(\frac{1}{2}) = 0$. It is then possible to use this solution for g_1' in (8.22) to determine f_1', leading to the following analytical solutions for the velocity components: for $0 \leq z_1 \leq \frac{1}{2}$,

$$r_1 f_1' = z_1 \ln z_1 - (2 + \ln \frac{1}{2}) z_1 + 1, \tag{8.55}$$

$$g_1' = -\frac{1}{2} \ln z_1 + \frac{1}{2} \ln \frac{1}{2}, \tag{8.56}$$

and for $\frac{1}{2} \leq z_1 \leq 1$,

$$r_1 f_1' = -(1 - z_1) \ln (1 - z_1) + (2 + \ln \frac{1}{2})(1 - z_1) - 1, \tag{8.57}$$

$$g_1' = \frac{1}{2} \ln (1 - z_1) - \frac{1}{2} \ln \frac{1}{2}. \tag{8.58}$$

In this case the azimuthal velocity no longer varies with the radius at large radii and the radial component decays like $\frac{1}{r_1}$. These solutions are illustrated in Figure 8.2. The non-dimensional normal velocity is now given by $\frac{w_D}{\omega s_D} =$

$w = -f$ and so

$$w = \epsilon w_1 = \frac{\epsilon}{r_1}\left(\frac{z_1^2}{2}(\ln z_1 - \ln\frac{1}{2}) - \frac{5z_1^2}{4} + z_1\right), \tag{8.59}$$

which is also illustrated in Figure 8.2.

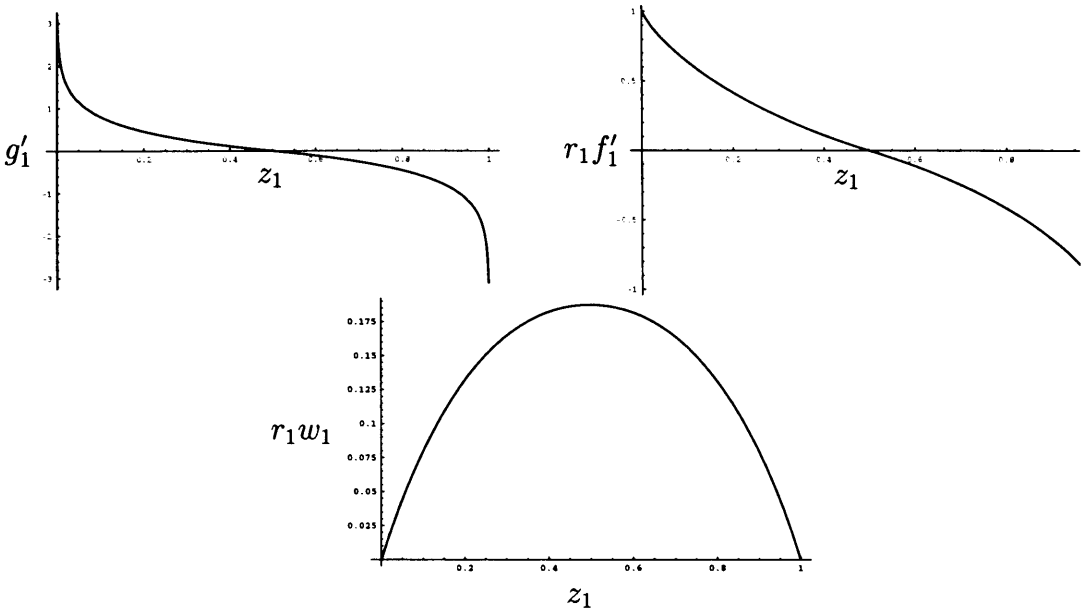

Figure 8.2: *Analytical large radii result for* g_1' *(top left),* f_1' *(top right) and* w_1 *(bottom).*

Consideration is now given to the results of Cooper & Reshotko. To enable direct comparison to be made with the present work, their form of the eddy viscosity needs to be examined as $r_1 \to \infty$. At large radii (8.5) becomes

$$\delta_m^* = 0.0131 R_r^{\frac{1}{2}}. \tag{8.60}$$

As, according to Cooper & Reshotko, both tiers of the Cebeci-Smith model can occur on this radial range it would appear necessary to extend the above analytical solution to include a two-tier model. This is relatively straightforward, and the details of this more general large radii limit are discussed in

Appendix E, but in fact it turns out that this is not immediately necessary. Of most practical importance is the relationship

$$\delta_m^* = \frac{z_{1k}}{2k_4}, \tag{8.61}$$

which holds at large radii as a consequence of continuity of eddy viscosity at the junction position. The unknown junction position can therefore be readily determined from specification of δ_m^*. Since $z_{1k} = 2k_4\delta_m^*$ this suggests that as $R_r \rightarrow \infty$, and hence $r_1 \rightarrow \infty$, $z_{1k} \rightarrow \infty$ also. However by definition $z_{1k} \leq \frac{1}{2}$ and thus for large radii it again appears that only the inner form of the Cebeci-Smith model is present. From (8.60) and (8.61) this is taken to occur at approximately $R_r^{\frac{1}{2}} = 268.8$ and so in the upper range of values considered by Cooper & Reshotko, the outer tier appears to be no longer present. Hence it is now possible to compare the analytical solution determined here with $z_{1k} = \frac{1}{2}$ and the (narrow-gap) results of Cooper & Reshotko (their work is shown as two straight curves as this is a reasonable approximation and it is not possible to determine the numerical values from the graph of their results more accurately). These are shown in Figure 8.3. Comparison is restricted to the narrow-gap results of Cooper & Reshotko as their wide-gap results appear unlikely to relate to the flow at such large radii as considered here.

As can be seen from Figure 8.3 the present analytical solution is loosely in agreement with the numerical results of Cooper & Reshotko. The discrepancies between the two results are perhaps due to the assumption of antisymmetry which is not truly valid at this value of the Reynolds number and of course the analytic solution is based on the assumption that $r_1 \gg 1$ whereas the above comparison is made at $r_1 \approx 2$ as Cooper & Reshotko's work is limited to this range. The numerical predictions shown disagree far more widely with both other sets of data. This may also arise as a consequence of the assumption of

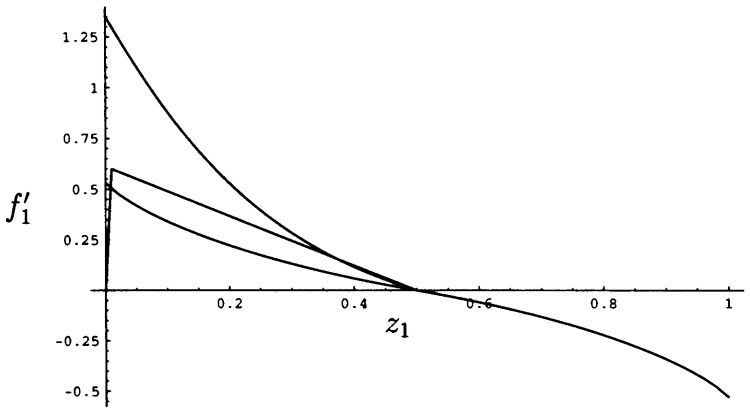

Figure 8.3: *Comparison of the narrow-gap numerical work of Cooper & Reshotko (middle curve) and the current large radii analytical solution with* $z_{1k} = \frac{1}{2}$ *(lower curve). The subsequent comparable numerical results produced in* §8.4.2 *are also shown here (top curve). These results are taken at* $r_1 = 1.8759$ *and* $R_r = 5.76 \text{ x } 10^6$.

antisymmetry although the marked discrepancy with the analytical predictions and those of Cooper & Reshotko is alarming.[1]

Finally we now use this analytical solution to show how the eddy viscosity used by Wilson[80] cannot be applied to this current problem. If such a Cebeci-Smith model is used it is now necessary to replace $\overline{k}_4$ with $k_3 = 0.105$ and $\delta_m^* = -g_1(0)$. $g_1(0)$ is then determined from the above large radii analytic solution for g_1' using the condition $g_1(\frac{1}{2}) = 0$. This is then substituted into (8.61) to determine an estimate for z_{1k} at large radii. Unfortunately this leads to the solution that $z_{1k} > 1$, which is clearly not possible as, by definition, z_{1k} must certainly be less than unity for the outer tier to be present. Therefore this choice of eddy viscosity is not valid here, at least at a radial position at which the large radii analytical solution holds, which is the regime of interest here.

1. This discrepancy is discussed in §8.4.3.

8.4.2 Numerical Solution

We can now solve (8.22) and (8.23) numerically. As in Chapters $2-5$, for the purposes of the numerical solution, the laminar sublayers are ignored and a solution for just the ITL is determined. Actually, the azimuthal momentum equation in both sublayers is the same as that on a rotating disc and hence an equivalent analytical solution is possible, although as the asymptotic behaviour in the matching with the ITL is different so will be the solution. Moreover, as the required approach is identical to that used in Chapter 3 it is not deemed necessary to repeat it here. Similarly, since the numerical method involved here is precisely the same as the lower half of the numerical problem solved in Chapter 3 no further details are discussed here. Instead a full description for the case where both tiers of the Cebeci-Smith model are included is contained in Appendix E.

8.4.3 Numerical Results

Numerical results for the ITL are now sought. Such results are shown in Figure 8.3 where comparisons are also made with the work of Cooper & Reshotko, and as already noted, the numerical results differ widely from those of Cooper & Reshotko as well as from the large radii analytical solution. Results for varying step length for use with the RKF algorithm are not shown here as instead such a comparison is made when numerical results are generated for both tiers of the Cebeci-Smith model (§8.4.4), showing that once the step length is sufficiently small the results produced remain approximately unchanged.

Interestingly, numerical results are only possible for the approximate radial range $r_1 \leq 15$. Beyond such values of r_1 this present method seems incapable of producing results.[1] Combined with the alarming disagreement

1. Specifically, when calculations are performed for $r_1 > 15$ the program used crashes and fails to produce any output.

between our numerical results and our analytical work, and indeed those of Cooper & Reshotko, there appears to be serious problems with our numerical formulation. In particular, several possibilities are raised as a result of these problems;

1. there may be an otherwise undetected flaw in our numerical algorithm;
2. perhaps (in order to produce more reliable results or to generate results at a larger radii) an outer tier to the eddy viscosity is required after all;
3. the inner tier used is inappropriate.

If there is an undetected flaw with the numerical scheme used, an alternative method might be possible but one is not attempted here. Instead, a 'test' case is used involving a new, somewhat speculative, form of the Cebeci-Smith model. With this particular eddy viscosity it now becomes possible to generate results for large radial values (at least as large as $r_1 \approx 1000$) and good agreement is found between the numerical and analytical results produced. The details of this test case are now described in more detail.

8.4.4 An Alternative Cebeci-Smith Model

Here we discuss a test case for our numerical method. This involves the use of an unorthodox choice of eddy viscosity which is of the same form as that used by Cooper & Reshotko but with a new definition for δ_m^*. The particular choice used actually arose due to an initial mistake in the formulation of the numerical problem (using the same form for the eddy viscosity as Cooper & Reshotko, the quantity δ_m^* was initially treated as an unknown to be determined as part of the numerical scheme and an extra, incorrect, boundary condition - $f(0) = 0$, as

well as $f(\frac{1}{2}) = 0$ - was imposed). With hindsight this mistake was eventually uncovered and our approach corrected. The delay in recognizing this mistake arose as a result of the very good agreement between the subsequent numerical and analytical results. On closer inspection, the results produced by imposing the incorrect boundary conditions correspond to using the correct conditions and setting $\delta_m^* = \frac{J_0}{r_1}$ with $J_0 = 35$, which is an otherwise unjustifiable condition.

The close correlation which was found between the different predictions leads us to include these results as they provide some validation of our numerical approach and show that the numerical method can be used to provide solutions at very large (perhaps infinitely large) radial positions which is not the case when only the inner tier of the Cebeci-Smith model is used.

Employing the technique used earlier and using both tiers of the Cebeci-Smith model, this new decaying form for δ_m^* (and hence the junction position) produces the following solution for the case where $z_{1k} = 0.45$, see Figure 8.4. Now we compare our numerical results for the case where $z_{1k} = 0.45$

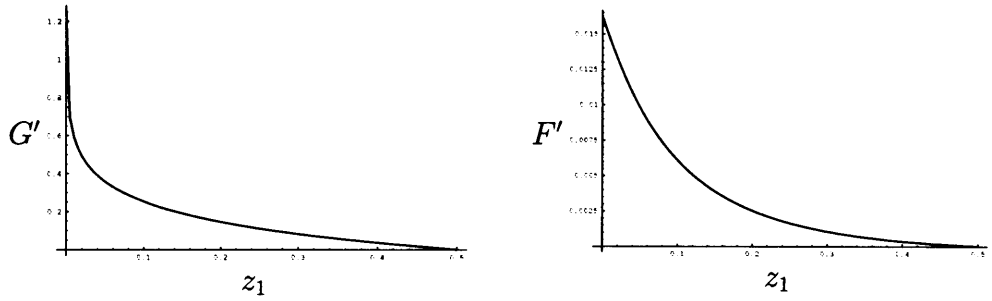

Figure 8.4: *Left: Azimuthal numerical results with* $z_{1k} = 0.45$. *Right: Radial numerical results for* $z_{1k} = 0.45$. F' and G' are the scaled velocity components as defined in Appendix E.

with varying step length. As can be seen in Figure 8.5 once the step length is sufficiently small our results are independent of step length. Next a comparison is made between the numerical and analytical results for varying values of the

junction position z_{1k} and hence varying values of the radius r_1 (Figure 8.6).

As can be seen from the comparison of our numerical and analytical results, the solutions are in close agreement for the azimuthal velocity and in broad agreement with the radial velocity, and, as anticipated, as the radius increases, corresponding to z_{1k} decreasing, the numerical results agree more closely with the large radii analytical solution. We can also compare our analytic prediction for the relationship between δ_m^* and z_{1k} with that produced by our numerical solution. Again we find that particularly as z_{1k} decreases the two sets of results are in very good agreement.

Interestingly, it is now only possible to produce results for the case when $r_1 \geq 13$ and that no upper bound on the radial range at which numerical results are achievable has been reached ($r_1 \approx 1000$ is the largest radii at which results have been produced but results at greater radii appear possible). The fact that, albeit using an otherwise unjustified eddy viscosity, it is possible to produce numerical results which agree well with the large radii analytical solution (and a further analytical solution subsequently derived) provides some evidence for the reliability of our approach. However, the limitations of the method when only the inner tier of the Cebeci-Smith model is used is concerning and further investigation would be highly desirable (although not undertaken here). Instead a new analytical solution (based on the assumption of a decaying form for δ_m^*, and hence decaying junction position) is produced.

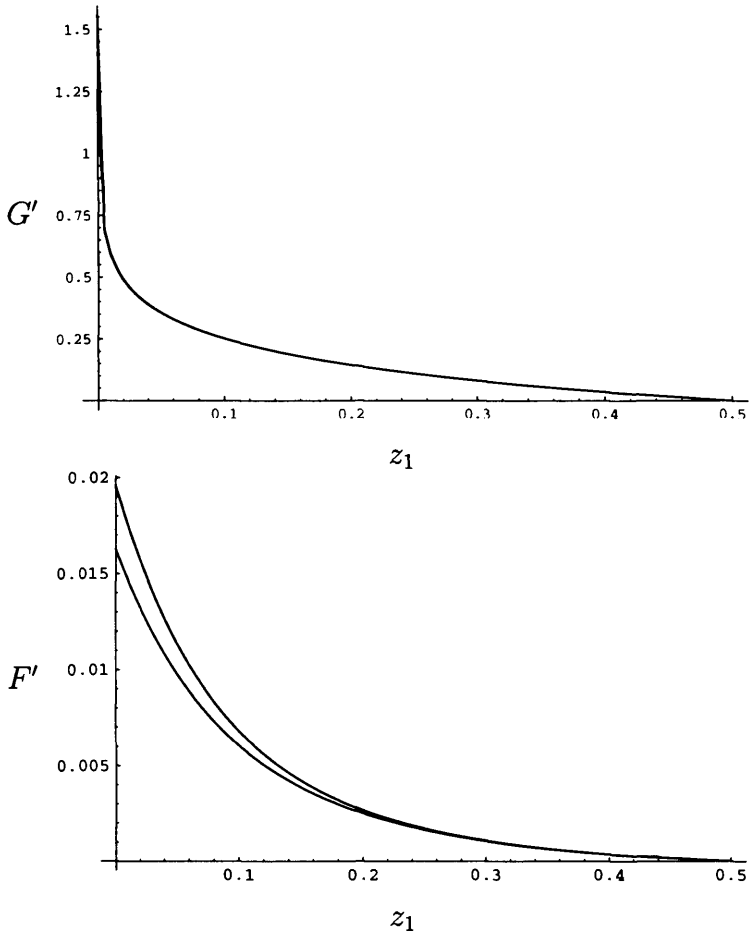

Figure 8.5: *Left: Azimuthal numerical results for* $z_{1k} = 0.45$ *with varying step length. Right: Radial numerical results for* $z_{1k} = 0.45$ *with varying step length. Although the individual curves are not always discernible, in both cases the uppermost curve corresponds to* $h = -0.000001$*, the middle curve* $h = -0.00001$*, and the lower curve* $h = -0.0001$.

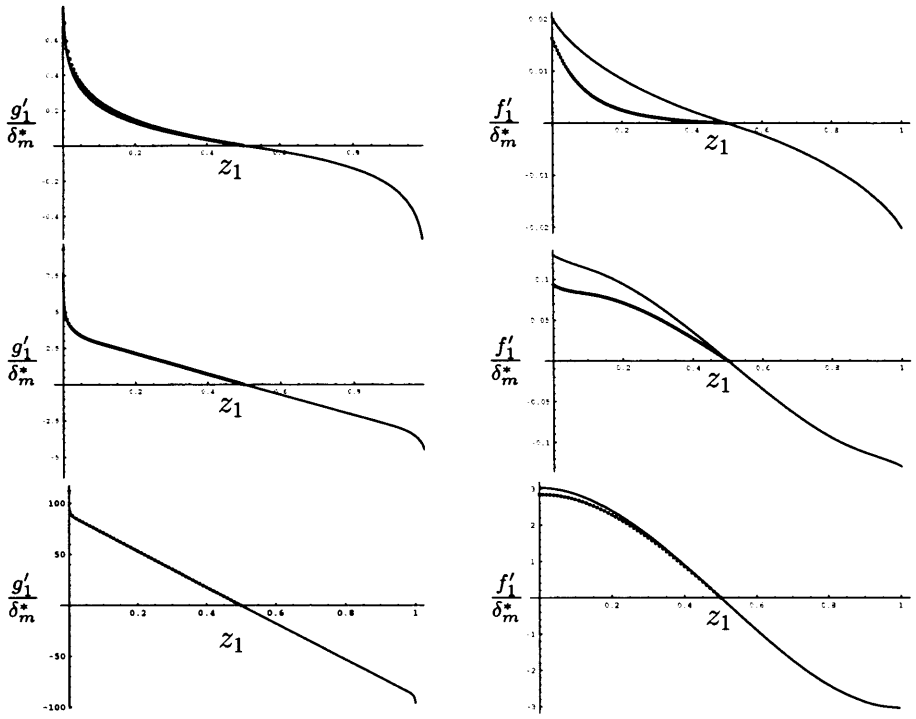

Figure 8.6: *Comparison of analytical and numerical azimuthal results with* $z_{1k} = 0.45$ (*left top*), *radial results with* $z_{1k} = 0.45$ (*right top*), *azimuthal results with* $z_{1k} = 0.1$ (*left middle*), *radial results with* $z_{1k} = 0.1$ (*right middle*), *azimuthal results with* $z_{1k} = 0.02$ (*left bottom*), *radial results with* $z_{1k} = 0.02$ (*right bottom*).

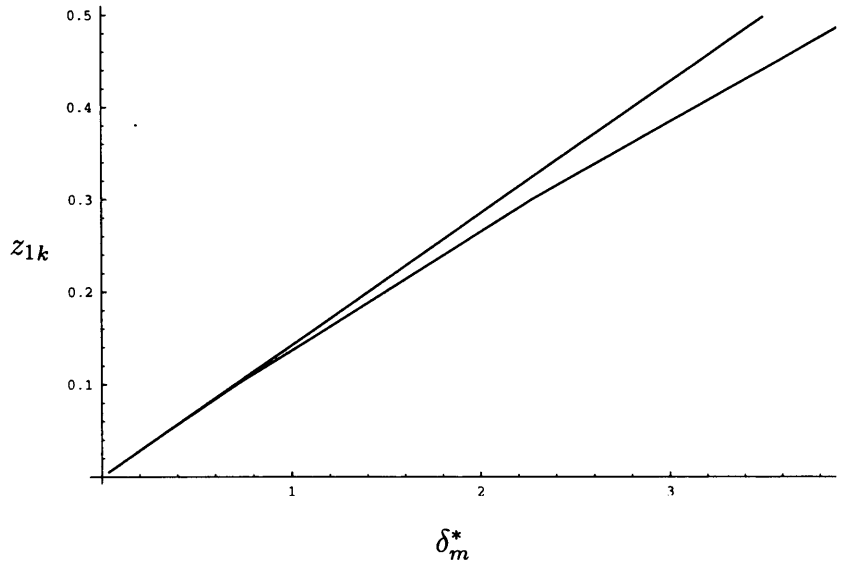

Figure 8.7: *Comparison of analytical (top curve) and numerical predictions for the relationship between* δ_m^* *and* z_{1k}.

8.4.5 Analytical Solution with Decaying Junction Position

Now supposing that $\delta_m^* \rightarrow \frac{J_0}{r_1}$ as used in the preceding numerical results, and that $|g_1''| \gg |f_1''|$ as is expected from consideration of the behaviour at large radii, the ITL can be taken to be comprised of two regions: firstly the 'core' layer, which is the bulk of the total layer, where $g_1' = O(1)$, $z_1 = O(1)$ and where the eddy viscosity is given by the outer form of the Cebeci-Smith model (in the core region here t is now used instead of z_1 to avoid any possible confusion with the ITL which is sometimes also referred to as the core); secondly there is now a thin sublayer where $z_1 = r_1^{-1}T$ and which contains the junction position between the outer and inner forms of the Cebeci-Smith model. We note that the same matching conditions between the ITL and the LS now apply to the matching between the laminar sublayer and this new sublayer, where (8.22) and (8.23) are now

$$0 = \frac{\partial}{\partial T} \begin{cases} k_4 J_0 f_1'' & \text{for } T \geq T_k, \\ T^2 |g_1''| f_1'' & \text{for } T \leq T_k, \end{cases} \tag{8.62}$$

and

$$0 = \frac{\partial}{\partial T} \begin{cases} k_4 J_0 g_1'' & \text{for } T \geq T_k, \\ T^2 |g_1''| g_1'' & \text{for } T \leq T_k. \end{cases} \tag{8.63}$$

Thus

$$0 = \begin{cases} k_4 J_0 f_1'' & \text{for } T \geq T_k, \\ T^2 |g_1''| f_1'' & \text{for } T \leq T_k, \end{cases} \tag{8.64}$$

and

$$-\frac{1}{4} = \begin{cases} k_4 J_0 g_1'' & \text{for } T \geq T_k, \\ T^2 |g_1''| g_1'' & \text{for } T \leq T_k, \end{cases} \tag{8.65}$$

from consideration of the matching conditions

$$g_1' \rightarrow -\frac{1}{2}\ln T, \tag{8.66}$$

$$f_1' \rightarrow T, \tag{8.67}$$

as $T \rightarrow 0$. Hence as $T \rightarrow \infty$

$$g_1'' \rightarrow -\frac{1}{4k_4 J_0}, \tag{8.68}$$

$$f_1'' \rightarrow 0. \tag{8.69}$$

Matching with the core region then suggests that in the core

$$g_1' \rightarrow C, \tag{8.70}$$

$$f_1' \rightarrow D, \tag{8.71}$$

with C and D constants which need to be determined, as $t \rightarrow 0$. In the core region we have

$$-g_1' = k_4 J_0 f_1''' \tag{8.72}$$

and

$$f_1' = k_4 J_0 g_1''', \tag{8.73}$$

which we can combine to yield

$$-g_1' = (k_4 J_0)^2 g_1''''' \tag{8.74}$$

and

$$-f_1' = (k_4 J_0)^2 f_1'''''. \tag{8.75}$$

This produces the solution

$$g_1' = Re[A_1 \exp a_1 t + A_2 \exp a_2 t + A_3 \exp a_3 t + A_4 \exp a_4 t] \tag{8.76}$$

and

$$f_1' = Re[B_1 \exp a_1 t + B_2 \exp a_2 t + B_3 \exp a_3 t + B_4 \exp a_4 t] \tag{8.77}$$

with

$$a_1 = (\frac{1}{2k_4 J_0})^{\frac{1}{2}}(1+i), \tag{8.78}$$

$$a_2 = (\frac{1}{2k_4 J_0})^{\frac{1}{2}}(-1+i), \tag{8.79}$$

$$a_3 = (\frac{1}{2k_4 J_0})^{\frac{1}{2}}(-1-i), \tag{8.80}$$

$$a_4 = (\frac{1}{2k_4 J_0})^{\frac{1}{2}}(1-i). \tag{8.81}$$

Inserting the solutions (8.76) and (8.77) into (8.72) and (8.73) yields

$$B_1 = iA_1, \tag{8.82}$$

$$B_2 = -iA_2, \tag{8.83}$$

$$B_3 = iA_3, \tag{8.84}$$

$$B_4 = -iA_4. \tag{8.85}$$

and the boundary conditions $g_1'(0) = C$, $f_1'(0) = D$, $g_1'(\frac{1}{2}) = 0$ and $f_1'(\frac{1}{2}) = 0$, are now equivalent to

$$A_1 + A_2 + A_3 + A_4 = C, \tag{8.86}$$

$$A_1 - A_2 + A_3 - A_4 = -iD, \tag{8.87}$$

$$A_1 \exp\frac{a_1}{2} + A_2 \exp\frac{a_2}{2} + A_3 \exp\frac{a_3}{2} + A_4 \exp\frac{a_4}{2} = 0, \tag{8.88}$$

$$A_1 \exp\frac{a_1}{2} - A_2 \exp\frac{a_2}{2} + A_3 \exp\frac{a_3}{2} - A_4 \exp\frac{a_4}{2} = 0. \tag{8.89}$$

Hence

$$A_1 = \frac{C - iD}{2(1 - \exp a_1)}, \tag{8.90}$$

$$A_2 = \frac{C + iD}{2(1 - \exp a_2)}, \tag{8.91}$$

$$A_3 = -A_1 \exp a_1, \tag{8.92}$$

$$A_4 = -A_2 \exp a_2. \tag{8.93}$$

We now determine the unknown constants C and D through the conditions $g''(0) = -\frac{1}{4k_4 J_0}$ and $f''(0) = 0$ (from matching with the sublayer) and which leads to

$$C = 12.483, \tag{8.94}$$

$$D = 0.413. \tag{8.95}$$

Taking $k_4 J_0 = 2.5$ (from $k_4 = 0.071$ and $J_0 = 35$) we have the following solution as illustrated in Figure 8.8. We can also compare these solutions with our earlier numerical results and our large radii analytical predictions.

As can be seen from Figure 8.8 the three sets of results are all in very good agreement at large radii as is hoped, and at the very least this work acts as a useful means to verify the accuracy of the three types of solution derived, although it must be noted that this is based on the arbitrary assumption that $\delta_m^* = 35/r_1$.

8.4.6 Comparison of Free Disc and Enclosed Disc Results

In the two-disc problem we have concentrated on the inner, bounded, surface of the rotating disc. Now we assume that the free surface[1] behaves like the rotating disc of Chapter 3, so that the presence of the stationary disc has no impact on the flow here. Assuming that the earlier results of Chapter 3 now apply to the free surface of the rotating disc, we can make comparisons between the flow on both sides of a rotating disc with a stator beneath it.

1. Here the free surface of the rotating disc is taken to be the opposite face of the disc to that facing the stationary disc.

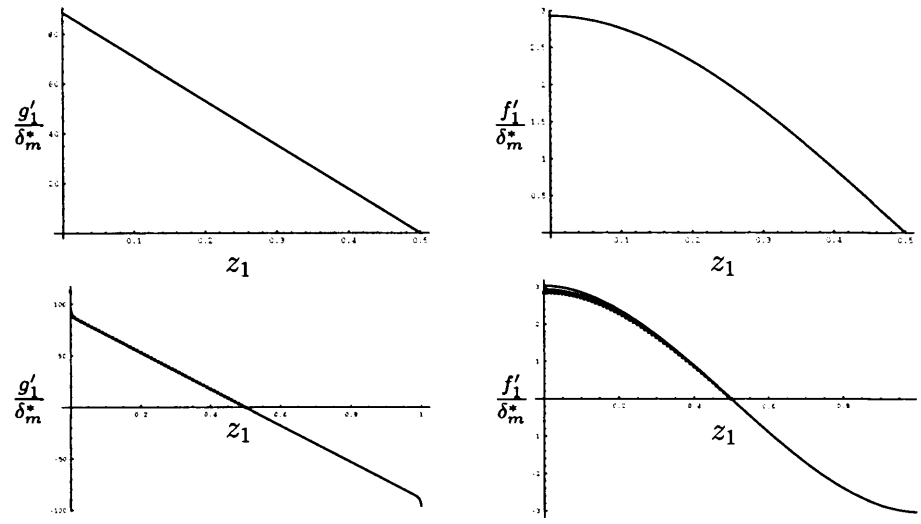

Figure 8.8: *Left top: Analytical result for* g_1'. *Right top: Analytical result for* f_1'. *Left bottom: Comparison with numerical results and large radii limit for* g_1'. *Right bottom: Comparison with numerical results and large radii limit for* f_1'. *All results are shown for junction position* $z_{1k} = 0.02$.

Figure 3.8 shows the radial velocity on a free rotating disc and Figure 8.2 the analytical solution for f_1' in the two-disc problem. As those two graphs show, the magnitude of the radial velocity in the free disc case is far greater than for the confined system. Moreover in the present problem, f_1' decays with the radius whilst the radial velocity perturbation for the free disc, also denoted f_1', does not. In contrast however, the azimuthal velocity on either side of the rotating disc is far more similar. This comparison is shown in Figure 8.9.

8.4.7 Skin Friction

In the laminar sublayer on the rotating disc we have the following azimuthal momentum equation,

$$0 = g_2''' + \frac{\partial}{\partial \eta_2}(\eta_2^2 |g_2''| g_2''). \tag{8.96}$$

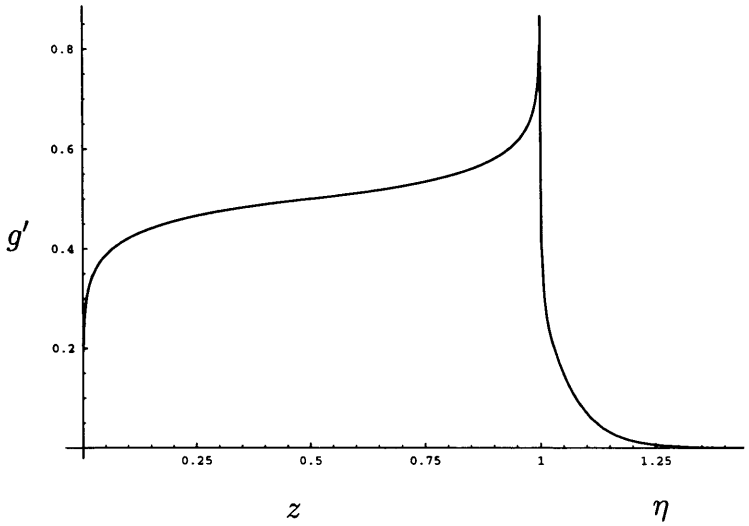

Figure 8.9: *Comparison of the present large radii analytical prediction for the non-dimensional azimuthal velocity $g'(z)$ and the numerical results for the non-dimensional azimuthal velocity $g'(\eta)$ on a free rotating disc, from Chapter 3. Results are presented for Reynolds number $R_r = 10^6$ and the two-disc results are shown on the non-dimensional height range $0 \leq z \leq 1$ whilst the free disc solution is given on the similarity height interval $1 \leq \eta \leq 1.5$. In both cases the rotating disc is at $z = \eta = 1$. For the two-disc flow, the stationary disc is at $z = 0$.*

As with the free disc problem we can use this equation to determine the skin friction through knowledge of the asymptotic behaviour of g_2'. As in Chapter 3, (8.96) can be integrated to obtain

$$-\frac{1}{4} = g_2'' + \eta_2^2 |g_2''| g_2'', \tag{8.97}$$

using the fact that $g_2' \to -\frac{1}{2}\ln\eta_2$ as $\eta_2 \to \infty$. Thus as $\eta_2 \to 0$ we have

$$-\frac{1}{4} = g_2''(0), \tag{8.98}$$

which leads to the following form for the skin friction $c_{f\theta}$,

$$c_{f\theta} = \frac{k_1^2 \epsilon^2}{2}, \tag{8.99}$$

where the skin friction is defined as in the free disc case and is derived in exactly the same way. This process can be repeated for the laminar sublayer on the stationary disc and, since the azimuthal momentum equation is the same for both sublayers and the azimuthal asymptotic behaviour is of the same magnitude, an identical result is achieved.

We now compare our predictions for the skin friction with the asymptotic behaviour as found by Cooper & Reshotko. From above we have

$$c_{f\theta} = \frac{0.08}{(\ln R)^2}, \tag{8.100}$$

and hence

$$c_{f\theta} = \frac{0.08}{(\ln R_r)^2}, \tag{8.101}$$

as $R_r \rightarrow \infty$, whereas Cooper & Reshotko, based on the work of Coles[18], propose the form

$$0.173718(\frac{2}{c_{f\theta}})^{\frac{1}{2}} + \log(\frac{2}{c_{f\theta}}) = \log(\frac{\omega s_D^2}{\nu}) + \log R_r + 1.13512, \tag{8.102}$$

which as $R_r \rightarrow \infty$ becomes

$$0.173718(\frac{2}{c_{f\theta}})^{\frac{1}{2}} = \log R_r, \tag{8.103}$$

and hence

$$\begin{aligned} c_{f\theta} &= \frac{2(0.173718)^2}{(\log R_r)^2} \\ &= \frac{0.32}{(\ln R_r)^2}, \end{aligned} \tag{8.104}$$

which is the same as that on a free disc and four times greater than our predictions, although as can be seen from Appendix D, our results are comparable to those of Afzal for turbulent Couette flow. Interestingly, the asymptotic result of Cooper & Reshotko provides further support for our own predictions for the skin friction on a free rotating disc, since, as stated, Cooper & Reshotko's prediction is based on the work of Coles for a free disc.

8.5 Possible Extensions of the Two-Disc Problem

Some brief potential extensions to this model are now considered. In particular the system can be modified to include asymmetry about the gap centre line and two new aspects which are of interest with respect to rotor dynamics. These are the influence of side structures on the flow and the inclusion of non-axisymmetry in the two-disc flow.

8.5.1 Asymmetric Flow between Two Discs

The antisymmetric case studied to date in this chapter has the distinct advantage of being a simpler problem to solve as the system can be reduced to solving for just one half of the gap region. However the lack of a definitive eddy viscosity model for use here, combined with the relative unimportance (from an engineering perspective) of flow at such large radii means that the asymmetric phase is of more direct significance. Therefore this flow is now discussed.

Boundary Layer Structure

It is possible to produce numerical results based on the method used by Cooper & Reshotko, specifically using their choice of eddy viscosity model and hence δ_m^*, treating β_p as an unknown parameter of the flow. As this has already been performed by Cooper & Reshotko, it is not undertaken here and instead the boundary layer structure is discussed and the governing equations for each layer derived. It is supposed that in the core region of the boundary layer the azimuthal velocity is $O(\beta_p)$ (so that the inertial and pressure terms balance in

the leading order expansion in the IITL) where β_p is defined as

$$\beta_p^2 = \frac{1}{\rho\omega^2 r_D}\frac{\partial p}{\partial r}. \tag{8.105}$$

Hence, in the ITL

$$r = \epsilon^{-1} r_1, \tag{8.106}$$

$$z = z_1, \tag{8.107}$$

$$g' = \beta_p + \epsilon g_1', \tag{8.108}$$

$$f' = \epsilon f_1'. \tag{8.109}$$

These substitutions, (8.106) - (8.109), produce the following equations for the ITL

$$-2\beta_p g_1' = r_1 \frac{\partial}{\partial z_1} \begin{cases} k_4 \delta_m^* f_1'' & \text{for } z_1 \geq z_{1k}, \\ z_1^2 (f_1''^2 + g_1''^2)^{\frac{1}{2}} f_1'' & \text{for } z_1 \leq z_{1k}, \end{cases} \tag{8.110}$$

and

$$2\beta_p f_1' = r_1 \frac{\partial}{\partial z_1} \begin{cases} k_4 \delta_m^* g_1'' & \text{for } z_1 \geq z_{1k}, \\ z_1^2 (f_1''^2 + g_1''^2)^{\frac{1}{2}} g_1'' & \text{for } z_1 \leq z_{1k}. \end{cases} \tag{8.111}$$

Following the same matching analysis as for the antisymmetric case it is found that

$$g_1' \sim -(1-\beta_p)\ln z_1, \tag{8.112}$$

$$g_1' \sim \beta_p \ln(1-z_1), \tag{8.113}$$

as $z_1 \to 0$ and $z_1 \to 1$ respectively, and likewise

$$f_1' \sim \frac{2\beta_p}{r_1} z_1 \ln z_1, \tag{8.114}$$

$$f_1' \sim -\frac{2\beta_p}{r_1}(1-z_1)\ln(1-z_1), \tag{8.115}$$

In the two laminar sublayers the height scaling and velocity expansions are unchanged from the antisymmetric case but now the pressure gradient has

changed and so, with $0 \leq \beta_p \leq \frac{1}{2}$, the governing equations in the laminar sublayers on the rotating and stationary discs are

$$\beta_p^2 - 1 = f_2''' + \frac{\partial}{\partial \eta_2}(\eta_2^2 | g_2'' | f_2''), \tag{8.116}$$

$$0 = g_2''' + \frac{\partial}{\partial \eta_2}(\eta_2^2 | g_2'' | g_2''), \tag{8.117}$$

and

$$\beta_p^2 = f_3''' + \frac{\partial}{\partial \eta_3}(\eta_3^2 | g_3'' | f_3''), \tag{8.118}$$

$$0 = g_3''' + \frac{\partial}{\partial \eta_3}(\eta_3^2 | g_3'' | g_3''), \tag{8.119}$$

respectively. As stated, a numerical solution is not attempted here and instead an analytical prediction for the skin friction is now derived.

Skin Friction in the Asymmetric Flow Region

The same derivation for the skin friction used previously for the antisymmetric flow problem and in Chapter 3 for the free disc case can be extended to the present asymmetric system. The appropriate asymptotic behaviour for this phase is given by (8.112) and (8.113) and yields the following form for the skin friction on the rotating disc and on the stationary disc respectively,

$$c_{f\theta} = 2(1 - \beta_p)^2 k_1^2 \epsilon^2, \tag{8.120}$$

$$c_{f\theta} = 2\beta_p^2 k_1^2 \epsilon^2. \tag{8.121}$$

Note that as $\beta_p \to 0$ (and hence as the flow approaches that of a free disc, or alternatively as $r_1 \to 0$) the skin friction on the stationary disc tends to zero, whilst that on the rotating disc tends to that on a free disc.

8.5.2 An Enclosed Rotating Disc

The present two-disc problem is designed to model ground effect but this is not the only physical interaction of interest in helicopter dynamics. The influence of nearby structures such as buildings are also important. Thus to try to model this behaviour a horizontal cylindrical enclosure (wall) is included and which is taken to surround the two discs. For this problem it is assumed that the clearance from the edge of the two discs is roughly the same as the gap distance and both these distances are considered to be $O(\epsilon)$ relative to the radius of the discs.

In this case the flow in the gap between the two discs and the enclosure can be considered as a quasi 2D problem in the radial and normal directions with the system governed by the 2D Euler equations. Bernoulli's equation therefore holds and can be used to relate the pressure on the rotating disc to the pressure on the enclosure:

$$p_e + \frac{1}{2}\rho(u_{De}^2 + w_{De}^2) = p_W + \frac{1}{2}\rho(u_{DW}^2 + w_{DW}^2), \tag{8.122}$$

where the subscripts e and W respectively denote the values measured at the edge of the disc and on the wall. For ease p_W is determined at a stagnation point on the wall. From the earlier analytical large radii solution, $u_D(0) = \frac{\omega s_D}{k_1^2}$ and $w_D(0) = 0$. Combining these velocities with the pressure, determined earlier as $p = \frac{\rho\omega^2 r_D^2}{8}$, yields

$$p_{stag} = \frac{\rho\omega^2 a^2}{8} + \frac{\rho\omega s_D}{k_1^2}, \tag{8.123}$$

where p_{stag} is the pressure on the wall at the stagnation point and a is the radius of the rotating disc. This suggests that once the radius is sufficiently large (so that the analytical solution above applies) then the pressure at the stagnation point is approximately the same as that at the edge of the disc.

8.5.3 A Cut-Disc and a Stationary Disc

Having examined the problem of the flow between a stationary and a rotating disc as a model for the flow generated by a set of rotors in ground effect, we now attempt to improve our model by briefly examining the problem of the flow generated by a rotating cut-disc which rotates in a plane parallel to a stationary disc at a fixed distance, s_D. This problem is of interest to us as it enable us to examine the influence of ground effect on flows without axisymmetry. Furthermore, in the same way that the NATBL on a cut-disc is relevant to the flow generated by a set of rotors because it is possible to reduce the turbulent boundary layer on a set of rotors to that on a cut-disc, we might also suppose that once we can understand the flow generated by a rotating cut-disc and a stationary disc, it will be possible to gain some understanding of the NATBL on a set of rotors in ground effect. As discussed in the previous chapter, whilst the flow generated by a rotating and a stationary disc has been examined previously, leading to a range of experimental and numerical research on the topic, there unfortunately does not appear to be any such research into this non-axisymmetric problem.

The steady dimensional Reynolds equations for a non-axisymmetric boundary layer, in cylindrical polar co-ordinates in a frame of reference rotating with angular velocity, ω, are taken as

$$\begin{aligned} &u_D\frac{\partial u_D}{\partial r_D} - \frac{v_D^2}{r_D} + \frac{v_D}{r_D}\frac{\partial u_D}{\partial \theta} + w_D\frac{\partial u_D}{\partial z_D} - 2\omega v_D - \omega^2 r_D = -\frac{1}{\rho}\frac{\partial p_D}{\partial r_D} \\ &+\nu\frac{\partial^2 u_D}{\partial z_D^2} + \frac{\partial}{\partial z_D}\begin{cases} \overline{k_4}\delta_m^*(\frac{\tau_w}{\rho})^{\frac{1}{2}}\frac{\partial u_D}{\partial z_D} & \text{for } \overline{z}_D \geq \overline{z}_{Dk}, \\ \overline{z}_D^2\left|\frac{\partial u_D}{\partial z_D}\right| + \frac{\partial v_D}{\partial z_D}\left|\frac{\partial u_D}{\partial z_D}\right| & \text{for } \overline{z}_D \leq \overline{z}_{Dk}, \end{cases} \end{aligned} \tag{8.124}$$

and

$$u_D\frac{\partial v_D}{\partial r_D}+\frac{u_D v_D}{r_D}+\frac{v_D}{r_D}\frac{\partial v_D}{\partial\theta}+w_D\frac{\partial v_D}{\partial z_D}+2\omega u_D=-\frac{1}{\rho r_D}\frac{\partial p_D}{\partial\theta}$$
$$+\nu\frac{\partial^2 v_D}{\partial z_D^2}+\frac{\partial}{\partial z_D}\begin{cases}\overline{k_4}\delta_m^*(\frac{\tau_w}{\rho})^{\frac{1}{2}}\frac{\partial v_D}{\partial z_D} & \text{for } \overline{z}_D\geq\overline{z}_{Dk},\\ \overline{z}_D^2|\frac{\partial u_D}{\partial z_D}+\frac{\partial v_D}{\partial z_D}|\frac{\partial v_D}{\partial z_D} & \text{for } \overline{z}_D\leq\overline{z}_{Dk}.\end{cases} \tag{8.125}$$

with continuity equation

$$\frac{1}{r_D}\frac{\partial(u_D r_D)}{\partial r_D}+\frac{1}{r_D}\frac{\partial v_D}{\partial\theta}+\frac{\partial w_D}{\partial z_D}=0. \tag{8.126}$$

Here we are using the same eddy viscosity as Cooper & Reshotko for the flow between a stationary and a rotating disc. Now we make the substitutions

$$r_D = \frac{s_D}{k_1^2}r, \tag{8.127}$$
$$z_D = s_D z, \tag{8.128}$$
$$u_D = \omega r_D f'(r,\theta,z), \tag{8.129}$$
$$v_D = \omega r_D g'(r,\theta,z), \tag{8.130}$$
$$p_D = \rho\omega^2 r_D^2 p(r,\theta), \tag{8.131}$$

where the radius is also scaled against k_1^2 for convenience and which, from the continuity equation, yields

$$\frac{w_D}{\omega s_D}=-2f-r_D\frac{\partial f}{\partial r_D}-\frac{\partial g}{\partial\theta}. \tag{8.132}$$

Equations (8.127) - (8.131) lead to the following equations

$$f'^2-3ff''-g'^2+g'\frac{\partial f'}{\partial\theta}-f''\frac{\partial g}{\partial\theta}-2g'-1 \tag{8.133}$$
$$=-\frac{\partial p}{\partial r}+\frac{1}{R_s}f'''+\frac{\partial}{\partial z}\begin{cases}\overline{k_4}\delta_m^*|g''(0)|^{\frac{1}{2}}f'' & \overline{z}\geq\overline{z}_k\\ \overline{z}^2(f''^2+g''^2)^{\frac{1}{2}}f'' & \overline{z}\leq\overline{z}_k\end{cases}$$

and

$$2f'g' - 3fg'' + g'\frac{\partial g'}{\partial \theta} - g''\frac{\partial g}{\partial \theta} + 2f' \tag{8.134}$$
$$= -\frac{1}{r}\frac{\partial p}{\partial \theta} + \frac{1}{R_s}g''' + \frac{\partial}{\partial z}\begin{cases} \overline{k_4}\delta_m^*|g''(0)|^{\frac{1}{2}}g'' & \overline{z} \geq \overline{z}_k \\ \overline{z}^2(f''^2 + g''^2)^{\frac{1}{2}}g'' & \overline{z} \leq \overline{z}_k. \end{cases}$$

Although no further analysis of this problem will be undertaken here, we might suppose that we have the following boundary layer structure - a laminar sublayer on the stationary disc; a laminar sublayer on the rotating cut-disc; a laminar sublayer in the wakes of the cut-disc; and a core, outer layer. This could then be applied to the Reynolds equations derived above in order to simplify the problem.

8.6 Summary

In this chapter we have examined the flow between two discs, one stationary and the other rotating, and concentrated on the flow at large radii. Here the flow is assumed to be antisymmetric about the midpoint of the gap between the discs.

The simplifications employed in this chapter, such as the assumption of antisymmetry and the slightly arbitrary decision made on the choice of eddy viscosity used, renders this problem rather contrived but does enable some initial features to be outlined. These include a description of the boundary layer (one which is readily extended to the asymmetric flow case) and an analytical solution valid at large radii (which is easily modified to include any suitable form for the Cebeci-Smith eddy viscosity). An analytical prediction for the skin friction follows simply from the boundary layer structure used here and is in agreement with that for turbulent Couette flow (as deduced by

Afzal). Moreover, on consideration of the asymmetric flow problem, our skin friction prediction 'fits' in with the equivalent prediction for the free rotating disc. There is substantial disagreement with the asymptotic results of Cooper & Reshotko regarding skin friction (which they predict to be the same as that on a free disc) however their work is based on that of Coles who examined a free disc (this suggests that the good agreement with our results for a free disc is not surprising and that perhaps it is not appropriate to extend the results of Coles to an enclosed disc flow).

More alarming is the stark difference between the present numerical results and those of Cooper & Reshotko (and the present analytical results) and the limitations of the numerical scheme used here (such as the inability to produce results for large radial positions when only an inner tier of the Cebeci-Smith model is used). A more comprehensive study of this problem, in particular involving a more sophisticated numerical method,[1] is therefore highly desirable (the test case used in §8.4.4 may provide some insight into a more suitable numerical scheme and at least shows good agreement with the large radii analytical solution).

As mentioned, a few speculative extensions to this problem have been briefly considered although no major progress has been achieved (or indeed attempted). These are nonetheless included as they indicate the possible avenues in which it is hoped this research may be extended and to, hopefully, encourage these avenues to be explored.

1. For instance one which solves for the entire gap region and does not assume antisymmetry.

Chapter 9

Conclusions and Further Work

9.1 Summary

The main new features described in the present study may be listed immediately. They are the enhanced thickness of the turbulent boundary layer on a moving wall; likewise that on a rotating disc; the agreements with empirical and other previous methods on the above two fundamental problems; the boundary layer thickness on a rotating cut-disc; the effects of vertical asymmetry and of ground clearance; and the flow structures of all the above. (It was found after the writing up of this thesis that enhanced boundary layer thickness has also been found recently in independent work by Scheichl[63] in a quite different setting). A more detailed summary is as follows.

In **Chapter 2** an effective viscosity was used as a means of describing the turbulent stresses which occur in the flow past a flat plate with a moving surface, and a particular form used: the Cebeci-Smith model. The boundary layer height was then taken to be order k_1^2 where $k_1 = 0.4$ is von Karman's constant. These assumptions appear to be at least partially substantiated by

the accuracy with which the current predictions for skin friction, velocity and displacement thickness agree with existing work.

Encouraged by the success of the description of the turbulent boundary layer used in the previous chapter, **Chapter 3** proceeded to examine a rotating disc in an unbounded fluid, again based on a new suggestion for the boundary layer structure. Once more, the results generated for the skin friction and the fluid velocity within the boundary layer agree well with the work of other authors but now the displacement thickness is found to grow more rapidly (in fact more-or-less linearly) with radius than is found in earlier research. This may arise due to the assumption of a similarity solution for this flow.

Chapter 4 introduced non-axisymmetry into rotating flows. The appropriate Reynolds equations were derived following the same approach as Smith & Cebeci[66] with azimuthally dependent terms retained. These equations were then coupled with a four-region structure for the turbulent boundary layer. Crucial to the success of this new model is the existence of two 'outer' layers where there is a balance between inertial and turbulent terms. For the most part the non-axisymmetric turbulent boundary layer (NATBL) is azimuthally invariant to leading order. The solution here was related to that of a free disc where the velocities are scaled by the parameter $a^{\frac{1}{2}}$ with a the surface (disc) solidity.

In **Chapter 5** the flow due to a cut-disc was considered as an early model for a rotor. In this problem a numerical solution was produced for the 'buffer' layer, i.e. the outer region which has θ-dependence. The results produced were for a variety of flows with the disc solidity and the number of blades in the cut-disc both varied. Blade inclination was then incorporated in a simple way (i.e. without considering the free wake shape) as a means of

introducing interaction between both halves of the flow. Several low solidity limits were then analyzed. Firstly the earlier numerical procedure was used to study the flow profiles as a became small and these results seemed to indicate the existence of a limit as a tends to zero. Next an analytical solution to the flow in a region close to the blade was derived and which is in general agreement with the relevant numerical work. Moreover, this analytical solution tends to the solution for the flow on an isolated flat plate as found by Neish & Smith[50] and shows how the flow past a cut-disc reduces to the flow past a set of isolated blades as a shrinks to zero. Finally another analytical solution was derived, this time for the near-wake region, and also compared with the equivalent numerical solutions. In this case, as a became small, the analytical and numerical solutions were found to be in very good agreement.

Chapter 6 then involved solving for a cut-disc with vertically symmetric blade thickness. Smith & Timoshin[68] have shown that the Prandtl shift reduces such boundary layers to that on a flat cut-disc and that the pressure outside the boundary layer can be described by Laplace's equation subject to a condition on the normal pressure gradient which is based on the blade shape. This has been verified for the particular turbulent flow of interest here and illustrated with a solution for a limited type of blade configuration and possible blade shape.

Vertical blade asymmetry has been considered in a 2D context in **Chapter 7**. Here the work of Smith & Timoshin[69] has been extended to the turbulent flow regime of interest here, and in the case of an infinite number of thin identical blades, the global solution for the pressure and the fluid downwash is shown to be periodic. A global complex potential for the flow has been derived and used, in conjunction with an image potential, to extend the problem to one

incorporating ground effect. As the gap between the blades and the ground decreases to zero, the pressure difference on the blades and the magnitude of the fluid downwash in the wakes doubles. This then leads to an decrease in the power required by the blades, for a given rotation rate and in accordance with Bramwell and Seddon, to maintain hover.

Chapter 8 then considered ground effect over a viscous length scale by examining the flow between two discs, one rotating and the other stationary. The behaviour at large radii, relative to the gap distance between the discs, was investigated with the use of the Cebeci-Smith eddy viscosity model and with the flow assumed to be antisymmetric. Several analytical solutions were considered, in particular one where the radius tends to infinity. Initially the flow at large radii was determined assuming that only the inner tier of the eddy viscosity was required. This solution was found to have broad agreement with the numerical results of Cooper & Reshotko but disagreed quite significantly with our own numerical results. Moreover, our numerical procedure can only produce results for a small range of Reynolds numbers unless an outer tier to the Cebeci-Smith model is used. In this test case, assuming a decaying junction position between the two tiers, the large radii analytical solution and the numerical results agree very well as the radius increases (corresponding to the junction position decreasing to zero). A further analytical solution based on a decaying junction position also correlated well with these two sets of results. Predictions for the asymptotic form of the skin friction are found to be four times smaller than that derived by Cooper & Reshotko who predict that the skin friction is the same as in the case of a free disc. On the other hand, our results do agree with Afzal[1] for turbulent Couette flow. It has also been possible to make comparisons between the velocity profiles in both this

two-disc problem and the free disc case of Chapter 3. It transpires that the azimuthal velocity in the vicinity of the rotating disc is broadly similar in both flows but the radial velocity of the free disc is by far the greater of the two radial components. Three possible extensions were also discussed. Firstly the boundary layer structure and skin friction coefficients for asymmetric flow were described. Secondly the pressure at the stagnation point of a cylindrical enclosure surrounding the two discs was calculated and found to be broadly the same as the pressure at the edge of the rotating disc itself. Finally the governing equations for the flow between a rotating cut-disc and a stationary flat disc were presented.

9.2 Application to Turbulent Jets

It is now also noted that the possible application of the preceding work, on boundary layers attached to moving surfaces (and in the subsequent wakes), to the problem of turbulent jets has been considered by the author. Although it transpires that there appears only a little value and novelty in applying the turbulence model (in particular the structure of the turbulent boundary layer) used herein, this problem merits further consideration and is briefly discussed.

Jet flow has numerous applications in engineering including jet engines, exhausts and outlet gas pipes. The relevance to earlier work in this thesis comes from the geometry of jet flow, specifically that the typical length of a jet is much greater than its width (Schlichting[64]). This suggests that the boundary layer approximations may also apply here. Moreover, in the case of a turbulent jet, the flow is driven by an outflow of fluid in (initially at least) a relatively thin region. This jet then interacts with the fluid around it, transferring momentum to previously unperturbed surrounding layers and

causing the jet to expand. Parallels can be drawn, in the two-dimensional case at least, with the flow on a flat plate with a moving surface where the non-zero surface velocity draws nearby areas of fluid along at (almost) the same rate, in turn leading to a transfer of momentum to regions of the fluid further from the plate. The obvious distinction to be noted here is that the centre line velocity of a turbulent jet (analogous to the speed of the moving surface in Chapter 2 say) is not maintained at a constant rate along the length of the flow, and, indeed, might intuitively be expected to decay as the distance from the jet aperture increases. Nonetheless it seems reasonable to wonder if the enhanced boundary layer structure used for the flow on the flat plate with a moving surface in Chapter 2 may also be valid here.

Jet flow is a widely examined problem and one which is discussed extensively, for a variety of different scenarios, including Prandtl[57], Schlichting[64], Lin[43], Cebeci & Bradshaw[12], Dahm & Dimotakis[24], Papanicolaou & List[53], Papantoniou & List[54] and Peterson & Plesniak[55]. In the case of 2D jets Schlichting derives several properties of the flow. A similarity solution can be applied and shows the jet width growing linearly with distance along the jet, with the centre line velocity decaying as the square root of the distance. These results are not exclusive to Schlichting and are found throughout literature on this topic. Analogous results also exist for other types of jet (such as round and axisymmetric jets). Crucially Schlichting also presents an account of the solution determined by Goertler[35]. In this case Goertler derived an analytical answer using an eddy viscosity equivalent to that in the upper tier of the Cebeci-Smith model used previously in this thesis. Pre-dating this work is that of Tollmien[76] who modelled the eddy viscosity as similar to the lower tier of the Cebeci-Smith form (it should be noted that the mixing length used

by Tollmien grows linearly with distance along the jet as opposed to growing linearly with distance normal to the centre line as is the case with the Cebeci-Smith models used herein). It seems likely that it is possible to combine the work of Tollmien and Goertler to model the turbulent stresses using a Cebeci-Smith type eddy viscosity, and it would be interesting to see how such results compare with experimental work and the predictions of Tollmien and Goertler. This is not something that was attempted here and instead the possibility of the two-dimensional turbulent boundary layer (2DTBL) structure used in Chapter 2 is considered.

This structure involves having a thin sublayer with an order unity velocity and, in the formal extension to jet flow, two thicker outer layers where the velocity is significantly smaller in magnitude. Unfortunately this requires logarithmic asymptotic behaviour as the jet centre line is approached. As with the flow in the wake of a flat plate considered by Neish & Smith[50] and for the non-axisymmetric turbulent boundary layer considered in Chapter 4, this logarithmic behaviour contravenes the condition of symmetry about the jet centre line. Instead the velocity decays as the square root of distance from the centre line. Since this asymptotic behaviour is unable to bridge the two order of magnitudes corresponding to the sublayer and the two outer layers, such a structure cannot be applied. Instead it appears that the jet is comprised of a large region where the velocity is of the same order as the wake centre line and where either the velocity in this thick layer decays to zero at the edge of the jet or there exists a thin outer layer at the edge in which the relatively large core velocity reduces to a much smaller order of magnitude. This latter scenario bears some resemblance to the flow between two discs (Chapter 8) with a large core region and two thin sublayers.

However, for the types of turbulent stress model considered, this discussion of the 2DTBL structure is academic since it is principally used to simplify the Reynolds equations so that they can be solved more easily. As Tollmein and Goertler have shown, the full Reynolds equations taken with Cebeci-Smith type eddy viscosities can be solved directly without resorting to a simplifying structure for the flow. Hence there seems to be little direct relevance of the work of this thesis to the problem of 2D jets. Nonetheless, the physical similarities between these two types of flow hint that there may be applications of the present work to jet flows. In particular in cases where the Reynolds equations are not as easily solved (for instance where a different eddy viscosity is used, when the flow geometry is more complicated or when the jet is in the presence of a crossflow) then a turbulent structure for the jet may be required. In this scenario the earlier boundary layer structures used in this thesis may provide insight into the solution for such jets.

9.3 Further Work

Below are listed possible and desirable extensions to the present work. There are various avenues of investigation which can be explored further and these relate to aspects of those flows studied herein as well as to new flow problems which are pertinent to helicopter dynamics and to alternative otherwise unconnected engineering and physical applications. The following examples of further work can be loosely categorized into two types: those aspects which follow immediately from the present investigation and those which pose a tougher problem and which are designed to bridge the gap between the level of rotor blade complexity which is admissible analytically here and that experienced on a daily basis in engineering. The former category of work is considered here

first.

1. Throughout this investigation a particular turbulence model was used: the Cebeci-Smith two-tier eddy viscosity model. Other types of turbulence closure models are available however, and it would be useful to see how the current work compares with results produced using other eddy viscosity models and with more detailed turbulence (Reynolds) stress models.

2. It is possible to extend the work of Chapter 5 to include cut-disc configurations which consist of more than one blade size or where the blades have different fixed inclinations. These are straightforward problems which require relatively little extra effort, but which would produce results which may be interesting to see. These options were not considered here as the practical use in helicopter dynamics is limited although it may be more relevant in other applications.

3. The cut-disc problem of Chapter 5 (and hence the rotating disc problem of Chapter 3 by necessity) could be solved numerically without recourse to a similarity solution. Although, particularly in the inner inertial-turbulent layer of the cut-disc, this may be a complicated and computationally-intensive procedure, it would produce several benefits. Firstly it would enable a comparison to be made with the existing work on a rotating disc, especially in terms of our present predictions for the displacement thickness. In terms of our present work the use of a similarity solution leads to a linearly growing displacement thickness which is more rapid growth than found by von Karman or Cooper. More importantly though, this would allow a comparison to be made between

the far-field behaviour of a radial cut-disc and one with perhaps more realistically shaped blades (as Smith & Timoshin considered in the analogous laminar problem). Finally, a fully three-dimensional solution for the cut-disc flow would allow the symmetric blade problem of Chapter 6 to be extended to include configurations of one or two blades and with more realistic lengthwise blade shape.

4. Similarly, a fully 3D solution (as opposed to the similarity transformation used at present) to the flow in the outer inviscid region of a pair of rotors with symmetric blade shape would enable the current problem to be extended to blades with chordwise[1] blade shape, as actually occurs in practical scenarios, and not just limited to those with particular blade curvature as is presently the case.

5. The two-disc flow of Chapter 8 could be extended to a solution for all radii using the same Cebeci-Smith model as that of Cooper & Reshotko[22]. This would enable comparisons to be made with the results of Cooper & Reshotko for the skin friction and the radial pressure gradient, as well as the velocity profiles. This problem could also be developed to take in the related flows of co/counter rotating discs.

6. In general in this investigation, consideration has been given to the application to helicopter dynamics primarily. However it is possible to take this work further by considering the possible use with respect to other types of rotors, such as propellers, turbines, etc.

Now we discuss those wider challenging areas of further work which are designed to improve the realism of the flows which can be modelled.

1. i.e. where the thickness of the blade varies from the leading edge to the trailing edge of the blade.

1. A crucial aspect of the asymmetric flows considered here which it has not been possible to address is the determination of the free wake shape in three-dimensional flows. Instead the present investigation has been limited to either specifying the vertical wake shift as in Chapter 5 or working in two dimensions as in Chapter 7. Thus an important further piece of research would be to solve for the free wake shape generated by a set of inclined blades and a set of rotors with vertically asymmetric thickness.

2. There are also numerous other aspects of rotor blade dynamics which have not been considered and some examples of these include:

   - Spiralling downward wakes;
   - Smoothly varying blade inclination; and
   - The shedding of tip vortices, as well as other edge effects.

3. The two-disc flow with a cylindrical enclosure could also be examined more completely to help develop greater understanding of the influence of side structures on rotating flows.

4. A solution to the flow between a rotating cut-disc and a stationary disc could also be attempted. Although this is a fully 3D problem, if it is assumed that the velocity in the bulk of the gap is independent of θ (as may be a reasonable assumption in the case of low solidity) then the system reduces to one in which the radius can be treated as just a parameter of the flow (as occurred in the two-disc problem) and the governing equations which result from this are similar to those for the inner inertial-turbulent layer on a cut-disc. That suggests that a finite-difference technique may also work well for this problem. This system

has the interesting feature that, as a similarity solution is not invoked, there is no restriction to having radially-defined blades or thickness, and so realistic rotor shapes and configurations could be considered.

Appendices

Appendix A

A Runge-Kutta-Fehlberg Algorithm

Throughout this thesis, Runge-Kutta-Fehlberg algorithms of varying order are used to solve systems of ordinary differential equations. For the reader's benefit a third-order example (as used in Chapter 2) is now described (the analogous higher and lower order equivalents of this algorithm follow immediately from the definition presented below). No explanation for the validity of this algorithm is given, instead the reader is referred to Applied Numerical Analysis[33], from which this algorithm is taken.

If the equations to be solved are

$$\frac{\partial a}{\partial t} = f_1(t, a, b, c), \tag{A.1}$$

$$\frac{\partial b}{\partial t} = f_2(t, a, b, c), \tag{A.2}$$

$$\frac{\partial c}{\partial t} = f_3(t, a, b, c), \tag{A.3}$$

and we define the following quantities (for $i = 1$, 2 and 3),

$$k_{i1} = df_i(t_n, a_n, b_n, c_n), \tag{A.4}$$

$$k_{i2} = df_i(t_n + d/4, a_n + k_{11}/4, b_n + k_{21}/4, c_n + k_{31}/4), \tag{A.5}$$

$$\begin{aligned} k_{i3} = {} & df_i(t_n + 3d/8, a_n + 3k_{11}/32 + 9k_{12}/32, b_n + 3k_{21}/32 + 9k_{22}/32, \\ & c_n + 3k_{31}/32 + 9k_{32}/32), \end{aligned} \tag{A.6}$$

$$\begin{aligned} k_{i4} = {} & df_i(t_n + 12d/13, \\ & a_n + 1932k_{11}/2197 - 7200k_{12}/2197 + 7296k_{13}/2197, \\ & b_n + 1932k_{21}/2197 - 7200k_{22}/2197 + 7296k_{23}/2197, \\ & c_n + 1932k_{31}/2197 - 7200k_{32}/2197 + 7296k_{33}/2197), \end{aligned} \tag{A.7}$$

$$\begin{aligned} k_{i5} = {} & df_i(t_n + d, \\ & a_n + 439k_{11}/216 - 8k_{12} + 3680k_{13}/513 - 845k_{14}/4104, \\ & b_n + 439k_{21}/216 - 8k_{22} + 3680k_{23}/513 - 845k_{24}/4104, \\ & c_n + 439k_{31}/216 - 8k_{32} + 3680k_{33}/513 - 845k_{34}/4104), \end{aligned} \tag{A.8}$$

$$\begin{aligned} k_{i6} = {} & df_i(t_n + d/2, \\ & a_n - 8k_{11}/27 + 2k_{12} - 3544k_{13}/2565 + 1859k_{14}/4104 - 11k_{15}/40, \\ & b_n - 8k_{21}/27 + 2k_{22} - 3544k_{23}/2565 + 1859k_{24}/4104 - 11k_{25}/40, \\ & c_n - 8k_{31}/27 + 2k_{32} - 3544k_{33}/2565 + 1859k_{34}/4104 - 11k_{35}/40), \end{aligned} \tag{A.9}$$

where $a_n = a(t_n), b_n = b(t_n), c_n = c(t_n)$ and d is the step length of each iteration, then

$$\begin{aligned} a_{n+1} = {} & a(t_n + d) = a_n + 25k_{11}/216 + \\ & 1408k_{13}/2565 + 2197k_{14}/4104 - k_{15}/5, \end{aligned} \tag{A.10}$$

$$\begin{aligned} a^*_{n+1} = {} & a^*(t_n + d) = a^*_n + 16k_{11}/135 + \\ & 6656k_{13}/12825 + 28561k_{14}/56430 - 9k_{15}/50 + 2k_{16}/55, \end{aligned} \tag{A.11}$$

$$b_{n+1} = b(t_n + d) = b_n + 25k_{21}/216 + \quad \text{(A.12)}$$
$$1408k_{23}/2565 + 2197k_{24}/4104 - k_{25}/5,$$
$$b^*_{n+1} = b^*(t_n + d) = b^*_n + 16k_{21}/135 + \quad \text{(A.13)}$$
$$6656k_{23}/12825 + 28561k_{24}/56430 - 9k_{25}/50 + 2k_{26}/55,$$

$$c_{n+1} = c(t_n + d) = c_n + 25k_{31}/216 + \quad \text{(A.14)}$$
$$1408k_{33}/2565 + 2197k_{34}/4104 - k_{35}/5,$$
$$c^*_{n+1} = c^*(t_n + d) = c^*_n + 16k_{31}/135 + \quad \text{(A.15)}$$
$$6656k_{33}/12825 + 28561k_{34}/56430 - 9k_{35}/50 + 2k_{36}/55.$$

The quantities a_n, b_n and c_n are fourth-order Runge-Kutta formulae and a^*_n, b^*_n and c^*_n are fifth-order formulae. The purpose of calculating two different predictions for each quantity a, b and c is to allow us to calculate the error. For this RKF algorithm, the error in calculating a_n, E_a, is given by

$$E_a = a^*_n - a_n \quad \text{(A.16)}$$

with the errors for b_n and c_n defined similarly.

Appendix B

Further Aspects of the Non-axisymmetric Turbulent Boundary Layer

Here we finally consider two aspects of the NATBL which were not included in Chapters 4 and 5. First, the matching of the asymptotic expansions in each region of the NATBL. Despite the relative importance of such work (especially in establishing the importance of the disc solidity) it is a somewhat cumbersome process and, in truth, contains no more complications than those already discussed in Chapters 2 and 3. As such it is included as an appendix for the ease of the reader.

Secondly, we consider a linearized solution to the flow in the IITL (really just to see if one is possible) which whilst being a model problem and one which lacks any direct relevance to the problems considered in this thesis, is considered worthy of inclusion.

B.1 Matching in the NATBL

To begin we examine the matching between the IITL and the LSB. Here we have

$$\begin{aligned} f' &= \epsilon C_1 + \epsilon^2 (\ln \epsilon)^2 f_2' + \epsilon^2 F_2' \\ &\sim \epsilon C_1 + \epsilon^2 (\ln \epsilon)^2 A_5 \eta_2 + \epsilon^2 C_1 \ln \eta_2, \\ f' &= \epsilon^2 F_3' + \epsilon^{-2} R^{-1} f_3' \\ &\sim \epsilon^2 C_1 \ln \eta_3 + \epsilon^{-2} R^{-1} A_7 \eta_3 \\ &= \epsilon^2 C_1 (\ln \eta_2 + 2 \ln \epsilon + \ln R) + A_7 \eta_2, \end{aligned} \tag{B.1}$$

and

$$\begin{aligned} g' &= -1 - a^{\frac{1}{2}} \epsilon \ln \epsilon - \epsilon g_2' \\ &\sim -1 - a^{\frac{1}{2}} \epsilon \ln \epsilon - \epsilon A_6 \ln \eta_2, \\ g' &= \epsilon g_3' \\ &\sim \epsilon A_8 \ln \eta_3 \\ &= \epsilon A_8 (\ln \eta_2 + 2 \ln \epsilon + \ln R). \end{aligned} \tag{B.2}$$

At first it appears that the leading order terms in the matching of the radial velocity components between these two layers are not of the same order of magnitude. However it must be remembered that the expansion of the radial velocity in the IITL is based on the asymptotic form for f' in the OITL and for a rotating disc. As such when $\eta = O(\epsilon)$ the expansion used is correct but when $\eta = O(\epsilon^{-1} R^{-1})$ as is the case when the flow approaches the LSB then the leading order term has the asymptote $f_2' \sim \eta_2 (\ln \eta_2)^2$. Therefore the asymptotic behaviour $f' \sim \epsilon^2 (\ln \epsilon)^2 \eta_2$ should be replaced by $f' \sim \eta_2$ in this matching (since here $\ln \epsilon$ is replaced by $\ln \eta_2$ and, as is true for the rotating

disc problem, when $\eta_2 = O(\epsilon^{-1}R^{-1})$, $\ln \eta_2 \sim \epsilon^{-1}$). This means that the two radial asymptotes are now of the same order. Hence $A_6 = -A_8 = 1$. We might also infer that $A_5 = A_7$ however this later leads to a contradiction and so is neglected. Instead we find that the correct asymptotic coefficients are determined from consideration of the governing equations for the IITL and the LSB, and that in fact, $A_5 \neq A_7$.

Now we look at the matching between the OITL and the IITL, where

$$\begin{aligned} f' &= \epsilon f_1' \\ &\sim \epsilon C_1 + \epsilon A_1 \eta_1 (\ln \eta_1)^2, \\ f' &= \epsilon C_1 + \epsilon^2 (\ln \epsilon)^2 f_2' \\ &\sim \epsilon C_1 + \epsilon^2 (\ln \epsilon)^2 A_3 \eta_2 \\ &= \epsilon C_1 + \epsilon (\ln \epsilon)^2 A_3 \eta_1, \end{aligned} \tag{B.3}$$

and

$$\begin{aligned} g' &= -1 + \epsilon g_1' \\ &\sim -1 - \epsilon A_2 \ln \eta_1, \\ g' &= -1 - a^{\frac{1}{2}} \epsilon \ln \epsilon - \epsilon g_2' \\ &\sim -1 - a^{\frac{1}{2}} \epsilon \ln \epsilon - \epsilon A_4 \ln \eta_2 \\ &= -1 - a^{\frac{1}{2}} \epsilon \ln \epsilon - A_4 (\ln \eta_1 - \ln \epsilon), \end{aligned} \tag{B.4}$$

and so $A_1 = A_3$ and $A_2 = -A_4$.

Finally we consider the matching between the IITL and the LSW.

$$\begin{aligned} f' &= \epsilon C_1 + \epsilon^2(\ln\epsilon)^2 f_2' + \epsilon^2 F_2' \qquad \text{(B.5)} \\ &\sim \epsilon C_1 + \epsilon^2(\ln\epsilon)^2(\overline{f_4} + A_9(\theta)\eta_2{}^{\frac{1}{2}}) + \epsilon^2\frac{3C_1}{2}\ln\eta_2, \\ f' &= \epsilon^2 F_4' + \epsilon^2(\ln\epsilon)^2\overline{f_4}(\theta) + \epsilon^{\frac{4}{3}}R^{-\frac{1}{3}}(\ln\epsilon)^2 f_4' \\ &\sim \epsilon^2 C_1 \ln\eta_4 + \epsilon^2(\ln\epsilon)^2\overline{f_4}(\theta) \\ &\quad +\epsilon^{\frac{4}{3}}R^{-\frac{1}{3}}(\ln\epsilon)^2 A_{11}(\theta)\eta_4{}^{\frac{1}{2}} \\ &= \epsilon^2\frac{3C_1}{2}(\ln\eta_2 + \frac{2}{3}\ln R + \frac{4}{3}\ln\epsilon) + \epsilon^2(\ln\epsilon)^2\overline{f_4}(\theta) \\ &\quad +\epsilon^2(\ln\epsilon)^2 A_{11}(\theta)\eta_4{}^{\frac{1}{2}}, \end{aligned}$$

and

$$\begin{aligned} g' &= -1 - a^{\frac{1}{2}}\epsilon\ln\epsilon - \epsilon g_2' \qquad \text{(B.6)} \\ &\sim -1 - a^{\frac{1}{2}}\epsilon\ln\epsilon - \epsilon(-\overline{g_4} + A_{10}(\theta)\eta_2{}^{\frac{1}{2}}), \\ g' &= -1 - a^{\frac{1}{2}}\epsilon\ln\epsilon + \epsilon\overline{g_4}(\theta) + \epsilon^{\frac{1}{3}}R^{-\frac{1}{3}}g_4' \\ &\sim -1 - a^{\frac{1}{2}}\epsilon\ln\epsilon + \epsilon\overline{g_4}(\theta) + \epsilon^{\frac{1}{3}}R^{-\frac{1}{3}}A_{12}(\theta)\eta_4{}^{\frac{1}{2}} \\ &= -1 - a^{\frac{1}{2}}\epsilon\ln\epsilon + \epsilon\overline{g_4}(\theta) + \epsilon A_{12}(\theta)\eta_2{}^{\frac{1}{2}}, \end{aligned}$$

and so $A_9 = A_{11}$ and $A_{10} = -A_{12}$. Substituting the asymptotic forms for the velocity components $f'(\eta)$ and $g'(\eta)$ for each region into the appropriate

governing equations yields

$$A_1 = -A_2, \tag{B.7}$$

$$A_3 A_4 = -a, \tag{B.8}$$

$$A_5 A_6 = -a, \tag{B.9}$$

$$A_7 A_8 = -1, \tag{B.10}$$

$$\frac{1}{4} A_9 A_{10} = -1 - \frac{d\overline{f_4}}{d\theta}, \tag{B.11}$$

$$\frac{1}{4} A_{10}^2 = -\frac{d\overline{g_4}}{d\theta}, \tag{B.12}$$

$$\frac{1}{4} A_{11} A_{12} = -1 - \frac{d\overline{f_4}}{d\theta}, \tag{B.13}$$

$$\frac{1}{4} A_{12}^2 = -\frac{d\overline{g_4}}{d\theta}. \tag{B.14}$$

In addition, it is also necessary for our solution to be periodic. Integrating (4.40) with respect to η_2 leads to

$$-\frac{\partial}{\partial\theta}\int_0^\infty g_2' d\eta_2 = [\eta_2^2 g_2''^2]_0^\infty, \tag{B.15}$$

and so to ensure periodicity we must have

$$\frac{\partial}{\partial\theta}\int_0^\infty g_2' d\eta_2 = 0. \tag{B.16}$$

Integrating with respect to θ from 0 to 2π, and noting that the blade area is equal to $2\pi a$ and $a \leq 1$, leads to

$$-\int_0^\infty g_2' d\eta_2 = \int_0^{2\pi} [\eta_2^2 g_2''^2]_0^\infty d\theta \tag{B.17}$$

$$= 2\pi(A_2^2 - a). \tag{B.18}$$

So taking $|A_2| = a^{\frac{1}{2}}$ we have

$$\int_0^\infty g_2' d\eta_2 = 0 \tag{B.19}$$

and hence, a periodic solution. Therefore the asymptotic coefficients have been determined as

$$A_1 = -a^{\frac{1}{2}}, \tag{B.20}$$

$$A_2 = -a^{\frac{1}{2}}, \tag{B.21}$$

$$A_3 = -a^{\frac{1}{2}}, \tag{B.22}$$

$$A_4 = a^{\frac{1}{2}}, \tag{B.23}$$

$$A_5 = -a, \tag{B.24}$$

$$A_6 = 1, \tag{B.25}$$

$$A_7 = -1, \tag{B.26}$$

$$A_8 = -1, \tag{B.27}$$

and the following asymptotic forms are:

$$f_1' \sim -a^{\frac{1}{2}}\eta_1(\ln\eta_1)^2, \tag{B.28}$$

$$g_1' \sim -a^{\frac{1}{2}}\ln\eta_1, \tag{B.29}$$

as $\eta_1 \to 0$;

$$f_2' \sim -a^{\frac{1}{2}}\eta_2, \tag{B.30}$$

$$g_2' \sim a^{\frac{1}{2}}\ln\eta_2, \tag{B.31}$$

as $\eta_2 \to \infty$;

$$f_2' \sim -a\eta_2, \tag{B.32}$$

$$g_2' \sim \ln\eta_2, \tag{B.33}$$

as $\eta_2 \to 0$ over the blade;

$$f_2' \sim \overline{f_4} + A_9(\theta){\eta_2}^{\frac{1}{2}}, \tag{B.34}$$

$$g_2' \sim -\overline{g_4} + A_{10}(\theta){\eta_2}^{\frac{1}{2}}, \tag{B.35}$$

as $\eta_2 \to 0$ in the wake;

$$f_3' \sim -\eta_3, \tag{B.36}$$

$$g_3' \sim -\ln \eta_3, \tag{B.37}$$

as $\eta_3 \to \infty$; and

$$f_4' \sim A_{11}(\theta)\eta_4{}^{\frac{1}{2}}, \tag{B.38}$$

$$g_4' \sim A_{12}(\theta)\eta_4{}^{\frac{1}{2}}, \tag{B.39}$$

as $\eta_4 \to \infty$. The functions A_i, with $i = 9, 10, 11$ or 12, are given by the, as yet, unknown wake functions $\overline{f_4}$ and $\overline{g_4}$, by means of $(B.11)$ and $(B.14)$.

B.2 A Linearized Solution in the IITL

In order to test our model for the structure of the NATBL described in §4.3, we now examine the case where the flow in the IITL differs only slightly from that on a rotating disc but where the flow is now non-axisymmetric, and seek to determine whether a periodic linear solution exists. Since the perturbation of the present flow from that on a rotating disc is taken to be small, it is supposed that the boundary layer here is, for the most part, the same as that for a flat disc but that there exists a small layer on the surface where this perturbation is 'felt'. This layer corresponds to the IITL. The azimuthal momentum equation for the IITL is

$$-\frac{\partial g_2'}{\partial \theta} = \frac{\partial}{\partial \eta_2}(\eta_2^2(\frac{\partial g_2'}{\partial \eta_2})^2), \tag{B.40}$$

and since the perturbation is small, we suppose that the velocity in this layer is perturbed by just a small factor, $O(\gamma)$, from the asymptotic behaviour of the flat disc near the surface. Hence the azimuthal velocity component is written

as $g_2' = \ln \eta_2 + \gamma \overline{v}$ with $\overline{v} \to \overline{c} \ln \eta_2$ as $\eta_2 \to \infty$, where $\gamma \ll 1$. This then leads to

$$-\frac{\partial \overline{v}}{\partial \theta} = 2\frac{\partial}{\partial \eta_2}(\eta \frac{\partial \overline{v}}{\partial \eta_2}). \tag{B.41}$$

Differentiating $(B.41)$ and letting $T = \eta \overline{\tau}$, where $\overline{\tau} = \frac{\partial \overline{v}}{\partial \eta_2}$, then results in the following linearized equation:

$$-\frac{\partial T}{\partial \theta} = 2\eta \frac{\partial^2 T}{\partial \eta^2}. \tag{B.42}$$

Next, in light of the requirement of periodicity, a solution of the type

$$T = Re[\sum_{n=0}^{\infty} f_n(\eta_2) \exp(in\theta)], \tag{B.43}$$

is attempted, and yields

$$-inf_n = 2\eta f_n'', \tag{B.44}$$

$\forall n$. Due to the variation from flat disc flow we suppose that $\overline{v}(0) \neq 0$ and $T(0) \neq 0$ and that, in general, the flow would not be symmetric in θ. Thus $f_n \to b_n$ as $\eta \to 0$, for some constants $b_n \neq 0$ which are determined by the particular deformation from the flat disc flow. We also require $T \to \overline{c}$ as $\eta \to \infty$, and hence that $f_n \to 0$, for $n \neq 0$, and $f_0 \to \overline{c}$ as $\eta \to \infty$. A contour integral solution of the form

$$f_n = \int_{C_n} \exp(\omega\eta)\phi_n(\omega)d\omega, \tag{B.45}$$

is now suggested for $n \neq 0$. From this we have

$$f_n'' = \int_{C_n} \omega^2 \exp(\omega\eta)\phi_n(\omega)d\omega \tag{B.46}$$

and so

$$\int_{C_n} in \exp(\omega\eta)\phi_n(\omega) + 2\eta\omega^2 \exp(\omega\eta)\phi_n(\omega)d\omega = 0. \tag{B.47}$$

Integration by parts results in

$$\int_{C_n} in \exp(\omega\eta)\phi_n(\omega) - 2(\omega^2\phi_n(\omega))' \exp(\omega\eta)d\omega \qquad \text{(B.48)}$$
$$+2[\omega^2 \exp(\omega\eta)\phi_n(\omega)]_{C_n} = 0.$$

Defining C_n such that

$$[\omega^2 \exp(\omega\eta)\phi_n(\omega)]_{C_n} = 0, \qquad \text{(B.49)}$$

means that we then need to find $\phi_n(\omega)$ satisfying

$$in\phi_n - 2(\omega^2\phi_n)' = 0. \qquad \text{(B.50)}$$

Hence

$$in\phi_n - 4\omega\phi_n - 2\omega^2\phi_n' = 0, \qquad \text{(B.51)}$$

$$\frac{in - 4\omega}{2\omega^2} = \frac{\phi_n'}{\phi_n}, \qquad \text{(B.52)}$$

$$\ln\phi_n = -2\ln\omega - \frac{in}{2\omega} + \ln A_n, \qquad \text{(B.53)}$$

$$\phi_n = A_n \exp(-\frac{in}{2\omega})\omega^{-2}, \qquad \text{(B.54)}$$

where A_n is an arbitrary constant, and now

$$f_n = \int_{C_n} A_n\omega^{-2} \exp(\omega\eta - \frac{in}{2\omega})d\omega \qquad \text{(B.55)}$$

subject to

$$[\exp(\omega\eta - \frac{in}{2\omega})]_{C_n} = 0. \qquad \text{(B.56)}$$

This condition is satisfied if C_n is defined to be any contour on which $Re[\omega] \rightarrow -\infty$ at one end of the contour and $Im[\omega] \rightarrow +0$ at the other end. Thus C_n can be taken to be the straight line in the complex plane given by

$$\omega = r \exp(a\pi i) \qquad \text{(B.57)}$$

with $\frac{1}{2} < a < 1$ and $0 \leq r < \infty$. Note that the condition on a is to ensure that $Re[\omega] < 0$ and $Im[\omega] > 0$ to satisfy the conditions above. Thus f_n is now given by

$$f_n = A_n \exp(-a\pi i) \int_0^\infty r^{-2} \exp(r\eta(s+ti) - \frac{n(si+t)}{2r}) dr \tag{B.58}$$

where $\exp(a\pi i) = s + ti$. This represents one of the two possible solutions to $(B.44)$. To ensure that it is the correct solution we need to see if it satisfies the appropriate boundary conditions. For $n \neq 0$ we have the conditions

$$f_n(0) = b_n, \tag{B.59}$$

$$f_n(\infty) = 0. \tag{B.60}$$

Taking $\eta = 0$ we have an exact integral for f_n and find

$$\frac{2A_n \exp(-a\pi i)}{n(si+t)} = b_n, \tag{B.61}$$

and since

$$si + t = i \exp(-a\pi i) \tag{B.62}$$

we have

$$A_n = \frac{inb_n}{2}. \tag{B.63}$$

Thus defining the arbitrary constant A_n by $(B.63)$ ensures that the boundary condition at $\eta = 0$ is satisfied.

For the limit as $\eta \to \infty$ we note that

$$|f_n| = |A_n||\exp(-a\pi i)|| \int_0^\infty r^{-2} \exp(r\eta(s+ti) - \frac{n(si+t)}{2r}) dr| \tag{B.64}$$

and hence

$$|f_n| \leq |A_n| \int_0^\infty r^{-2}| \exp(r\eta(s+ti) - \frac{n(si+t)}{2r})| dr. \tag{B.65}$$

Therefore

$$|f_n| \leq |A_n| \int_0^\infty r^{-2} \exp(r\eta s - \frac{nt}{2r}) dr. \tag{B.66}$$

Thus as $\eta \to \infty$, in order to satisfy $f_n \to 0$ it is sufficient to show that

$$\int_0^\infty r^{-2} \exp(r\eta s - \frac{nt}{2r}) dr \to 0. \tag{B.67}$$

For this purpose we examine $r = r_0 + \alpha\bar{r}$ where $\alpha \ll 1$ and r_0 is the value of r at which $\exp(r\eta s - \frac{nt}{2r})$ is maximal for a given value of η. Substituting this into the integral above produces

$$I_n = \int_{-\infty}^\infty \alpha r_0^{-2} \exp[(r_0 + \alpha\bar{r})\eta s - \frac{nt}{2r_0}(1 - \frac{\alpha\bar{r}}{r_0} + \frac{\alpha^2\bar{r}^2}{r_0^2})] d\bar{r}. \tag{B.68}$$

By definition then,

$$r_0 = (-\frac{nt}{\eta s})^{\frac{1}{2}}, \tag{B.69}$$

and hence $\alpha\bar{r}\eta s + \frac{nt\alpha\bar{r}}{2r_0^2} = 0$. Note that by definition of a, $s < 0$ and $t > 0$, and as both n and η are also positive, r_0 is real, as is necessary. Now we have

$$\frac{I_n}{\alpha} = \int_{-\infty}^\infty r_0^{-2} \exp(r_0\eta s - \frac{nt}{2r_0} - \frac{\alpha^2 nt\bar{r}^2}{2r_0^3}) d\bar{r} \tag{B.70}$$

and thus

$$\frac{I_n}{\alpha} = \exp(r_0\eta s - \frac{nt}{2r_0}) \int_{-\infty}^\infty r_0^{-2} \exp(-\frac{\alpha^2 nt\bar{r}^2}{2r_0^3}) d\bar{r}. \tag{B.71}$$

Since

$$\int_{-\infty}^\infty r_0^{-2} \exp(-\frac{\alpha^2 nt\bar{r}^2}{2r_0^3}) d\bar{r} \tag{B.72}$$

is finite, we have

$$\int_0^\infty r^{-2} \exp(r\eta s - \frac{nt}{2r}) dr \sim A(\eta) \exp(-B\eta^{\frac{1}{2}}). \tag{B.73}$$

as $\eta \to \infty$, where

$$A = \int_{-\infty}^\infty r_0^{-2} \exp(-\frac{\alpha^2 nt\bar{r}^2}{2r_0^3}) d\bar{r}, \tag{B.74}$$

$$B = -\frac{s}{(-nst)^{\frac{1}{2}}} + \frac{1}{2}(-n^3 st^3)^{\frac{1}{2}}. \tag{B.75}$$

By definition of n, s and t, $B > 0$, and from $(B.69)$, it is apparent that

$$A(\eta) \sim \exp(-\eta^{\frac{3}{2}}). \tag{B.76}$$

Thus

$$f_n = A_n \exp(-a\pi i) \int_0^\infty r^{-2} \exp(r\eta(s+ti) - \frac{n(si+t)}{2r}) dr \to 0 \tag{B.77}$$

as $\eta \to \infty$. For the special case $n = 0$, $f_0'' = 0$, and so

$$f_0 = K_1\eta + K_2 \tag{B.78}$$

for some constants K_1 and K_2 to be determined from the boundary conditions. These are

$$f_0(0) = b_0 \tag{B.79}$$

$$f_0(\infty) = \bar{c} \tag{B.80}$$

and so a solution is only possible if $b_0 = \bar{c}$ and then

$$K_1 = 0 \tag{B.81}$$

$$K_2 = \bar{c} \tag{B.82}$$

$$f_0 = \bar{c}. \tag{B.83}$$

This shows that a linearized solution to the flow in the IITL exists and that the NATBL structure described in §4.3 can be applied to a physical (if somewhat idealized) system.

We can now verify the analysis described above by evaluating the left hand side of $(B.67)$, which is

$$I(\eta) = \int_0^\infty r^{-2} \exp(r\eta s - \frac{nt}{2r}) dr, \tag{B.84}$$

numerically. First we define the following quantities,

$$\eta^* = -\eta nst \tag{B.85}$$

$$r^* = \frac{r}{nt}, \tag{B.86}$$

thus the LHS of $(B.67)$ is equivalent to

$$ntI(\eta) = I^*(\eta^*) = \int_0^\infty r^{*-2} \exp\left(-r^*\eta^* - \frac{1}{2r^*}\right) dr^*, \tag{B.87}$$

with the integral $I^* \to 0$ as $\eta^* \to \infty$, to satisfy $(B.67)$ for all $n \neq 0$. Now $r^{*-2} \exp\left(-r^*\eta^* - \frac{1}{2r^*}\right)$ is numerically integrated over the range $r^* = 0$ up to $r^* = L$ where L is taken to be sufficiently large so that the integral

$$\int_0^L r^{*-2} \exp\left(-r^*\eta^* - \frac{1}{2r^*}\right) dr^* \tag{B.88}$$

varies only negligibly if the value of L is increased. In practice $L = 100$ is used. For the purposes of the integration Simpson's Rule is used and the calculation repeated for a variety of values of η^*. These calculations can also be verified by evaluating the integral I^* using Mathematica. Figure $B.1$ illustrates these results. When calculating the integral in $(B.87)$ using Simpson's rule it becomes apparent that as η increases the interval length required for a converged solution decreases to the extent that the calculation was prohibitively slow. This can be seen in Figure $B.1$ where two curves, corresponding to two different interval lengths, are included along with the values determined using Mathematica. Using very small interval lengths for some values of η^* we are able to generate accurate and converged solutions which agree well with those values determined using Mathematica and are presented in Table $B.1$ for guidance.

Since a very small interval length is required to produce an accurate answer sing Simpson's rule, such calculations were only performed at a limited number

η^*	I^*
1	0.8753
10	0.0653
100	6.98×10^{-6}
1000	6.39×10^{-14}

Table B.1: *Numerical evaluation of $I^*(\eta^*)$ using Simpson's Rule.*

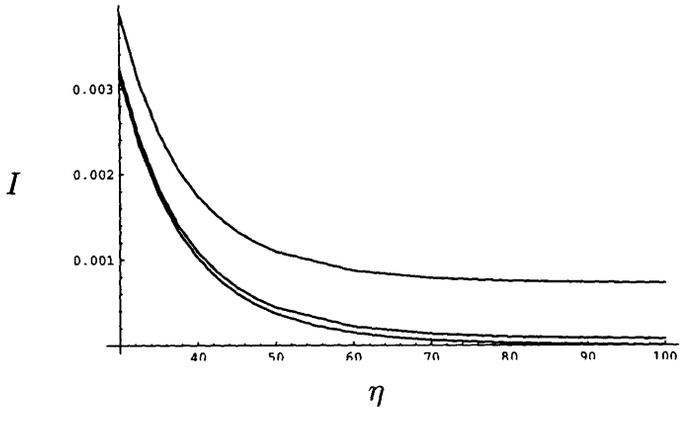

Figure B.1: *Plot of integral I^* against η^* using Mathematica (lower curve) and Simpson's rule using a coarse interval length (upper curve) and a fine interval length (middle curve).*

of values of η^*, hence the slightly jagged appearance of the two numerical curves.

These results (Table $B.1$ and Figure $B.1$) indicate that $I^*(\eta^*) \rightarrow 0$ as $\eta^* \rightarrow \infty$ as required and so the solution derived analytically satisfies the necessary boundary condition at infinity.

Appendix C

The Prandtl Shift

The Prandtl shift is a useful tool in simplifying aerodynamical flow problems (see Smith & Timoshin or Purvis). As such, and since it has been used several times in this thesis, it is now described, using the notation used in Chapters 6 and 7.

The Prandtl shift is defined as

$$h_D = z_D - F(r_D, \theta) \tag{C.1}$$

$$s_D = w_D - u_D \frac{\partial F}{\partial r_D} - \frac{v_D}{r_D}\frac{\partial F}{\partial \theta} \tag{C.2}$$

where the blade shape is given by $F(r, \theta)$. These substitutions are introduced into the non-axisymmetric dimensional Reynolds equations:

$$\frac{\partial u_D}{\partial t} + u_D\frac{\partial u_D}{\partial r_D} - \frac{v_D^2}{r_D} + \frac{v_D}{r_D}\frac{\partial u_D}{\partial \theta} + w_D\frac{\partial u_D}{\partial z_D} - 2v_D - 1 = \tag{C.3}$$
$$\nu\frac{\partial^2 u_D}{\partial z_D^2} + \frac{\partial}{\partial z_D}(\nu_{tD}\frac{\partial u_D}{\partial z_D})$$

and

$$\frac{\partial v_D}{\partial t} + u_D\frac{\partial v_D}{\partial r_D} + \frac{u_D v_D}{r_D} + \frac{v_D}{r_D}\frac{\partial v_D}{\partial \theta} + w_D\frac{\partial v_D}{\partial z_D} + 2u_D = \tag{C.4}$$
$$\nu\frac{\partial^2 v_D}{\partial z_D^2} + \frac{\partial}{\partial z_D}(\nu_{tD}\frac{\partial v_D}{\partial z_D}),$$

with

$$\nu_{tD} = \begin{cases} k_2 \omega r_D \delta_D^* & \text{for } z_D \geq z_{Dk}, \\ k_1^2 z_D^2 [1 - \exp(-\frac{z_D}{26\nu}(\frac{\tau_{WD}}{\rho})^{\frac{1}{2}})]^2 |\frac{\partial u_D}{\partial z_D} + \frac{\partial v_D}{\partial z_D}| & \text{for } z_D \leq z_{Dk}, \end{cases} \tag{C.5}$$

and continuity equation

$$\frac{1}{r_D}\frac{\partial (u_D r_D)}{\partial r_D} + \frac{1}{r_D}\frac{\partial v_D}{\partial \theta} + \frac{\partial w_D}{\partial z_D} = 0. \tag{C.6}$$

Upon making this substitution we must replace the partial derivatives in the Reynolds equations as follows

$$\frac{\partial}{\partial z_D} \rightarrow \frac{\partial}{\partial h_D}, \tag{C.7}$$

$$\frac{\partial}{\partial r_D} \rightarrow \frac{\partial}{\partial r_D} - \frac{\partial F}{\partial r_D}\frac{\partial}{\partial h_D}, \tag{C.8}$$

$$\frac{\partial}{\partial \theta} \rightarrow \frac{\partial}{\partial \theta} - \frac{\partial F}{\partial \theta}\frac{\partial}{\partial h_D}, \tag{C.9}$$

and that having replaced the partial derivatives in this way, we now find that

$$\frac{\partial u_D}{\partial t} + u_D\frac{\partial u_D}{\partial r_D} - \frac{v_D^2}{r_D} + \frac{v_D}{r_D}\frac{\partial u_D}{\partial \theta} + s_D\frac{\partial u_D}{\partial h_D} - 2v_D - 1 = \nu\frac{\partial^2 u_D}{\partial h_D^2} + \frac{\partial}{\partial h_D}(\nu_{tD}\frac{\partial u_D}{\partial h_D}) \tag{C.10}$$

and

$$\frac{\partial v_D}{\partial t} + u_D\frac{\partial v_D}{\partial r_D} + \frac{u_D v_D}{r_D} + + \frac{v_D}{r_D}\frac{\partial v_D}{\partial \theta} + s_D\frac{\partial v_D}{\partial h_D} + 2u_D = \nu\frac{\partial^2 v_D}{\partial h_D^2} + \frac{\partial}{\partial h_D}(\nu_{tD}\frac{\partial v_D}{\partial h_D}) \tag{C.11}$$

with continuity equation

$$\frac{1}{r_D}\frac{\partial (u_D r_D)}{\partial r_D} + \frac{1}{r_D}\frac{\partial v_D}{\partial \theta} + \frac{\partial s_D}{\partial h_D} = 0. \tag{C.12}$$

The additional terms which arise from changing the derivatives are cancelled out by the choice of substitution for the normal velocity component. Hence the

governing equations are unchanged but now apply to the range $0 \leq h_D \leq \infty$ as opposed to $F(r,\theta) \leq z_D \leq \infty$ as before. Hence we have reduced the boundary layer problem to that of a turbulent boundary layer on a flat surface instead of one with thickness. This is known as the Prandtl shift and we shall invoke this transformation whenever we are examining the flow past blades with shape or inclination. It is important to note here that the blade shape reappears when we consider the pressure in the outer inviscid region.

Appendix D

Turbulent Couette Flow

D.1 Asymptotic Behaviour

Now we briefly consider the similarities between the flow between a rotating and a stationary disc and the 2D problem of the flow between a channel with one moving and one stationary wall. This flow has been examined by Afzal[1] and determines the following asymptotic form for u, the dimensional velocity component in the direction of the channel, as $y \to 0$

$$\frac{U_c - u}{u_\tau} = -\frac{1}{k_1} \ln y, \tag{D.1}$$

where the stationary wall is at $y = 0$, U_c is the centre line velocity and u_τ is the friction velocity. Also

$$\frac{U}{u_\tau} = \frac{2}{k_1} \ln R_\tau + 12.4 \tag{D.2}$$

where U is the velocity of the moving wall and R_τ is a Reynolds number based on the friction velocity and defined by

$$R_\tau = \frac{u_\tau h}{\nu}. \tag{D.3}$$

In this problem, h is the half-width of the channel (i.e. the channel width is $2h$) the channel width is $2h$ and ν is the kinematic viscosity. Defining

$$\bar{\epsilon} = (\ln R_\tau)^{-1} \tag{D.4}$$

then as $y \to 0$,

$$u = U_c + \bar{\epsilon}\frac{U}{2}\ln y. \tag{D.5}$$

As $R_\tau \to \infty$, Afzal has shown that $U_c \to \frac{U}{2}$, so $(D.5)$ becomes

$$(\frac{u}{U}) = \frac{1}{2} + \frac{\bar{\epsilon}}{2}\ln y \tag{D.6}$$

as $y \to 0$. In the flow between a stationary and a rotating disc we find that

$$R_\tau = \frac{u_\tau s}{2\nu} \tag{D.7}$$

$$= \frac{\epsilon k_1}{4}(\frac{\omega r s}{\nu})^{\frac{1}{2}} \tag{D.8}$$

$$= \frac{\epsilon k_1}{4}(\frac{\nu s}{\omega r^3})^{\frac{1}{2}} R_\tau \tag{D.9}$$

and hence as $R_\tau \to \infty$ it is assumed that $\bar{\epsilon} \approx \epsilon$. Thus equating $(\frac{u}{U})$ with g' our prediction for the asymptotic form for the azimuthal velocity agrees with that of Afzal for the asymptotic behaviour of turbulent Couette flow.

D.2 Skin Friction

Again it is now possible to compare our work with that of Afzal's for turbulent Couette flow. In this case, Afzal's prediction for the skin friction is

$$c_f = \frac{2u_\tau^2}{U^2}. \tag{D.10}$$

Combining this with $(D.2)$ leads to

$$c_f = \frac{k_1^2\bar{\epsilon}^2}{2}. \tag{D.11}$$

Again now assuming that $\bar{\epsilon} \to \epsilon$ as $R \to \infty$, as in §$D.1$, our prediction for the skin friction is the same as Afzal's for the flow in a channel with one moving and one stationary wall.

Appendix E

Solutions to the Flow Between a Rotating and a Stationary Disc

In Chapter 8 we examined (in a highly simplified form) the flow between a rotating and a stationary disc. One of the major assumptions made involved the choice of eddy viscosity, specifically that the form used was simply the lower tier of the form used by Cooper & Reshotko. Using this assumption analytical and numerical results were presented for the velocity profile. These solutions can be extended to include a two-tier eddy viscosity akin to that of Cooper & Reshotko and these extensions are now described.

E.1 Large Radii Limit

In the case where both tiers of the Cebeci-Smith eddy viscosity is used we have the following large radii analytical solution in terms of the unknown junction

position z_{1k}: for the outer region,

$$r_1 f_1' = \frac{z_1^3}{6z_{1k}^2} - \frac{z_1^2}{4z_{1k}^2} - \frac{1}{2}(z_1 - \frac{1}{2}) + \frac{1}{24z_{1k}^2}, \tag{E.1}$$

$$g_1' = -\frac{z_1}{2z_{1k}} + \frac{1}{4z_{1k}}; \tag{E.2}$$

for the inner region on the rotating disc,

$$r_1 f_1' = z_1 \ln z_1 - z_1 - (\frac{1}{2z_{1k}} + \ln z_{1k})z_1 + \frac{1}{2} + \frac{2z_{1k}}{3} + \frac{1}{24z_{1k}^2}, \tag{E.3}$$

$$g_1' = -\frac{1}{2}\ln z_1 - \frac{1}{2z_{1k}}(z_{1k} - \frac{1}{2}) + \frac{1}{2}\ln z_{1k}; \tag{E.4}$$

and for the solution in the inner region of the stationary disc,

$$r_1 f_1' = -(1 - z_1)\ln(1 - z_1) + (1 - z_1) + (\frac{1}{2z_{1k}} - \ln z_{1k})(1 - z_1) - \frac{1}{2} - \frac{2z_{1k}}{3} - \frac{1}{24z_{1k}^2}, \tag{E.5}$$

$$g_1' = \frac{1}{2}\ln(1 - z_1) + \frac{1}{2z_{1k}}(z_{1k} - \frac{1}{2}) - \frac{1}{2}\ln z_{1k}. \tag{E.6}$$

This solution is illustrated in Figure $E.1$. Interestingly the azimuthal velocity seems to vary only a small amount as the junction position changes although the radial velocity varies far more considerably.

Note that this solution yields the relationship

$$\delta_m^* = \frac{z_{1k}}{2k_4}, \tag{E.7}$$

so the unknown junction position can be readily determined from specification of δ_m^*.

E.2 Numerical Solution for the Flow Between Two Discs

Next we describe a general numerical scheme (capable of solving for either a one or two-tier eddy viscosity such as that used in Chapter 8 or by Cooper &

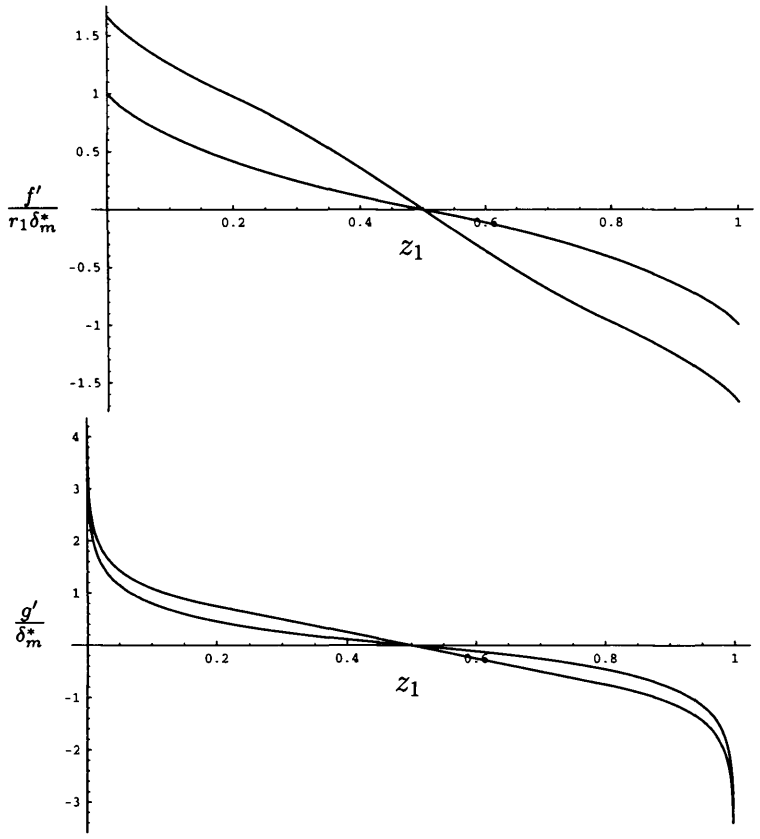

Figure E.1: *Analytic solution of* f_1' *(top) and* g_1' *(bottom) as* $r_1 \to \infty$ *with varying junction position* $z_{1k} = 0.2$ *(upper curves) and* $z_{1k} = 0.5$ *(lower curves).*

Reshotko). In practice the method varies slightly depending on whether one or both tiers are present and such differences will be highlighted where relevant. Since the numerical solution derived here will only be concerned with the ITL,

the following boundary conditions and asymptotes are used

$$f_1(\frac{1}{2}) = 0, \tag{E.8}$$

$$f_1'(\frac{1}{2}) = 0, \tag{E.9}$$

$$f_1''(z_{10}) = \frac{\ln z_{10} + 1}{r_1}, \tag{E.10}$$

$$g_1(\frac{1}{2}) = 0, \tag{E.11}$$

$$g_1'(\frac{1}{2}) = \frac{1}{2}, \tag{E.12}$$

$$g_1''(z_{10}) = -\frac{1}{2z_{10}}, \tag{E.13}$$

where $z_{10} \ll 1$. Now the following substitutions are made in (8.22) and (8.23)

$$f_1 = JF, \tag{E.14}$$

$$g_1 = JG, \tag{E.15}$$

$$r_1 = \frac{\overline{r}}{J}, \tag{E.16}$$

where J is taken to be either $|g_1''(\frac{1}{2})|$ or δ_m^* respectively depending on whether the solution is determined when one or both tiers of the Cebeci-Smith model are present. This yields

$$-G' = \overline{r}\frac{\partial}{\partial z_1}\begin{cases} k_4\frac{\delta_m^*}{J}F'' & \text{for } z_1 \geq z_{1k} \\ z_1^2(F''^2 + G''^2)^{\frac{1}{2}}F'' & \text{for } z_1 \leq z_{1k} \end{cases} \tag{E.17}$$

and

$$F' = \overline{r}\frac{\partial}{\partial z_1}\begin{cases} k_4\frac{\delta_m^*}{J}G'' & \text{for } z_1 \geq z_{1k} \\ z_1^2(F''^2 + G''^2)^{\frac{1}{2}}G'' & \text{for } z_1 \leq z_{1k} \end{cases} \tag{E.18}$$

subject to

$$F'(\frac{1}{2}) = 0, \tag{E.19}$$

$$F(0) = 0, \tag{E.20}$$

$$G(\frac{1}{2}) = 0, \tag{E.21}$$

$$G'(\frac{1}{2}) = 0, \tag{E.22}$$

$$F''(z_{1k})^2 + G''(z_{1k})^2 = (\frac{k_4 \delta_m^*}{J z_{1k}^2})^2. \tag{E.23}$$

Now the following substitutions are introduced so that the above equations can be expressed in a form suitable for solution through an RKF algorithm:

$$s_1 = F(z_1), \tag{E.24}$$

$$s_2 = F'(z_1), \tag{E.25}$$

$$s_3 = F''(z_1), \tag{E.26}$$

$$s_4 = G(z_1), \tag{E.27}$$

$$s_5 = G'(z_1), \tag{E.28}$$

$$s_6 = G''(z_1). \tag{E.29}$$

The problem then separates into two sets of equations. The first corresponds to $z_1 \leq z_{1k}$,

$$\frac{ds_1}{dz_1} = s_2, \tag{E.30}$$

$$\frac{ds_2}{dz_1} = s_3, \tag{E.31}$$

$$\frac{ds_3}{dz_1} = [s_2 - 2z_1\overline{r}|s_3 + s_6|s_6 - (\overline{r}z_1^2 s_6|s_3 + s_6|^{-1} + \overline{r}z_1^2|s_3 + s_6|)\frac{ds_6}{dz_1}] \tag{E.32}$$
$$/(\overline{r}z_1^2 s_3 s_6|s_3 + s_6|^{-1})$$

$$\frac{ds_4}{dz_1} = s_5,$$

$$\frac{ds_5}{dz_1} = s_6, \tag{E.33}$$

$$\frac{ds_6}{dz_1} = [(s_2 - 2z_1\overline{r}|s_3 + s_6|s_6)(\overline{r}z_1^2(s_3|s_3 + s_6|^{-1} + |s_3 + s_6|)) \tag{E.34}$$
$$+(s_5 + 2z_1\overline{r}|s_3 + s_6|s_3)(\overline{r}z_1^2 s_3 s_6|s_3 + s_6|^{-1})]/$$
$$[(\overline{r}z_1^2 s_6^2|s_3 + s_6|^{-1} + \overline{r}z_1^2|s_3 + s_6|)(\overline{r}z_1^2(s_3|s_3 + s_6|^{-1} + |s_3 + s_6|))$$
$$-(\overline{r}z_1^2 s_3 s_6|s_3 + s_6|^{-1})^2]$$

with boundary conditions

$$s_1(z_{10}) = 0, \tag{E.35}$$

$$s_2(z_{10}) = C_1 + \frac{z_{10}}{\overline{r}}\ln z_{10}, \tag{E.36}$$

$$s_3(z_{10}) = \frac{\ln z_{10} + 1}{\overline{r}}, \tag{E.37}$$

$$s_5(z_{10}) = C_2 - \frac{1}{2J}\ln z_{10}, \tag{E.38}$$

$$s_6(z_{10}) = -\frac{1}{2Jz_{10}}. \tag{E.39}$$

The second set, corresponding to $z_1 \geq z_{1k}$, is

$$\frac{ds_1}{dz_1} = s_2, \tag{E.40}$$

$$\frac{ds_2}{dz_1} = s_3, \tag{E.41}$$

$$\frac{ds_3}{dz_1} = -\frac{J}{k_4 \overline{r} \delta_m^*} s_5, \tag{E.42}$$

$$\frac{ds_4}{dz_1} = s_5, \tag{E.43}$$

$$\frac{ds_5}{dz_1} = s_6, \tag{E.44}$$

$$\frac{ds_6}{dz_1} = \frac{J}{k_4 \overline{r} \delta_m^*} s_2, \tag{E.45}$$

with boundary conditions

$$s_1(\frac{1}{2}) = 0, \tag{E.46}$$

$$s_2(\frac{1}{2}) = 0, \tag{E.47}$$

$$s_3(\frac{1}{2}) = s_{3c}, \tag{E.48}$$

$$s_4(\frac{1}{2}) = 0, \tag{E.49}$$

$$s_5(\frac{1}{2}) = 0, \tag{E.50}$$

$$s_6(\frac{1}{2}) = s_{6c}, \tag{E.51}$$

where s_{3c} and s_{6c} are the unknown values at the centre line, $z_1 = \frac{1}{2}$ (although if J is taken to be $|g_1''(\frac{1}{2})|$ then $s_{6c} = -1$). When both tiers of the eddy viscosity are used it is also necessary to satisfy

$$(\frac{k_4}{z_{1k}^2})^2 = s_3(z_{1k})^2 + s_6(z_{1k})^2 \tag{E.52}$$

to satisfy continuity of the eddy viscosity. These equations are now in a suitable form to be solved using an RKF algorithm.

If both tiers of the eddy viscosity occur then one of the unknown parameters in this problem is the unknown junction position z_{1k}. As we use an RKF

algorithm the height is discretized according to the step length used and this could pose a problem when trying to determine the exact value of the junction position. Where necessary, to negate this problem it is assumed that the junction position varies with radius, and as such, for the sake of the numerical scheme a solution is sought for a given junction position and the radius $\overline{r}$ is iterated on until a suitable solution is found.

To begin we consider the two cases possible here, namely whether one or both tiers of the Cebeci-Smith model is present. In the latter case δ_m^* is specified and initial estimates for s_{3c}, s_{6c} and $\overline{r}$ are made and the RKF algorithm run down from $z_1 = \frac{1}{2}$ to the junction position and a check is performed to see if $(E.52)$ is satisfied. If it is not satisfied to within a suitable accuracy (specifically to within 10^{-6}) we then iterate on s_{6c} using Newton's method until $(E.52)$ is satisfied. We then proceed to run our algorithm down to a suitably small value for the height, z_{10}, for example 0.0001, and then check to see if the conditions

$$s_3(z_{10}) = \frac{\ln z_{10} + 1}{\overline{r}}, \tag{E.53}$$

$$s_6(z_{10}) = -\frac{1}{2\delta_m^* z_{10}}, \tag{E.54}$$

hold (to within an accuracy of 10^{-4}) for some choice of δ_m^*. Again, if these conditions are not satisfied to sufficient accuracy, s_{3c} and $\overline{r}$ are iterated on until suitable values are determined. In the case where only the inner tier of the Cebeci-Smith model occurs this numerical problem is much simpler and now a value of $\overline{r}$ is specified and with $s_6(\frac{1}{2}) = -1$, $s_3(\frac{1}{2})$ is varied until $(E.53)$ holds.

E.3 Alternative Analytic Solution for the Flow Between Two Discs

Finally, a further possible analytical solution is discussed.

In the inertial-turbulent layer

$$-g_1' = r_1 \frac{\partial}{\partial z_1} \begin{cases} k_4 \delta_m^* f_1'' & \text{for } z_1 \geq z_{1k} \\ z_1^2 (f_1''^2 + g_1''^2)^{\frac{1}{2}} f_1'' & \text{for } z_1 \leq z_{1k} \end{cases} \tag{E.55}$$

and

$$f_1' = r_1 \frac{\partial}{\partial z_1} \begin{cases} k_4 \delta_m^* g_1'' & \text{for } z_1 \geq z_{1k} \\ z_1^2 (f_1''^2 + g_1''^2)^{\frac{1}{2}} g_1'' & \text{for } z_1 \leq z_{1k} \end{cases} \tag{E.56}$$

which upon differentiation produces

$$-g_1'' = r_1 \frac{\partial^2}{\partial^2 z_1} \begin{cases} k_4 \delta_m^* f_1'' & \text{for } z_1 \geq z_{1k} \\ z_1^2 (f_1''^2 + g_1''^2)^{\frac{1}{2}} f_1'' & \text{for } z_1 \leq z_{1k} \end{cases} \tag{E.57}$$

and

$$f_1'' = r_1 \frac{\partial^2}{\partial^2 z_1} \begin{cases} k_4 \delta_m^* g_1'' & \text{for } z_1 \geq z_{1k} \\ z_1^2 (f_1''^2 + g_1''^2)^{\frac{1}{2}} g_1'' & \text{for } z_1 \leq z_{1k}. \end{cases} \tag{E.58}$$

Now we introduce the substitution

$$f_1'' = R(r_1, z_1) \cos\theta(r_1, z_1), \tag{E.59}$$

$$g_1'' = R(r_1, z_1) \sin\theta(r_1, z_1), \tag{E.60}$$

which leads to

$$R = r_1 \begin{cases} k_4 \delta_m^* (2R'\theta' + R\theta'') & \text{for } z_1 \geq z_{1k} \\ 4z_1^2 RR'\theta' + 4z_1 R^2 \theta' + z_1^2 R^2 \theta'' & \text{for } z_1 \leq z_{1k} \end{cases} \tag{E.61}$$

and

$$0 = r_1 \begin{cases} k_4 \delta_m^* (R'' - R\theta'^2) & \text{for } z_1 \geq z_{1k} \\ 2z_1^2 RR'' + 2z_1^2 R'^2 + 8z_1 RR' + 2R^2 - t^2 R^2 \theta'^2 & \text{for } z_1 \leq z_{1k} \end{cases} \tag{E.62}$$

where $'$ denotes differentiation with respect to z_1. Thus for $z_1 \geq z_{1k}$ we have

$$R^2 = r_1 k_4 \delta_m^* R(2R'\theta' + R\theta'') \tag{E.63}$$

$$= r_1 k_4 \delta_m^* (R^2\theta')' \tag{E.64}$$

and

$$R'' = R\theta'^2, \tag{E.65}$$

thus

$$\theta' = (\frac{R''}{R})^{\frac{1}{2}}. \tag{E.66}$$

Combining these results we have the following equation for $R(r_1, z_1)$

$$R^2 = r_1 k_4 \delta_m^* (R^{\frac{3}{2}} R''^{\frac{1}{2}})'. \tag{E.67}$$

Whilst it is possible to solve this equation and compare with our previous numerical results for $|f_1'' + g_1''| = R$, this substitution has not led to a simplification of the problem and hence there seems little value in solving this modified problem fully.

Bibliography

1. Afzal, N., *Asymptotic Analysis of Turbulent Couette Flow*, Fluid Dynamics Research, Volume 12, pages 163-171, 1993.

2. Afzal, N., *Turbulent Boundary Layer on a Moving Continuous Plate*, Fluid Dynamics Research, Volume 17, pages 181-194, 1996.

3. Bayley, F., J. & Owen, J., M., *Flow Between a Rotating and a Stationary Disc*, The Aeronautical Quarterly, Volume 20, Part 4, pages 333-354, 1969.

4. Bhattacharyya, S. & Pal, A., *On the Flow Between Two Rotating Disks Enclosed by a Cylinder*, Acta Mechanica, Volume 135, pages 27-40, 1999.

5. Bowles, R. G. A. & Smith, F. T., *Interactive Flow Past Multiple Blades and Wakes*, Q. Jl. Mech. appl. Math., Volume 53 (2), pages 207-251, 2000.

6. Bowles, R. G. A. & Smith, F. T., *Lifting Multi-Blade Flows with Interaction*, J. Fluid Mech., Volume 415, pages 203-226, 2000.

7. Bradshaw, P., Ferriss, D. H. & Atwell, N. P., *Calculation of Boundary Layer Development using the Turbulent Energy Equation*, J. Fluid Mech., Volume 28, pages 593-616, 1967.

8. Bramwell, A. R. S., Done, G. & Balmford D., *Bramwell's Helicopter Dynamics: Second Edition*, Butterworth Heinemann, 2001.

9. Bush, W. B. & Fendell, F. E., *Asymptotic Analysis of Turbulent Channel and Boundary-Layer Flow*, J. Fluid Mech., Volume 56, pages 657-681, 1972.

10. Carrier, G. F., Krook, M. & Pearson, C. E., *Functions of a Complex Variable*, McGraw-Hill, 1966.

11. Cebeci, T. & Abbott, D. E., *Boundary Layers on a Rotating Disc*, AIAA Journal, Volume 13, pages 829-832, 1975.

12. Cebeci, T. & Bradshaw, P., *Momentum Transfer in Boundary Layers*, McGraw-Hill, 1977.

13. Cebeci, T. & Smith, A. M. O., *Analysis of Turbulent Boundary Layers*, Academic Press, 1974.

14. Cham, T. S. & Head, M. R., *Turbulent Boundary-Layer Flow on a Rotating Disc*, J. Fluid Mech., Volume 37, Part 1, pages 129-147, 1969.

15. Clauser, F. H., *The Turbulent Boundary Layer*, Advances in Applied Mechanics, Volume IV, pages 1-51, 1956.

16. Cochran, W. G., *The Flow Due to a Rotating Disc*, Proc. Cambridge Phil. Soc., Volume 30, pages 365-375, 1934.

17. Coles, D., *The Problem of the Turbulent Boundary Layer*, ZAMP, Volume 5, Part 3, pages 181-203, 1954.

18. Coles, D., *The Law of the Wall in Turbulent Shear Flow*, 50 Jahre Grenzschlicht Forschung, pages 153-163, 1955.

19. Conlisk, A. T., *Modern Helicopter Aerodynamics*, Annual Review of Fluid Mechanics, Volume 29, pages 515-567, 1997.

20. Cooper, P., *Turbulent Boundary Layer on a Rotating Disc Calculated with an Effective Viscosity*, AIAA Journal, Volume 9, pages 255-261, 1971.

21. Cooper, P., *Turbulent Fluid Friction of Rotating Discs*, thesis submitted in partial fulfillment of the requirements for the Degree of Doctor of Philosophy, Cape Western Reserve University, 1972.

22. Cooper, P. & Reshotko, E., *Turbulent Flow between a Rotating Disc and a Parallel Wall*, AIAA Journal, pages 573-578, 1974.

23. Curle, N. & Davies, H. J., *Incompressible Flow*, Modern Fluid Dynamics, Volume 1, Van Nostrand, 1968.

24. Dahm, W. J. A. & Dimotakis, P. E., *Measurements of Entrainment and Mixing in Turbulent Jets*, AIAA, Volume 25, No. 9, pages 1216-1223, 1987.

25. Daily, J. W. & Nece, R. E., *Chamber Dimension Effects on Induced Flow and Frictional Resistance of Enclosed Rotating Discs*, Transactions of the ASME, Series D: Journal of Basic Engineering, Volume 82, pages 217-232, 1960.

26. Daniels, W. A., Johnson, B., V. & Graber, D., J., *Aerodynamic and Torque Characteristics of Enclosed Co & Counter Rotating Disks*, Journal of Turbomachinery, Volume 113, pages 67- 74, 1991.

27. Dijkstra, D. & van Heist, G. J. F., *The Flow Between Two Finite Rotating Disks Enclosed by A Cylinder*, J. Fluid Mech., Volume 128, pages 123-154, 1983.

28. Durbin, P. A., *Near-wall Turbulence Closure Modelling without Damping Functions*, J. Theoretical and Computational Fluid Dynamics, Volume 3, pages 1-13, 1991.

29. Erian, F. F. & Tong, Y. H., *Turbulent Flow Due to a Rotating Disc*, The Physics of Fluids, Volume 14, pages 2588-2591, 1971.

30. Firthmann, E., *Turbulent Jet Expansion*, NACA TM 789, 1936.

31. Gan, X., Kilic, M. & Owen, J. M., *Flow Between Contrarotating Disks*, Journal of Turbomachinery, Volume 117, pages 298-305, 1995.

32. Gent, R., Miller, J., Soliman, M. & Young, C., *Personal correspondence*, QinetiQ.

33. Gerald, C. F. & Wheatley, P. O., *Applied Numerical Analysis: Fifth Edition*, Addison Wesley, 1994.

34. Glauert, H., *The Elements of Aerofoil and Airscrew Theory*, Cambridge University Press, 1948.

35. Goertler, H., *Berechnung von Aufgaben der freien Turbulenz auf Grund eines neuen Naherungsansatzes*, ZAMM, Volume 22, pages 244-254, 1942.

36. Gradshteyn, I. S. & Ryzhik, I. M., *Table of Integrals, Series' & Products*, Academic Press, 5th Edition, 1994.

37. *Jane's Defence Weekly*

38. Jasmine, H. A. & Gajjar, J. S. B., *Absolute Instability of the Von-Karman, Bodewadt and Ekman flows between a Rotating-Disk and a Stationary Lid*, Article submitted to Royal Society, 2004.

39. Jones, M. A. & Smith, F. T., *Fluid Motion for Car Undertrays in Ground Effect*, Journal of Engineering Mathematics, Volume 45, pages 309-334, 2003.

40. Jones, M. A., *Mechanisms in Wing-in-Ground Effect Aerodynamics*, PhD thesis, Univ. of London, 2000.

41. Kerwin, J. E., *Marine Propellers*, Annual Review of Fluid Mechanics, Volume 18, pages 367-404, 1986.

42. Knudsen, J. G. & Katz, D. L., *Fluid Dynamics and Heat Transfer*, McGraw-Hill, 1958.

43. Lin, C. C., *Turbulent Flows and Heat Transfer*, Volume V High Speed Aerodynamics and Jet Propulsion, Oxford University Press, 1959.

44. Lingwood, R. J., *An Experimental Study of Absolute Instability of the Rotating-Disc Boundary-Layer Flow*, J. Fluid Mech., Volume 314, pages 373-405, 1996.

45. Littell, H. S. & Eaton, J. K., *Turbulence Characteristics of the Boundary Layer on a Rotating Disc*, J. Fluid Mech., Volume 206, pages 175-207, 1994.

46. Mellor, G. L., *The Large Reynolds Number, Asymptotic Theory of Turbulent Boundary Layers*, International Journal of Engineering Science, Volume 10, pages 851-873, 1972.

47. Milne-Thompson, L. M., *Theoretical Hydrodynamics*, Dover Publications, 1996.

48. Muskhelishvili, N. I., *Singular Integral Equations*, Noordhoff, 1953.

49. Nakayama, A., *Characteristics of the Flow Around Conventional & Supercritical Airfoils*, J. Fluid Mech., Volume 160, pages 155-179, 1985.

50. Neish, A. & Smith, F. T., *The Turbulent Boundary Layer and Wake of an Aligned Flat Plate*, Journal of Engineering Mathematics, Volume 22, pages 15-42, 1988.

51. Neish, A., *An Asymptotic Theory of the Two-Dimensional Turbulent Boundary Layer Separation and Aligned Flat Plate-Wake Behaviour*, PhD thesis, Univ. of London, 1988.

52. Noble, B., *The Wiener-Hopf Technique*, Pergamon Press, 1958.

53. Papanicolaou, P. N. & List, E., *Investigations of Round Vertical Turbulent Buoyant Jets*, J. Fluid Mech., Volume 195, pages 341-391, 1988.

54. Papantoniou, D. & List, E., *Large-Scale Structure in the Far Field of Buoyant Jets*, J. Fluid Mech., Volume 209, pages 151-190, 1989.

55. Peterson, S. N. & Plesniak, M. W., *Evolution of Jets Emanating from Short Holes into Crossflow*, J. Fluid Mech., Volume 503, pages 57-91, 2004.

56. Prandtl, L., *Uber die neues Formelsystem fur die ausgebildete Turbulenz*, Nachr. Akad. Wiss., Gottingen, Math.-phys. KL. 1945.

57. Prandtl, L., *Essentials of Fluid Dynamics*, Blackie & Son Ltd, 1952.

58. Purvis, R., *Rotor Blades and Ground Effect*, PhD thesis, Univ. of London, 2001.

59. Quackenbush, T. R., *"Smart Duct" Quiet Steering Control*, Continuum Dynamics, Inc., 2004.

60. Riley, M. J. & Brotherhood, P., *Comparative Performance Measurements of Two Helicopter Blade Profiles in Hovering Flight*, RAE Technical Report 74008, 1974.

61. Sakiadis, B., *Boundary Layer on Continuous Solid Surface. I Boundary-Layer Equations for Two-Dimensional and Axisymmetric Flow*, A. I. Ch. E. J., Volume 7, Part 1, pages 26-27, 1961.

62. Sakiadis, B., *Boundary Layer on Continuous Solid Surface. II The Boundary Layer on a Continuous Flat Surface*, A. I. Ch. E. J., Volume 7, Part 2, pages 221-225, 1961.

63. Scheichl, B., *Asymptotic Theory of Marginal Turbulent Separation*, PhD thesis, Vienna University of Technology, 2001.

64. Schlichting, H., *Boundary Layer Theory*, McGraw-Hill Series in Mechanical Engineering, 4th Edition, 1960.

65. Seddon, J., *Basic Helicopter Aerodynamics*, BSP Professional Books, 1990.

66. Smith, A. M. O. & Cebeci, T., *Numerical Solution of the Turbulent Boundary Layer Equations*, Report no. DAC 33735, McDonnell Douglas Corp., 1967.

67. Smith, F. T., *Personal correspondence on the flow on a cut-disc*, 2002.

68. Smith, F. T. & Timoshin, S. N., *Blade-wake Interaction and Rotary Boundary Layers*, Proc. R. Soc. London, Volume 452, pages 1301-1329, 1996.

69. Smith, F. T. & Timoshin, S. N., *Planar Flows Past Thin Multi-Blade Configurations*, J. Fluid Mech., Volume 324, pages 355-377, 1996.

70. Smith, F. T. & Timoshin, S. N., *Vortex-Generator Jets: Theoretical Prediction and Design*, United Technologies Research Centre, UTRC94-43, 1994.

71. Spalart, P. R. & Allmaras, S. R., *A One-equation Turbulence Model for Aerodynamic Flows*, AIAA, Volume 32, 1992.

72. Spalart, P. R., *On the Simple Actuator Disk*, J. Fluid Mech., Volume 494, pages 399-405, 2003.

73. Stepniewski, W. Z. & Keys, C. N., *Rotary Wing Aerodynamics*, Dover Publications, 1984.

74. Sychev, V. V., Ruben, A. I., Sychev, V. V. & Korolev, G. L., *Asymptotic Theory of Separated Flows*, Cambridge University Press, 1998.

75. Szeri, A., Z., Schneider, S., J. & Labbe, F., *Flow Between Rotating Disks. Part One. Basic Flow*, J. Fluid Mech., Volume 134, pages 103-131, 1983.

76. Tollmein, W., Calculation of Turbulent Expansion Processes, NACA TM 1085, 1945.

77. Tsou, F. K., Sparrow, E. M. & Goldstein, R. J., *Flow and Heat Transfer in the Boundary Layer on a Continuous Moving Surface*, Int. J. Heat Mass Transfer, Volume 10, pages 219-235, 1967.

78. Van dyke, M., *Perturbation Methods in Fluid Mechanics*, The Parabolic Press, 1975.

79. von Karman, Th., *Laminare und Turbulente Reibung*, ZAMM, Volume 1, No. 4, pages 233-252, 1921.

80. Wilson, P., L., *On the Core Flow and Turbulent Boundary Layer in a Curved Duct*, PhD thesis, Univ. of London, 2003.

81. Wu, X. & Squires, K. D., *Prediction and Investigation of the Turbulent Flow over a Rotating Disc*, J. Fluid Mech., Volume 418, pages 231-264, 2000.

82. Yihua, C., Zhiqiang, Y. & Yuan, S., *A Coupled Free Wake - CFD Method for The Simulation of Helicopter Rotor Flow*, Canadian Aeronautics and Space Journal, Volume 48, No. 4, pages 251-258, 2002.

83. Strawn, R. & Ahmad, J., Hovering Rotor and Wake Calculations with an Overset-Grid Navier-Stokes Solver, Proceedings of the 55th AHS Annual Forum, 1999.